

Self-organizing Processes in Non-Crystalline Materials: from Lifeless to Living Objects

M.I. Mar'yan*, A. Szasz**

* Uzhgorod National University, Department of Solid State Electronics Uzhgorod, Ukraine

**Department of Biotechnics, St. Istvan University, Godollo, Hungary

Published: Budapest-Uzhgorod, OncoTherm GmbH, 2000

Mar'yan M.I., Szasz A. Self-organizing Processes in Non-Crystalline Materials: from Lifeless to Living Objects. – Budapest-Uzhgorod. OncoTherm. 2002.

This book deals with self-organizing processes. These processes play an extremely important role in the phenomena occurring in the living and lifeless nature. One can hardly solve a variety of medical, biological, and technological problems without studying such processes, since the main goal of synergetics (i.e. the science which studies self-organizing systems) is to reveal the general regularities of self-organizing processes in the systems of different nature. This is the reason for the analysis performed in this book concerning fundamental theoretical problems, modelling and investigations of the self-organizing processes in inorganic and organic materials with different levels of complexity, from atomic systems to living organisms.

Keywords: synergetics, self-organization, non-crystalline state

Written for: graduate students, researchers, engineers

MAR'YAN M.I. Associate Professor, Uzhgorod National University, Uzhgorod, Ukraine

SZASZ A.

**Private Professor, Szent Istvan University,
Godollo, Hungary
Visiting Professor of Strathclyde University,
Glasgow, UK**

© OncoTherm GmbH, 2000

INTRODUCTION

When solving problems concerning various fields of science ranging from physics and biology to economics and ecology, the formation and conservation of the functional organization, its development and self-complication is both the goal of the study and its paramount stage [1-5]. The following two examples are peculiar here. The first one concerns problems related to the development and preparation of materials with structural-sensitive properties and various ordering degrees. In the majority of cases, the most important factor is the creation of the required spatial or spatial-temporal ordering. Another example is the operation of living organisms and the related simulation of ordered structures in biological objects. The question about the optimal ordering and organization is also topical when studying global problems, i.e. energy, ecological and other problems, which require immense resources. The trial-and-error method is not appropriate here. Knowledge of inherent properties of the system and the regularities of its evolution is more reasonable. In this case, it is difficult to overestimate the importance of self-organization and ordering formation laws in physical, biological and other systems.

For this reason, an interdisciplinary field of science has been created, i.e. the new theory of self-organization or synergetics, which explores the general principles of the formation of spatial, time and spatial-temporal structures in thermodynamically open systems of different nature away from the equilibrium state [6-10]. Thus, the first cause beneficial for the creation of synergetics was the exit from the framework of the classical (equilibrium and linear) thermodynamics and the subsequent necessity of the description of highly non-equilibrium systems.

The second cause of synergetics creation is the necessity to analyze various complicated processes by means of new mathematical methods when solving a series of scientific and technical problems. One is forced to deal more frequently with non-linear phenomena where more intense external actions result in the qualitatively new behaviour of the system [11-13].

Non-crystalline materials are the specific example here. It should be noted that the principal trends in the practical application of non-crystalline solids (i.e. vitreous and amorphous materials) have been clearly defined so far [14]. The more ample use of such solids and the quest for new areas of application require fundamental scientific research, which will provide new ideas for applied development in the future. The main tendencies of fundamental studies of non-crystalline solids start from the analogy with the well-known structure and properties of crystalline solids and liquids, while non-crystalline solids are considered disordered systems [15-17].

At considerable deviations of the system from equilibrium and under the influence of substantial external fields, the dominant role is played by synergetic effects and by the energy transformation mechanism that can be studied by means of the ideas of non-equilibrium thermodynamics. From this standpoint, the creation of non-crystalline solids is the self-organizing process accompanied by the formation of ordered structures on the macroscopic scale. Such an approach to non-crystalline solids is in the initial state. Hand in hand with this, it enables one to describe the formation of non-crystalline solids, their structure and the peculiarities of the interaction with the external fields based on the unified physical principle. The solution to this problem correlates with the simulation of the vital activity of living objects [18-23].

The present work is dedicated to studies on the formation of ordered structures in the condensed matter (non-crystalline solids, water, bio-objects), by invoking the ideas of synergetics and considering the interaction of electromagnetic radiation with the related media.

Contrary to a number of known publications on the order-disorder problem, this book contains both the mathematical background and a number of experimental facts, concerning glasses, water, and bio-matter. Therefore, it may be interesting for the professionals working in this field of science and for those readers who just try to comprehend deep interconnections in the materials science and living objects without mathematical proof. An important problem of the influence of different fields on the metastable matter is successively analyzed in many aspects, and leads to understanding of the

essential importance of investigations in this direction, especially for living objects and for the metastable matter in general.

The material is divided into chapters so that from chapter to chapter the considered problems become more and more clear, and appropriate mathematical models of self-organizing processes – more visual. Each chapter starts with a brief, popular scientific presentation of the developed concept without a loss of strictness. In the appendix, the data, calculations and results of the calculations are presented, allowing the readers possessing the necessary mathematical apparatus to evaluate the reliability and persuasiveness of arguments in favour of the mathematical models used.

That is why this book will be useful for a wide community of scientists and engineers working in the fields of material science, biology, and medicine, and also for students.


Most of the results outlined in this book have been obtained by the authors.

ACKNOWLEDGEMENT

The authors would like to thank Prof. Alexander Kikineshy for his fruitful remarks, ideas and discussions on the subject and a lot of work during the formation of the content, which was essential for the edition.

NOTATIONS

\square	amplitude of the mode	$(dS)_e$	entropy flux due to the matter and energy exchange with the environment
\vec{A}	vector dipole	E	energy of state
$A(t), B(t)$	arbitrary operators	\tilde{E}	self-consistent energy of system
a, b	potential constants	\vec{E}	electrostatic field vector
a	average interatomic distance	$E(t)$	emission initiation of laser
a_r	relaxation process constant	E_g	energy gap
a_{ij}	matrix elements	$E(\vec{r}, t)$	electromagnetic wave
\vec{B}	induction vector	F	free energy functional; force
C_p	heat capacity	F_0	free energy functional for equilibrium state
C_i	reagent concentration	\square	external force
$C(t)$	product concentration	\square_0	amplitude of the external force
CN	co-ordination number	\square_c	critical value of amplitude external force
$c(\tau)$	correlation function	$\square\{x(t)\}$	fourier-transformation of the function
c_0	correlation function constant	\mathfrak{S}	transformation function
\vec{D}	shift vector	$F(t)$	correlation function
D	diffusion coefficient	$F(X, \lambda)$	non-central function of reagent concentration in the Belousov-Zhabotinsky reaction
$D_0(x)$	soft domain of the diffusion constant	$F_1(\sigma), F_2(y_l), F_3(y_t)$	non-linear functions
$\tilde{D}_{ll'}^{\alpha\beta}$	self-consistent mean-square of atomic displacements	σ, y_l, y_t	
d	space dimensionality	$\tilde{F}'_1(\sigma)$	the first derivative $\tilde{F}_1(\sigma)$ with respect to σ
d_f	fractal dimensionality	f	- stochastic process frequency
d_l	layer thickness	f	- elastic constant
dE	energy increase	\tilde{f}	- effective force constant
dN_k	particle number of the k-th component increase	f_T	- force which results in the production of the thermal fluxes
dS	entropy increase		
dV	volume increase		
dW_t	random variable W_t increase		
$(dS)_i$	entropy production inside the system		

f_N	force which results in the production of the diffuse fluxes	N	number of atoms
	function of state	N_o	defect states density
$f_\lambda(X(r,t))$	non-linear functional dependence	N_e	number of equal parts
f_1, f_2, f_3	transformation coefficients	N_E	number of edges
G	photo-generation rate	N_F	number of faces
G_{\min}	minimum value of power radiation	N_V	number of vertices
$G(l', t)$	Green's function	N_{grain}	number of grains
$G(k, \omega)$	Green's function in k -representation	N_1	number of atoms in the solid-like state
$G(\delta)$	non-central potential	N_2	number of atoms in the soft-like state
$\tilde{G}(\delta)$	self-consistent interaction non-central potential	N_f	number of atoms in the f state
G_0	non-central potential parameter	N_{norm}	normalization factor
$G(T)$	heat source	$\mathfrak{N}(\vec{r})$	local physical quantities
g	force constant	n_s	number of pentagons
\tilde{g}	effective force constant	n_i	number of face-polygons
\mathbf{g}	gravitational acceleration	P	pressure
g_f	statistical weight	P^*	reduced pressure
$g(x, r, t)$	distribution function	\mathfrak{R}	probability density
H	Hamiltonian	$\mathfrak{R}(y, t / x, s)$	probability density for Fokker-Planck equation
\tilde{H}	effective Hamiltonian	\mathfrak{R}_s	stationary probability density for Fokker-Planck equation
\vec{H}	magnetic field vector	\square	laser radiation power
H_f	Hamiltonian of subsystem f	\square_c	critical value of power
$H(\{\mathcal{X}\})$	configuration Hamiltonian	\tilde{P}	reduced laser radiation power
\hbar	Plank's constant	\vec{P}	electric polarization vector
I	intensity density of the incident wave	p	parameter of relaxation process
$I(x)$	intensity distribution across laser beam cross-section	p_S, q_S	Schlaflly symbols
I_0	constant of laser beam	$p(l)$	atom momentum
$\tilde{I}_\alpha(l, l')$	self-consistent interaction potential	$p([\delta s])$	generalized entropy
J_e	current density	\vec{Q}	reciprocal lattice vector
$J(\eta, t)$	probability flux	Q_i	distribution parameter which characterizes the disordering in the system
$J_m(x) - m^{th}$	order-Bessel function	$Q(T)$	heat exchange with the environment
k	wave- vector	q	cooling rate
k_c	critical wave-vector	q_c	critical cooling rate
k_B	Boltzmann constant	\tilde{q}	reduced cooling rate
k_F	Fermi wave-vector	\tilde{q}_c	reduced critical cooling rate
L	length	\mathbf{q}	heat flux
L_S	short-range order distance	R	radius
L_M	mesoscopic media-range order distance	R	constant molecular gas
L_c	dissipative structure period	\vec{R}_l	average equilibrium position of the l -th atom
L_a	transition energy difference	r	inter-atomic distance
$L_{bistable}$	domains for bistable-element dimension	\vec{r}_l	radius-vector of the l -th atom
L_{multi}	domains for multi-vibrating-element dimension	$r_m, r_{m0}, r_{m\infty}$	parameters of Fejchenbaum's mapping
L_{auto}	domains for auto oscillating-element dimension	$r_0(\eta), r_1(\eta)$	transformation function
\vec{M}	magnetic polarisation vector	S	entropy
M	mass		

$S(f)$	spectral density function power	z	number of closest neighbours
s	short-range order parameter	Z	average coordination number
S_F	Forster's constant	α	optical absorption coefficient
S_0	beam cross section	α_T	linear expansion coefficient
T	temperature	α_{ij}	matrix quasi-stationary solutions elements
T_1, T_2	temperature of liquid layer lying between two parallel planes	$\tilde{\alpha}_i$	reduced matrix elements
T_m	melting temperature	α_a	non-linearity parameter
$T_f(l)$	kinetic energy of the l -th atom	α_{norm}	normalization parameter
\tilde{T}_f	self-consistent kinetic energy of the f -th subsystem	β	parameter of relaxation process
t	time	β	quantum yield
t_η, t_κ	reduced time	β_T, β_N	distribution constants
U	optical transmission	β_0	diffusion soft domains constant
$U_f(\vec{r}_i)$	one-particle potential	$\Gamma(x)$	Gamma-function
$U(\vec{r}_1, \vec{r}_2, \dots, \vec{r}_N)$	potential energy of system	γ	damping constant
$u(l)$	dynamic displacement of atom	γ_i	parameter of Landau-Khalatnikov regression equation
$u_{\alpha\beta}(l, l')$	relative displacement	γ_o	absorption coefficient prior to lighting
V	volume; potential	$\gamma(\omega)$	absorption coefficient
\tilde{V}	reduced volume	γ_{colour}	constant of the colour noise
V_0	parameter of potential	Δ	Laplacian
V_{grains}	volume of grains	ΔT	temperature gradient
V_{total}	total volume	ΔT_c	critical value of temperature gradient
$V_{product}$	product volume	$\Delta\omega_2$	short-range disordering destroying
$V_{extended}$	extended volume	$\Delta y_i(\tilde{q})$	reduced thermal displacements of particles in the equilibrium state along the bondings
$V(x)$	rate of the change in the soft domain dimensions	δ	deflection of the atom in the plane normal to the direction of the bond
$W(R_i)$	relaxation rate	δ_i	mean-square displacement
X_i	general extensives belonging to the i -th interaction	$\delta(t)$	Kronecker symbol
$X(\vec{r}, t)$	state system parameter	$\delta(x)$	Dirac function
$X_s(\vec{r}, t)$	state system stationary parameter	δF	free energy functional variation
x	distance	$\delta\tilde{\phi}_f^{\alpha\beta}$	force constant variation
\vec{x}	n -dimensional vector with the components x_1, x_2, \dots, x_n	$\delta\sigma$	fraction of atoms in the liquid-like states variation
\vec{x}_s	n -dimensional vector in the stationary state	$\delta y_{\alpha\beta}$	mean-square relative displacements of atoms variation
\dot{x}	velocity	δT	temperature field variation
\bar{x}	average size of the sort configuration domain	δg	distribution function variation
x_o, y_o	initial condition of the phase trajectory	δN_2	number atoms in soft configuration variation
Y_i	general intensities belonging to the i -th interaction	$\delta\eta(r, t)$	order parameter variation
$y_{\alpha\beta}(l, l')$	the mean-square relative displacement of the l, l' atoms	$\partial_y, \partial_{yy}$	first and second derivative with respect to y
y_l	reduced mean-square displacement of atom along the bond	ε	dielectric susceptibility
y_t	reduced mean-square displacement of atom normally to the bond	ε	Bethe's parameter
		ε_m	measure of the removal from the white noise approximation
		π	3.14
		$\theta(t - t')$	Heaviside's function

θ	angle deviation	$\Phi(r, t)$	reduced temperature field
θ	temperature expressed in Boltzmann constants	Φ_s	stationary temperature field
\mathcal{G}_E	energy band deformation potential	$\Phi(r)$	pair potential
η	order parameter	$\Phi_1(r)$	long-range component of the pair potential
η_s	stationary solutions of the order parameter	$\Phi_2(r)$	short-range component of the pair potential
η_h	heat exchange constant	$\tilde{\Phi}_f$	self-consistent potential energy of the f -th subsystem
Λ	wave length	$\phi(\eta, q)$	non-linear function in equation bifurcation diagram
λ	external control parameter	$\bar{\phi}(\eta, q)$	non-linear function in a stable stationary state
λ_i	eigenvalues	$\phi_{ff'}(\vec{r}_{ll'})$	interatomic interaction potential
λ_t	external parameter for a system with white noise	$\tilde{\phi}_f^{\alpha\beta}(l, l')$	force constant
$\lambda(k)$	damping decrement	φ	soft states potential
λ_{\max}	maximum value of the function $\lambda(k)$	$\varphi(x_n)$	point mapping function
μ	chemical potential	χ_o	effective beam radius
μ_k	chemical potential of the k -th component	χ_l^f	local characteristic function
ν	frequency	$\Psi(r, t)$	Lyapunov's functional
$\vec{\nu}(l)$	vector static displacement of the l -th atom	$\tilde{\Psi}(r)$	self-consistent central interaction potential
$\nu_\alpha(l/m)$	static displacements of the l -th atom when the atom m is in the liquid-like state	$\psi(r)$	central Morse-like potential
ν_{0f}	geometrical-structure factor	$\omega(\vec{k})$	frequency vibration of atoms
ξ	fluctuation around the average value	ω_0	external force frequency
ξ_p	anisotropy for different potentials parameter	ω_{0k}	resonant frequency
ξ_d	activation energy diffusion	ω_L	maximum vibrational frequency
$\vec{\xi}(t)$	negligibly small vector	ω_f	fraction of atoms in the f -th state
ρ	material density	ω_2^e	fraction of atoms in the equilibrium disordered state
κ	compression modulus		
κ_o	heat conduction coefficient		
$\tilde{\kappa}$	reduced heat conduction coefficient		
ρ_e	electric charge density		
σ	long-range order parameter		
σ	external noise intensity		
$\sigma_f(l)$	configurational function of two microscopic states		
σ_2	fraction of atoms in the liquid-like states		
$\sigma[\delta s]$	generalized entropy production		
τ	reduced temperature		
τ_m	reduced melting temperature		
τ_c	reduced critical temperature		
τ_0	reduced synthesis temperature		
τ_g	reduced softening temperature		
τ_p	exposure time		
τ_i	relaxation time		
τ_t	reduced time		
τ_{cor}	correlation time		
τ_{life}	life-time		

SELF-ORGANIZING PROCESSES IN DIFFERENT-NATURE SYSTEMS

Self-organizing processes play an extremely important role in the surrounding life, i.e. in the phenomena occurring in the living and lifeless nature. One can hardly solve a variety of medical, biological, and technological problems without studying such processes since the main goal of synergetics (i.e. the science which studies self-organizing systems) is to reveal the general regularities of self-organizing processes in different-nature systems [1-4].

1.1. Synergetics: principal definitions

Synergetics today covers not only various areas of science, featuring processes of self-organization in an alive and lifeless nature, but also permeates into various fields of human activity. The Professor of Stuttgart University and the Director of the Institute of Theoretical Physics and Synergetics H. Haken is recognized as the author of the term "synergetics" [5]. According to Haken, synergetics studies the behaviour of systems comprising a great number of subsystems (parts, components). In its precise sense, the term "synergetics" means the joint action, thus distinguishing the coordination in the functioning of the parts, reflected in the behaviour of the system as a whole¹.

The advantage of synergetics is that the systems, representing the subject of study and considered as a whole, can very different in nature and may be studied by each of the sciences separately (for example, by physics, biology, chemistry, mathematics, sociology, economy and so on). Each of such studies its "own" nature of the system by its intrinsic methods and produces the results of research in its "own" language. At the existing differentiation of the science, this means that the achievements of one science frequently become inaccessible to the attention and comprehension of the representatives of other sciences. A similar situation takes place with interfacing sciences originating from the junction of two sciences in a more or less wide frontier field (for example, in biophysics, physical chemistry and so on). Therefore, physics studies the physical nature of systems using physical methods, while biophysics is engaged in the research of biological objects by physical methods. Therefore, contrary to the traditional areas of science, synergetics is interested in common legitimacies of the evolution of the systems of any nature, which stipulates its generalized interdisciplinary character.

Synergetics studies a common character of regularities and dependences, not appealing to the nature of systems, by means of specific resources, having a common character in relation to private sciences. The unity and integrity of synergetics in studying systems is illustrated by Fig. 1.1.1.

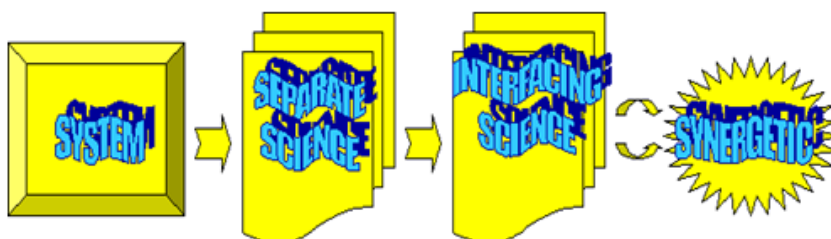


Fig. 1.1.1. Synergy as an interdisciplinary field of science.

¹ The predecessor of Haken's synergetics was that of the physiologist Sherrington, who studied the consistent action of flexors and extensors at limb operation, as well as the synergy, i.e. junction of a man and God in a pray.

Due to the fact that synergy removes the specific nature of investigated systems, it acquires the ability to describe the formation development, by working out a common model of phenomena occurring in an organic and inorganic nature. Synergetics appears to be a link in understanding the relationship between the substance and the life. The most apparent feature of the objects of an alive nature is that they are capable of self-organization, i.e. the spontaneous formation and development of complicated structures. The necessary premise for the self-organizing effects consists of an openness of systems (energy, mass, information exchange with environment). Due to this flux from the outside, the system becomes active, i.e. gaining the ability of the spontaneous formation of the structures. Apparently, the effects of self-organization cannot be an exclusive property of biological objects, and, thus, they are also observed (in simpler form) in the systems of an inorganic origin.

Therefore, synergetics combines the studies of the system as a whole and those of its separate parts at different levels. It makes a bridge between them using two levels of description, due to their coordination, synchronization and coherence. As a result, the system acquires the properties that are not inherent in its separate parts. This circumstance has essential importance and allows one to define synergetics as a science exploring self-organization. Thus, the macroscopic manifestations of the processes occurring at the microscopic level arise "independently", due to self-organization, with no "guiding hand" that operates outside the system. The self-organization is born by the system itself as a result of a loss of stability of the state. Thus, self-organization is reduced to the selection among the spatially active systems, potentially possessing a great number of degrees of freedom at a small number of order parameters (variables) defining the dynamics of the whole system. A small amount of order parameters and scarce possibilities, which they reflect in defining separate states, testify to the fact that in compound systems, only a few structures are possible and available, being consistent through a combined action of the elements.

There are no separate control elements (units) of the system in charge of a certain property. The complicated structural formations in the nature are simultaneously both determined (predictable) and stochastic (unpredictable), i.e. they exhibit a dualism of determined and stochastic. In synergetics, there is nothing predetermined at a level of preset computer program – except the structures and systems, which following a loss of stability can give rise to some new states. The system becomes unpredictable, not by virtue of our ignorance, but by virtue of its nonlocal properties, such as complexity, nonlinearity, openness, and non-equilibrium. At a point of a loss of stability the new functioning mechanisms with new parameters are self-organized. It should be noted, that the parameters of the state do not disappear – they remain, but in cases related to self-organization, the system selects the order parameters itself. We obtain a sort of ready oblate information on the system. Even when the separate elements of the system have a complex internal structure, their entire internal complexity is not revealed in their mutual interaction, and, from the point of view of a macrosystem, they function as simple enough objects with a small number of effective degrees of freedom. Otherwise, no structure ordering occurs in the system.

It should be noted that it is possible to describe more or less adequately self-organizing phenomena at one level. The investigation of the phenomena between various levels is so far problematic. The chaos at one level leads to the structuration at the other. This approach is one of the basics of synergetics. The thermal oscillations and diffusion act as the chaos at the microlevel. However, for a number of self-organizing systems of organic and inorganic origin, this process plays a principal role in the formation of ordering at the mesoscopic (average) level order. The chaos at one level results in self-organization and the appearance of an order parameter at the other level (spatial or temporary). The systems behave in a chaotic manner; however, at the particular stages of the process or at some characteristic moments, they result in the appearance of the formations, for which the structural representation is adequate. Such structures can be considered those of the next level with their definite functioning parameters. At the next level, the ordering may arise again, and so on.

A convenient image of nonlinear dynamics are the fractal structures, for which the description obeys the same rules with the change of spatial or temporary scales [6-8]. The term "fractal structures" is widely used for the description of self-organization in the energy, mass, and

information – open systems, since in this case, in the non-linear dynamics tasks, we do not deal with unstructured random processes, but just with the results of self-organization, i.e. the creation of complex, coherent structures.

Synergetics describes the birth and creation of spatially and temporally branched structures under the scripts of interchanging periods of stability and instability. At the initial stage, the system, wandering in the state space, forms controlling parameter values; the first is the attractor (attractor is the steady state, to which the system tends and for which the predictability and reproducibility of the modes is peculiar). Then, skipping into the other domain due to a loss of stability and fluctuations, it forms a second attractor, and so on. Due to this, the contour of the states of the system – i.e. the domain of stability, singular points, tunnels of transitions from one domain to another – is formed. The concept of a path of self-organization of the complex system arises, which can be conveniently described by the fractals. The task of synergetics consists of the search for studies of the models of self-organizing systems, which result from the most typical assumptions, the properties of separate active elements and the laws of interaction between them. The theory of dissipative structures, Thom's theory of catastrophes and the theory of mappings and attractors belong to the most spread synergetic methods [5,9-15] (Fig. 1.1.2).



Fig. 1.1.2. Methods of synergetics.

Consider the above methods.

1.2. Methods of synergetics

1.2.1. Dissipative structures: general characteristics

G. Haken was among the first to draw attention [5] to the commonness of the dissipative structure formation process with phase transitions in non-equilibrium systems (in ferromagnetics, ferroelectrics, superconductors, etc.). This allowed him to call the dissipative structure formation processes the non-equilibrium transitions [5]. The latter are much more diversified than the equilibrium ones and play a prime role not only in the physical processes but also in biological and chemical processes.

The notion of dissipative structures as one of the most general notions of thermodynamics of non-equilibrium processes was first introduced by I. Prigogine [15]. This term emphasizes the fact that these structures arise in dissipative systems during the non-equilibrium (irreversible) processes. The temporal, spatial and spatial-temporal dissipative structures are distinguished.

Note the necessary conditions for formation of the dissipative structures [15-22].

- Dissipative structures can be produced only in open systems. In such systems, the energy influx or matter exchange may occur, compensating the losses and providing the existence of ordered states. In this connection, the external supply of "negative entropy" exists together with the production of entropy.
- Dissipative structures arise in macroscopic systems comprising a large number of particles (atoms, molecules, cells, etc.). This allows one to apply equations for the functions averaged over the physically infinitesimal volume (the local equilibrium condition). The ordering in these systems is also co-operative in character, since a great number of objects are involved.

- Dissipative structures arise only in the non-linear systems described by the non-linear function.
- To admit the occurrence of dissipative structures, linear equations must allow (at certain values of parameters) the appearance of solutions with other symmetries, for instance, transition from the laminar flow to the turbulent one accompanied by changes in velocity.

Based on the examples considered above, one may distinguish three types of active media elements in which self-organizing processes are observed [22]: bistable, multi-vibrating (excited) and auto-oscillating elements (Fig. 1.2.1.).

Bistable elements have two stationary states, and may remain in each of these states for an infinitely long time. An external action may cause the transition from one state to another. To induce transition, the intensity of this action must exceed a certain threshold.

Multi-vibrating elements have a single distinguished rest state, which is stable with respect to comparatively weak external actions. However, such systems differ from passive ones by their response to the actions, exceeding the threshold level. As a response to this quite intense external action, the system produces a flash of activity, i.e. a certain sequence of active transitions takes place, and only after this does the system return to the initial rest state.

Auto-oscillating elements act like the *perpetuum mobile*. They autonomously perform cyclic transitions via a certain group of states. An external action is able to decelerate or accelerate this cyclic movement only, but not to stop it.

The examples considered illustrate the basic properties of the stationary structures produced. First of all, each of these structures is a stable formation, the form and size of which are resumed at slight perturbations. The same distributed system can possess a huge number of different stationary non-equilibrium structures. Which of the stationary states is realized in experiment depends on the initial conditions and the external random field. For such structures, besides the local interaction, the active medium elements are involved in long-range feedback. The properties of dissipative structures set up in the medium depend tangibly on the type of elements composing this medium, i.e. bistable, excited or auto-oscillating elements (Fig. 1.2.1).

If the active medium, in which self-organizing processes are realized, consists of bistable elements, then it comprises a family of domains with $L_{bistable}$ -order dimensions in which the state of the medium is close to one of the two stable states of the separate element. These domains are separated by transient L -wide layers.

If the medium comprises the multi-vibrating elements, then it possesses only a homogeneous stationary rest state. In the one-dimensional case, this structure is a set of narrow L_{multi} -wide strata spaced by $\sim L$ distances. In the domains between the strata, the medium is in the state lying close to the resting one. In two-dimensional or three-dimensional cases, the dissipative structure is an aggregate of little drops.

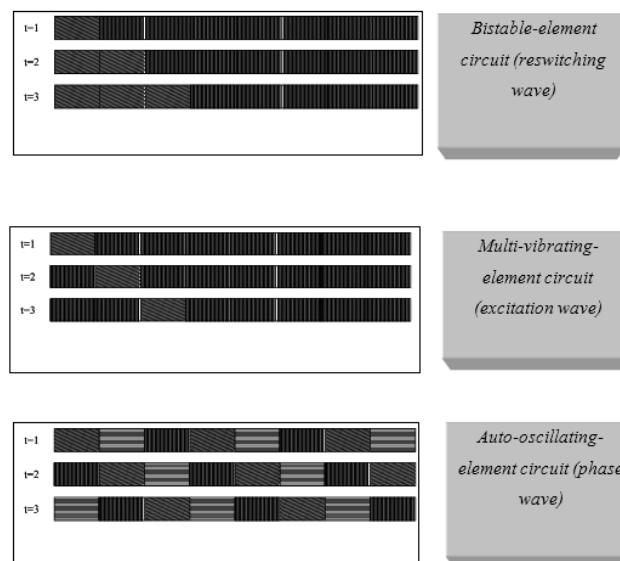


Fig. 1.2.1. Types of active media elements.

If one separate element of the medium undergoes periodic auto-oscillations, then the stationary homogeneous state of the active medium is absolutely unstable. Stationary structures are formed in it in the form of L_{auto} -long strata separated by transient layers (Fig. 1.2.1).

The occurrence of dissipative structures away from the equilibrium is due to the presence of fluctuations and it was therefore called "order via the fluctuations". This type of ordering is an essential approach to the conditions of the vital activities of biological objects, since the organisms are open systems far from equilibrium. Dissipative structures of biological origin have been discovered at various levels of complexity:

- at the molecular level, i.e. the variations of the substrate density during the reactions catalyzed by the ferments;
- at the cellular level, i.e. the induction-type vibrations and genome repressions described by Jacobo and Mono;
- at the organism levels (the circadian and similar rhythms);
- on the population level, i.e. the variation of a number of organisms within biocenosis. While in physicochemical systems, the feedback, similar to autocatalysis, occurs extremely rarely, but it is a necessary condition for the biological organization in living systems.

The term "whole" in relation to the concept of dissipative structures is treated as the result together with its formation, distinguishing and combining; thus, this is the process of formation and the result. The dissipative structures in the biological objects are not a constant notion, but are in a permanent formality.

The degree of steady integrity, which is peculiar to the dissipative structure as an organic whole at the levels mentioned above and is necessary to promote the development of the structures at the higher level of organization, is determined by the minimum energy dissipation. We should define fundamental dissipative structures as the result of self-organization at the appropriate molecular-organism levels. A quantitative measure of each level is the intensity of interaction with the medium external with respect to a considered level, which defines the binding energy of the stable system produced. The hierarchy of levels of structural organization ("a quantum ladder") is considered the result of a prior self-organization.

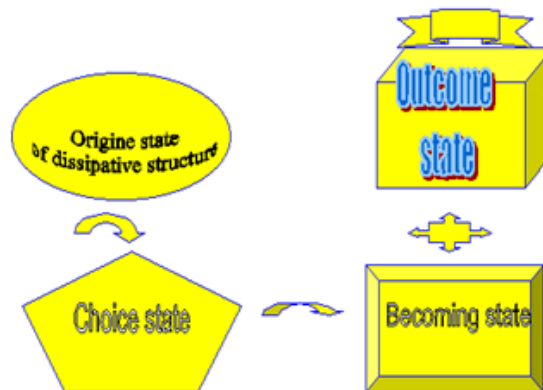


Fig. 1.2.2. Visual representation of dissipative structure development.

One may distinguish some stages of the formation of the dissipative structure at certain levels (visually this process is illustrated in Fig. 1.2.2). The first stage describes the initial state, which comprises different possibilities of structuring the medium in the minimized (not evident) form. In the physical aspect, this stage is associated with that initial "vacuum", the fluctuations of which are potentially uniformly distributed over the whole system. The second stage is defined by a state on the verge of possible and true, in which a set of principally essential and possible, but not yet stable structures, appear to be open. The third stage is related to a choice of the possibility of structural complications up to the formation. At the fourth stage, the manifestation and implementation of the stable structures occurs.

However, a principal difference exists between the appearance of the order via fluctuations in the systems far from equilibrium and in the living systems. This difference is that in the first case, we deal with the process of dissipative structure self-organization, whereas in the second case, the self-regulating phenomenon occurs which provides the stability of the state of the biological system far from equilibrium. In the first case, the cause/effect relations are of a spontaneous type, while in the second case, they are strictly determined by the genetic programme. Thus, dissipative systems are non-linear [14,18-20] and, taking into account the necessity to be as general as possible, we may consider them in a common mathematical model.

The non-linearity of the problem being studied motivates the possibility of a qualitative change in solutions, which describes the behaviour of the system at continuous variation of the parameters. In this case, a slight variation in system parameters may result in a considerable change in solution. The simplest example of a non-linear equation is an ordinary quadratic equation. We can continuously increase one of the coefficients and find that at any small increment in the vicinity of some quantities, real solutions can both be produced or vanish.

The models of the turbulent motion of liquids, the ecological models and the Belousov-Zhabotinsky reactions are the recognized examples of non-linear processes. Non-linear dynamic systems may have extremely complicated motion modes, i.e., depending on the parameters, their dynamics may be either regular or chaotic. One of the paradoxical peculiarities of the systems specified by non-linear mathematical models is the property of self-organization. In complex systems with many interacting subsystems, the qualitative peculiarities may arise as they are not possessed by any component. As a result, a new structure and the relevant operation appear at the macroscopic level.

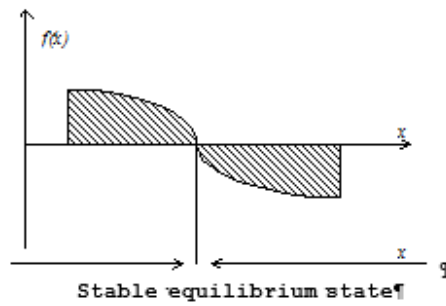
1.2.2. Non-linear differential equations and mathematical analysis of instabilities

The choice of mathematical model of the dynamic object is reduced to the construction of differential equations. The model of the non-linear dynamic system can also be constructed in a class of non-linear algebraic functions [5,14,18]. Consider the first approach, because the second follows from the first one. In some cases, the behaviour of the dynamic system is described by the first-order differential equation:

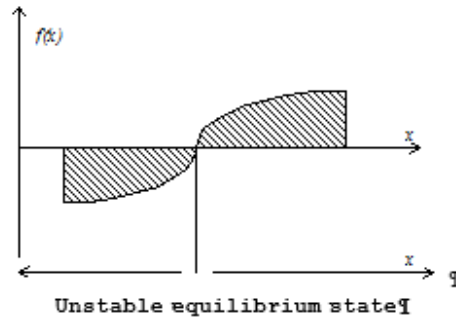
$$\frac{\partial \bar{x}}{\partial t} = f(\bar{x}), \quad \bar{x}(0) = \bar{x}_0, \quad (1.2.1)$$

where $\bar{x} = \{x_1, x_2, \dots, x_n\}$ is the n-dimensional vector with the components x_1, x_2, \dots, x_n , $f(\bar{x})$ is the non-linear function of the state. The points \bar{x}_s , for which the right side $f(\bar{x})$ of equation (1.2.1) equals zero, i.e. $f(\bar{x}) = 0$, are called the equilibrium positions or the stationary (singular) points of the system. The position of equilibrium can be both stable and unstable. The notion of the stability of the dynamic system is of great importance and may be considered one of the basic concepts. In particular, the character of the evolution of the system from the stationary state depends considerably on the type of equilibrium, i.e. stable or unstable equilibrium. For the case of the unstable equilibrium, the system can be flung away from the stationary state, even due to extremely small deviations from the initial state, and either the motion becomes chaotic or the system transitions to the other stationary state.

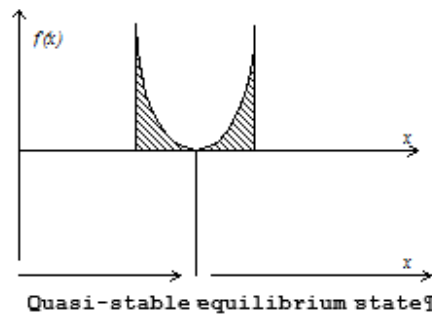
The system is in the stable equilibrium state \bar{x} if the system remains close to \bar{x}_s for any t, even at slight deviations from it. In the mathematical language, this statement is written as follows. Let the system (1.2.1) at a certain moment of time t_0 be in the state $\bar{x}(t_0)$ close to the equilibrium state: $\bar{x}(t_0) = \bar{x}_s(t) + \bar{\xi}(t)$,



Case-1.¶
f(x) function changes its sign close to x_s (from "-" to "+"). Here $\partial f(x)/\partial x > 0$, i.e. the function increases with x .¶



Case-2.¶
f(x) function changes its sign close to x_s (from "-" to "+"). Here $\partial f(x)/\partial x > 0$, i.e. the function increases with x . This means that the illustrative point located in a close proximity to the equilibrium state will move away from the equilibrium state. → ¶



Case-3.¶
f(x) function does not change its sign close to x_s with increasing x . This means that the illustrative point located rather close to x_s on one side will approach it, while this point being located on the other side will move away. In this case $\partial f(x)/\partial x = 0$.¶

Fig. 1.2.3. Possible cases of $f(x)$.

where $\xi(t)$ is negligibly small compared with \bar{x}_s . Lyapunov's theory states [22] that if all eigenvalues λ_j of the matrix $a_{ik} = \left(\frac{\partial f}{\partial x_k} \right)_{x_s}$ obey the inequality:

$$\text{Re } \lambda_j < 0, \quad (j = 1, 2, 3, \dots, n), \quad (1.2.2)$$

then the equilibrium position \bar{x}_s is stable. If among all eigenvalues λ_j the only one exists that:

$$\text{Re } \lambda_j > 0, \quad (j = 1, 2, 3, \dots, n), \quad (1.2.3)$$

then the singular point \bar{x}_s of the system (1.2.1) is unstable. The eigenvalues λ_j of the matrix are defined from the relation:

$$\det |a_{jk} - \lambda_j \delta_{ik}| = 0, \quad (1.2.4)$$

which is called the characteristic equation, where δ_{ik} is the Kronecker symbol.

Let us analyze the behaviour of $f(x)$ close to x_s in the one-dimensional case. Since $f(x_s) = 0$, three cases appear to be possible (Fig. 1.2.3).

1.2.3. Iteration procedure of point mapping

We revert to the differential equation (1.2.1) and shall apply the iteration procedure of point mapping. Consider for simplicity the one-dimensional case. For the initial conditions x_0 , we shall

draw the phase trajectory, e.g., vertically upward from the point $\{x=x_0, y=0\}$, until it crosses curve y at the point $\{x_0, y_0(x_0)\}$. Then, we draw the horizontal line from point (x_0, y_0) until it crosses y at point $\{\varphi(x_0), y_0\}$, i.e. transforms point x_0 into point $x_1 = \varphi(x_0)$. Thus, we obtained a certain set of points which transit sequentially into each other, indicating the occurrence of a certain function φ , which relates the locations of two sequential points x_n and x_{n+1} :

$$x_{n+1} = \varphi(x_n). \quad (1.2.5)$$

This relation defines the point mapping. The sequential application of the mapping (1.2.5) allows the infinite sequence of points to be obtained:

$$x_0, x_1, x_2, x_3, \dots, x_n, \quad (1.2.6)$$

this is uniquely determined by the coordinate of the initial point x_0 . The use of point mapping instead of differential equations when studying the dynamics of certain systems is of interest both from the standpoint of clarity and in relation to numerical analysis, since the dimension of the system is reduced by a unit in going to mapping.

A set of $x_1, x_2, x_3, \dots, x_n$ iterations is called the orbit or the mapping trajectory. A motionless point x_s is called stable if, for sufficiently small values of the external parameter, the iterations x_n converge to x_s regardless of the initial value of x_0 . A motionless point x_s is called unstable if for almost all x_n the iteration process diverges.

Consider the construction of the bifurcation diagram, i.e. branching of the x_n solutions on the r_m parameter, for the one parameter square Fejchenbaum's mapping:

$$x_{n+1} = r_{m0}x_n(1-x_n), r_{m0} = 4r_m, \quad (1.2.7)$$

where r_m, r_{m0} are the parameters of Fejchenbaum's mapping [5,22].

The values of parameters for which the topological (or qualitative) change in movement regimes in the system occurs, are called bifurcation values, and this change is called bifurcation. Let us gradually increase the r_{m0} parameter within the 0 to ∞ range.

- $0 \leq r_{m0} \leq 1$. In this case, the square reflection has only one immobile point $x_n = 0$, which is stable.
- $1 < r_{m0} \leq 3$. For $r_{m0} > 1$, the immobile point $x_n = 0$ loses its stability, because $d\varphi(x_n)/dx_n > 1$, and one more immobile point $x_n = 1 - 1/r_{m0}$ appears in the range $[0,3]$. The immobile point will be stable, because $d\varphi(x_n)/dx_n = 2 - r_{m0}$ (Fig.1.2.4 and Fig. 1.2.5).
- $3 < r_{m0} \leq 1 + \sqrt{6}$. If $r_{m0} > 3$, the mapping again is subjected to a new bifurcation, the immobile point $x_n = 1 - 1/r_{m0}$ becomes unstable. A double circle appears, which is created by two immobile points

$$x_2^{(1),(2)} = (r_{m0} + 1 \pm (r_{m0}^2 - 2r_{m0} - 3)^{1/2}) / 2r_{m0} \quad (1.2.8)$$

- $1 + \sqrt{6} < r_{m0} = 3.5699$. When the r_{m0} parameter crosses the $1 + \sqrt{6} = 3.45$ value, a new bifurcation takes place: the double circle $\{x_1^{(1)}, x_2^{(2)}\}$ loses its stability, but a new four-fold circle appears. For $r_{m0} \geq 3.54$, this circle becomes unstable and is replaced by a new stable circle with a period 2, and so on. The successive bifurcations of double periods take place at $r_{m\infty} = 3.5699$.
- For $r_{m\infty} < r_{m0} \leq 4$ the mapping has circles with an arbitrary period, including aperiodic trajectories. The dynamics of the dissipative structure becomes complicated and versatile; it has an ergodic property and mixing with exponential scattering of close trajectories.

Similarly to Fig.1.2.5, the bifurcation pattern will also be observed for an arbitrary point mapping with a single maximum, which is approximated by the square parabola. Therefore, the complicated chaotic evolution regimes are observed for non-linear dynamic systems.

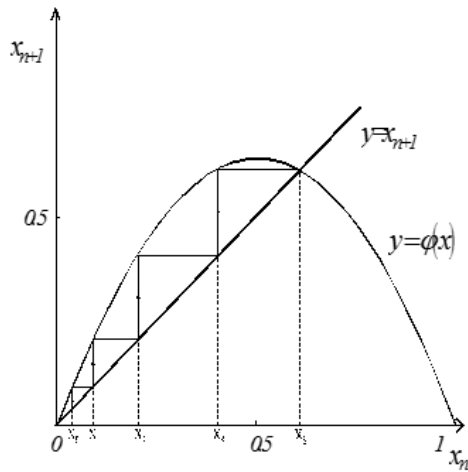


Fig. 1.2.4. Point mapping of $x_{n+1} = \varphi(x_n)$ for $r_m = 0.6, x_0 = 0.05, x_s = 0.583$.

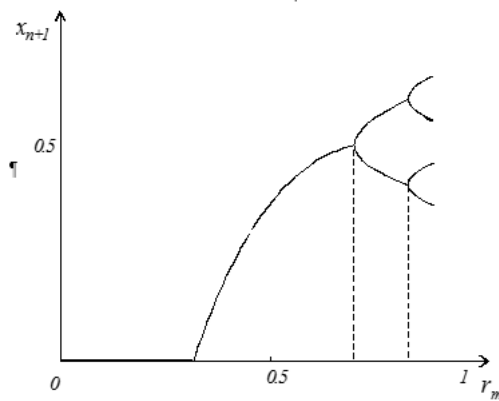


Fig. 1.2.5. Bifurcation diagram $\{x_{n+1}, r_m\}$.

1.2.4. Fractal peculiarities of the chaos

A peculiarity of the simplest dynamic systems to qualitatively change the character of their motion at the transition from the regular to random at slight variation of some external parameters is such an unusual one that all possible regularities of rearrangement occurring in this case should be clarified only by studying the fundamental properties of non-linear dynamics [6-8, 21-27].

1.2.4.1. Regular and stochastic fractals

The dimensional properties of these systems create new characteristics. They have their origins in the notion of fractals inherent in a wide circle of natural objects. Fractals are used to describe irregular forms in such physical systems as non-crystalline materials, porous solids and polymers.

Snowflakes are the classical examples of such structures. The fractal clusters are produced in ferroelectrics or at the crystallization and dielectric breakdown, when the branched structure of current trajectories or a turbulent flow occur. These systems can be called the rarefied or branched objects, and their shape is one of the most intriguing geometric properties. The concept of fractals was first introduced by Mandelbrot [6]. The fractal dimensionality d_f is used as the quantitative measure of structurality of these objects. Consider first a spherical object of mass M and radius R . They are related by the following expression:

$$M(R) = R^d \quad (1.2.9)$$

where d is the space dimensionality, which we usually work with (the dimensionality of a straight line is $d = 1$, that for the surface is $d = 2$, etc.). For many cases, we cannot be satisfied by this definition, since some curves exist which are hard to be distinguished from the surface. The trajectory of the Brownian particle is a simple example (Fig. 1.2.6). For small intervals of investigation time, $d = 1$. At the same time, the larger the observation time, the larger the number of trajectories filling the surface. The question arises here of whether it is possible to indicate some topological characteristics of the degree of complexity of the particle trajectory in the phase space. This gives us the tool which distinguishes the chaotic degree of motion by the shape of its trajectory. This problem is especially essential in those cases, when the chaos is evoked by the regular interactions in the dynamic systems, since just in that case we meet the variety of transient states of motion from regular to stochastic.

An object, whose mass and size obey the relation (1.2.9), is called a compact object. In this case, the scale relation for the density $\rho = M / R^d$ has a form $\rho = R^0$. The relation between mass and a specific size of the object can be defined in a more general form [24]:

$$M(R) = R^{d_f} \quad (1.2.10)$$

The object is called fractal if it obeys the relation (1.2.10) with d_f , other than the space dimensionality d . In this case, the density is not the same for all R and is scaled as:

$$\rho(R) = (M / R)^{d_f} = R^{d_f - d}$$

Since $d_f < d$, the density decreases with size. This relation is a quantitative measure of the notion that fractals are the rarefied or branched structures.

The meaning of equation (1.2.10) is that the fractal objects are self-similar, i.e. they look similar in any spatial scale. To clarify the significance of self-similarity, consider an example of Koch's regular fractal (Fig. 1.2.7), i.e. the object which is self-similar at all length scales. Let us introduce the unit length section and partition it into three parts, with each being $1/3$ long (a). Then, remove the central $1/3$ of the section (b), thus producing the triangular hump in a curve, whose overall length becomes $4/3$. At the next step (c), each $1/3$ long segment is partitioned into three parts, each being $1/9$ long, and this procedure is repeated an infinite number of times producing an infinitely long curve comprising an infinite number of small segments. This curve is called the triangular Koch's curve.

Consider the dimensionality of the regular Koch's fractal. For the unit length section, partitioned into N_l equal parts each of L length, $N_l = 1 / L$. Similarly, for the square lattice, we have $N_l = 1 / L^2$. Thus, for the d_f -dimensional object, $N_l = 1 / L^{d_f}$. Hence, after logarithmically transforming, we obtain [6,24]:

$$d_f = \log(N_l) / \log(1 / L), \quad (1.2.11)$$

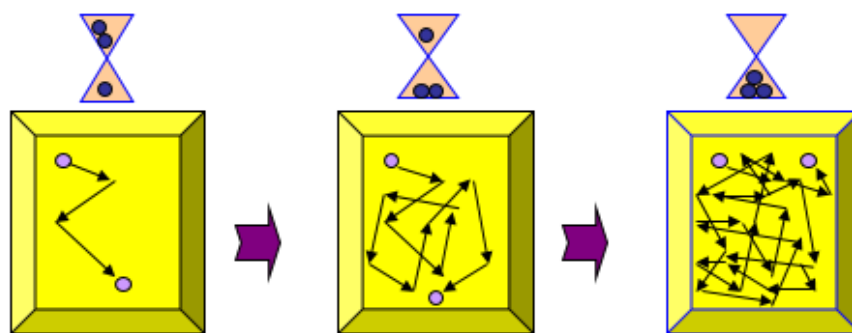


Fig. 1.2.6. Trajectory of Brownian particle.

For the Koch's curve, at each reduction in length L by a factor of 3, the number of segments increases four times. Therefore, for Koch's curve, $N_l = 4, L = 1 / 3$ and

$d_f = \log(4) / \log(3) = 1.262$. Thus, Koch's curve is not just a one-dimensional object, but rather a two-dimensional one.

Similarly, the regular fractals of the square Koch's curve, Serpinsky spacer and Serpinsky carpet (Fig. 1.2.7), are built.

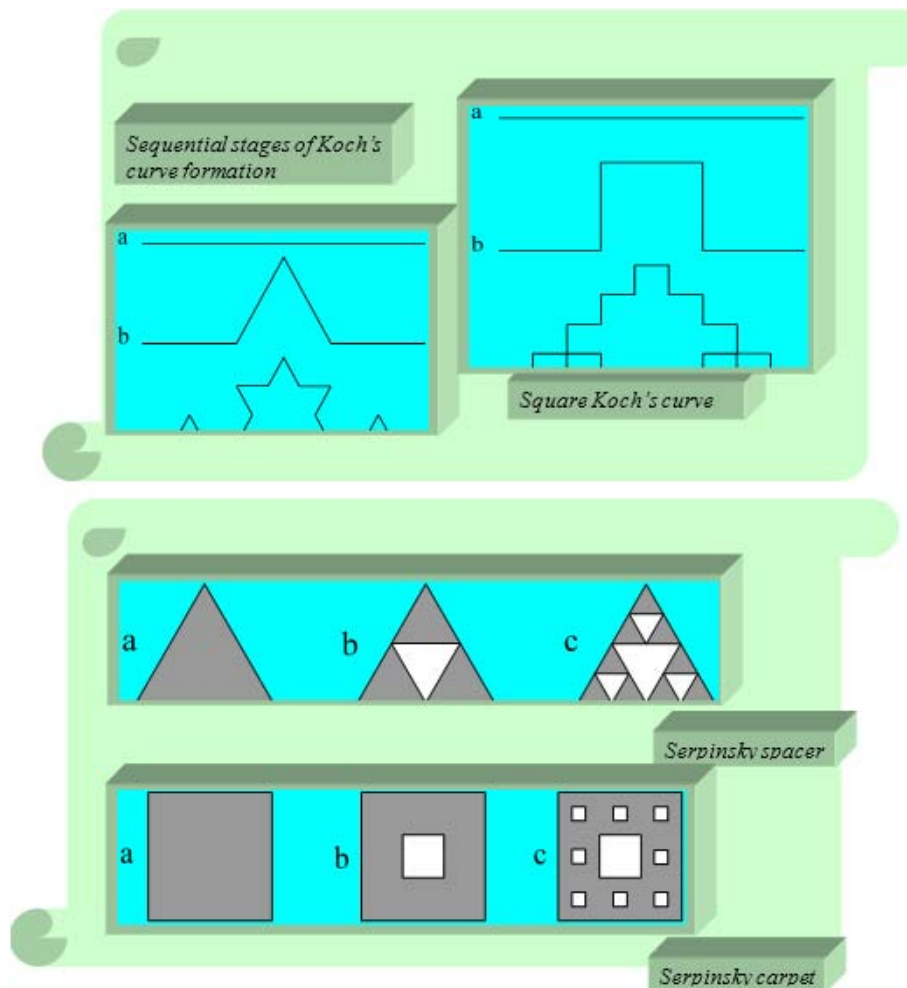


Fig. 1.2.7. Regular fractals of the square Koch's curve, Serpinsky spacer and Serpinsky carpet.

Thus, the sequential stages for the Serpinsky spacer are as follows. The unit triangles are partitioned into nine equal parts and the central triangle is removed. The same procedure is repeated for each of the remaining parts, and the shaded regions are removed. We considered three quite similar examples of fractals. In the case of Brownian motion, at the surface, the numerical analysis shows that $d_f = 2$, whereas $d = 1$. Thus, fractals can be regular (e.g., the Koch's curve) and stochastic (for instance, the Brownian motion trajectory).

For all cases, $d_f > d$, which corresponds to a certain physical sense and just features the complication of multitudes. If this is a curve ($d = 1$), then it can be complicated by an infinite number of bendings to the point where its fractal dimensionality reaches two for the case, when it tightly covers the finite plane, or three, if the curve fills the cube.

It should be noted that the example with Brownian motion testifies that the chaos described by the dynamic equations is essentially fractal. Its fractal character first results from the property of trajectories, which transforms them from regular or periodic to stochastic. Indeed, if the regular trajectory has a $d = 1$ dimensionality, then the local instability complicates the trajectory, making it increasingly more cumbersome and unpredictable.

1.2.4.2. Fractal structure of the relaxation processes

Considerable attention has been recently drawn to studies of relaxation processes in non-crystalline condensed media. This is primarily due to the experimental fact that in numerous systems, the time-dependence of correlation functions $F(t)$ is governed by the Kohlrausch exponential law [7,26]:

$$F(t) = \exp(-t / \tau)^\beta, \quad 0 < \beta < 1 \quad (1.2.12)$$

Parameters β and τ depend on the material and may be the functions of external variables, e.g. temperature or pressure. The relation (1.2.12) describes a number of interesting processes in disordered systems, energy transfer in condensed molecular media, electron and hole transfer in disordered semiconductors, and diffusion in porous materials.

Consider the methods of simulating these objects by fractal structures taking into account both the spatial and time disorder. It should be noted that the time inhomogeneity being related to the random location of doping molecules in a matrix or with that of atoms in amorphous semiconductors, for example, results in the microscopic transition velocity range appearing to be quite wide: the spatial disorder causes the temporal and, sometimes, energy disorder. This complicated situation cannot be described analytically. One has to develop models like the fractals considered below.

Let us analyze the space and time correlations.

Self-similarity is the basic feature of the fractals, i.e. each separate object or ensemble of objects possesses invariance with respect to the group of scale transformations. Consider the excitation damping law for the chosen donor located at the origin of coordinates due to the direct energy transfer to the defects located at the sites R with the preset structure. The relaxation function, i.e. the possibility of the donor residing in the excited state within the time interval t , is:

$$F_i(t) = \exp(-t / W(R_i)), \quad (1.2.13)$$

where $W(R_i)$ is the relaxation rate that defines the relaxation time $\tau_i = 1 / W(R_i)$. For a fixed configuration of a number of defects located at the sites R_i , we have:

$$F_{\{R_i\}} = \prod_{i=1} \exp(-tW(R_i)). \quad (1.2.14)$$

Let us average (1.2.6) over all possible defect configurations. For the case when the defects are located randomly and the possibility of the given site to be occupied by the defect is exactly equal to p ; therefore, one may write:

$$F(t) = \prod_{i=1} (1 - p) + p \exp(-tW(R_i)) \quad (1.2.15)$$

that for $p \ll 1$ gives:

$$F(t) = \exp\{-p \sum (1 - \exp(-tW(R_i)))\}. \quad (1.2.16)$$

Taking into account that the site density is:

$$\rho(R) = \sum_i \delta(R - R_i)$$

we shall convert the sum into the integral [7]:

$$F(t) = \exp\{-p \int dR \rho(R) (1 - \exp(-t/W(R)))\}. \quad (1.2.17)$$

If $\rho(R) = \text{const}$ and the interaction is described by the relation

$$W(R) = aR^{-s_F}, \quad (s_F \geq 6 \text{ is the Forster constant}) \quad (1.2.18)$$

we obtain:

$$F(t) = \exp((-t/d)^{d/s_F}) \quad (1.2.19)$$

(d is the space dimensionality).

Non-exponential damping results from the parallel relaxation processes and from the existence of the distance hierarchy. To generalize this result to the case of the transfer along the fractal structure with the fractal dimensionality d , one has to substitute d_f for d [24].

1.3. Self-organizing systems: lifeless and living objects

Recently, much attention has been paid to the theoretical and experimental studies of self-organizing processes in various physical, chemical and biological systems [28-32]. The processes are non-equilibrium and accompanied by energy dissipation.

Many examples of the formation of ordered states during non-equilibrium processes are known in physics. In this case, the ordering may occur both in time (time-dependence, e.g., the appearance of limiting cycles in auto-oscillating systems) and space (standing strata in gas discharges, the Benar's cells at the convectional movement in liquids, the transition of the laminar flow to the turbulent one in the liquid) [5]. The formation of spatial-temporal ordered states (e.g., auto-wave processes in classic and quantum generators (lasers)) is also possible.

1.3.1. Non-equilibrium self-organizing processes in the systems of lifeless nature

The studies of self-organizing processes in condensed systems (i.e. liquids, crystals, glasses) and in biological objects, which receive energy from the external sources, are characterized by continuous energy dissipation and redistribution among active elements. When some of these elements are locally interlinked and form the distributed active medium, the production of various stationary or time-dependent spatial structures is observed in this medium. Fundamental notions such as consistency, mutual action, and ordering are the constituents of both physics and biology, i.e. the possibility to describe the behaviour of both living systems and common physical systems by using these notions is an outstanding achievement. For most cases, the properties of the whole system cannot be explained on the basis of the simple superposition of the properties of its components, since these subsystems interact with each other. In addition, the system acquires the properties which contrast qualitatively with those of separate subsystems. Such subsystems [3-5] may be atoms, molecules, and cells, as well as the human communities.

First of all, the self-organizing processes in physical systems should be considered. These processes in liquid (gaseous) layers at the presence of temperature inhomogeneities are known as the Benar's heat convection (Fig. 1.3.1). The heat convection provides the basis for various phenomena observed in nature. Among them are atmospheric and ocean circulations, which define the climate change for a short or long period. Another example is the drift of continents or, in other words, the motion of continental platforms caused by the large-scale cloak movements. Heat convection underlies the heat and matter transfer inside the Sun, which substantially defines the solar activity.

The heat convection is also related to the production of so-called Benar's cells [4,5] in the liquid layer between two parallel planes to which the temperature gradient ΔT is applied: $\Delta T = T_2 - T_1 > 0$.

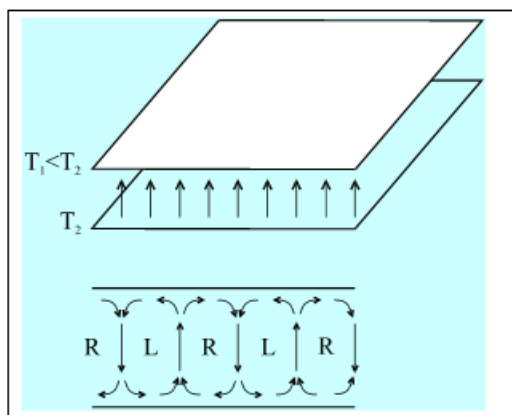


Fig. 1.3.1. Convective Benar's cells.

At low temperature gradients, ΔT , in the system, a single state is established for which the heat transfer from the lower layer of liquid to the upper one is specific and the latter transfers the heat to the environment providing the constant T_1 (Fig. 1.3.1). The temperature, as well as density and pressure, are not homogeneous, and due to the heat conduction, vary almost linearly from the warm domain (T_2) to the cold one (T_1). In this state, reached by the system in a form of a response to the external restriction, the stability dominates.

When the system deviates from equilibrium with the increase of ΔT , at a certain critical value, ΔT_c , the bulk of liquid starts to move. This motion will not be chaotic. The liquid is structured in the form of cells noticed first by Benar and, thus, called the Benar's cells (Fig. 1.3.1). These cells are placed along the horizontal axis, and the liquid moves sequentially clockwise (R) and counter-clockwise (L) inside them.

The qualitative explanation of this phenomenon is as follows. Due to thermal expansion, the liquid is stratified, and that part which is close to the bottom plane possesses a lower density compared to the upper layers. This causes the density gradient to be directed opposite to the gravity force direction. Evidently, such a configuration is unstable. Consider, for example, a small volume of liquid close to the bottom plane. Imagine now that this element of volume moves slightly upwards due to perturbation. Entering a colder (and, thus, denser) domain, the selected element is a subject of the upward Archimedean force, which tries to enhance the motion. On the other hand, if the drop which is first close to the upper plane moves downwards, it enters the low-density domain and the resulting force of Archimedean and gravity forces will accelerate the downward movement. Therefore, in this liquid layer, up- and downward fluxes may originate, resulting in the production of cells. The reason for such fluxes not being observed at low ΔT is related to the stabilizing effect of the viscous liquid, resulting in the initiation of internal friction forces directed against the movement. The heat conduction is also the stabilizing factor due to which the temperature difference between the displaced drop and its environment tries to escape. This, in particular, explains the occurrence of the symmetry violation and transition from the simple behaviour to the complex one. The notions of ordering and consistency of the system are the specific features of such transitions. When ΔT is less than the critical value ΔT_c , the homogeneity of the liquid makes its different parts independent of each other. In contrast to this, each volume element above the threshold value ΔT_c affects the state of the other element. Such pattern implies the presence of correlations, i.e. the statistical dependence of remote parts of the system. Specific dimensions of Benar's cells are within the millimetre region (10^{-1} cm), whereas the specific spatial scale of intermolecular forces lies within the Ångstrom region (10^{-8} cm), i.e. the Benar's cell involves almost 10^{21} molecules. The fact that such a considerable amount of particles

may demonstrate coherent behaviour, in spite of the random thermal motion of each part, is one of the principal properties, which characterizes the occurrence of the self-consistent behaviour.

A specific feature related to Benard's cells is that this laboratory experiment is characterized by the reproducibility, i.e. at $\Delta T = \Delta T_c$ the convective pattern arises. On the other hand, the liquid is structured into the clockwise and counter-clockwise-rotation cells, which are the random quantities. Thus, aside from the determinability of the occurrence of the cell structure, the direction of motion in the cells is not predictable and uncontrollable. Only in the case of one or other perturbation, which dominates at the given moment, defines the motion of the liquid in the cell. Thus, a peculiar combination of the accident and definiteness is seen. This analogue dualism known in biology as a manifestation of fluctuations and natural selection is revealed in physics in the quantum-mechanical approach to the description of microscopic phenomena.

In conclusion, in the case of remoteness from equilibrium, the system can adapt itself to external restrictions in the environment in different ways. From the mathematical viewpoint, in this situation, at the same values of parameters, one can obtain several different solutions. Only the chance defines which one of them will be obtained. The fact that one variant has been chosen among numerous possible variants provides a system with the historical dimensionality, i.e. a specific memory about the former events, which have happened at the critical moment and defined the influence on evolution.

At large $\Delta T = \Delta T_c$, the most suitable for the heat transfer convection regime is established in the liquid (at ΔT_c the immobile heat-conducting liquid regime becomes unstable). The convection cells form a more highly-organized structure, which results from the collective motion in the liquid.

Similar self-organizing processes are also specific for the occurrence of a coherent emission [30]. In this case the transition of atoms to the excited state is induced by an external influence. These atoms act as a microscopic antenna (Fig.1.3.2). At low pumping powers $P < P_c$ (P_c is the critical power value), atoms generate light packets independently of each other, and the laser is operating similarly to a common lamp (the radiation field $E(t)$ consists of separate uncorrelated packages). At $P > P_c$ powers, all of the atomic antennas start to oscillate in phase and generate one giant packet of coherent laser emissions. Let the dependence of the emission intensity on the pumping power be the same. The generation mode corresponds to the hypercritical cell production. The light field in a laser is generated by excited atoms. Furthermore, the field exerts an opposite effect upon the atoms; the stimulated emission arises, being interfered with two factors: a permanent dissipation and fluctuations which perturb the emission process by their random action. For these reasons, the stimulated emission field in the subcritical regime is damped out. Above a certain pumping power value, the amplitude begins to rise. As a rule, the dampening dies away for one mode, the amplitude of which acts as an order parameter.

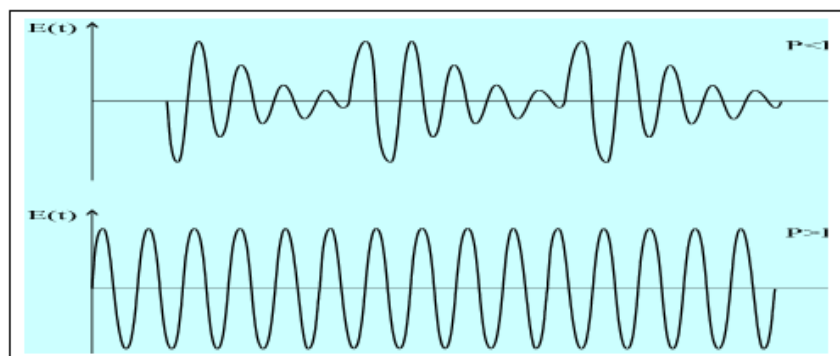


Fig. 1.3.2. Coherent emission initiation in lasers.

Consider another example of self-organizing processes, i.e. a periodically excited pendulum. The equation of motion of the pendulum is written as [5]:

$$\frac{d^2\theta}{dt^2} + \gamma \frac{d\theta}{dt} + g \sin(\theta) = F_0 \cos(\omega_0 t),$$

where θ is a deviation angle, g is the gravitational acceleration, γ is a damping constant, ω_0 is the frequency of the external force with F_0 amplitude (the mass is taken equal to unit).

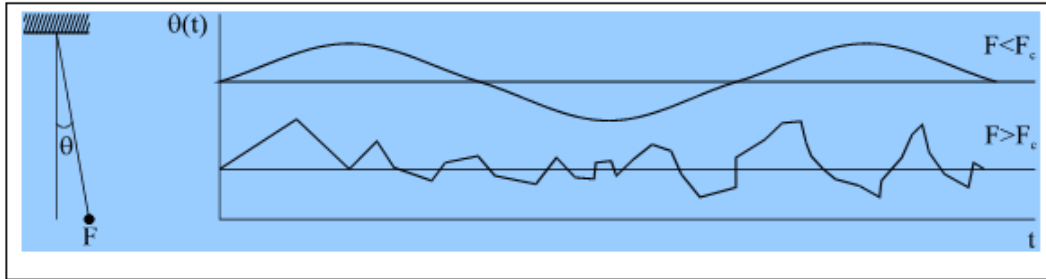


Fig. 1.3.3. A pendulum with the external force F applied.

A numerical solution of the equation is shown in Fig. 1.3.3. The time dependence of angle $\theta(t)$ becomes chaotic if the amplitude F of the force exceeds the threshold value F_c .

The next experimental physicochemical system, in which the formation of spatial and temporal structures has been studied in detail, is the Belousov-Zhabotinsky reaction [4,5,18]. The organic molecules (e.g. the malonic acid molecules) are oxidized by bromate ions during the catalysis of the oxidation-reduction system (Ce^{4+}, Ce^{3+}). The reagents are $Cl_2(SO_4)_3$, $NaBrO_3$, $CH_2(COOH)_2$, H_2SO_4 being involved in 18 elementary reactions [5].

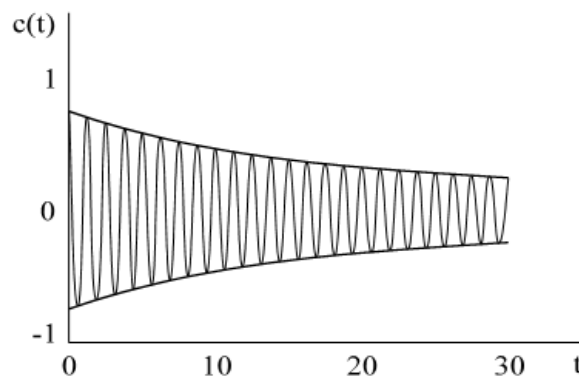


Fig. 1.3.4. Belousov-Zhabotinsky reaction.

The generalized equations for the reagent concentration $\{C_i\}$ in the system of chemical reactions have a form of system of non-linear 1st-order differential equations:

$$\frac{dF(X, \lambda)}{dX} = F(X, \lambda)$$

where $X = (C_1, C_2, \dots, C_k)$, $F(X, \lambda)$ is a non-linear function $\{C_i\}$, and λ is an external control parameter. The variable which possesses a chaotic behaviour in the Belousov-Zhabotinsky reaction, is the Ce^{4+} ion concentration C , measured by the selective light absorption by these ions. The average time spent by the substance in the flowing reactor (Fig. 1.3.4) is an external control parameter.

1.3.2. Self-organizing processes in bio-matters

Among all of the natural objects, biological ones are functionally and morphologically the most complex and highly organized. During the protracted period of biological evolution, functioning away from the equilibrium state, they permanently receive the energy and matter flux, and preserve the memory of the forms and functions attained within this period [33-45].

The important balance is reached between short- and long-range effects, controlled by the energetic situation. The system always tries to realize the lowest available energy (which is the cluster (in microscopic range) with a five-fold symmetry). On the macroscopic scale, it is the ordered occupation of space, which eliminates the five-fold symmetries and therefore contradicts the microscopic requirements. This delicate balance leads to dynamic vibrations, which can be easily frozen by one of the forces dominating in the system. A protein, with its saturated-desaturated states in the living process (balancing between the low-energy state at the microscopic level, which is the saturated molecule, and the low energy state required by the metabolism, which is a non-saturated state), also shows this basic dynamic construction and builds a system called life. Self-organizing builds up this dynamic equilibrium in all of the organizing levels from water-transfer through proteins and up to the organism as well. The dynamic vibration is effective for the whole living organism. It has an effect on every level of organization of the system: starting from the protein building up the total unity.

Accordingly, the system creates a balance between nutrients and end-products that breakdown the energy stored in the chemical bonds of nutrients and creates the end-products, in which the chemically stored energy is low. At the same time, certain biological systems (plants) are capable of executing this process in reverse, for which they receive their energy from the solar energy and electromagnetic radiation (This process is a fundamental conversion, which makes the nutrients available to other life processes which are not capable of such conversion).

The cell is the traditional object of biophysical research. Cellular biophysics processes as well as the processes of energy and information exchange typical of biological systems are also inherent in cells. The substantial inhomogeneities are also observed at the cellular level [31].

A knowledge of the principal regularities of the formation of structures in the media open with respect to the energy and mass exchange allows one to turn to the purposive creation of distributed dynamic systems, which form one or another spatial structures. One of the principal applications in this case are the problems of digital processing of information. The use of spatial structures, not discrete signals, as the elementary unit of information processing, allows the computer efficiency in the artificial intellect tasks to be increased drastically. There is some evidence that similar mechanisms underlie functioning of the human brain [36-40,45].

As already known, the brain is a giant network of tens of billions nervous cells (neurons) bound by the branches (dendrites and axons). The number of bindings of a single neuron may reach tens of thousands. The mechanism of action of a separate neuron is responsible for the fact that the nervous cell may be in one of three discrete states – rest, excited and refractive (the latter corresponds to the unexcited state). The interstate transitions are controlled both by intracellular processes and electric signals coming from the other neurons through the branches. The change from the resting state to the excited one occurs in a threshold manner at the almost simultaneous reception of a great number of pulsed excitation signals. The neuron spends a certain amount of time in the excited state and then transitions independently to the refractive state. This state features quite a high excitation threshold: the neuron almost fails to respond to the excitation signals received. After a period of time, the excitation ability is restored, and the neuron relaxes to the rest state.

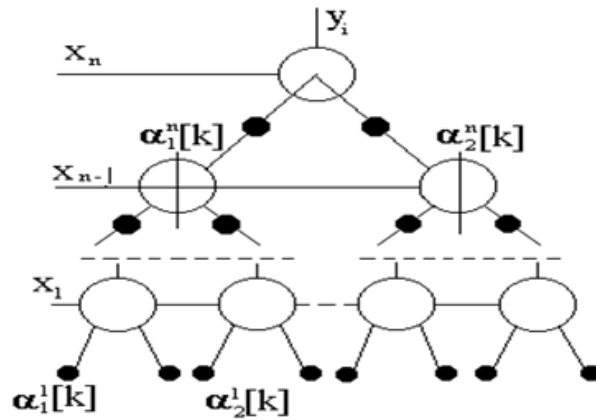


Fig. 1.3.5. Structure of a neuron network ($\alpha_s^i[k]$. Is an exit the s -th neuron at the i -th level in discrete time k , x_i and y_i are the state parameters network).

During the excitation, the excitation pulse is generated in the output branch (axon) and propagates along it at the 1–100 m/s speed [27, 45]. A change in the axon membrane local conduction with respect to sodium or potassium ions forms the basis of the propagation process, i.e. the essential inhomogeneities are observed at the cellular level. The potassium ion concentration inside the nervous cells (neurons) is considerably higher than that outside of cells, whereas the opposite situation takes place for sodium ions. These differences, which imply the strong non-equilibrium of the state, form the basis for nervous excitation propagation-type processes, which play an essential role in the life. Such non-equilibrium is sustained by the active transport operation and bioenergetic reactions (such as glycolysis and breathing). No direct electric contact occurs between neurons. The heat is transferred from the axon to the input branch (dendrite) of the other neuron within a special domain (synapse), where the endings of two nervous cells lie close to each other. Some of the synapses are peculiar. Under the influence of excitation signals, they form the inhibition pulse of the opposite electrical polarity in the dendrite. At the simultaneous arrival to the neuron, these pulses can damp the excitation signals (Fig. 1.3.5).

Thus, common physical and chemical systems may possess a complex behaviour with a series of peculiarities belonging to the living systems. A question arises naturally: whether one is able to explain some of these peculiarities by the transitions induced by non-equilibrium and relevant instability mechanisms (say, chemical autocatalysis).

Besides the structure of a separate nervous cell, the global aspects of brain activity, i.e. the specialization of its large areas and functional communications between these areas are also studied relatively well. At the same time, little is known about the method of information processing at the intermediate level inside the neuron network areas, involving only tens of thousands of nervous cells. The brain is quite frequently compared with a computer. In addition, it is assumed that each excitation pulse carries the unit information, while neurons play a role of logical switches completely similar to the computer elements. However, in our opinion, the brain functioning is based on other principles completely. There is no rigid communication structure between the neurons in the brain similar to that in a computer. The reliability of separate brain elements (neurons) is considerably worse than that of the modern computer units. The damage of even those areas, which comprise quite a large amount of neurons, does not occasionally affect the efficiency of information processing in this area of a human brain. Part of the neurons dies during aging of the organism.

The computer network resembles the multicellular organism. After the program, i.e. the repertoire of reactions of each computer and the initial status of all of them, is indicated, the network starts to live its own life and simulates the corresponding process. From that viewpoint, one can assume that the brain stores and processes the information in images. It operates as a computer, in which the surrounding world is mapped in the spatial-temporal structures of neuron activities. An evocative simulation allows the future events and schedules of actions to be

predicted. Such a mechanism of the brain operation was probably developed during the course of biological evolution. In animals, the basic function of the nervous system is to transform the senses prompted by the environment into a certain motional activity [32].

A viewpoint that the human brain operation is based on the learning principles seems to have recently received much recognition. Consider, for instance, the possible sequence of steps expected to be performed for solving the problem of how to distinguish the triangle among all other polygons. The first step is to distinguish the lines and check whether their quite large areas are close to the straight-line sections. Then, one has to choose vertices, i.e. the points where two lines cross. The next step is to create the intermediate concise image of a pattern – its graph. This graph fixes only the existence of relations between the vertices independently of lengths and orientation of the lines, which realize these relations. Now, when each graph corresponds to the whole class, one has to recognize graphs, thus giving the final answer for the problem stated. Therefore, the possibility to solve this simple task requires the creation of semantic structures – graphs. Each graph, in turn, may also be considered a certain notion (e.g., a triangle graph) and act as the elements involved in the semantic structure of the next hierarchic level. All of the necessary operations with semantic structures are executed in the brain in the analogue way, similarly to certain dynamic processes in the complex distributed non-linear system. The brain is like the medium where semantic structures evolve, interact and compete with each other.

The process of development of living organism does not require the interference of external controlling forces, and there is a sequence of independent acts of self-organization. Handling of this process can be carried out with the help of inappreciable effects of controlling parameters. They influence the choice of path of development at the moments when the developing structure is able to bifurcate in the presence of several possible paths of evolution.

With the help of synergetics, various aspects of human medicine in particular are being researched [45]. In the normal operation of almost all systems of vital activity, the intermediate mode between chaos and order (the so-called determined chaos) is characteristic. Thus, for the processes of respiration, palpitation and mental equilibrium, the particular measure of the chaos necessary for maintaining the health of a human is peculiar. For example, the extreme modes of heart rate (arrhythmia and excessively ordered rhythms) are dangerous and testify to illness; a fragile heart is not able to react to varying external conditions. Health defines a particular balance between chaos and order. The concept of dynamic illness in the recognition and treatment of disease, and also as a warning of illness, will be utilized. The stabilization of vital activity is reached through instability, and the stationary values of change. The questions are how much chaos can a human bear without becoming ill, when are random oscillations normal, and when are they dangerous? These problems are considered with the help of synergetics and are studied in this book.

2.1. Metastability, bistability, self-organization

Materials with compositionally, topologically and/or morphologically metastable states are important in both pure and applied physics. In the past three decades, these states have played a central role among new materials which have been produced. Many of the early stimuli to activity, directed towards the synthesis, study and exploitation of novel metastable structures, especially in metallurgy, can be demonstrated by some metal alloys being quenched to the amorphous phase. During the quenching process, the system is "frozen" ("configurationally frozen") into one of the thermodynamically intermediate states between the initial and final equilibrium. Upon annealing, these phases often evolve into other interesting and useful metastable states. The question of the stability of metastable states is still at the stage of rapid development. Not only are solid and highly-technological materials metastable, but all of the open dissipative systems (i.e. the systems ready to be self-organized) are also metastable. Their stable reference-state would be isolated and thermodynamically closed.

2.1.1. Metastability and bistability

Metastability pertains to the energy state located above the stable (equilibrium) state and isolated from it by an energy barrier, which is characterized by the activation energy (Fig. 2.1.1). Most chemical reactions in bio-system-metabolism follow the metastable potential. This allows the reactions to be performed in small steps, which do not liberate too much energy in one reaction. The small-step chemical reaction-chain procedure controls the stable conditions of bio-reactions and the production of non-pulsed energy.

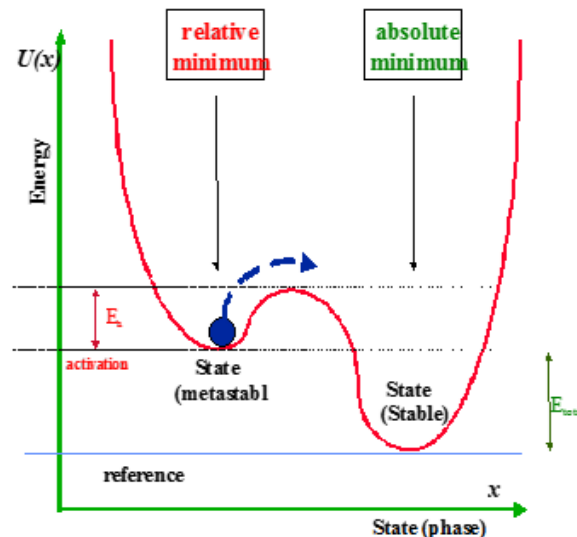


Fig. 2.1.1. Energy scheme of metastability.

The stability questions for metastable states concentrate on the height and origin of isolating barriers in most cases. The most important factors creating this barrier from the material-science point of view were developed for metal physics. There are three relevant factors:

- ◆ Chemical factors, (Hume-Rothery [1], Pauling [2], Pearson [3], etc.): chemical bonds, electrochemical differences, electronegativity differences, etc.
- ◆ Geometric factors, (Hume-Rothery [4], Laves [5], Frank and Kasper [6], etc.): size factors, tendency of proper (translational) space-filling, etc.

- ◆ Electronic factors, (Hume-Rothery [4], Jones [7], Mott [8], etc.): electronic band effects, collective quantum-effects, etc.

All of these factors are connected with electronic bonds and bands, and are different manifestations of the electronic properties of solids. We will show later that these conditions are important in every open system, even in living matter. The factors listed are not equal: no chemical and geometric effects are understandable without the essential electronic effects. Electronic states are a priori responsible for metallic and other types of bonds in any material structure based only on the electromagnetic interactions (the systems are considered, in which among the four basic interactions only the electromagnetic interaction is active). A special bistable potential arrangement (the double-well potential, Fig. 2.1.2) is responsible for bifurcation processes. In the energetic case, the particle has the same probability of exposing one of the possible states. At a definite energy, the equal probability is broken (the symmetry is broken) and the particle seeks one of the minima at a further decrease of energy. In many practical cases, the final state has an extreme probability (like with the tossing of a coin: one state has a probability of 1 and the other 0 at the end). However, these are interesting cases; when the final stable state is not extreme, and the two (or more) states are not frozen, their occupation has a probability less than 1. These states dynamically share the final state in a definite position. The only point is that no state exists between the final ones; however, a definite split of the states exists (like the spin-states).

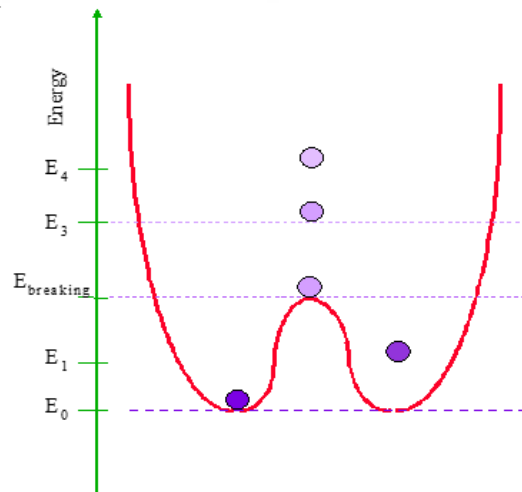


Fig. 2.1.2. Energy scheme of bistability.

2.1.2. Bifurcation processes

The best example of the everyday games is coin tossing (heads or tails), or the hill-valley situation with a ball. In both cases, the probability of either side (valleys) being seen is equal (Fig. 2.1.3). When the coin is being tossed (we can say that it is energetic or, in other words, “hot”), both of the final states are equally possible. The identical probability of a tail and head decreases when the coin collides with something and loses its energy. One side will be more probable than the other. This means that circumstances determine the probability. As a result, there is a 100% probability for one side of the coin and zero for the other. The symmetry of chances changes in this way with the energy states; there is a tendency for one state over the other (Note, this decision is an intrinsic behaviour of the actual conditions, property of the “matter”). In principle, the states of probability, like tossing coins, can be described with a double-well potential, with the same probability for these two states. The barrier between them (like a hill between two valleys at sides) isolates the states and determines the definite states of occupation. If the state has a higher energy than the isolating barrier, the probability of occupation of the states will be the same. This can be formulated in such a way that when the energy is equal to the barrier height (the change of

probability: symmetry-breaking point), the system bifurcates: the system is “frustrated”, unable to “choose” a definite state. This frustration mechanism is the essence of tossing a coin as well.

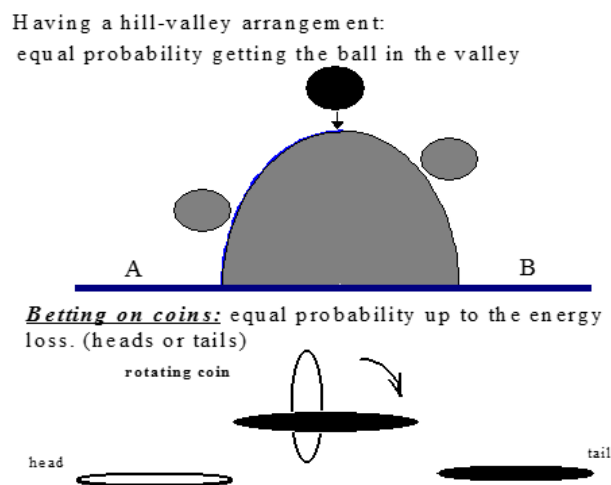


Fig. 2.1.3. Two simple practical bistabilities.

A multi-valley potential arrangement is also possible. To model the equal multiple possibilities, roulette in a casino is the best example (Fig. 2.1.4). Every possible position is equal for betting (multi-furcation) if the ball is energetic. During the gradual loss of ball-energy, symmetry breaking occurs and one of the states is exposed. It is trivial to derive the non-equal multi-well potentials (multiple metastabilities) from the equal one.

Roulette betting in the CASINO has 37 minima,
which are equal. The running ball equally canchoose!

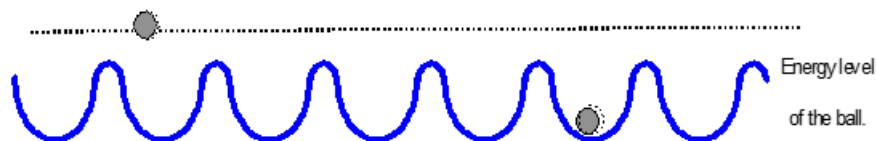


Fig. 2.1.4. Multi-choice of potential arrangement.

By rearranging the wells, a metastable cascade (like a small-step bio-reaction), can be constructed (Fig. 2.1.5). To reach the next well with lower energy, it is necessary to surmount the barrier.

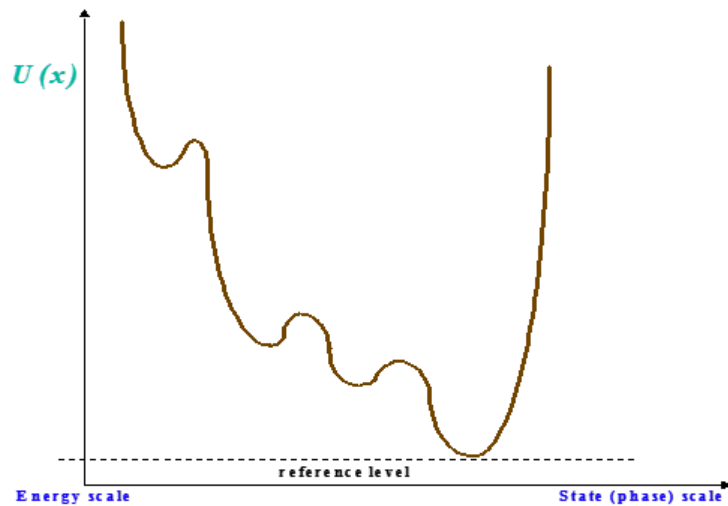


Fig. 2.1.5. Draft of the serial of bio-reactions: “small-step procedure”.

2.1.3. Dynamic description

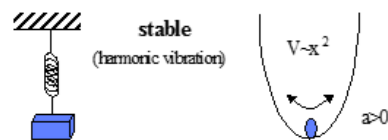
In dynamic approaches, the potential of the non-linear force law can form a typical double-well potential, causing bifurcation in that pair-interaction (Fig. 2.1.6; F is the force, V is the potential, and x is the distance, with a and b denoting constant parameters). The linear force law and its consequent quadratic potential

$$F = -ax, \quad V = \frac{a}{2}x^2 \quad (2.1.1)$$

are most trivial in the case of an elastic spring. It can be realistic to model the actual interactions in case of the proper elasticity (excluding all the dissipative processes). If the force ($F(x)$) has non-linear terms,

Linear approach

$$F = -ax \quad V = \frac{a}{2}x^2 \geq 0$$



Non-linear approach

$$F = -ax - bx^3 \quad V = \frac{a}{2}x^2 + \frac{b}{4}x^4$$

(HFröhlich)

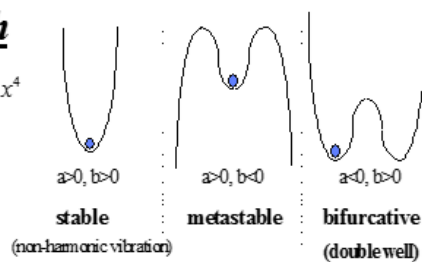


Fig. 2.1.6. Construction of the bistable potential by non-linear force law.

$$F = -ax - bx^3, \quad V = \frac{a}{2}x^2 + \frac{b}{4}x^4 \quad (2.1.2)$$

the system can be anharmonic (Fig. 2.1.7). If the force has only terms with odd exponents, however, the potential becomes symmetrical, and the situation is typically bifurcative. If the force has even terms as well,

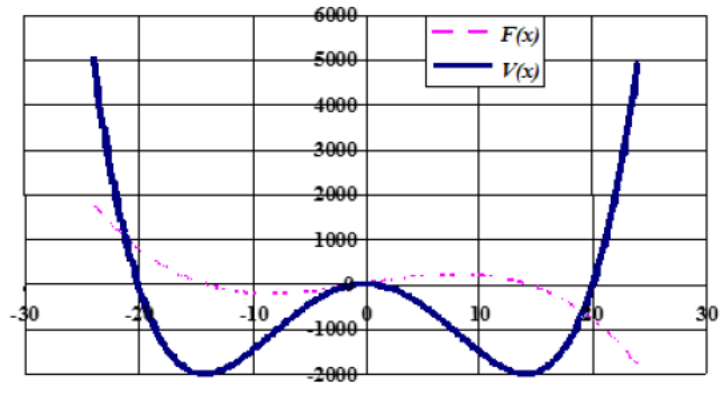


Fig. 2.1.7. Numerically calculated anharmonic force $F(x)$ and potential $V(x)$.

$$V = \frac{a}{2}x^2 + \frac{b}{4}x^4, \quad a=40, b=0.2.$$

$$F = -ax - cx^2 - bx^3, \quad V = \frac{a}{2}x^2 + \frac{c}{3}x^3 + \frac{b}{4}x^4 \quad (2.1.3)$$

the potential will not be symmetrical, and one of the minima will be dominant (global) (Fig. 2.1.8).

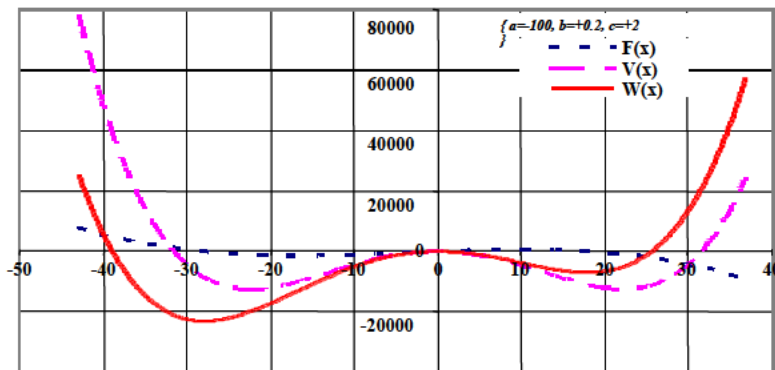


Fig. 2.1.8. Numerically calculated asymmetric non-linear force $F(x)$ and potential $W(x)$ (comparison with the symmetric one $V(x)$).

$$F = -ax - cx^2 - bx^3 \quad W = \frac{a}{2}x^2 + \frac{c}{3}x^3 + \frac{b}{4}x^4 \quad (a = -100, b = +0.2, c = +2)$$

Physically, the bifurcative situation comes from the sum of a repulsive (with the same direction as that of the movement) linear force and an attractive (opposite to the movement direction) non-linear force (with an odd exponent). The origin of the potential asymmetry is also an attractive term with even exponents.

The non-linearity is one of the most common behaviours in all self-organizing systems. A small modification (“ b ” is one order of magnitude smaller than “ a ”) can be efficient enough.

The actual geometric arrangement can determine the shape of the potential wells. During dynamic processes, the potential well can also change.

2.1.4. Example of mechanical self-organization

A mechanical self-organizing procedure can be delighted with a simple process: let us have a bowl of cherries in the disordered structure. If we shake the bowl, the cherries will be ordered in a self-arrangement manner (Fig. 2.1.9).

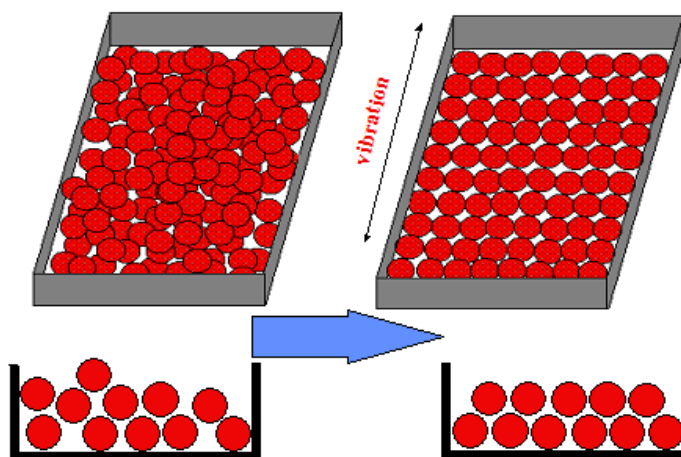


Fig. 2.1.9. Long-range ordering by vibration effects.

The individual cherries take the opportunity to occupy more stable sites; their partial (local) energy minimum changes to the global one (Fig. 2.1.10). This procedure drastically changes the actual potential curve (Fig. 2.1.11.), and the actual geometric arrangement determines the shape of the potential well to optimize the long-range order in the system². Here the dynamic parameters of the particles also play a role [9].

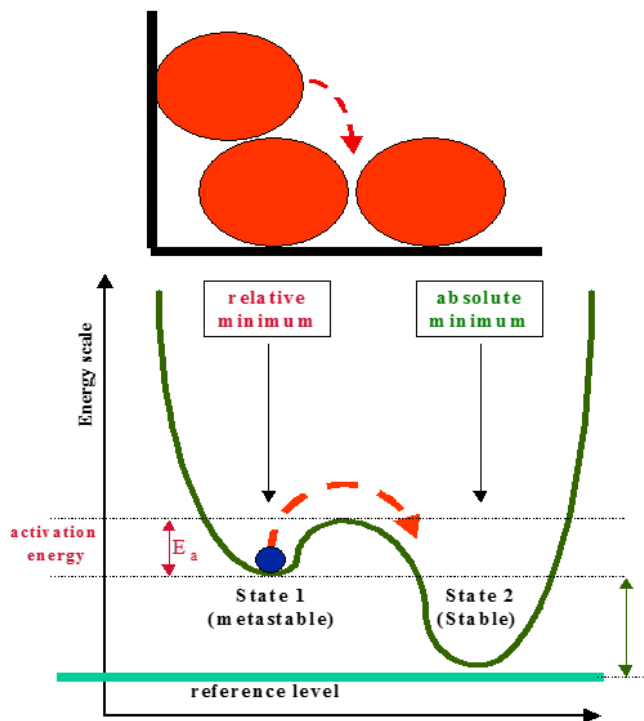


Fig. 2.1.10. Search for a global stability by mechanical vibration.

² This procedure changes the symmetries in micro- and macro-environments of the system. Consequently, it is a classical phase transition (both the entropy and volume of the system suddenly change) induced by an outside mechanical vibration. Hence, this procedure is a simple example of noise-induced phase transitions as well.

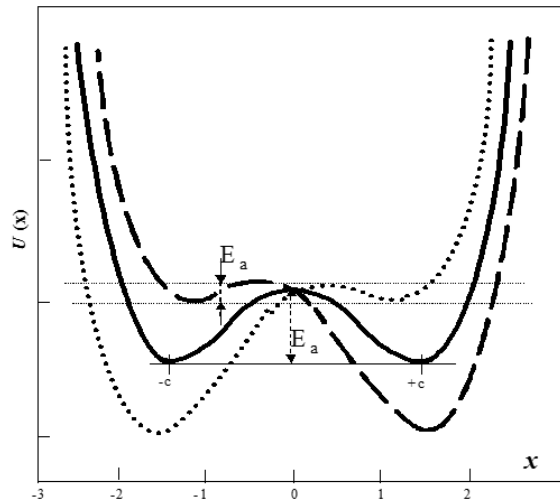


Fig. 2.1.11. Change in the shape of the potential wells during the mechanical vibration.

More generally, an interesting self-organizing mechanism can be followed by the properties of the granular materials (powder, sand, etc.) [10]. The vibration-induced arrangement in granular materials is a subject of scientific studies [11]. Even a simple mechanism like the shaping of a sand-pile occurs in a self-organized way [12], [13]. Grains fall randomly onto a pile growing vertically and reorganizing itself by the lateral motion of specific branches of grains (avalanches).

One of the easiest and most widely used methods of following the microscopic procedure is molecular dynamics (MD). This calculation can characterize the physical parameters of the system [14], [15]. The MD computer simulation involves a numerical integration of the classical Newton's equations of motion, enabling the particles in a given ensemble to reach the best (most available stable) positions. The particles generally interact with each other through different pair-potentials. The number of considered particles is determined by computer capacity only.

Molecular dynamics is also a perfect tool with which to calculate the radial pair-correlation function [16]. Its temperature-dependence is a good sign of the rearrangement induced by thermal energies. We can follow the rearrangement of different kinds of particles by the partial-pair-correlation function [16]. We can also determine the contacts of metalloids in a special amorphous alloy [17]. The MD calculation makes it possible to follow the dynamics of changes, even of a treatment with rapid and slow cooling modes [18].

2.1.5. Example of thermodynamic self-organization

Here, we start to study a refrigeration procedure in an initially homogeneous system. The grains of the actual precipitate grow over time.

Consider the grain (product-island)-volume $V_{\text{grain}}(t_0, t)$ relation of a time-dependent isotropic reaction, which was started at time t_0 , and with $S(\xi)$ being the isotropic reaction velocity by the actual running time ξ :

$$V_{\text{grain}}(t_0, t) = \frac{4\pi}{3} \left| \int_{t_0}^t S(\xi) d\xi \right|^3 \quad (2.1.4)$$

If the number of nuclei (grains) is N_{grain} , then the entire product volume is:

$$V_{\text{product}}(0, t) = N_{\text{grain}}(t) V_{\text{grain}}(0, t)$$

the total volume (connecting the intact, not changed phase) is:

$$V_{\text{total}} = V_{\text{product}}(0, t) + V_{\text{intact}}(0, t) \quad (2.1.5)$$

If we assume a dilute situation $[V_{\text{product}}(0, t) \ll V_{\text{intact}}(0, t)]$, during the process of evolution, the grain number and grain size grow as follows:

$$V_{product}(t) = V_{total} \left\{ N_{grain}(t) V_{grain}(0, t) + \int_0^t K_{grain}(\tau) V_{grain}(\tau, t) d\tau \right\} \quad (2.1.6)$$

where $K_{grain}(t)$ is the reaction rate from newly born grains.

A problem arises when the reaction develops. The product volume ($V_{product}$) becomes high enough for the interaction and/or overlapping of the product-islands (grains), so the mixture of initial and final products is no longer dilute. To avoid double-counting, Johnson, Mehl [199], Avrami [200] and Kolmogorov [21] introduced the so-called “extended volume” formalism. This extends the volume on the size, which is considered to be dilute, so that the complication can be eliminated. This calculates a larger volume for the product:

$$dV_{product} = \left(1 - \frac{V_{product}}{V_{total}} \right) dV_{extended}$$

hence:

$$V_{extended} = -V_{total} \ln \left(1 - \frac{V_{product}}{V_{total}} \right) \quad (2.1.7)$$

Introducing the product concentration $C(t)$:

$$C(t) = \frac{V_{product}(0, t)}{V_{total}} \quad (2.1.8)$$

we get:

$$-\ln(1-C(t)) = \frac{4\pi}{3} \left\{ N_{grain}(0) \int_0^t S(\xi) d\xi \Big|_0^3 + \int_0^t K_{grain}(\tau) \int_0^t S(\xi) d\xi \Big|_0^3 d\tau \right\} \quad (2.1.9)$$

In the isotherm case, when K is time-independent $\{K_{grain}(t) = K_{grain}\}$, we have:

$$-\ln(1-C(t)) = (kt)^n \quad (2.1.10)$$

so, the non-reacting specific volume vanishes exponentially with the time:

$$\left(\frac{V_{int\ act}}{V_{total}} \right) = 1 - C(t) = \exp(-(kt)^n) \quad (2.1.11)$$

It could be derived in the other way as well, where the V_{intact} changes proportionally by its value:

$$dV_{int\ act} = -kV_{int\ act} \quad \text{than} \quad \ln \left(\frac{V_{int\ act}}{V_{total}} \right) = -kt \quad \text{so} \quad \frac{V_{int\ act}}{V_{total}} = \exp(-kt) \quad (2.1.12)$$

which corresponds to the $\nu=1$ case. If the change in volume is specially polynomial time-dependent, then:

$$dV_{int\ act} = -V_{int\ act} (kt)^{n-1} \quad (2.1.13)$$

and so:

$$\ln \left(\frac{V_{int\ act}}{V_{total}} \right) = -(kt)^n \quad \Rightarrow \quad \left(\frac{V_{int\ act}}{V_{total}} \right) = \exp(-(kt)^n) \quad (2.1.14)$$

The n -exponent is typical for the reaction mechanisms of the processes and:

$$n = \frac{\ln\left(-\ln\left(\frac{V_{intact}}{V_{total}}\right)\right)}{\ln(kt)} \quad (2.1.15)$$

which shows an intrinsic similarity of the reactions, if their “n” exponent is identical.

These exponents are observable in different reactions, as shown in Table 2.1.1 (for solids [22] and for bio-matter [23]).

Solids		Bio-matter	
process	exponent	process	exponent
Beginning of	v=3	Growth of bacteria	v= 4
Nucleation with constant	v=4	K+ conductance decay in a nerve	v= 1.9
Nucleation with growing	v >4	K+ leakage from a poisoned muscle	v=1.7
Starting nucleation and surface	v=2	Growth (weight) of a rat	v=2.0
Diffusional growth from	v=1.5	Growth (length) of a salamander	v=2.3
Diffusional growth from growing	v=2.5	Growth (height) of a sunflower	v=1.9
Diffusional growth in 1 or 2	v=1	Synthesis of chlorophyll in maize	v=2.2
Limited different growth in 1 or 2 dimensions	v=1.5	Muscle tension during contraction	v=1.21
		Myosin splitting of ATP	v=1.24
		Fresh green leaf IR phosphorescence	v=1.0
		Dried green leaf IR phosphorescence	v=1.28
		Melanin IR phosphorescence decay	v= 1.08
		Cytochrome IR phosphorescence	v=1.16

Table 2.1.1. Comparison of Avrami exponents from solid- and bio-reactions.

The calculated Avrami function is the so-called Sigmoid type, which is typical for thermodynamic self-organisation (Fig. 2.1.12).

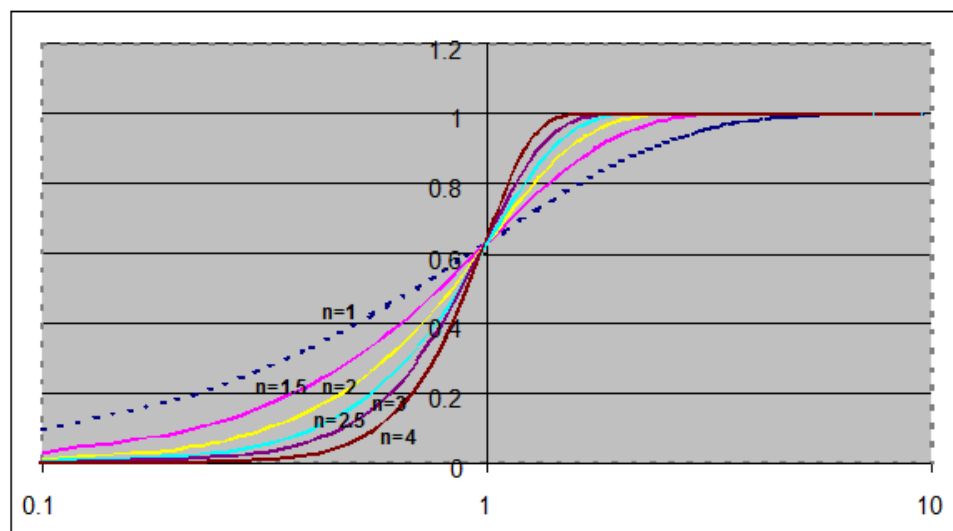


Fig. 2.1.12. Some Avrami functions by various exponents ,n’.

There are other sigmoid type functions, such as the exponential:

$$c * \exp(-d * \exp(-et))$$

Also, there is the Fermi-distribution-like:

$$1 - \frac{k}{1 + \exp(-at)}$$

Other types of sigmoid functions are shown in Fig. 2.1.13.

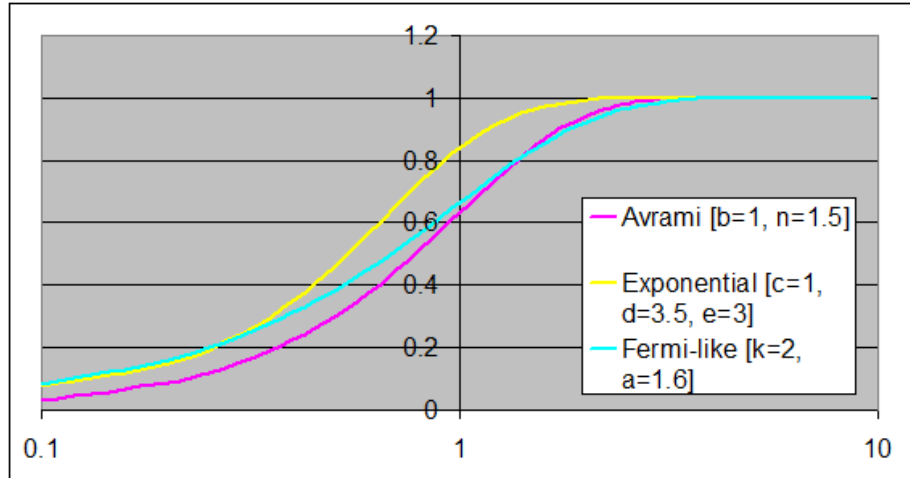


Fig. 2.1.13. Different Sigmoid curves.

These functions are close to each other; they can be identical within 3.5% at a special set of parameters (Fig. 2.1.14).

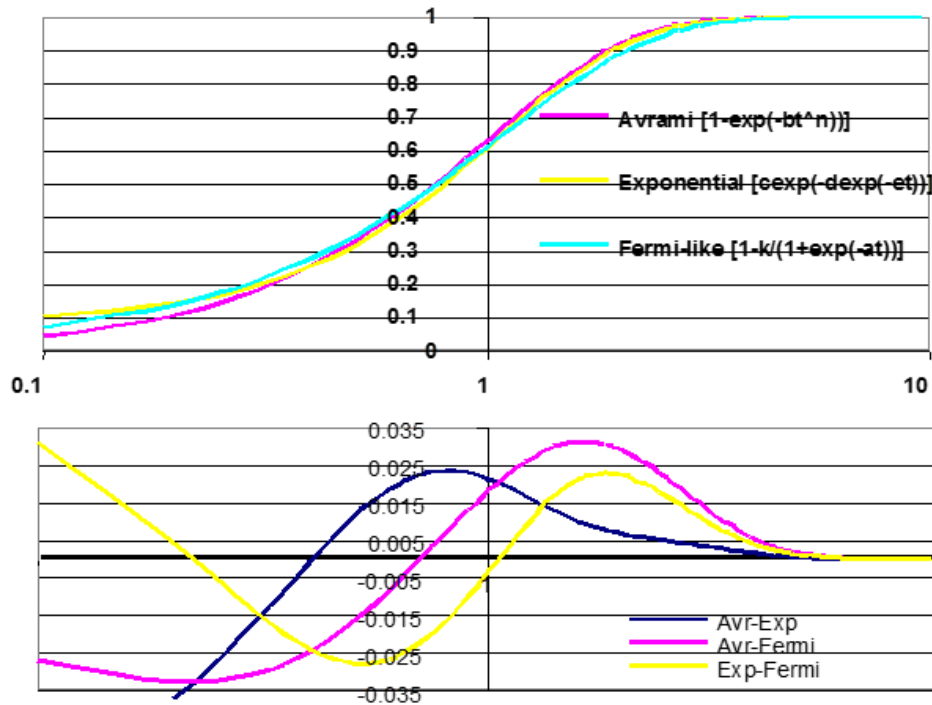


Fig. 2.1.14. A special set of parameters allows the curves to be identical within 3.5%.

2.2. Order characterization

According to the basic thermodynamic equation:

$$dE = TdS - pdV + \sum_k \mu_k dN_k + \sum_i Y_i dX_i \quad (2.2.1)$$

where E , T , S , p , V , μ_k , N_k are the widely accepted notations for energy, temperature, entropy, pressure, volume, chemical potential of the k -th component and a particle number of the k -th component, respectively. X_i and Y_i are the general extensives and intensives belonging to the i -th interaction, respectively. Any interaction that can give an energetic term creates an $X - Y$ pair. For example³, in the mechanical interactions:

$$\{Y_i dX_i\} \Rightarrow (\vec{F} \cdot d\vec{x}) \quad (\text{force and displacement}),$$

$$\{Y_i dX_i\} \Rightarrow (\vec{\sigma} \cdot d\vec{A}) \quad (\text{surface tension and surface size}),$$

whereas in electromagnetic interactions:

$$\{Y_i dX_i\} \Rightarrow (\vec{E} \cdot d\vec{P}) \quad (\text{electric field and polarization}),$$

$$\{Y_i dX_i\} \Rightarrow (\vec{H} \cdot d\vec{M}) \quad (\text{magnetic field and magnetization}),$$

etc. The driving force of the ordering is basically the entropy.

Contrary to a very simple notation of the entropy in the basic thermodynamic equation (Eq. 2.2.1), its change can be complex. From the geometric point of view, the configurational entropy and the collectivisation entropy are important. Both kinds of entropy-terms are connected with the actual geometric arrangement of the involved particles:

The **configurational entropy** characterizes the ordering procedure, derived from the configurational specific heat. This heat term describes the heat-exchange of the system during the geometric rearrangement.

The **collectivization entropy** characterizes particle interactions, and their energy contribution. If the system has no interaction potentials (ideal gas), then the "collectivization" is observed only by the collective modes (like waves) in the system. These entropy-parts are well connected, so their pure discussion is impossible.

2.2.1. Order parameters

The structure characterization by entropy is connected to the co-operative phenomena in the arrangement. To describe a system, we introduce the short-range order (SRO) and long-range-order (LRO) parameters, σ and s , respectively. To establish these parameters, we have to study the first co-ordination sphere connections. By definition [24], σ is defined as the difference between the number of pairs of different atoms and the number of pairs of identical ones divided by the total number of pairs. In case of N particles with the average co-ordination number Z , the number of pairs is $(Z/2)N$. Let us model a binary system with A and B particles on the α and β positions. The system is regarded as ordered if every A and B particle occupies its own α and β position, respectively. If only a p -portion of A atoms is in the ordered position, then α -positions occupied by A-particles and β -positions occupied by A-particles are $(1/2)Np$ and $(1/2)N(1-p)$, respectively. Hence the $p=1/2$ and $p=1$ correspond to the complete disorder and complete order, respectively. Consequently, the LRO is characterized by p . For practical purposes, Bethe introduced the s parameter for LRO which ranges from 0 to 1: $s = 2p-1$. Actually, we denote the A(α)-A(β) pairs by $(Z/2)N\xi$, then we have [25] for the SRO:

³ In this case their product is scalar.

$$\sigma = \frac{\frac{Z}{2}N(1-2\xi) - \frac{Z}{2}N2\xi}{\frac{Z}{2}N} = 1-4\xi \quad (2.2.2)$$

which we can express in the Bethe-approximation [26] by two Bethe parameters ε and η :

$$1-\sigma = \left(\frac{4\varepsilon\eta}{1+\varepsilon\eta} \right) \left(\frac{1}{1+\varepsilon^{\frac{z}{z-1}}} \right) \quad (2.2.3)$$

where ε and η are connected and can be parameterized by δ :

$$\begin{aligned} \varepsilon &= \exp(-2\delta(Z-1)) \\ \eta &= \frac{sh((z-2)\delta)}{sh(z\delta)} \end{aligned} \quad (2.2.4)$$

The LRO parameter may be presented:

$$s = \frac{(\varepsilon\eta+1)^z - (\varepsilon+\eta)^z}{(\varepsilon\eta+1)^z + (\varepsilon+\eta)^z} \quad (2.2.5)$$

Numerical calculation of the above parameters shows (Fig. 2.2.1, Fig. 2.2.2) that, when $\varepsilon = 1$ (critical temperature T_c), η is also maximal. The LRO parameter at T_c is zero (this is one of the definitive behaviour of the T_c , Fig. 2.2.3) while SRO remains finite.

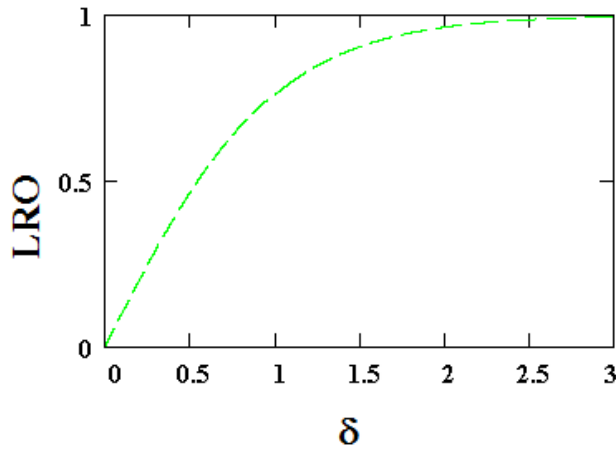


Fig. 2.2.1. Changes of LRO parameter by δ (does not depend on Z).

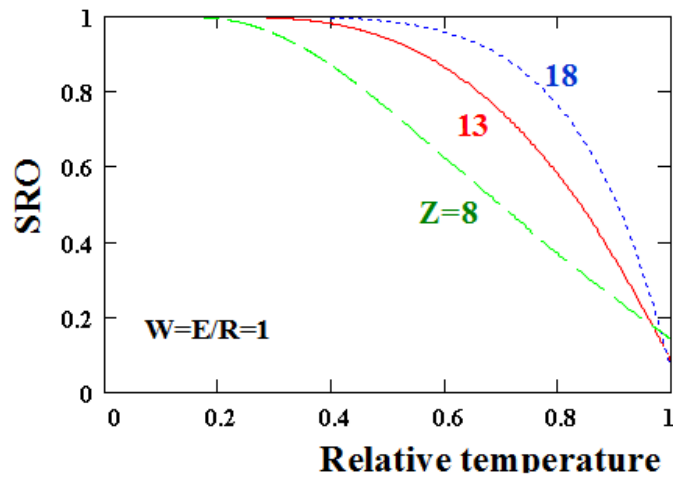


Fig. 2.2.2. Changes of SRO parameters by δ at different Z (various packages).

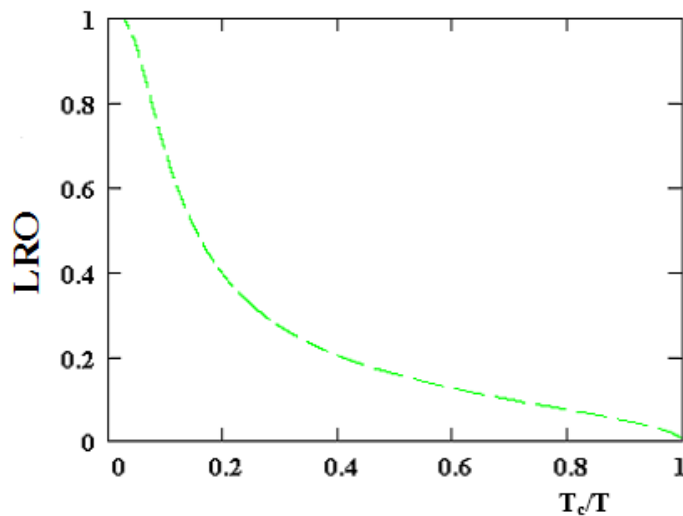


Fig. 2.2.3. LRO parameter versus T_c/T (relative temperature).

The (σ/s) ratio has a minimum (Fig. 2.2.4), which has not too much change with the average Z in its realistic (close packed [27]) values. The free energy dependence can be calculated on the long-range order [28]. This is shown in Fig. 2.2.5 – Fig. 2.2.7 by different s -parameters and temperatures. Note the definite free-energy minimum below T_c (characteristically no minimum above). The minimum indicates that the order parameter and stability of the actual state are very much connected, and the stability (free-energy minimum) is connected with different order-parameters at various temperatures. It is also important to note that the depth of the potential increases with cooling. The SRO is calculated by the metallic ordering procedures based on the electronic band approximations [29-30].

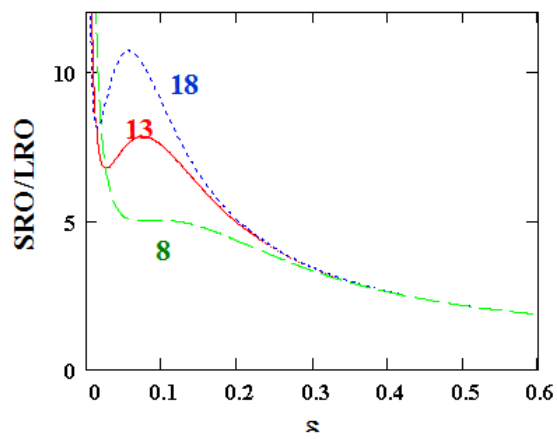


Fig. 2.2.4. Change of the SRO/LRO ratio by δ at $Z=8, 13$ and 18 .

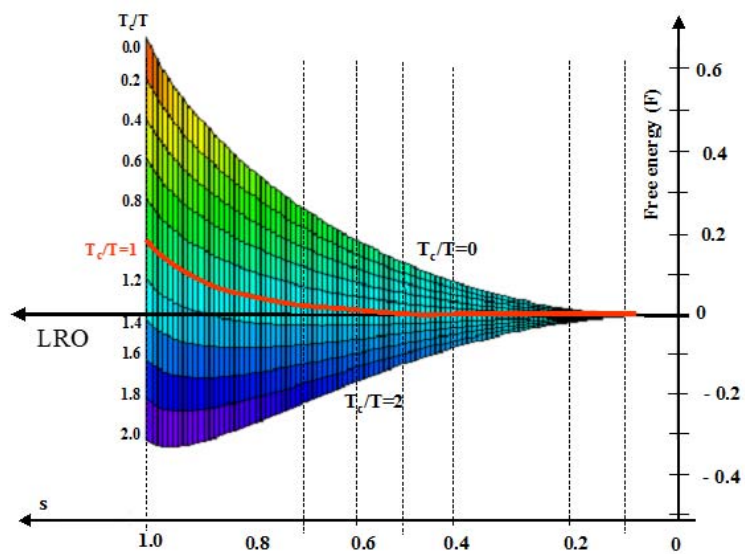


Fig. 2.2.5. The free energy curves versus LRO in Bethe approximation.

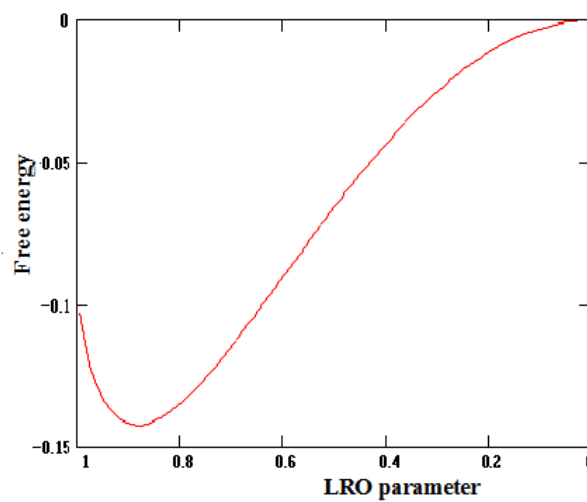


Fig. 2.2.6. Free energy versus LRO at $E=29.8$ J/K/mole [H-bridge bonding], $T=15$ K and $z=13$ [close packing].

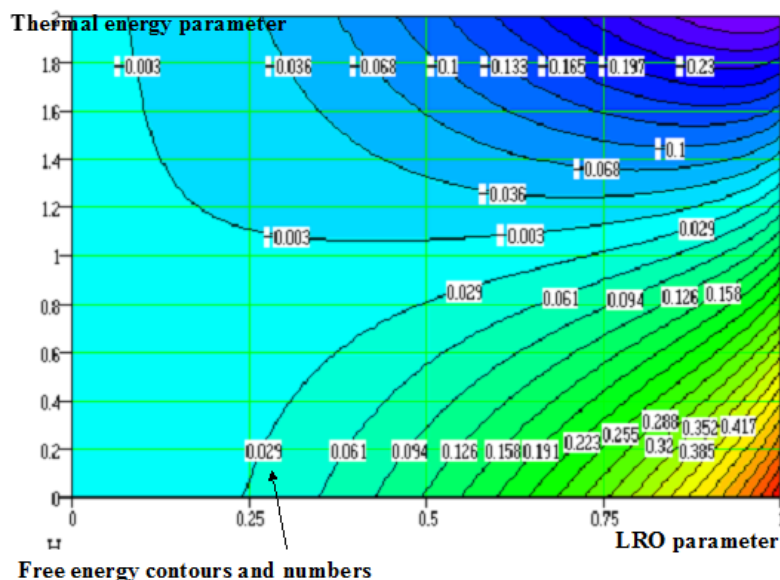


Fig. 2.2.7. The free energy dependence on LRO and the energy parameter zE/RT (R is the universal gas-constant, T is the temperature, z is the coordination number and E is the bonding/activation energy).

2.2.2. Dynamic properties

At zero temperatures (general reference state), both LRO and SRO are maximal (there is an entire order on every scale). With the temperature growth, LRO monotonically decreases and reaches a point (critical point) when the global order disappears. The local order (SRO) is different; the decrease of LRO from the global order destroys SRO as well. Because of the procedure that breaks the internal bonds to destroy the long-range order, the short-range order decreases even more rapidly.

However, when the system is broken into small clusters, SRO is stabilized, while LRO decreases further. The critical size is the cluster, which is stable individually, and its conditions depend on the actual potential in the substance.

Do we reach a special point during the increase in temperature? When does a geometric frustration (bifurcation) procedure appear? If the system is on the border of the different energetic optima of SRO and LRO, the system “cannot decide”, and the situation for the geometric vibration is ready.

This bifurcation point is also achievable at the constant temperature by changing the interaction potential or the pressure. The pressure controls the average distance between the particles and through this parameter the cluster stability can be tuned. Three intensive parameters (temperature T , chemical potentials μ_i and pressure P) are responsible for the stabilization of the special point for bifurcation (geometric frustration) procedure. If we take into account the electromagnetic interaction as well (outside the electromagnetic fields), then two other intensities (the electric E and magnetic fields H) are also able to tune the system to the frustration. As a consequence, the pairing extensives (S , Ni , V , P and M , respectively) are important to stabilize the system energetically. During the frustration, the global intrinsic energy of the system is not changed, but inside terms in the basic thermodynamic equation fluctuate intensively, keeping the sum constant.

2.2.3. Structural properties

Filling up the space with equal geometric units (by translational repetition of the units to make a proper tessellation) has been proven to be more contradictive than previously thought.

The different topologically close-packed structures are important in studying structural stability, which was intensively studied by Laves [5] and Frank & Kasper [6]. It was pointed out

that many complex intermetallic compounds could be understood as being determined by the geometric conditions of the sphere packing. The sphere packing requires tetrahedral micro-clusters and, in general, the energy conditions of the packing favours the structures with triangular faces and tetrahedral cells.

A regular tetrahedron has the most compact arrangement that can be constructed by identical hard spheres. This compactness is accompanied by minimal system energy. Therefore, these forms of clusters will spontaneously appear in various situations. We can construct the most compact arrangement by tetrahedrons. A cluster involving twenty tetrahedrons sharing one vertex has the lowest cluster energy. This arrangement has some gaps between spheres (Fig. 2.2.8).

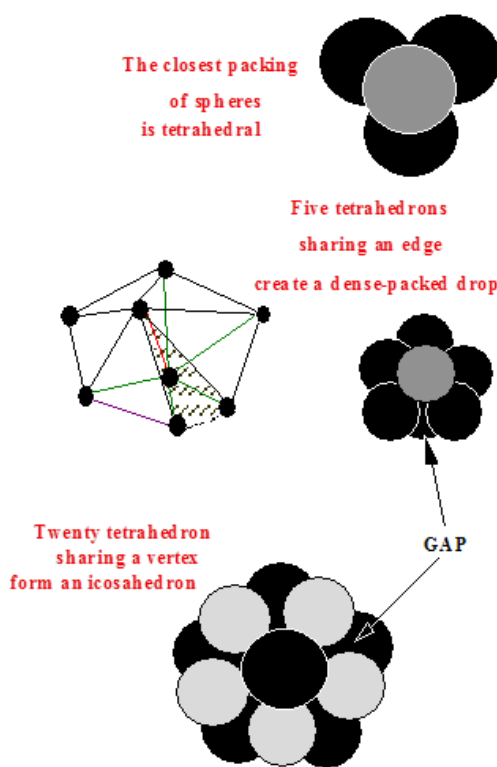


Fig. 2.2.8. Construction of icosahedron by hard spheres.

With a little pressing, this becomes a regular unit (one of the five Platonic bodies): the icosahedron. The icosahedron has a five-fold symmetry; it is not possible to fill the space periodically with the repetition of these units only. However, the macroscopic energy-minimization requires a periodic translational repetition (crystals). The holes formed by tessellation in between the units decrease the compactness (density), smear the potential-wells and decrease the cluster stability.

The packing individual cluster by the uniform spheres prefers the co-ordination number (CN) of 12. Three types of the close-packed co-ordination with CN = 12 are available: the face-centred cubic (FCC), the hexagonal close-packed (HCP) and the icosahedral close-packed (ICP). FCC and HCP are closed-packed, translationally space-filling structures. Their periodic repetition fills the space properly. These two structures appear very commonly in crystalline materials, having a well-defined long-range order (LRO) with dense packing. This crystalline order has definite translation symmetry (translational repetition of a given unit).

The ICP structure, however, is very peculiar: it fails to translationally fill the space properly. Its five-fold symmetry is strictly prohibited in every crystalline structure: no crystal exists with this. The space-group has no five-fold element [J.]. It has a typical central symmetry and builds up the structure from a centre. Its continuation is also the central procedure: spherically packing the next particles onto the cluster surface, continuing the procedure always by spherical symmetry

from a fixed point (the centre of the icosahedron). The ICP structure leads to the densest cluster packing [6]. The regular icosahedron contains twenty slightly distorted regular tetrahedrons (their height is reduced by a factor of 0.925) sharing one vertex, the centre of the icosahedron (Fig. 2.2.9).

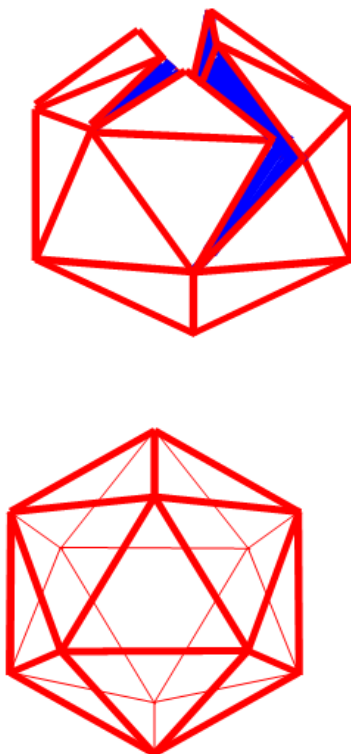


Fig. 2.2.9. Construction of icosahedron.

Contrary to the densest cluster-structure, the average density of the ICP is lower than the FCC or HCP. Exactly this is the main internal topological contradiction: the global optimization (system density) and local optimization (cluster density) are different.

The tight tetrahedral cluster packing prefers the icosahedral arrangement. The total binding energy of ICP (calculated by the Lennard-Jones potential [31]), is deeper than $-41J$, (where J denotes the binding energy [bond strength]) of a pair. The closed packed FCC has only the binding energy. Consequently, the ICP structure with hard equal spheres contains more than 10% of deeper bonds. Hence, it is more stable. If we include the 12 next-nearest-neighbour-bonds, the binding energy difference is a driving force that spontaneously deforms the HCP and FCC structures into ICP [32]. The deepest binding energy of ICP has also been calculated within a simple potential-well approximation [33]. The ICP is the energetically most stable clustering, even if it constructs the system with relatively soft (deformable) spheres for packing. This structure, as well as other clusters having non-translational symmetry (7-, 8-, 9-,...-fold axes), form the basic clusters of each non-crystalline material. All of the non-crystalline-fitting (non-translational) clusters fix the system in a metastable state, which cannot reach the crystalline order and the deepest system-energy minimum. The main difference between the crystalline and non-crystalline matter is as follows: in the crystalline material, a five-fold symmetry is strictly prohibited, while in the non-crystalline matter, five-fold (and other non-translational) clusters are the basic units.

In clustering processes, the short-range order (SRO) strives for the icosahedral formation under certain conditions. This process was experimentally observed in various liquids and amorphous solids [34], in the formation of extremely small clusters [35], moreover even in the austenitic stainless steel [36]. The icosahedral co-ordination occurs in metallic crystals [37] and in non-metallic compounds [38] and was well observed in the metal-carbonyl clusters [39], playing an important role in catalysis. Its critical role in biomatter will be discussed in Chapter 4.

2.2.4. Ordering procedure

To study the local structures the concept of the so-called Voronoi polyhedron [40] has been introduced in general. These polyhedrons represent the first co-ordination shells of every atom by a convex polyhedron formed by the perpendicular bisecting planes of each atomic bond [41]. In crystalline materials, this construction is called the “Wigner-Seitz cell”. This is different from the co-ordination polyhedron, where the actual particles are in its vertices (this is the well-known “elementary cell”). The co-ordination polyhedron and the Voronoi polyhedron are geometric duals [42]. Geometric duals can be constructed by bisecting of the edges of a given polyhedron by planes. So the tetrahedral is self-dual, the cube and icosahedron have their geometric duals – octahedron and dodecahedron, respectively.

First, the principles of polyhedron identification should be clarified. Let us introduce the symbol $\{p_s, q_s\}$, which denotes a polyhedron (regular solid) having $\{p_s\}$ polygons at its faces, and $\{q_s\}$ of polygons meet at each vertex. According to Euler’s formula, $\{p_s, q_s\}$ determines the number of vertices N_V , the number of edges N_E and the number of faces N_F . Euler’s formula is:

$$N_V - N_E + N_F = 2 \quad (2.2.5)$$

Due to the polyhedron regularity:

$$q_s N_V = p_s N_F = 2 N_E \quad (2.2.6)$$

Hence:

$$N_V = \frac{4p_s}{2q_s + 2p_s - q_s p_s}, N_F = \frac{4q_s}{2q_s + 2p_s - q_s p_s}, N_E = \frac{2p_s q_s}{2q_s + 2p_s - q_s p_s} \quad (2.2.7)$$

Bisecting the edges by planes makes the geometric dual of polyhedrons. In this way the $\{p_s, q_s\}$ polyhedron becomes $\{q_s, p_s\}$, which is generally the notation of the geometric dual.

When filling the space by the spheres, a five-fold symmetry is frequently preferred in the Voronoi polyhedron, seeking for the ICP arrangement [43]. Nevertheless, the short-range local preference of the icosahedral order does not agree with the global long-range requirements. The icosahedrons (and the dodecahedron as their dual [42] and simultaneously as its Voronoi polyhedron) have no perfect tessellation in the Euclidean-space due to their five-fold symmetry [44]. The statistics of the Voronoi polyhedrons in the system far from thermal equilibrium are difficult to describe by a well-defined analytic parameter. The polyhedrons show a large variation, and the geometric characterization complicates the evaluation and makes it difficult to follow the trends and changes in the system.

We are able to determine the actual particle arrangement in the given ensemble by MD calculations. It depends on the initial starting parameters (i.e. boundary conditions, initial distribution, pair-potential, integration method, etc.). The result allows one to calculate co-ordination statistics [45] or to decide on the micro-clustering preferences [46,47]. Simple molecular dynamics calculations were performed to clarify the role of different potentials in the actual SRO arrangement. These calculations show the dependence of the actual geometry (characterized by the radial distribution function (RDF)) on the given interaction potentials (Morse-, empirical- and pseudo-potentials) [45-48]. Generally the softer potentials lead to the more relaxed cases, reaching easier the global stability.

To evaluate the Voronoi polyhedrons, we used the statistics in the Coxeter notation [49]. We counted the edges of the faces and set them into a growing order. In this way, a polyhedron is denoted through a set of indices $n_3, n_4, n_5, n_6, n_7, \dots \{n_i\} \dots$, where ‘n’ is the number of faces with vertices ‘i’. Consequently (0,6,0,8), Fig. 2.2.8 denotes the Voronoi polyhedron of the BCC structure (it has 0, 6, 0, 8 three-, four-, five- and six-edged polygons, respectively.)



Fig. 2.2.10. Voronoi polyhedron of BCC (0,6, 0,8).

The Voronoi polyhedron of the FCC structure is a rhombododecahedron, with 12 equal rhombuses as its faces, so its Coexeter notation is (0,12,0,0) (note that this FCC Coexeter notation is identical for the HCP Voronoi cells as well. It indicates that the symmetries are not included in the notation, only the number of the surface polygons.) The Voronoi polyhedron of the icosahedron is a dodecahedron (its geometric dual). The relevant Coexeter symbol is (0,0,12,0)⁴. The statistics contains all the types of Voronoi polyhedrons realized in the actual state. Their shape and frequency are also calculated around both constituents. In general, various deformations of the well-known periodic structures and numerous intermediate polyhedrons [(0,3,6,4), (0,3,6,5), (0,4,4,6), (0,4,4,7)] appear. These and similar polyhedrons are generated from the distribution of the regular crystalline arrangements. The actual calculation, starting either from the LRO (crystalline) or SRO (amorphous) extreme always leads to the deformed intermediates shown in Fig. 2.2.11. The co-ordination number (CN) in the co-ordination polyhedrons must be calculated by a sum of the Coexeter-numbers. Consider some examples of CN: CN_(0,6,0,8)=14, CN_(0,4,4,0)=8, CN_(0,3,6,0)=9, CN_(0,2,8,4)=14, CN_(0,4,4,6)=14, CN_(0,2,8,5)=15, etc.

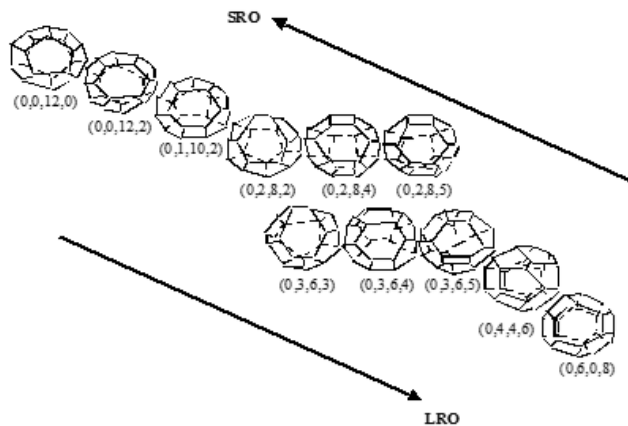


Fig. 2.2.11. A set of polyhedrons between the SRO and LRO conditions (Coexeter symbols are indicated).

To evaluate the trend of changes in the polyhedrons we have to take into account a topological rule: the crystalline order prefers only three-, four- and six-fold symmetries, prohibiting five-, seven- and so on symmetries. On the other hand, the amorphous structures prefer five- and seven-fold symmetries (Bernal-holes) (Fig. 2.2.12).

⁴ Note that not only the dodecahedron has this notation.

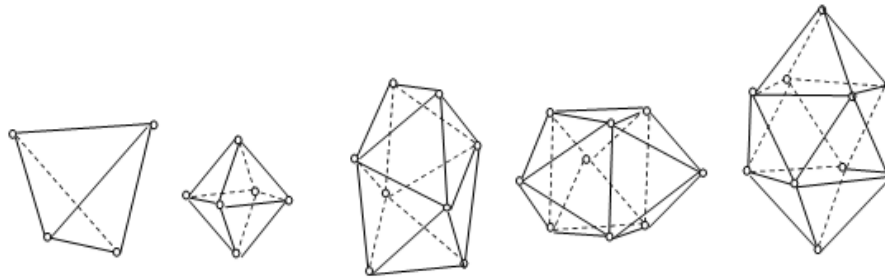


Fig. 2.2.12. Bernal-holes in amorphous structure (DRP model). Their geometric dual represents the Voronoi polyhedra.

In this way, we have a specific factor to distinguish on the actual trend: does it develop itself in the crystalline (LRO) or amorphous (SRO) direction? We have to assess the change in the relative number of non-crystalline (non-translational) symmetries. In fact, faces higher than 6-edge polygons are very scarce, so only the pentagonal faces have to be compared in different states. Let us introduce a parameter for the pentagonal dominance (denoted by “ P ” [50]) generated by the ratio of the number of pentagons (n_5) to the total number of face-polygons ($\sum_i n_i$) in a given Voronoi polyhedron:

$$p = \frac{n_5}{\sum_i n_i} \quad (2.2.8)$$

In general, considering all the crystalline symmetries in comparison with to the non-crystalline ones, we introduce [51,52] the c-parameter ‘c’ (crystalline-behaviour):

$$c = \frac{n_3 + n_4 + n_6}{\sum_i n_i} \quad (2.2.9)$$

This corresponds to:

$$c \leq 1 - p \quad (2.2.10)$$

because not only a five-fold symmetry can break the crystalline order.

Using the P -parameter, the Voronoi polyhedrons (Wigner-Seitz cells) of an ideal crystal can be characterised by $p_{(0,6,0,8)} = \frac{0}{14} = 0$, while a dodecahedron (the dual of the icosahedron, which is prohibited in a crystalline structure) has $p_{(0,0,12,0)} = \frac{12}{12} = 1$. The range of P with some example polyhedrons is shown in Fig. 2.2.13.

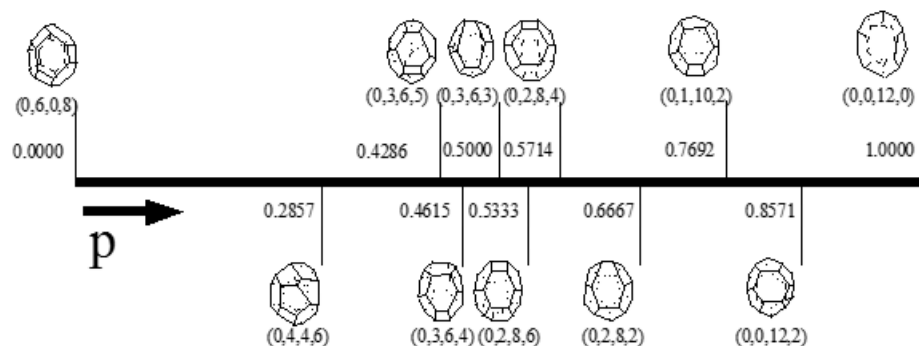


Fig. 2.2.13. Scale of the p -parameter (with some sample polyhedrons).

The pentagonal dominance can be different in the overlapping sub-lattices. The sub-lattices could have any pentagonal (or higher non-crystalline) symmetries without negatively affecting the translational symmetry requirements. For example note, the A15 structure, which is the complex of BC and ICP sub-lattices. The Frank-Kasper sub-lattices are also non-crystalline.

The translational symmetry and its topology recognize only the geometric conditions regardless of the actual properties of the involved particles (units, atoms, etc.). Consequently, the Voronoi analysis is independent of the actual particles involved. Voronoi analysis studies the topology only. However, counting the different Voronoi cells of the individual particles, we have to take into account which particle is in the centre. This means that the regular Voronoi analysis follows the geometry only; sub-lattices (clusters of identical atoms) are not calculated.

Using this, we can calculate the role of different constituents in fixing the actual state by following the development of CN-polyhedrons of different components. For example, a microstructure calculation has been performed for Al-Mn classical quasicrystal [53] to study the geometric role of Mn in Al-matrix. In the same way, we can clarify the role of metalloids in creating the non-crystalline structure in metal-metalloid systems [18]. The numerical solution of the Newton equations (MD) gives even more facilities: the mass-dependence of the Voronoi analysis is also available [54]. The change in icosahedral order is shown in Fig. 2.2.14. In both cases, the impurity masses lower or higher than the matrix-atomic weight have a higher number of icosahedral clusters than the matrix itself. Two different structures have been observed by pair-correlation [50] depending on the particle mass:

- at small particle mass ($M < M_A$) the amorphous structure domains, while
- at large particle mass ($M > M_A$) the quasi-crystalline order is formed.

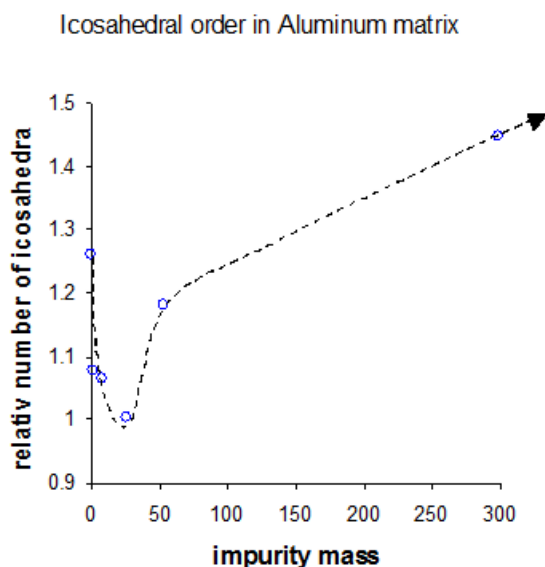


Fig. 2.2.14. Relative number of icosahedral clusters in Al-matrix versus the impurity mass.

The MD calculation of Voronoi polyhedrons by different potentials [55] (pseudopotential (PP)) and Lennard-Jones potential (LJ)) shows (Fig. 2.2.15) an important dependence of P -parameter on the softness of the potential. The wider and softer LJ allows more effective next-neighbour interactions than the harder PP, so PP increases the p -parameter more than LJ.

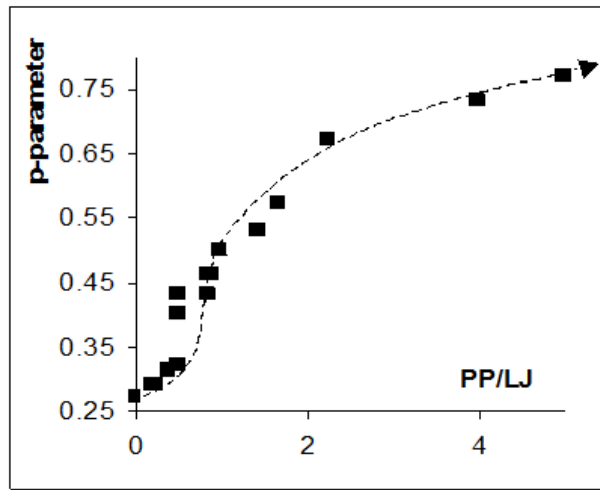


Fig. 2.2.15. *p*-parameter versus the ratio of the Lennard-Jones and pseudo-potential.

2.3. Intrinsic topological dynamism

2.3.1. Structural incompatibility

The most interesting fact from this point of view is the cluster formation in cluster beams. This shows a preference for some definite clusters if the number of atoms involved in these clusters produces the so-called “magic numbers”. The “magic numbers” can be described by the icosahedral arrangements [56]. Therefore, small clusters of atoms tend to form icosahedral (close-packed in SRO) clusters.

The formation of a few atoms cluster is governed by the closest packing. In two dimensions, this arrangement is a triangle, which has no topological contradiction at further growth (Fig. 2.3.1). However, in three dimensions, the tetrahedral arrangement is dominant. Twenty tetrahedrons (sharing a vertex) form an icosahedron, which is prohibited in crystalline structures. However, when increasing numbers of particles interact (forces become effective over a long range), symmetry breaking changes the overall symmetries (Fig. 2.3.1). Five-fold axes vanish and a normal crystalline structure is achieved.

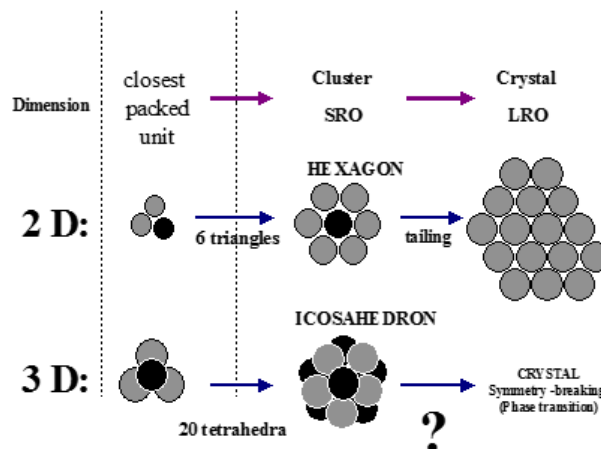


Fig. 2.3.1. Incompatibility of the icosahedron.

This process occurs at some kind of thin-film growth. In this process, the nucleation minimizes the free energy by the five-fold arranging, and when the nuclei start to interact, the

symmetry suddenly changes and the crystalline order appears. In order to characterize this symmetry breaking and the actual phase transition, one has to understand the ordering effects.

Consequently, the contradiction between the closest cluster packing (ICP) and the closest space packing (FCC) creates a non-usual situation: from the point of view of space filling the SRO prefers the ICP arrangement, while the LRO requirements favour the FCC (or HCP) structure. The build-up procedure starts by such clustering of ICP in equilibrium conditions. However, due to a periodic repetition of only icosahedrons, no proper translational space filling exists; the situation develops contradictory requirements. In this static meaning, the SRO and LRO arrangements contradict each other in the three-dimensional case⁵.

The balance of contradictory tendencies in the long- and short-range potentials has determined the actual stability of an arrangement. Consequently, there are two possibilities:

- To construct a state with the microscopic minimization of cluster energies. This is an icosahedral clustering. In a short-range order it is optimal, regardless of the imperfect space filling due to the periodic repetition (LRO) of the icosahedron.
- To satisfy the macroscopic requirements and arrange the units in a crystalline structure. In the long-range order it is optimal, regardless of the microscopic (SRO) requirements.

An LRO-stabilized (i.e. crystalline) system will not be the densest in the microscopic sense, so it will not satisfy the energy minimization at the cluster level. On the other hand, the densest icosahedral arrangement is no denser macroscopically than the crystalline close packing in LRO. If the short-range forces are dominant, the system structure will be different from the long-range force. The system, which is “soft” enough to change early its cluster-arrangements, has a topological (geometric) bifurcation (Fig. 2.3.2). This corresponds to a double-well potential with one state of the microscopic and the other of the macroscopic energy minima.

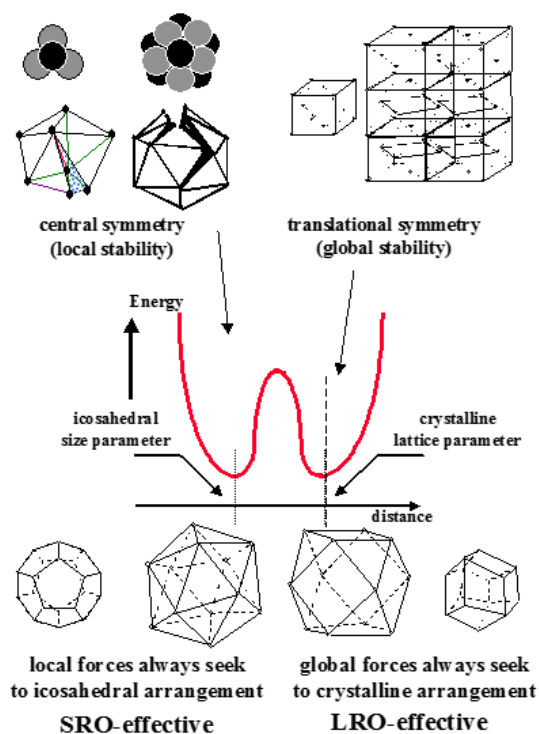


Fig. 2.3.2. Bifurcation of short-range order and long-range order.

⁵ The contradiction is only for the frozen (static) structures which exist in three dimensions. The dynamic situation could be different. Furthermore, in four (or higher) dimensions, this type of topological contradiction does not exist.

For the long-range potential term, various approximations are available:

- The simplest and, thus, most popular is the jellium model, which is widely applied in the theory of metallic clusters [57].
- The shell approximation with the spherical jellium model describes some observations of cluster creation in alkali metals [57].
- Lennard-Jones potential is effective for the states with icosahedral clusters.
- Using the spherically averaged pseudopotential, (SAPS [58]) or, in the case of another mesoscopic potential, an average Madelung energy proposed by Manninen [59], which is effective only in the mesoscopic range, the results obtained are closer to those of the experiments.

In general, good metallic materials prefer jellium-like (drop) clustering [60]. However, materials with large electron effective masses more likely form the ICP arrangement, which is generally described by the Lennard-Jones potential [61]. The local energy requirement leads to a special stability with clusters of five-fold symmetry [62]. The vacancy formation energy for different clusters is the highest for icosahedral clustering. In this way, the cluster arrangement gradually disappears during growth (as the influence of the long-range term is growing) [60]. It is clear from calculations [61] that alkali metals and molten liquid phases may overemphasise the spherical (jellium) structure. This spherical system suppresses the role of the packing geometry.

As mentioned above, the SRO potential minimum at the icosahedral cluster disappears when a cluster grows. It was shown by the Lennard-Jones potential calculation [33] that the growing cluster maintains its symmetry up to 13 outer co-ordination shells, and the most stable one is the formation with 8 co-ordination spheres (Fig. 2.3.3).

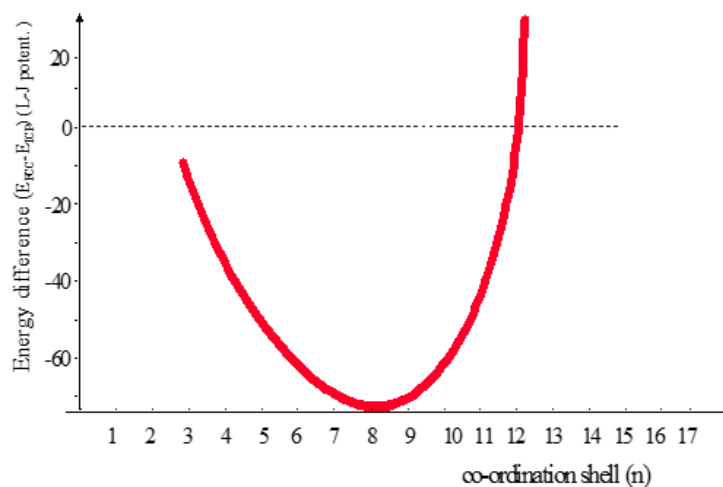


Fig. 2.3.3. Medium-range order (MRO) versus the co-ordination shells (Lennard-Jones potential).

Arranging the icosahedrons in the space means that the non-filled holes in between can be eliminated by attaching the icosahedrons to each other. We have two possibilities for this solid attachment:

- To deform the regular icosahedrons to the indefinite (irregular) but similar polyhedrons. Then, the periodic repetition (to fill up the space translationally) disappears.
- To use the regular icosahedrons, but to curve the space, and go into the four-dimensional case (this is similar to the two-dimensional problems with pentagons; there was also a solution to maintain the pentagons and curve the flat sheet into the three-dimensional space).

So, if we try to maintain the regularity, we have to interpret the static (rigid) arrangements in four dimensions. In this way, the shell-by-shell gradual growing procedure can be well described geometrically with the higher-dimension regular polyhedrons (so-called polytopes [49]). Let us use the Schläfli symbols $\{p,q\}$, a polyhedron having p faces of q edge regular polygons. The Schläfli

symbol of the four-dimensional polytope is $\{p,q,r\}$. The faces of this polytope are $\{p,q\}$ polyhedrons, and the vertex figure (dual) of the polytope has faces $\{q,r\}$. Hence, the geometric dual of the $\{p,q,r\}$ polytope is $\{q,r,p\}$ ⁶. The icosahedral polytope $\{3,3,5\}$ has $\{3,3\}$ tetrahedral faces, while its dual $\{5,3,3\}$ has $\{5,3\}$ dodecahedral faces. The icosahedral polytope ($\{3,3,5\}$) has 120 vertices (120 particles are involved). This finite unit is the largest available compact regular solid in any dimension (this means only in four dimensions, because in higher dimensions, the polytope with 5-fold-symmetry does not exist). The fragments of $\{3,3,5\}$ projected into the flat three-dimensional space show the subsequent co-ordination-shells (the most dense micro-packing with a central symmetry). Around the central atom, the next shell consists of 12, 12, 20, 12, 30, 12, 20, 12, and 1, respectively. The compact $\{3,3,5\}$ has eight co-ordination shells (including the central particle). Further co-ordination shells must be non-regular; their energy rapidly grows. One may conclude that the microscopically optimal packing even in any dimension, in principle, could not be continued to macroscopic ranges. In the regular polytope formulation, in the flat space, the co-ordination shell number 8 must be the most stable one, 7.

The cluster of the ICP closest packing cluster can be enlarged by the so-called disclination procedure [63] into the higher co-ordination arrangements. This procedure creates different Frank-Kasper polyhedrons with CN = 14, 15, 16. These are laser realized in different alloy structures in sub-lattice geometry (see Fig. 2.3.4). It is well established that the Frank-Kasper phases give the topologically ideal close packing in comparison with any other packing constructions [6]. These phases have a five-fold face on average [64], which emphasizes the crucial role of SRO in close packing.

The construction of long-range icosahedral order is also possible: either by the Frank-Kasper sub-lattices (like the A15 crystalline structure) or by quasi-crystals. In quasi-crystals, the joining icosahedrons are overlapping providing almost (but not perfect) translational symmetry in the material.

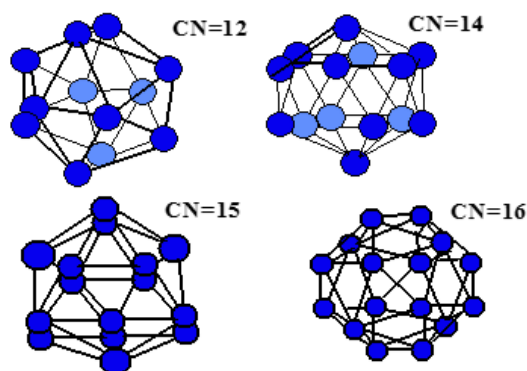


Fig. 2.3.4. Frank-Kasper polyhedrons (sublattices).

2.3.2. Dynamic properties: two-dimensional cases

The apparent contradiction of the space-filling (of the short range with the highest cluster densities, which have five-fold symmetries, and of the long range with the proper translational tessellation, where the five-fold symmetry is definitely prohibited) can be solved in different ways.

For simplicity, let us first consider the effect of the five-fold symmetry in a simple two-dimensional lattice containing regular pentagons translationally arranged in a sheet. The plane

⁶ There is a limited number of the possible polytopes existing: the ‘pentatope’ $\{3,3,3\}$; the hypercube $\{4,3,3\}$, its dual cross-polytope $\{3,3,4\}$, a self-dual $\{3,4,3\}$ and a dual pair having pentagons $\{5,3,3\}$ and $\{3,3,5\}$. In higher dimensions, altogether only three further regular polytopes exists: self-dual simplex $\{3^d\}$ and the hypercube and its dual $\{4,3^{d-1}\}$, $\{3^{d-1},4\}$.

⁷ This corresponds well to the Lennard-Jones calculations.

sheet cannot be covered properly by these pentagons; in addition, another polygon (rhombus) has to be applied for tiling (Fig. 2.3.5). This is one of the solutions when the short-range five-fold requirement is satisfied and the sheet is filled in. In this case, not all of the clusters are in the preferred pentagonal arrangement.

We note that the tessellation of the regular pentagons can be arranged in different ways, where the solutions are different from those described above, but the basic idea is applicable in each case (Fig. 2.3.6).

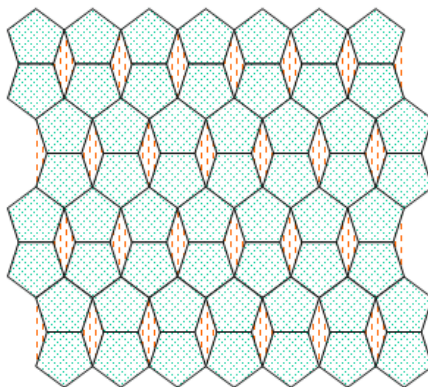


Fig. 2.3.5. Covering the sheet by regular polygons.

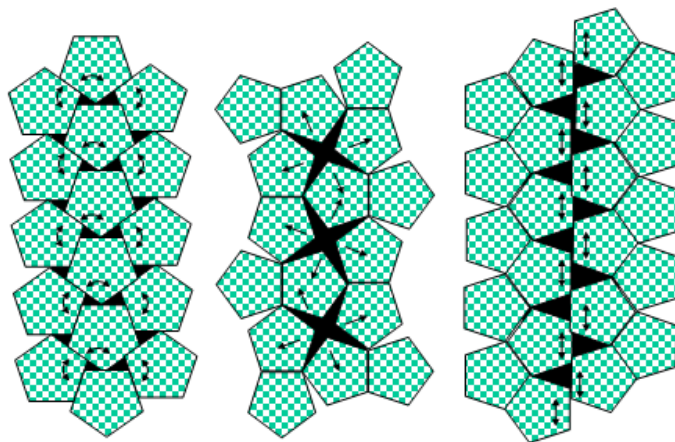


Fig. 2.3.6. Different arrangements of the pentagons in plane sheet.

Every system contains polygons far from the optimal pentagon. This frozen-in solution solves the SRO \leftrightarrow LRO contradiction, satisfying partially both of the requirements as well. Of course, the overlap of pentagons or non-regular ones also harmonizing with the LRO space filling, but the first co-ordination circles are not pentagonal in these cases, contradicting the initial conditions.

To study further the problem, a serious question should be considered: does a continuous transformation of the long-range ordered arrangements to the short-range favoured clustering exist? Without this transformation, the balance of SRO and LRO is not tuneable; the frustration picture is not realistic. The continuous transformation from a rectangular square lattice to the tiling for quasi-crystalline tessellation is solved [61] by tilting the lattice units.

A special deformation has been introduced [65] at the appropriate places, so the original square-network shrinks and expands into the regular pentagonal tessellation, as in Fig. 2.3.7. This effect corresponds to the special projection of the curved sheet into a plain 2D arrangement. The densest arrangement of the regular pentagon in a sheet is shown in Fig. 2.3.8.

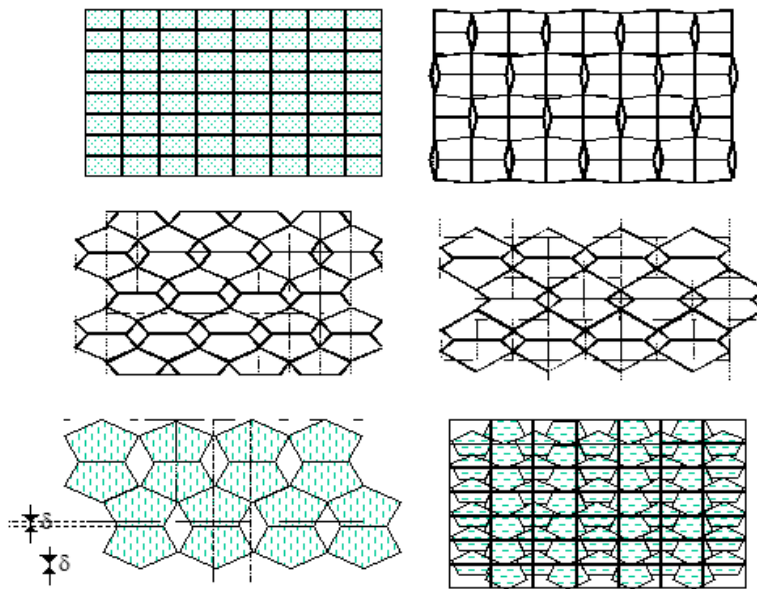


Fig. 2.3.7. Sample distortion of the square lattice to pentagonal covering.

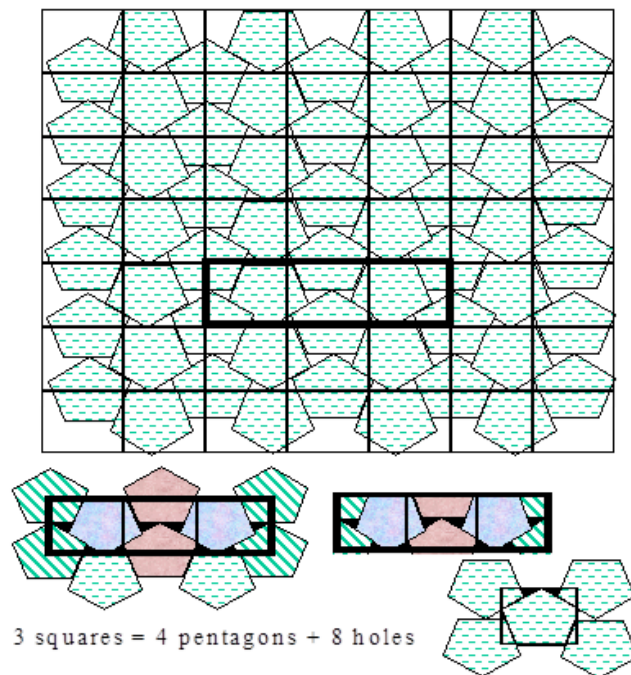


Fig. 2.3.8. Closest packing of pentagonal cover in the square-lattice.

The other possible arrangements (Fig. 2.3.9) are pentagons, which overlap with each other (Fig. 2.3.9(a)), or regular pentagons deformed into non-regular polygonal forms, where LRO can be easily satisfied (Fig. 2.3.9(b)). Non-pentagonal units are “cut out”, so the sheet becomes curved (Fig. 2.3.9(c)). These deformations are frozen-in and, thus, the optimum SRO is heavily damaged in each micro-arrangement. If these deformations are not frozen in, the particles in the fence chains become frustrated (soft bonding case). These atoms have no fixed optimum site and fluctuate on the given linear chain satisfying both the SRO and LRO requirements in a time-average of their motion (Fig. 2.3.9(d)). Consequently, the SRO \leftrightarrow LRO problem is soluble also in a non-frozen, dynamic coherent arrangement (Fig. 2.3.9(e)). The rigid puckered chains and soft, fluctuating fence chains could alter (Fig. 2.3.10.) The individual vibrations could be collectively organized and, thus, the rigid zigzags serve as a channel for the energy bag (soliton) which slides through the

material. This solution is very similar to the domino-row falling, when the instability bag glides by the row. If this arrangement somehow freezes, then both the long- and short-range requirements are broken.

In actual materials, the local (SRO) and global (LRO) energy requirements compete with each other to evolve the structure observed. It is proposed that their balance plays a central role in the formation of the actual phase, emphasizing the crucial role of the medium-range order (MRO) in the mesoscopic region.

Proper filling solutions:

- A.) Overlapping units
- B.) Non-regular units
- C.) Curved space
- D.) Vibration bridges
- E.) Coherent waves

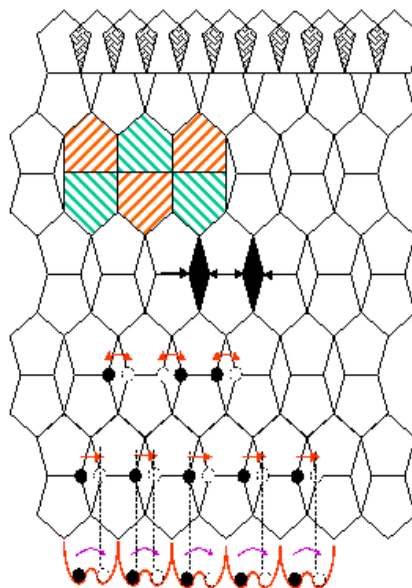


Fig. 2.3.9. Different solution of five-fold tessellation.

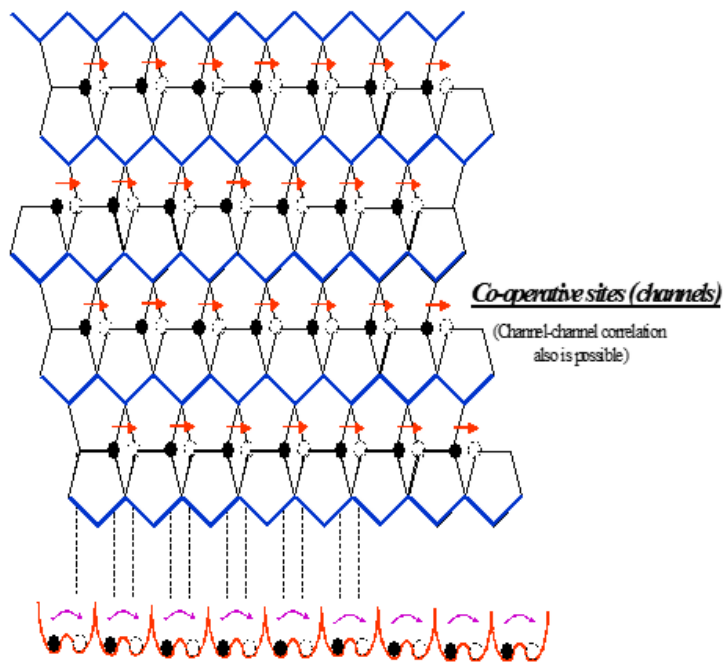


Fig. 2.3.10. Dynamic solution of pentagonal tessellation. Note the alternate structure and the solitary wave in channels.

2.3.3. Dynamic properties: three-dimensional cases

Having learnt the processes in 2D, we turn now to the 3D packing problem. The contradiction of the optimal structural energy in the local and global scales results from that locally the most stable icosahedral clustering is inapplicable alone for proper tessellation in the three-dimensional Euclidean space. If the short-range interactions are strong enough to influence the general energy balance, the structure has to be frustrated.

The competition of two antagonistic mechanisms can indeed produce a set of similar structures and equilibrium. The properly space-filled FCC or HCP clusters can spontaneously deform into the icosahedron [32] (Fig. 2.3.11) creating the densest packing in a cluster, so the possibility of the solution of LRO \leftrightarrow SRO contradiction by the same dynamic picture (as was described in 2D) exists. A slight deformation can transform FCC to ICP and vice versa (Fig. 2.3.12) [32]. The LRO preferred FCC (Fig. 2.3.13) can be continuously deformed (breathing mechanism) into a tessellation seeking the ICP clustering, and finally we get the tessellation by regular icosahedrons. This process is more spectacular for the corresponding Voronoi polyhedrons, where the continuous tilted deformation of the polyhedrons from the FCC Wigner-Seitz cell through a transition phase to the regular dodecahedron is clearly seen. Consequently, the apparent dynamic route is the same as in 2D. The similarity is obvious if we are close to instability, balancing between the preferable SRO and contradictory LRO clustering.

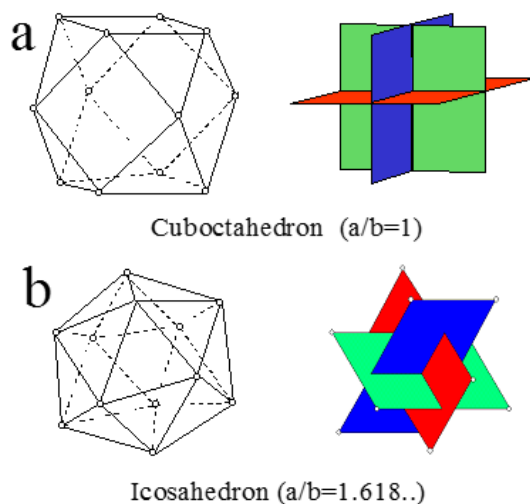


Fig. 2.3.11. Structure of closed packer LRO (a) and SRO (b).

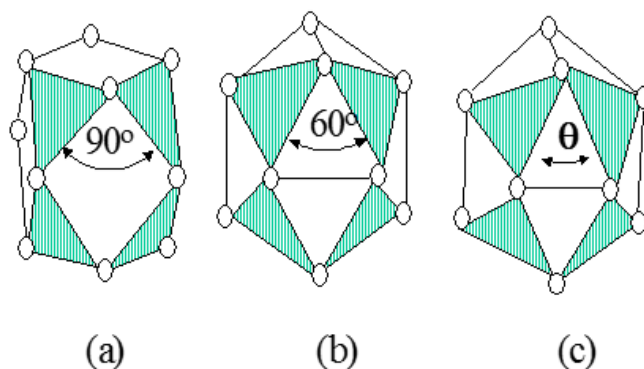


Fig. 2.3.12. Distortion between the cuboctahedron and icosahedron.

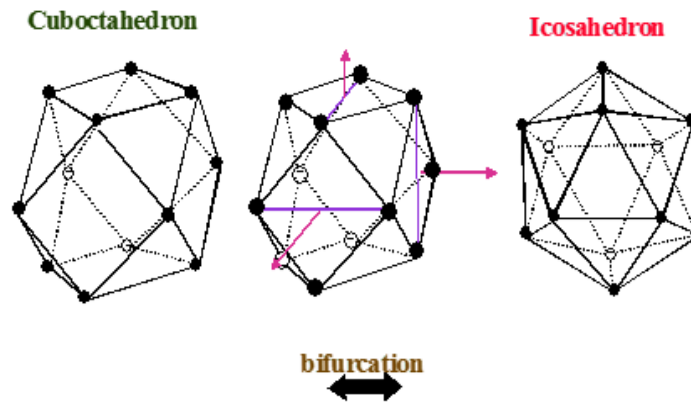


Fig. 2.3.13. Possible bifurcation mechanism between FCC and ICP.

The balance of the SRO \leftrightarrow LRO interaction (instability), to our mind, can be tuned by MRO of solids. To examine MRO, it is necessary to consider a system seeking icosahedral clustering with non-interacting spheres. When switching on an attractive potential between them, this tendency remains [32]. A strong potential minimum of the arrangements with tetrahedral cells and triangular faces [33] is observed. To describe atomic interactions, the Lennard-Jones potential is frequently used, which strongly stabilizes the ICP structure through a few (about 8-11) coordination shells [67]. Moreover, the number of atoms involved in a volume stabilized by icosahedral five-fold symmetry is relatively large, ranging between 10^5 and 10^7 [68].

There are two possible solutions for the SRO \leftrightarrow LRO contradiction: the static (frozen-in) and the dynamic ones. A structurally non-periodic space filling with as many icosahedral-clusters as possible can be created by a quasi-crystalline arrangement. Indeed, there is a strong indication for the quasi-crystalline ground state [61]. The other solution is dynamic in the sense that the coherent vibrations create a situation where the micro-clusters are momentarily the icosahedrons, and their nearest vicinity is far from the energy minimum. In the next step, the fluctuations lead to the opposite situation: the given cluster becomes distorted, and its vicinity seeks the icosahedral symmetries. In general, on average for a longer time-interval, all of the clusters are in the lowest energy state both microscopically and macroscopically. This dynamic equilibrium simultaneously satisfies both long- and short-range order requirements on average.

The freezing-in (static) considerations pertain to the ground state at zero temperature. With increasing temperature, the micro-instabilities (geometric frustration) vanish with longer mesoscopic effects. The frozen-in icosahedral clusters (similarly to the two-dimensional case) will be gradually transformed to the crystalline order at higher temperatures [33]. The same gradual-transformation occurs in the dynamic case: when the energy in clusters is too high, the microscopic stabilization requirements are not strong enough.

These problems have led to a hot discussion in the literature at present [69]. The optimal dynamic harmony in the local and long-range is stabilized, and its possible freezing depends on the range of interactions. The strong short-range forces without the medium effect in mesoscopic ranges cannot form a dynamic frustration, since any arrangement would be frozen-in all of the time. The coupled first co-ordination shells (local order of clusters) can be frustrated in a long range only by the active medium-range forces.

Note that the contradictory SRO \leftrightarrow LRO conditions can be harmonized statically as well as in the 2D pattern. If we pick-up the rhombuses from the tessellation in Fig. 2.3.14 and close the leakage in the space, the sheet becomes curved and the problem turns into a curved 2D-representation. Twelve pentagons form a regular dodecahedron, where pentagons fill the 2D-surfaces of the regular dodecahedrons in 3D, without any difficulties. Forming these dodecahedrons by each of twelve pentagons, the 3D-space will be filled up by dodecahedrons, but not completely. With further cutting out of the inter-polyhedral spaces between the dodecahedrons (shrinking in the space), the problem becomes one of the curved 3D space, giving a polytope

solution [49,70]. Here dodecahedrons can properly fill the space higher than three dimensions [49]. This is a static solution in more than three dimensions. In the 3D-case, the curved-space description has also been introduced for amorphous and quasi-crystalline structures [24,71,72]. Considering the relaxation effects [73] in the realistic models, the number of five-fold symmetries in Voronoi polyhedrons significantly increases [64]. It means that the energy contribution creates frustration in the medium range, including the domains as well [66].

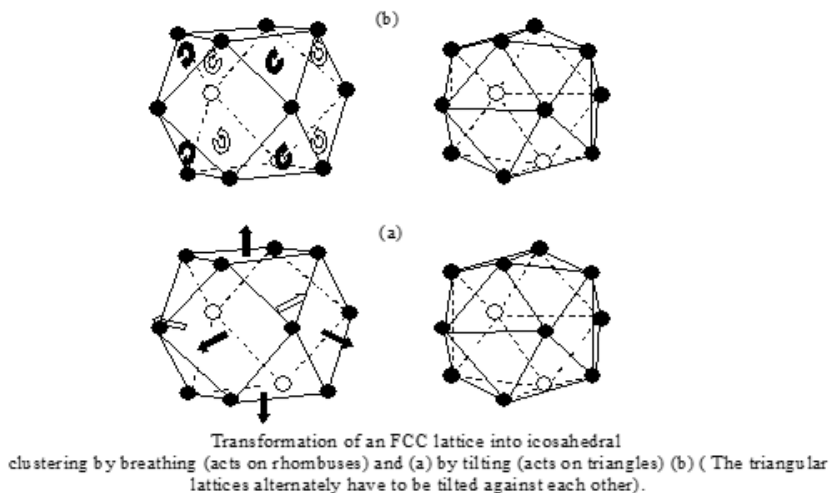


Fig. 2.3.14. Tilting and breathing mechanisms.

The compact SRO clusters with the almost regular Voronoi polyhedrons become deformed by the relaxation, promoting global regular space filling. The disclination lines can be introduced [74] to form a special, so-called “predominantly icosahedral material” (PIM) [75]. The density of disclinations is connected to the space curvature and is the easiest description of the structure [75]. In the three-dimensional space, this density is approximately proportional to the inverse square of the radius of space curvature, while in the case of LRO with a sub-lattice with five-fold symmetries (P- tungsten structure, Laves phases etc.), the positive and negative curvatures compensate each other exactly [76]; moreover, several complex structures can be described by a periodic network of disclination lines [63].

2.3.4. Transport caused by geometric frustration

The geometric "frustration" of the material makes a special transport phenomenon possible [77]: if a cluster stabilizes itself at the microscopic level, its neighbourhood becomes insatiable because of the larger space filling incompatibilities than the average ones. In this way, its neighbours, trying to lower the total (long-range) energy of the system, destroy a stable cluster. The lowered energy in the neighbourhood makes the microscopic stabilization possible for those clusters, which, in turn, will be destroyed by their neighbours (the process is very similar to the large-polaron effect [78,79]). The stable clustering moves towards the next cluster and pushes forward a stable cluster-bag without any particle transport. It can be visualized by a row of standing dominoes: if the first falls, then all of the others will gradually fall, without any transport of the dominoes themselves. Only the energy is transported. A moving, sliding "stability-bag" allows special transport in the cluster arrangement [80]. The phenomenon is very similar to the explanation of high-temperature superconductivity [81], and may be important for the transport and information exchange in living systems, including electron transport (charge transfer) in metabolic processes. This is a special solitary wave (soliton), which has an important role in biomatter as well (see Chapter 4).

2.4. Electron structure effect on the stability

The actual geometry and/or chemical arrangements definitely depend on the electron structure. *A priori*, the electronic structure of a solid is the most relevant stabilizing factor.

It was suggested [82,83] that metastable states in solids are stabilized within a small energy range by their electron (band) structure. The electron band is occupied by the lower energy in metastable phases than in their stable counterpart [84] (Fig. 2.4.1).

The main definitions of this topic are given in all textbooks of solid-state physics. We use the following:

Fermi-Surface (FS): the surface formed by the free or nearly free electron-sea in the energy-space;

Brillouin-zone (BZ): the cell of the impulse space which contains all of the energy states, which characterizes the crystal. Like the elementary cell in the normal space, which describes the structural (topological) purposes, the BZ describes alone all of the features of the electronic structure. BZ is a theoretical electronic construction; in the general case, it is not measurable.

Consequently, the energy-barrier, which provides limited stability to the actual metastable states, is modified by the electronic structure. The electronic band and, therefore, the energy barrier are basically dependent, but chemical bonds (SRO) at the cluster level stabilise the actual SRO arrangement as well.

The metastability of non-crystalline materials is characterized by the following parameters [3]: chemical, geometric and electronic ones. Their unique feature is the disordered structure and, thus, a loss of crystalline order. Despite the absence of crystallinity, the local clustering is relatively stable and surprisingly uniform. Long-range instability and the relatively stable short-range structures determine the metastability. Moreover, short-range geometry has five-fold symmetries, which are entirely incompatible with the crystalline order.

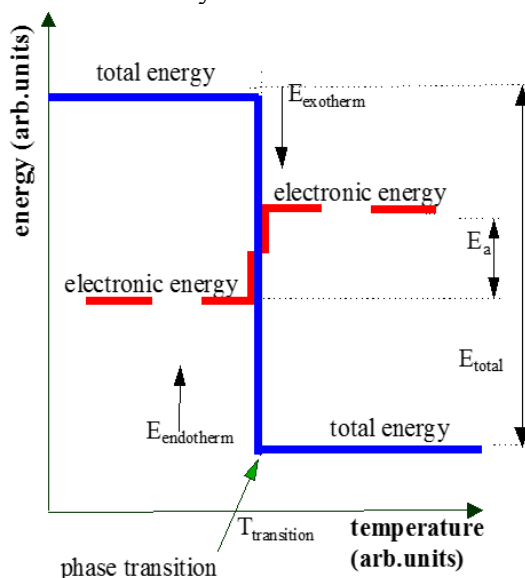


Fig. 2.4.1. Typical energy changes at the phase transition in the metastable situation.

2.4.1. Electronic structure and bistability

One of the oldest, semi-empirical stability criteria for the crystalline materials are the Hume-Rothery rules [4], relating the electron concentration in the alloys with the structure (Fig. 2.4.2). The basic idea is visualized by a classical picture, and the structural change is caused by a critical electron concentration⁸.

⁸ [(number of electrons)/(atoms)] or (e/a).

Mott and Jones reformulated the Hume-Rothery rules [8]. The idea is based on the interconnection of the electron structure with the crystal symmetries and, consequently, refers to the long-range effects.

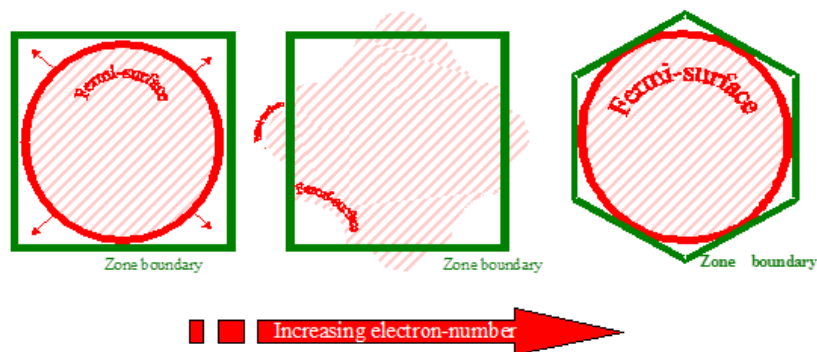


Fig. 2.4.2. The geometric change for the better accommodation of a given electron-number.

Also, the so-called Jones zone (JZ) [7], i.e. an extended and measurable Brillouin zone, was also introduced.

JZ has been defined as one of the Brillouin zones (BZ) (not reduced to the first one (Fig. 2.4.3)), chosen in the closest vicinity of the actual FS. This is experimentally detectable by the determination of the first non-vanishing structure factors in the experiments on X-ray diffraction by these planes. By definition, JZ is larger (or equivalent) in volume than the true first BZ.

Extended Brillouin zones in square lattice

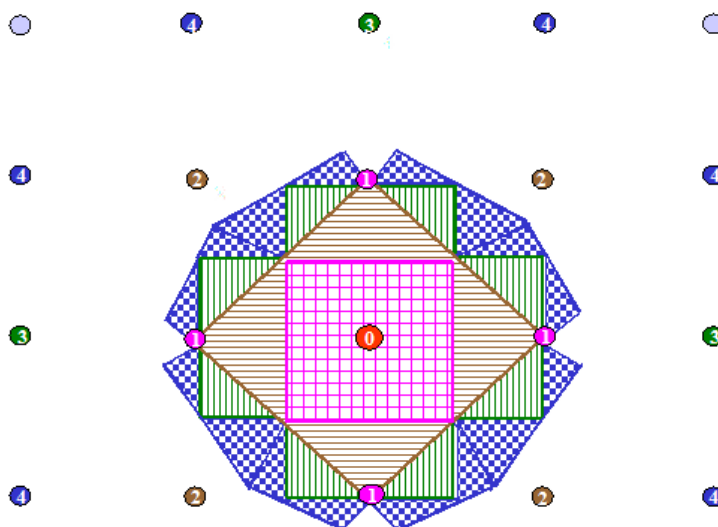


Fig. 2.4.3. First four Brillouin zones. The square-lattice points are numbered according to their role in the BZ-extension.

The BZ-construction is associated with the geometry of the elementary “unit cell” irrespective of whether or not the structure factor vanishes due to the internal arrangement of atoms inside the unit cell. JZ is not only a geometric construction formulated by Mott and Jones, but its position concerning the FS also becomes important in the phase stabilization.

The JZ boundaries correspond to the first non-vanishing structure factors, i.e. the planes at which an X-ray beam is strongly reflected. JZ geometry is strongly related to the symmetries of the real crystalline structure. JZ is a complex polyhedron bounded by the number of planes that increase with a higher number of atoms in the elementary cell. For complicated crystalline

structures, JZ becomes closer to the sphere. The stability idea is based on the Fermi-surface (FS) interaction with JZ, and is strongly determined by the FS-JZ interaction [1,8,85]. The FS boundaries are always curved (distorted spheres), while JZ always has a polyhedron shape with the plain faces. JZ becomes increasingly spherical-like (it has more and more faces) if the e/a ratio grows. In this case, due to the high volume/surface (V/S) ratio of JZ, the stability determined by the electron structure increases. The growth of e/a increases in parallel with the energy of the electron sea. To determine the optimal, most stable, ground state from the point of view of the electron structure, an optimum is searched. This is as small e/a as possible and, simultaneously, as spherical JZ as possible.

The most spherical cluster with the smallest number of particles (closest packing with the coordination number 12) is an icosahedron [6]. At the same time, it favours the most spherical JZ in the lowest level of e/a as well. The good nesting of FS in JZ causes stability of the icosahedral arrangement, because of the considerable energy required to surmount the energy gap due to the touching of surfaces [86] (Fig. 2.4.4). Consequently, the electronic structure itself is one of the driving forces to reach the icosahedral micro-arrangements, the FS nesting in JZ.

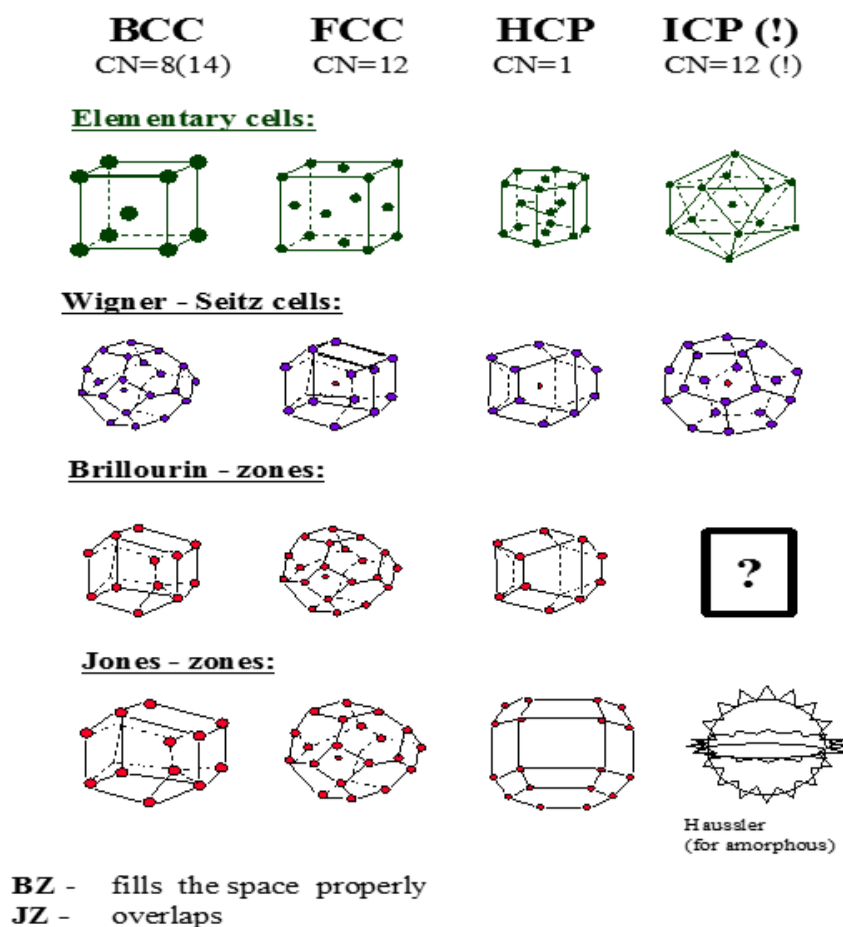


Fig. 2.4.4. Comparison of various zones.

The main energy term at this interaction is due to the energy gap created by touching JZ with FS. There are some contradictory opinions [87], however, stating that the stability does not really arise out of the van-Hove singularity at touching JZ with FS. At the time of popularity of the pseudo-potential methods, the stability criteria based on the FS-JZ interaction were out of favour. An almost negligible effect was calculated for the FS-JZ interaction [87]. Heine and Weaire pointed out that "there is no special stability that would be associated with zone faces touching either the Fermi-surface or Fermi sphere" [88], whereas Massalski and Mizutani emphasized [89]: "the test example.... was applied only to a hypothetical situation".

In fact, the condition of the FS-JZ interaction:

$$Q = 2k_f \quad (2.4.1)$$

is relevant in many cases to the stability of alloys (where Q is one of the vectors of the reciprocal lattice, and k_f is the Fermi wave-vector). The effect of touching JZ with FS opens a gap in the dispersion relation ($E(k_f)$) at $1/2Q$ (Fig. 2.4.5). This gap causes a local minimum in the density of states (DOS).

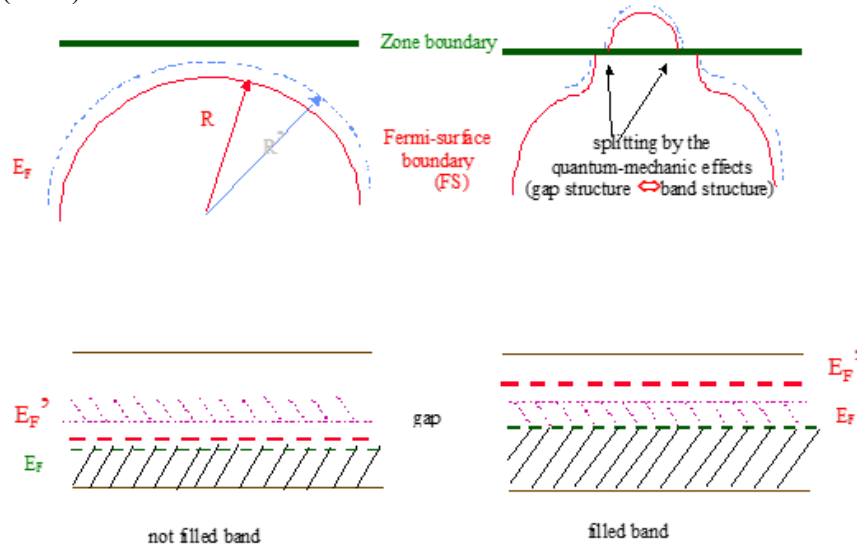


Fig. 2.4.5. Gap creation at the FS-JZ touching position.

Stroud and Ashcroft [90] emphasized that the condition in Eq. (2.4.1) was correct for the stability in many cases. However, the Hume-Rothery rule arises not so much out of the screening divergence itself as from the rapid variation of the dielectric function in the immediate vicinity of $2k_f$.

The pseudo-potential approximation to the stability problem of alloy phases was considered rather disappointing [91], and its usefulness in the stability is less obvious than before. In fact, there is a large category of alloys (electronic compounds or Hume-Rothery phases) where the FS-JZ interaction is essential for stability. Another example of the role of electron structure in the stability is the qualitative description of the stability of the BCC structures in the region $N=5-6$ (where N is the number of d and outer s -electrons per atom) [92]. This hypothesis was later generalized to a wider category of structures (HCP and FCC) for transition metals [93].

The interaction of different relevant factors affecting the stability is intensively used for the construction of the so-called “maps” [94] and in Miedema's rules [95] as well. These semi-empirical rules are continuously under detailed discussion [96].

During the study of the structure and stability of the binary alloys, Hafner recognized [97,98] that the electrostatic part of the energy strongly favours the distorted structures in LRO. The existing crystal structures are especially balanced between the electrostatic and band-structure potential contributions. The inter-atomic potentials of the compounds mainly define this balance. The observed inter-atomic distances of the compounds fit very well with the calculated minima of the potentials [99].

In fact, the FS-JZ interaction determines the stability in partially and/or totally disordered (LRO is lost) systems [100,102]. The homogeneous and isotropic disorder with SRO and MRO makes it possible to define a periodically continued neighbourhood [103] and quasi-Bloch states

[104] in one-electron approximation. For such materials, a sphere-like JZ has been measured by diffraction methods [105], and nearly-free electron behaviour has been observed [106] as well.

As a consequence, one of the most powerful ideas for amorphous metals stabilization (the Nagel-Tauc theory [107]) is based on the FS-JZ interaction [105]. In the nesting position (Fig. 2.4.6) due to the zone filling possibilities (Fig. 2.4.7), the stability is obvious.

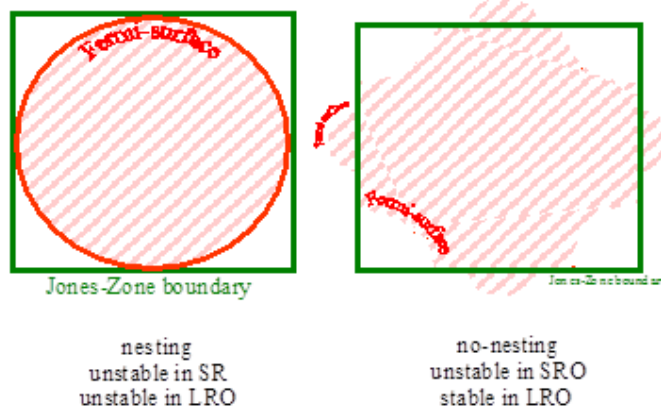


Fig. 2.4.6. The nesting situation.

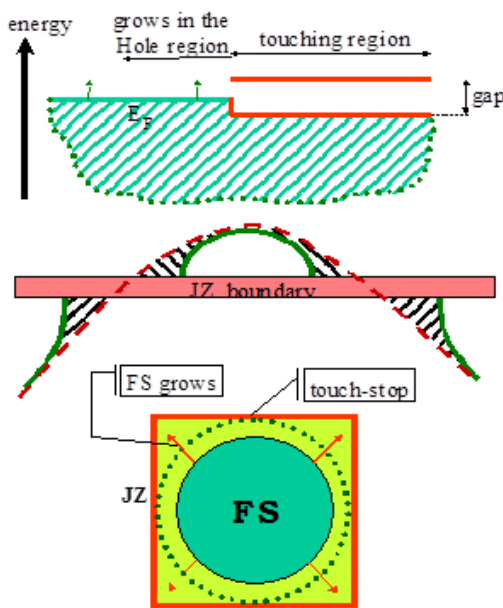


Fig. 2.4.7. Filling up the JZ in the touching region.

For the electronic stability, the perfect nesting of FS in JZ is the optimal case; the increase in electron number due to the energy-gap at FS requires a large energy to surmount the gap. To create this stable nesting, JZ should have polyhedrons close to the sphere [102], with a large number of faces at uniform distances from the centre of the zone. The FCC JZ has 8 faces for the first touching, while JZ of ICP (which is an icosahedron as well [101]) has 20 faces. Consequently, the icosahedral arrangement is the most stable, taking into consideration the JZ-FS interaction (and, of course, the appropriate number of electrons required to create the nesting of FS) [102].

The electron structure calculations show the stability of different LRO symmetries [108]. Two well-defined electron concentrations have been found where the material has no preferred LRO (Fig. 2.4.8). As a consequence of the non-definite LRO, these compositions have to have a strong SRO effect, seeking the icosahedral or other Frank-Kasper co-ordination, creating an optimal SRO for stable clustering. This SRO arranges a special MRO that is effective in a few co-ordination shells [109].

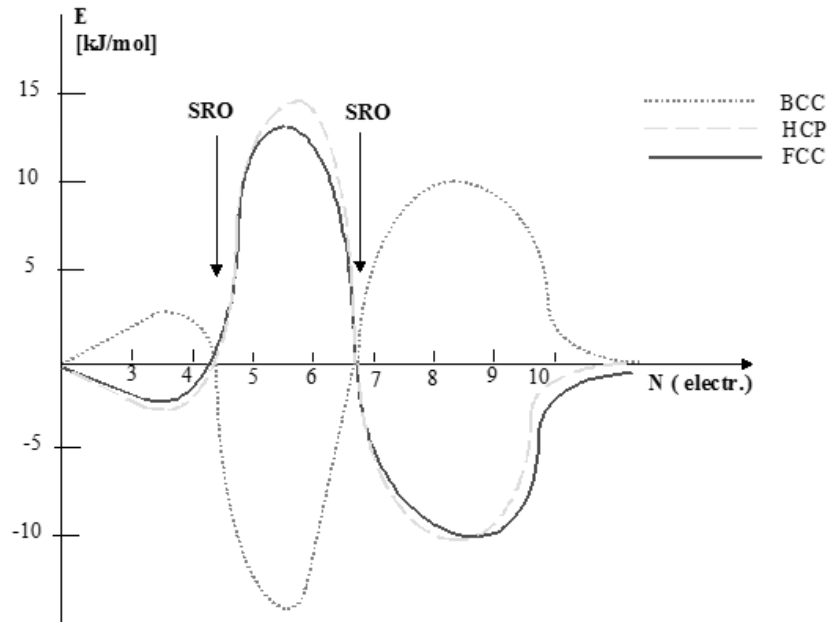


Fig. 2.4.8. Electronic stability and bistability points.

Based on a local instability, short-living ($\tau=10^{-13}$ - 10^{-12}) and large energy fluctuations were suggested [110] and applied in the kinetic theory of melting [111]. These instabilities exist in both the high- T_c and low- T_c superconductors [111]. We have suggested above the coherence of fluctuations. Thus, collective gliding of a stable arrangement is possible through the material. We mention that the coupling based on a short-range deformation has been suggested for the ferromagnetic clustering [68], which is, regarding the SRO-coupling, similar to these considerations. The concept of elementary excitations may be used in the case of frustration [71], similarly to the Bragg-condition in the crystalline material, and a spherical JZ can be assumed in amorphous materials with the $271/a$ radius (where a is the average distance between atoms). A soft-mode appears close to $k = 271/a$ in such solids where the frustration is in action. This is similar to the quasi-particle "solidon", introduced in He [112].

According to our suggestion [113,114], there is a collective excitation mediating the electron pairing in high- T_c materials; the soft mode c predicted near $k = 2\pi/a$ [111] acts close to the JZ-FS interaction, repeatedly emphasising the role of the electronic structure.

An idea of a spherical JZ was also introduced for amorphous alloys and, thus, the critical e/a was determined by the geometric coincidence of JZ with FS [105]. This was also supported by the Nagel-Tauc stability criterion [87], which is an exact extension of the Hume-Rothery rules for glassy metals.

However, there are some experimental [115] and theoretical [116] contradictions with Nagel-Tauc's theory. This fact and the limited applicability of the spherical JZ [105] require further investigation of the problem [104], leading to a refinement of the ideas.

2.4.2. Geometric conditions of the Fermi surface Jones interaction in the non-crystalline matter

Non-crystalline materials are in the metastable states, in which the thermodynamic conditions, and, first of all, the configuration behaviours and the short and medium-range orders (SRO and MRO) play an important role. The loss of long-range order (LRO), i.e. the loss of the translation symmetry, appears to characteristically dominate the locally stable arrangements. In spite of these facts, metallic amorphous alloys are relatively good conductors. Moreover, there are various data which show the applicability of the nearly free electron model in these alloys [106,107]. This model is theoretically confirmed on the basis of the quasi-Bloch-states [104] and the periodically

continued neighbourhood (PCN) [103] (Fig. 2.4.9), making it possible to describe the amorphous systems in the well-established framework of crystalline metals and alloys.

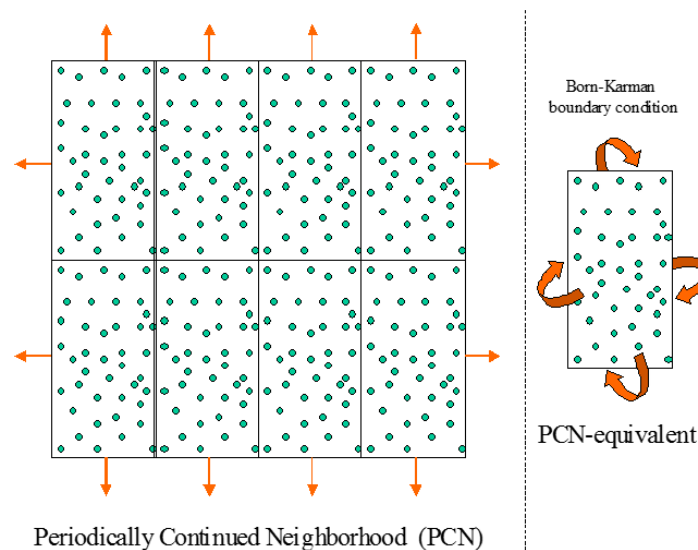


Fig. 2.4.9. Concept of the Periodically Continued Neighborhood, (extended picture) and its equivalent compressed picture (Born-Karman boundary condition).

Although the two characteristic surfaces, FS and JZ, are different constructions, their nesting may occur in some definite cases. The nesting situation is created by a special JZ-FS interaction [8], which makes an energy-gap at the point of touching. In the nesting case, a forbidden gap appears around FS to render the material non-metallic.

We propose providing a simple geometric calculation of the interaction between the typical quasi-polyhedral JZ and the quasi-spherical FS. We suppose that FS is entirely within the actual JZ and its sphere is distorted at the onset of the crossing (Fig.2.4.10). The icosahedral arrangement in a real space makes its JZ icosahedral as well [49]. A simple static-structure-factor calculation shows an icosahedral-seeking symmetry in the k_1 -space, which arises from a distorted icosahedral arrangement in a real space. The icosahedral-clustering has 12 first neighbours. For such a small number of atoms, only this close-packed arrangement makes such a great number of touching points in the smallest JZ volume. Consequently, this JZ characterizes the most stable arrangement among all possible close-packed clusterings. The amorphous material consists characteristically of this type of cluster. Since JZ is bounded by the planes, we can interpret the expression "spherical shape" to mean that the actual JZ assumes a polyhedral shape with more and more faces, but always having plane boundaries (Fig.2.4.11). Subsequently, Haussler [118] has noted an experimental evidence for an extension of Hume-Rothery's critical VEC's (valence electron concentration) to the amorphous phase, assigning $VEC=1.8$ to the amorphous state. For this state, he correctly invokes a 'limiting' spherical JZ, although, in our view [101], incorrectly implies that this becomes a true sphere. In the perfect crystals, the unperturbed long-range order leads to the regular JZ polyhedra filling the entire k -space. If we slowly 'switch on' the distortions in a crystalline material to form the amorphous metastable state, then the long-range order is gradually distorted. During this process, the crystal can be regarded as a mixture of short-range ordered clusters. Now, the JZ polyhedrons for each cluster develop more and more boundary planes. As the real structure becomes distorted and the PCN grows, JZ becomes more spherical, the X-ray diffraction peaks become diffuse and the long-range order is lost. Each almost spherical JZ would remain polyhedral but no longer fully unique in shape, only in volume [101]. Therefore, in this case, a satisfactory simplification would be an average to assume a unique JZ for the whole material, with spherical shape and diffuse boundary. This supposition is capable of explaining all of the above experimental findings, except those connected with FS-JZ contact effects. In this situation, the FS of the material with the short-range order cluster is no longer an ideal sphere, but

still resembles a sphere, depending on the exact cluster arrangement. A diffuse boundary sphere can also approximate this situation.

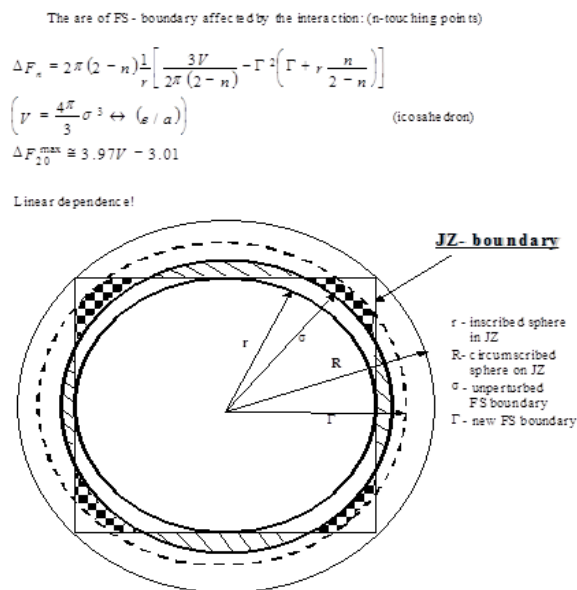


Fig. 2.4.10. Simple calculation of the nesting conditions [101].

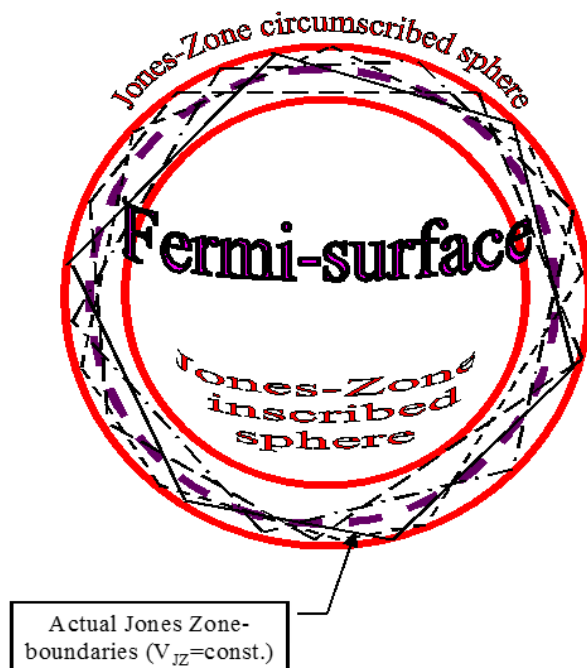


Fig. 2.4.11. Multi-polyhedral JZ (place-to place dependent) and ist FS.

The diffuse spherical shape of JZ has been observed by different diffraction methods [119]. Of course, the nesting here exists only on an average (as explained before). The average fitting of FS (quasi-free electron sea) with JZ (complex polyhedron, on an average a smeared sphere) causes a pseudo-gap at the Fermi-energy predicted by the Nagel-Tauc theory (Fig. 2.4.12).

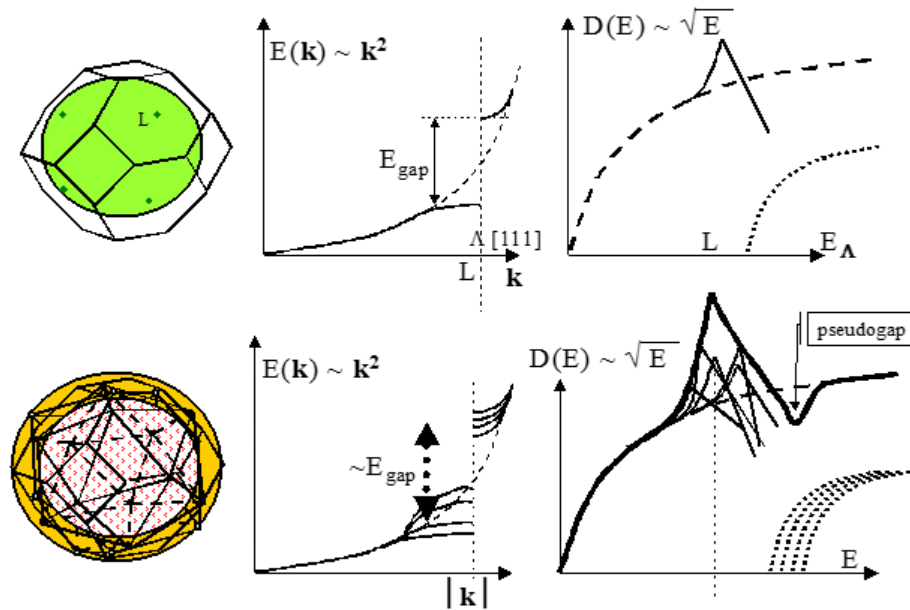


Fig. 2.4.12. Construction of the pseudogap by the FS-JZ touching.

There are some experiments verifying the linear dependence of the stability parameters on (e/a) . In the binary metallic Mg-based amorphous systems [120], as well as in the Sn-based binary amorphous alloys [121], a linear dependence is observed. Among the several investigations of metal-metalloid amorphous alloys, for example, in the case of the amorphous Fe-B-based ternary alloys, there is clear evidence for the predicted linear dependence [122,123]. The low-boron-content ternary alloys ($\text{Fe-TM}_x - \text{B}_{1-x}$, where TM is a transition metal, $9 < x < 15$) have been investigated [124]. In the case of $x = 13.5$, the crystallization is well separated from the precipitation of excess iron [125], and, thus, no polymorphic crystallization is expected. For these and other low-boron-content Fe-based ternary alloys a linear dependence has been found for the thermal parameters characterizing the stability (crystallization temperature and transition heat) versus e/a [57] (the deviation from the linearity at higher B concentration is due to the polymorphic crystallization).

2.4.3 Superconductivity and stability: a problem of the ground state

Metastability is meaningful only in comparison with the stable or reference state. Contrary to the lowest energy in stable state, the stability of the state is connected to the maximal available entropy in a closed system. The third-law of thermodynamics defines a ground state as an energy and entropy of reference.

The main requirement for the absolute ground state of a system is the lowest entropy (at $T = 0$ K the entropy constant could be chosen zero). This is similar to the lowest intrinsic energy (the quantum-mechanical zero-point energy). This state is a “global” order, and at $T \rightarrow 0$ the order tends to ideal. Let us study the “ideal order” from the configuration point of view. The actual equilibrium of a system configurationally requires a suitable space filling (to fill the available space homogeneously). The possible entropy maximum belongs to the most available homogenous arrangement.

In the equilibrium state of a particle collection, the individual particles (atoms, ions, etc.) are spherical. The sphericity is determined by the procedure of seeking for the smallest surface for the given volume. This is an individual trend of a local system (particle). The spherical particles (atoms, ions), however, cannot fill the space properly. A relaxation in the condensed phase of spherical atoms (ions) leads to an equilibrium, which differs from the overall behaviours of the independent sub-units.

The spheres become deformed. The hard touching of the units leads to increasingly more planes between the deformed spheres. With a small fantasy we can create this transition situation by growing the hard spheres with a soft cover. Then a particle will have a "cherry-like" composition: a hard ball inside (bone) and a soft surface layer outside. If we pump-up the soft interfaces (by increasing the volume), the system of cherries will soon fill up the spaces between the hard balls. The arrangement will be the realization of the Voronoi polyhedral structure. So, the units of the system become increasingly more polyhedral (instead of the curved surfaces, where we have more and more planes). This violates the energy minimum of the individual particles and yields a total free energy minimum of the system. This process is driven by the growth of the entropy in the condensed relaxed arrangement. Note that the entropy of the individual particles decreases due to the deformation procedure (the "neg-entropy", the information, which they represent, increases). The energy of the individual particles is higher, but their total free energy (the total energy of the particle-ensemble) in the case of the best possible space filling would be the lowest. In spite of the fact that the spherical form represents individually the lowest energy, the system lowest energy does not prefer it. In general, we can observe an individual energy minimum connected to the curved unit surfaces, while the system seeks the polyhedral units. The individual energy minimum is not compatible with general energy requirements of the systems. As a consequence of our three-dimensional space, there is a topological difference between the local and global approach. The local and total stability of the system is not in the exact correspondence.

Moreover, at the level of symmetries we realize the translational (or quasi-translational) symmetry in the "proper" tessellation, while the "prope" local unit has rotational (or quasi-rotational) symmetry. The local rotational symmetry could also be continued in a spherical (rotational) way, and only after a few co-ordination shells "vanish", the phase transition occurs [66].

However, it is impossible to fill the space properly (translationally) only by the icosahedral arrangements due to their five-fold co-ordination symmetries. Equilibrium will be stabilized by a relaxation process of the system. Due to this procedure the density of micro-clusters becomes inhomogeneous. If part of the micro-regions are to be denser (close to icosahedral), then their immediate proximity cannot be packed as densely. It is due to the packing problems of the five-fold clusters. This is manifested in the so-called "compensation" idea [41] developed for amorphous (non-crystalline) metals.

Due to the inherent inhomogeneity (based on the geometric frustration), different collective excitations could be introduced in the actual systems: the normal density fluctuation [64], the charge density waves [126], the bipolaronic excitation [38], etc. We guess that the intrinsic incompactness of the ground state is responsible topologically for the quantum zero energy.

The reason for this is that the space filling is microscopically unstable and the micro-stability requirements contradict the macro-stability. An entropy-stabilized equilibrium is created for the system, but a microscopic instability exists at the same time. This is the realization of the entropy bifurcation in the ground state [92].

Based on the above considerations about the structural and electron stability of solids, we can suggest that the ground state of the matter itself (geometrically) is metastable, which agrees well with the quantum-mechanical ground-state considerations. This metastability is connected with an inherent "vibrational" energy, corresponding to the ground-state energy declared by the quantum mechanics for other purposes. By this inherent energy, the local- and global-equilibrium incompactness is solved by time averaging: the inherent mobility bridges in the apparently contradicting topology continuously transform them into each other.

DISSIPATIVE STRUCTURE FORMATION IN NON-CRYSTALLINE MATERIALS

Recently, the ideas of the non-equilibrium thermodynamics predicting the possibility of the non-crystalline structure with new unique properties in strongly non-equilibrium conditions have been widely developed. In this case by the structure the method of the element organization and the spatial-temporal character of their inter-correlation are meant. The dissipative structure formation in the non-crystalline materials is related to the self-organizing phenomenon. That problem is of special interest not only for physics but also for biology and chemistry. Therefore, we will consider it in detail.

3.1. Synergetic approach to the non-crystalline solid formation

3.1.1. Non-crystalline condensed media: the dissipative structure

Non-crystalline solids are an extremely wide class of materials involving amorphous substances, glasses, crystals with high defect concentration, spin and magnetic glasses and biopolymer structures. The non-crystalline condensed media are much more abundant and no less important in practice than the idealized monocrystalline structures.

By the term "non-crystalline substance", the structural disruptions are most frequently manifested as the absence of the correlation of the physical quantity, which describes the present system at the distances defining the disordering scale. The non-crystalline solid state is usually considered a metastable one, which does not correspond to the minimum of the total energy and will transit in time to the stable equilibrium state. From this standpoint, the total order is the one that appears due to the non-vanishing correlation of all physical quantities across the total volume of the system. That approach to the non-crystalline solids is in the same relation and has the same specific features as, for example, the flat picture and the real three-dimensional image. Historically, such an approach to non-crystalline materials has been realized due to the description of the initially crystalline spatially ordered solids and the attempt to extend the results for the crystals to the disordered substances. The aforementioned consideration lays the "secondary" relation to the non-crystalline materials, when the essential peculiarities of their operation are rejected. The attempts to interpret the specific properties of certain non-crystalline materials result in the development and application of numerous representations and calculation techniques. In our opinion, the situation would change drastically if the structure and properties of the condensed media were started initially just from non-crystalline materials and the crystalline media were treated as a special case of more common non-crystalline ones. In this case a host of phenomena observed in non-crystalline materials would allow one to catch the general hypotheses and models which belong to the unified approach based on the ideas of synergetics. If the studies of the solid started from non-crystalline substances, not only physics but also biology and mathematics would achieve more success now.

One can formulate the following concepts of non-crystalline solid state:

- any substance can exist in the non-crystalline solid state in one or another form;
- non-crystalline materials are the dissipative structures formed as the method of system organization;
- non-crystalline substances are characterized by the criteria which define the domain of their stability in this state, i.e. the boundaries of the stability with respect to the control factors, which affect the system (i.e. the temperature, pressure, radiation and the rate of their variation, etc.);
- the role of non-linear modes in the formation of the non-crystalline non-equilibrium stationary system of any degree of complexity is equal and versatile;

- the main parameters, which specify the non-crystalline system, are the spatial-temporal correlation of physical quantities describing it and the life-time of the dissipative structure;
- the general regularities established for the non-crystalline state are also valid for the crystalline one.

In connection with the consideration of non-crystalline media, it is pertinent to recall the notion of the quasi-crystal as the object which is not periodic but has a long-range order. Such approach is of fundamental interest since it generalizes the definition of the crystal.

The study of peculiarities of the transition to the non-crystalline state (i.e. the dependence of the transition temperature on the control parameter as well as an anomalous increase in the structure relaxation time and thermodynamic properties in the transition region) within the framework of thermodynamic or relaxation approach in the linear approximation based on the system deviation from the equilibrium state allows only certain aspects of the present phenomenon to be explained. However, this approach fails to elucidate the whole pattern of the non-crystalline solid formation. Hand in hand with this, it is evident that the abundance and the complexity of the pattern are due to the strongly non-equilibrium character of the transition that requires the consideration of non-linear processes related to the interaction of various subsystems, i.e. the synergetic effects must be allowed for [1,2].

Since non-equilibrium is the main feature of non-crystalline structures, we shall analyze the transition to the non-crystalline state by using non-equilibrium thermodynamics regularities [1]. In accordance with this, the change in the entropy ds during the time interval dt can be divided into the sum of two contributions:

$$ds = (ds)_i + (ds)_e \quad (3.1.1)$$

where $(ds)_e$ is an entropy flux which exists due to the matter and energy exchange with the environment and $(ds)_i$ is the entropy production inside the system resulted from the irreversible process. It follows from the second law of thermodynamics that:

$$(ds)_i > 0 \quad (3.1.2)$$

and the equality sign corresponds to the equilibrium state.

For isolated system $(ds)_e = 0$, and we get from (3.1.2):

$$ds = (ds)_i > 0 \quad (3.1.3)$$

Thus, open systems differ from the isolated ones by the presence of an addendum corresponding to the exchange in the expression for the entropy variation. The $(ds)_e$ addendum has no definite sign, contrary to the $(ds)_i$ value, which never takes the negative sign. This allows one to present the transition to the non-crystalline state as the process in which the system reaches the state with the lower entropy as compared with the initial state:

$$\Delta S = \int_{\text{over path}} dS < 0$$

That state is extremely improbable from the viewpoint of the equilibrium state:

$$\mathfrak{R} \propto \exp\left(-\frac{E}{k_B T}\right)$$

where k_B is a Boltzmann constant, \mathfrak{R} is the probability of the system to be found in the state with the energy E . Moreover, this state may exist very long if the system reaches the stationary state, where:

$$ds = 0 \text{ or } (ds)_e = -(ds)_i < 0 \quad (3.1.4)$$

Consequently, if a sufficiently large negative flux of the entropy enters the system, a certain ordered configuration can be maintained in this system. Furthermore, the entropy delivery must occur in non-equilibrium conditions, otherwise, both $(ds)_e$ and $(ds)_i$ turn to zero. Hence, the fundamentally important principle follows that the non-equilibrium can serve as the source of the order, and the self-organization of dissipative fluctuational structures is the principal phenomenon, which constitutes the basis of structural transitions in non-crystalline media. Within the framework of that concept, the contradictions between dynamic and kinetic approaches to the non-crystalline solid formation are eliminated.

Consider general regularities in the formation of the short-range and medium-range order structure in the lowly non-equilibrium (quasi-crystalline) and highly non-equilibrium (non-crystalline) solids at the melt cooling depending on the cooling rate.

3.1.2. The structure modelling

In the atomic structure of non-crystalline substances, one may recognize the short-range order due to the correlation of the local physical quantities $\mathfrak{N}(\vec{r})$ at the distances $L_S \leq 0.1 \div 0.5$ nm and the mesoscopic media-range (intermediate order) due to the correlation of the parameters at the $L_M \leq 0.5 \div 5.0$ nm distances.

The expositions, which describe non-crystalline solid states, can be arbitrarily partitioned into the following three groups (see Fig. 3.1.1).

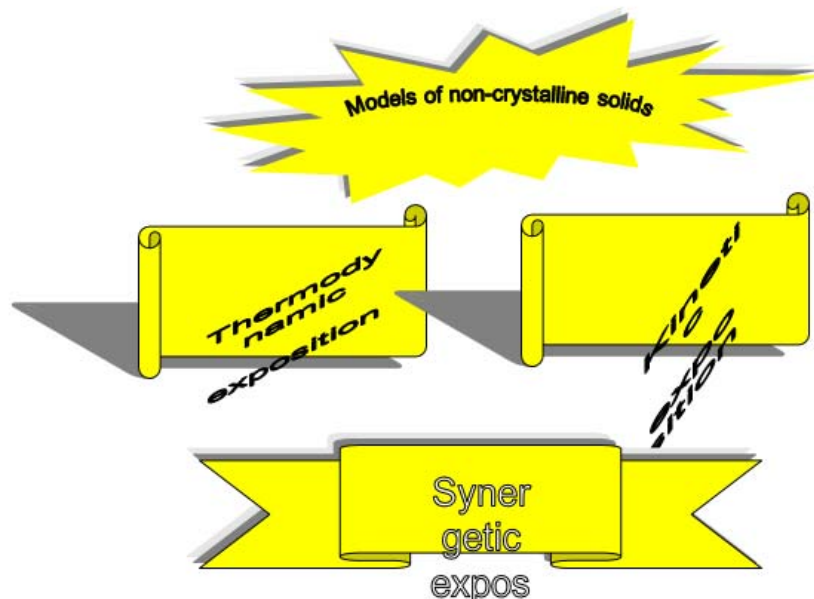


Fig. 3.1.1. Expositions of the non-crystalline state.

The first group models are founded on the thermodynamic exposition of non-crystalline skew fields. These models consider the thermodynamic properties of the systems at an inappreciable removal from balanced state in view of a particular degree of disorder. The given approach features a circle of appearances, which are determined by the behaviour of the structurally-responsive parameters, the thermodynamic functions in a transition range. Depending on the way a disorder is introduced into a system, they are subdivided into the next types:

- The models obtained by introducing the structural perturbations of ideally ordered structures (crystals). This class involves the models of the microcrystallites, hot solids, dislocations and random packing [4-6]. For most of them, it is assumed that the structural disordering combines the local violations of short-range order compared with the crystalline lattice matrix (violations of bond lengths and angles). Thus, for instance, the quasi-crystalline Gubanov's model assumes that the topological order in the crystalline lattice is retained. However, due to the bending and tension, it is so deformed that long-range order violation occurs at long distances (Fig. 3.1.2,a-b). The quasi-crystalline model also belongs to this class and considers the substance as the set of the crystallites, whose size is substantially larger in comparison with the free path length for electrons or phonons. In this case, the degree of the topological disordering is higher in the thin near-surface regions close to the crystallite boundaries, allowing one to consider the influence of the system dimension on the disordering degree [7-10].
- The models obtained by the randomly located structural units. This class comprises the hard-sphere close-packing models (the structural models of Bernal liquids, Fig. 3.1.2,c) [6,11,12]. By choosing the corresponding structural units and using the evolution procedure one can simulate physically available non-crystalline structures, in particular, the metal glasses. This class also comprises the cell disordering models, when physical properties of the structural matrix unit cells are not identical and vary in a random manner. The cell disordering is, for example, reduced to the substitutional disorder in the melts or A_xB_{x-1} -like compositions, when the regular alternation of A and B atoms and spin orientations in the lattice nodes are violated or the irregular distribution of different-type defects is observed (e.g., the vacancies, charged centres, etc.).

The models based on the numerical simulation by the "first principles". This class considers the methods of structural models construction by means of the computer modelling using the theoretical molecular dynamics apparatus and the theory-group analysis method [12-14]. Since the non-linear problems are solved analytically only in the specific cases, the computer modelling allows one to obtain a new instrument for the non-linear models studies (Fig. 3.1.2,d) [15].

- The continuum disordered models based on the structureless concept of solid, when the mass or potential energy distribution functions have a random and continuous character (Fig. 3.1.2,e). The macrostructure of the medium is ignored in this case. Thorp's model, which considers a substance as a family of spatial rigidity and non-rigidity domains, is one of the examples of such models [16,17]. The models are obtained by the topological mapping of the set of polyhedrons, which fill the space of the higher dimension of polytypes with a preset coordination of the structure under modelling onto the 3-D Euclidean space [18].

The models based on the kinetic (relaxational) approach belong to the second group [19-20]. The properties of non-crystalline media depend on the exterior factors (velocity of cooling, intensity of laser radiation), which means the presence of an interval of transition.

The two above concepts of exposition of non-crystalline solids reflect, at a first glance, two alternative approaches, each of them reflecting a particular circle of the experimental facts. The synergetic approach to the shaping and exposition of non-crystalline solid state enables to aggregate the indicated two concepts so that they do not exclude, but on the contrary, supplement each other [21-22]. Such an approach enables one to describe most adequately the structure and phase changes of the non-crystalline solid matter of an inorganic and organic origin that is a necessary stage in the transition from the lifeless to the alive nature. This is because synergetics takes into account the self-consistent interaction of all factors, both thermodynamic and dynamic. Within the framework of a given approach non-crystalline solid states are considered an outcome of the previous self-organization, during which the energy dissipation (transformation) is observed. This part of the book will be devoted to reviewing the given approach with a reference to media of an inorganic origin.

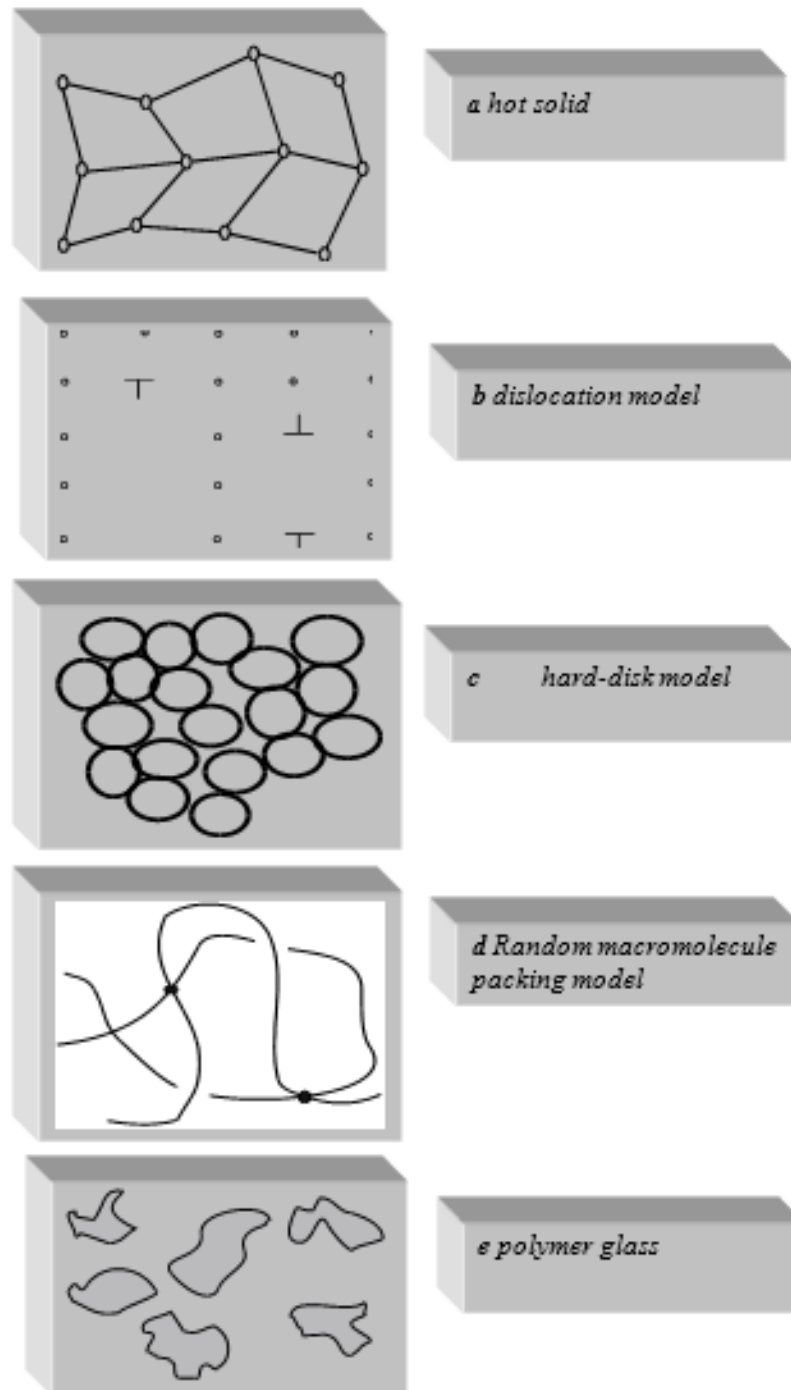


Fig. 3.1.2. The models of the non-crystalline materials.

3.2. Non-linear condensed media dynamics

3.2.1. Phase transition simulation in the system close to the equilibrium state and away from this state

As the temperature of the solid is elevated to the melting temperature, the concentration of point defects (of the interstitial atom (vacancy) type) or extended defects (of the dislocation type) increases sufficiently. Such defects taken separately are not the disordered phase nuclei. However, if they are accumulated within a certain macroscopic domain, then such area of disordering corresponds to the structure inherent to the liquid-like (soft) states, i.e. it has a shearing instability,

a high level of dynamic displacements and the instability related to the defect formation. Hence, within the phase transformation interval along with homogeneous fluctuations (i.e. the thermal displacements of atoms) the effect of heterophase fluctuations increases, being the formation of the liquid-like macroscopic domains inside the solid-phase state under study [21,22]. The schematic of the potential relief of that system is shown in Fig. 3.2.1 (*a* denotes the solid-like localized states, while *b* corresponds to the liquid-like delocalized (soft) states).

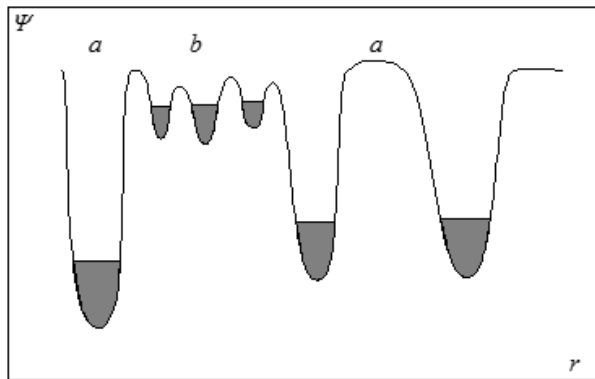


Fig. 3.2.1. Schematic of the potential relief of mixed systems: *a* – crystal-like states; *b* – liquid-like states.

The "soft" states are specific structural states with an additional degree of freedom in the configurational space. These states exist due to the spatial fluctuations of the short-range order parameters (the number and the length of the bonds, the inter-bond angles) near their average values and the formation of the defect states in the highly non-equilibrium conditions. They are intrinsic for non-crystalline solids. Atoms in the "soft" states possess a considerable level of static displacements and, consequently, the vibrational anharmonism and the ability to create spatial rearrangements. The bonding topology and the configurational parameters which describe the "soft" states, are accounted for and detailed in terms of certain structural models. We shall analyze the general tendencies of the formation of the macroscopically ordered structures in the non-crystalline solids away from the equilibrium state. Therefore, we shall use the universal characteristics of the "soft" states.

Now a reasonably large number of the experimental data are available allowing one to state that the structural formations of a certain chemical composition may exist within the $T < T_m$ temperature range as well as in the melt or in the non-crystalline solid [23,24]. The presence of heterophase fluctuations is confirmed by the studies of the semiconductor melts, the viscosity coefficient and the internal friction at the vitrification of liquid as well as by the Mossbauer spectroscopy, Raman spectroscopy and the X-ray structural analysis data [23-28]. The probability of the heterophase fluctuation formation and the relationship between various microscopic states are defined by conditions of the interphase equilibrium for the equilibrium phase transformation [22] and by the degree of deviation from the equilibrium state for highly non-equilibrium transformations [29,30].

Consider the system of N similar atoms of mass M , the portion N_1 of which being in the solid-like state and the portion $N_2 = N - N_1$ being in the liquid-like state. The Hamiltonian H of the system can be presented within the binary atom interaction approximation in the following form:

$$H = \sum_{l=1}^N \sum_f T_f(l) \sigma_f(l) + \frac{1}{2} \sum_{l \neq l'} \sum_{f, f'} \Phi_{ff'}(\vec{r}_{ll'}) \sigma_f(l) \sigma_{f'}(l'), \quad (3.2.1)$$

where $T_f(l) = \frac{\vec{P}^2(l)}{2M}$ is the kinetic energy of the l -th atom, $\vec{P}(l)$ is the momentum of the l -th atom, $\Phi_{ff'}(\vec{r}_{ll'})$ is an interatomic interaction potential, $\vec{r}_{ll'}$ is the interatomic distance and $\sigma_f(l)$ characterises two sets f of locally observed microscopic states:

$$\sigma_f(l) = \begin{cases} 1, & \text{if the atom } l \text{ is in the state } f; \\ 0, & \text{if the atom } l \text{ is not in the state } f. \end{cases}$$

The possibility of the formation of the liquid-like states in the solid is, consequently, $\sigma_f = \langle \sigma_f(l) \rangle = N_f / N$. Let us introduce the effective Hamiltonian \tilde{H} of the system (see Appendix 1):

$$\begin{aligned} \tilde{H} &= \sum_f H_f + (1 - \sigma_2)^2 \sum_{l, l', \alpha} \tilde{I}_\alpha(l, l') v_\alpha(l), \quad v_\alpha(l) = \sum_m v_\alpha(l/m) \sigma_2(m), \\ H_f &= \sigma_f \sum_l T_f(l) + \frac{\sigma_f^2}{2} \sum_{l, l'} \sum_{\alpha, \beta} \left[\Phi(\bar{R}_{ll'}) + \frac{1}{2} u^\alpha(l, l') \tilde{\Phi}_f^{\alpha\beta}(l, l') u^\beta(l, l') \right], \end{aligned} \quad (3.2.2)$$

where $\tilde{\Phi}_f^{\alpha\beta}(l, l')$, $\tilde{I}_\alpha(l, l')$ is the self-consistent potential interaction, $\vec{r}_l = \bar{R}_l + \vec{u}_l + \vec{v}_l$ is a radius-vector of l -th atom, \bar{R}_l is the average equilibrium position of the l -th atom, \vec{u}_l and \vec{v}_l are the dynamic and the static displacements of the l -th atom, respectively, $u_\alpha(l, l') = u_\alpha(l) - u_\alpha(l')$ are the relative displacements, $v_\alpha(l/m)$ are the static displacements of the l -th atom when the m -th atom is in the liquid-like state. The model parameters, i.e. the fraction of atoms in the liquid-like states σ_f , the force constants $\tilde{\Phi}_f^{\alpha\beta}(l, l')$ and the mean-square relative displacements of atoms $y_{\alpha\beta}(l, l') = \langle u^\alpha(l, l') u^\beta(l, l') \rangle$ in equation (3.2.2) are calculated on the basis of the variational principle for the free energy functional:

$$F \leq F_0 + \langle H - \tilde{H}_0 \rangle_0, \quad F_0 = \sum_f F_{0f} - TS, \quad F_{0f} = -\Theta \ln \left\{ SP \left(e^{-\frac{H_f}{\Theta}} \right) \right\}. \quad (3.2.3)$$

Here F_0 is the free energy functional for the effective Hamiltonian, $S = -k_B \ln \left[\prod_f \left\{ \frac{g_f!}{N_f! (g_f - N_f)!} \right\} \right]$ is the entropy, g_f is a statistical weight of the state f , $\Theta = k_B T$. The variation of F over the parameters σ ($\sigma \equiv \sigma_2$), $\tilde{\Phi}_f^{\alpha\beta}(l, l')$, $y_{\alpha\beta}(l, l')$ at fixed temperature T and pressure P :

$$\delta F = \left[\frac{\partial F}{\partial \sigma} \right]_{y_{\alpha\beta}, \tilde{\Phi}_f^{\alpha\beta}} \cdot \delta \sigma + \left[\frac{\partial F}{\partial \tilde{\Phi}_f^{\alpha\beta}} \right]_{\sigma, y_{\alpha\beta}} \cdot \delta \tilde{\Phi}_f^{\alpha\beta} + \left[\frac{\partial F}{\partial y_{\alpha\beta}} \right]_{\sigma, \tilde{\Phi}_f^{\alpha\beta}} \cdot \delta y_{\alpha\beta} \quad (3.2.4)$$

allows one to determine their temperature dependence for the equilibrium ($\delta F = 0$) and non-equilibrium ($\delta F \neq 0$) transformations (see Appendix 2).

Consider the application of the above concepts to the studies of the stable and metastable states formation in the certain solid-state model. Let us describe the interatomic interaction through the effective pair potential of the following type:

$$\Phi(r) = \Phi_1(r) + \Phi_2(r), \quad (3.2.5)$$

where its short-range component $\Phi_2(r)$ can be approximated by the hard-sphere potential ($\Phi_2(r) = \Phi_0$ at $r < a$ and $\Phi_2(r) = 0$ at $r > a$, a is an average interatomic distance) and the long-range

component $\Phi_l(r)$ can be presented in the form of a sum of the central Morse-like potential $\Psi(r) \left(\Psi(r) = V_0 \left[\exp\left\{-12\frac{r-a}{r}\right\} - 2\exp\left\{-6\frac{r-a}{r}\right\} \right] \right)$ and the non-central potential $G(\delta) \left(G(\delta) = -G_0 \exp\left\{-4\left(\frac{\delta}{a}\right)^2\right\} \right)$, where δ is the deflection of the atom in the plane normal to the direction of the bond, G_0 and V_0 are the potential parameters. Calculating the self-consistent interaction potentials $\tilde{\Psi}(r)$ and $\tilde{G}(\delta)$:

$$\begin{aligned} \tilde{\Psi}(r) &= V_0 \left[\exp\left\{-12\frac{r-a}{r}\right\} \exp\{2y_l\} - 2\exp\left\{-6\frac{r-a}{r}\right\} \exp\left\{\frac{y_l}{2}\right\} \right], \\ \tilde{G}(\delta) &= -\frac{G_0}{1+2y_l} \exp\left\{\frac{-4\left(\frac{\delta}{a}\right)^2}{1+2y_l}\right\}, \end{aligned} \quad (3.2.6)$$

and using the conditions of the quasi-equilibrium of the solid at the presence of the external pressure ($P = -\frac{zN(1-\sigma)^2 r \Psi'(r)}{V}$, V is the volume of the solid, z is the number of the closest neighbours, $y_l = \frac{36y_l(0,l)}{a^2}$, $y_t = \frac{4y_t(\delta)}{a^2}$ are the reduced mean-square displacements of atoms along the bond and normally to it, respectively), it is possible to determine the average interatomic distance. Here, one has to take into account that the volume of the most of the solids increases with the transition to the liquid phase (exceptions are the ice, bismuth and some other substances) and the liquid retains the short-range order.

Then the interatomic distance r is:

$$r = a \left(1 + \frac{y_l}{4} - \frac{1}{6} \ln \left\{ \frac{B(y_l)}{2} \right\} \right), \quad (3.2.7)$$

where $B(y_l) = 1 + \left[\frac{P^* r^2 e^{y_l}}{6(1-\sigma)^2 a^2} \right]^{\frac{1}{2}}$ is a parameter of non-linearity, $P^* = \frac{PV}{6zNV_0}$ is a reduced pressure.

Hence, the effective force constants $\tilde{f}(r)$ and $\tilde{g}(r)$ are:

$$\begin{aligned} \tilde{f}(r) &= (1-\sigma)^2 \tilde{\Psi}''(r) - \frac{\eta_\Phi}{\tau_\Phi}, \quad \tilde{g}(r) = (1-\sigma)^2 \tilde{G}''(r) - \frac{\eta_G}{\tau_G} \\ g &= \frac{8G_0}{a^2}, \quad f = \frac{72V_0}{a^2}. \end{aligned} \quad (3.2.8)$$

Here f and g are the force constants, η_Φ and η_G are the order parameters, τ_Φ and τ_G are the relaxation times, $\tilde{\Psi}''(r)$ and $\tilde{G}''(r)$ are the second derivative $\tilde{\Psi}$ with respect to r .

Similarly, we define the self-consistent potential energy $\tilde{\Phi}_1, \tilde{\Phi}_2, \tilde{I}$ of the system:

$$\frac{\tilde{\Phi}_l}{N} = -\frac{z}{2} \left\{ V_0 e^{-y_l} \left[B(y_l) - \frac{P^* r^2 e^{y_l}}{12(1-\sigma)^2 a^2} \right] + \frac{G_0}{1+2y_l} \right\}, \quad \frac{\tilde{\Phi}_2}{N} = \frac{\varphi}{2}. \quad (3.2.9)$$

$$\frac{\tilde{I}}{N} = \frac{z}{2} \Psi' [r - v_r] v_r = \frac{6V_0 z}{\alpha} v_r \times \left[\exp\{-12(r - \alpha - v_r)/r\} \exp\{2y_l\} - \exp\{-6(r - \alpha - v_r)/r\} \exp\{y_l/2\} \right] \quad (3.2.10)$$

where $\varphi = \int \Phi_2(r) dr$ is a potential of the "soft" states.

Thus, using the expressions (3.2.8) to (3.2.10), we arrive at the following self-consistent system of equations with respect to the fraction of atoms in the "soft" states and the mean-square displacements:

$$F_1(\sigma) = \sigma \xi_p + (1 - \sigma) z \left\{ \frac{e^{-y_l}}{2} \left[B(y_l) - \frac{P^* e^{y_l}}{12(1 - \sigma)^2} \left(\frac{r}{a} \right)^2 \right] + \frac{G_0}{(1 + 2y_l)} \right\} - z(1 - \sigma) \sigma \left(1 + \frac{y_l}{4} - \frac{1}{6} \ln \frac{B(y_l)}{2} \right) A(y_l) - \tau \ln \frac{\frac{g_2}{\sigma} - 1}{\frac{g_1}{1 - \sigma} - 1} + \tilde{a}_0 \tilde{q} \eta - c \eta^2 - b \eta^3 = 0, \quad (3.2.11)$$

$$F_2(y_l) = \frac{3e^{-y_l} \tau}{8\sqrt{2}(1 - \sigma)} \left[B(y_l) + \frac{P^* e^{y_l}}{6(1 - \sigma)^2} \left(\frac{r}{a} \right)^2 \right]^{-1} \left(1 + \frac{0.022(1 + 2y_l)^{-2}}{e^{y_l} \left[B(y_l) + \frac{P^* e^{y_l}}{6(1 - \sigma)^2} \left(\frac{r}{a} \right)^2 \right]} \right) - \quad (3.2.12)$$

$$- y_l - \frac{\eta_{y_l}}{\tau_{y_l}} = 0,$$

$$F_3(y_l) = \frac{3(1 + 2y_l) \tau}{8(1 - \sigma) e^{\frac{y_l}{2}}} \left[B(y_l) + \frac{P^* e^{y_l}}{6(1 - \sigma)^2} \left(\frac{r}{a} \right)^2 \right]^{\frac{1}{2}} - y_l - \frac{\eta_{y_l}}{\tau_{y_l}} = 0. \quad (3.2.13)$$

Here $F_1(\sigma), F_2(y_l), F_3(y_l)$ are non-linear functions, $\tau = \frac{\Theta}{V_0}$ is a reduced temperature, $\xi_p = \frac{\varphi}{V_0}$ is a parameter of anisotropy potentials,

$A(y_l) = 0.62 \left[\exp\left\{ 0.36 - 0.91y_l + 1.94 \ln \frac{B(y_l)}{2} \right\} - \exp\left\{ 0.18 - 0.955y_l + 0.97 \ln \frac{B(y_l)}{2} \right\} \right]$ is a parameter, and the allowance was made for that $G_0/V_0 \approx 0.1$ and the static displacements are $v_r \approx 3 \cdot 10^{-2} r$ [22,23].

The first derivative $\tilde{F}'(\sigma)$ with respect to σ :

$$F_1'(\sigma) = \tilde{a}_0 \tilde{q} + \xi_p - z \left\{ \frac{e^{-y_l}}{2} \left[B(y_l) - \frac{P^* e^{y_l}}{12(1 - \sigma)^2} \left(\frac{r}{a} \right)^2 \right] + \frac{G_0}{(1 + 2y_l)} \right\} - z(1 - 2\sigma) \left(1 + \frac{y_l}{4} - \frac{1}{6} \ln \frac{B(y_l)}{2} \right) A(y_l) - \tau \ln \frac{\left(\frac{g_2}{\sigma} - 1 \right) \frac{g_1}{(1 - \sigma)^2} - \frac{g_2}{\sigma^2} \left(\frac{g_1}{1 - \sigma} - 1 \right)}{(g_1/(1 - \sigma) - 1)^2} = 0. \quad (3.2.14)$$

The critical temperature at which $a(T_c, P_c, q_c) = 0$ and $c(T_c, P_c, q_c) = 0$, is defined, respectively, by the solution of equations (3.2.11), (3.2.14) and the second derivative with respect to σ :

$$2z \left(1 + \frac{y_l}{4} - \frac{1}{6} \ln \frac{B(y_l)}{2} \right) A(y_l) - \tau \ln \frac{\left(\frac{g_2}{\sigma} - 1 \right) \frac{g_1}{(1-\sigma)^2} - \frac{g_2}{\sigma^2} \left(\frac{g_1}{1-\sigma} - 1 \right)}{(g_1/(1-\sigma) - 1)^4} = 0.$$

For the equilibrium transition "crystal–liquid", the ab area corresponds to the crystalline state (see Figs. 3.2.2, 3.2.3), the ef area denotes the liquid and bc , de areas correspond to the metastable states, i.e. to the overheated crystal and the overcooled liquid, respectively. With the temperature of the solid approaching the reduced melting temperature τ_m determined on the basis of the relation $F_1 = F_2$, a sharp increase in the mean-square displacement of atoms is observed (at the ab area we have $y_l \approx 0.3-0.5$, $y_t \approx 0.1-0.12$ and the amplitudes of vibrations are $(u_t^2)^{1/2} \approx (0.12-0.14)a$, $(\varphi^2)^{1/2} \approx (7-9)^\circ$ that results both from the anharmonism of atom vibrations, formation of more and more abundant and large domains of the "soft" states and the relevant increase in the fraction of atoms at $\tau \rightarrow \tau_m$, $\sigma(\tau_m) \approx 0.07$). It should be noted that τ_m increases with P^* :

$$\tau_m \approx 0.52(1 + 0.34P^*)$$

and approaches the melting curve for the real solids [23].

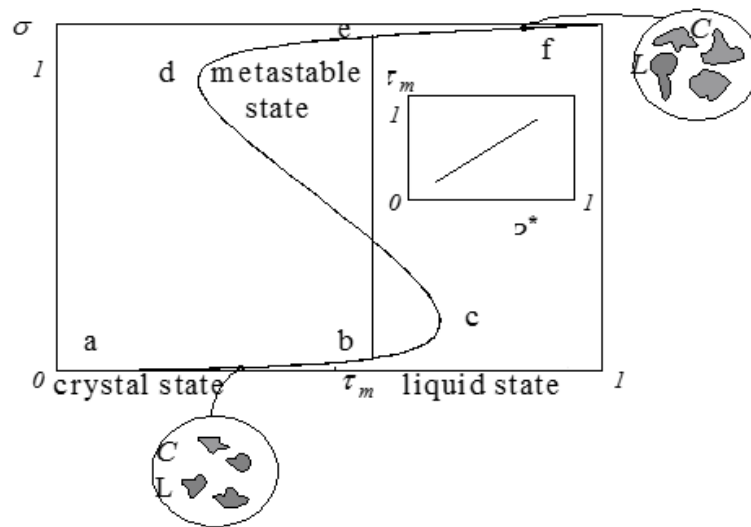


Fig. 3.2.2. The temperature dependence of the fraction of atoms in the „soft“ states at $q=-1$.

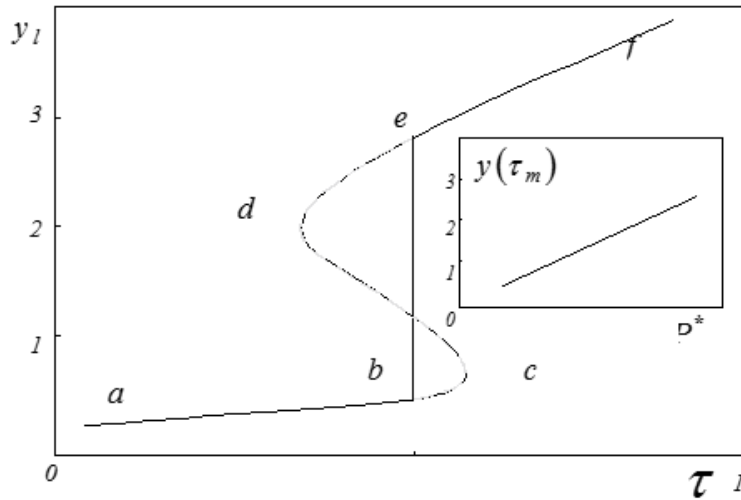


Fig. 3.2.3. The temperature dependence of the reduced mean-square displacements of atoms along the bond y_l at $q=-1$ and at different pressures.

Hand in hand with this, force constants decrease self-consistently. As $\tau > \tau_m$, the dynamic displacements of atoms increase essentially that governs the spasmodic rise of the fraction of atoms in the "soft" states and, consequently, the reduction of the force constants. Thus, the force constants of the central interaction of atoms, \tilde{f}/f , decrease by two orders during the transition to the melt, while a shear component of the interaction becomes almost zero ($\tilde{g}/g \approx 10^{-4}$) (see Figs. 3.2.4 – 3.2.6). It should be noted that the structural changes also occur during the transition to the melt as evidenced by the retention of the solid-like states ($\sigma(\tau > \tau_m) \approx 0.99$), for which the short-range order parameter fluctuations are slightly increased compared with the crystalline state.

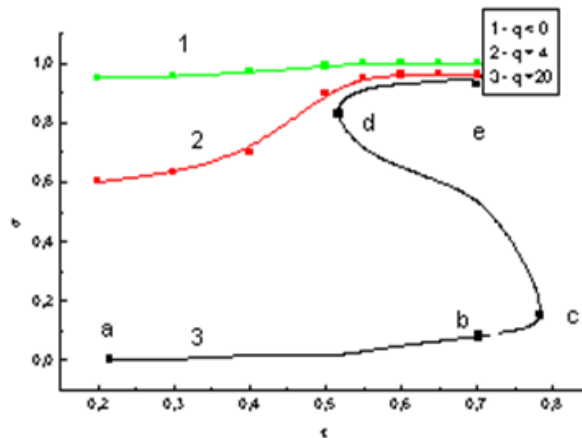


Fig. 3.2.4. The temperature dependence of the fraction of atoms in the "soft" states at different \tilde{q} .

At $\tilde{q} < q_c$, in the region of the transition temperature τ_m , the probability of the formation of the "soft" states and mean-square displacements of atoms undergo the leap, whose value decreases with \tilde{q} .

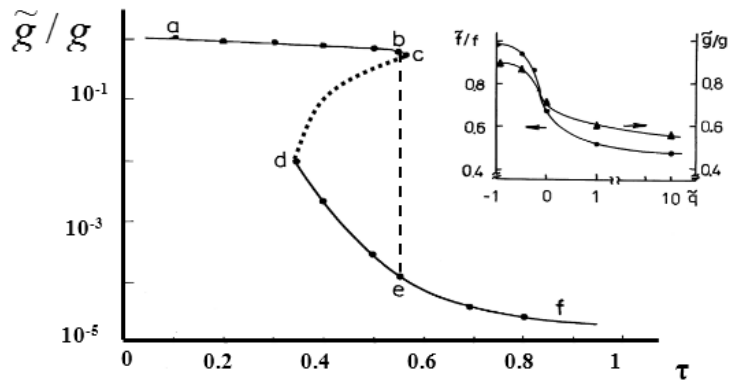


Fig. 3.2.5. Force constants of the \tilde{g}/g and \tilde{f}/f as the functions of τ .

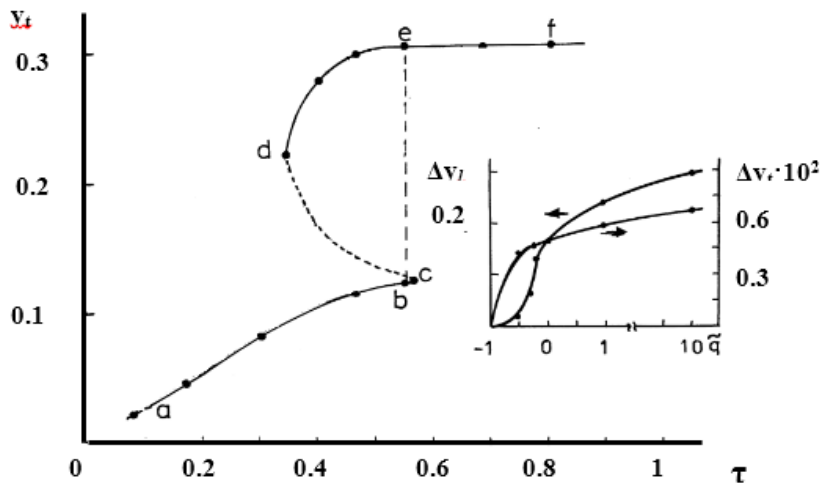


Fig. 3.2.6. The temperature dependence of the reduced mean-square displacements of atoms normally to the bond y_l at $\tilde{q} = -1$ and at different \tilde{q} .

3.2.2. The dissipative structure formation in the non-crystalline condensed matter

Let us analyze the temperature behaviour of the solutions of the system of equations (3.2.12) to (3.2.14) in highly non-equilibrium conditions, i.e. at $\tilde{q} \rightarrow \tilde{q}_c$. The temperature dependence of the fraction of atoms in the "soft" states and mean-square atom displacements have two specific domains. The first corresponds to the system cooling at $\tilde{q} < \tilde{q}_c$, when the transition to the solid state occurs with the spasmodic increase in the elastic constants and the decrease in the fraction of atoms in the "soft" states and mean-square atom displacements. Note that the value of the leap decreases with increasing \tilde{q} . The second domain observed at $\tilde{q} > \tilde{q}_c$ is characterized by the continuous anomalous increase, the development of a shear rigidity of the structure and the elastic constants, as well the continuous reduction of σ , y_l (see Figs. 3.2.7, 3.2.8). Consequently, the curve at $\tilde{q} = \tilde{q}_c$ demarcates the region of the existence of metastable (i.e. the overcooled liquid) and highly non-equilibrium (non-crystalline) condensed systems.

It defines the lower limit of the possible reduction of the mean-square atom displacements and the fraction of atoms in the "soft" states in the temperature range above τ_0 at $\tilde{q} < \tilde{q}_c$ (τ_0 is the temperature of synthesis, Fig. 3.2.9). The temperature τ_c in the curve \tilde{q}_c , at which metastable states are degenerated, is the temperature of coexistence of three states at a preset pressure, i.e.

crystalline, liquid and non-crystalline states: $\left(\frac{\partial^2 \sigma}{\partial \tau^2}\right)_{\tau_c} = 0$. The studies of the peculiarities in the behaviour of the thermodynamic properties of the system in the vicinity of $\{\tau_c, q_c\}$ are of doubtless interest. Note that the correlated reduction of the intensity of atom vibrations and the rise of the force constants at the transition from the metastable overcooled melt to the non-crystalline solid gives evidence for the occurrence of the collective macroscopic processes at the microstructural rearrangement level at which the non-crystalline structure with the inner order parameter \tilde{q} is formed depending on the control parameter values \tilde{q} . The order parameter used determines the degree of system deviation from the equilibrium state and correlates, in particular, with the fluctuations of system deviation from the Gaussian distribution. The non-equilibrium stationary structure produced at $\tilde{q} > \tilde{q}_c$ results from the instability of the ground thermodynamically non-equilibrium state and arises through the self-consistent enhancement of fluctuations (the mean-square atomic displacements and the fraction of atoms in the "soft" states) which reach the macroscopic level and make a new structure stable. That structure is a dissipative one.

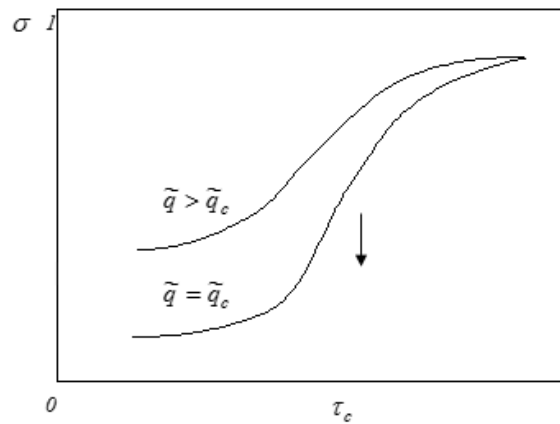


Fig. 3.2.7. The temperature dependence of the fraction of atoms in the „soft“ states at $(\tilde{q} \rightarrow \tilde{q}_c)$.

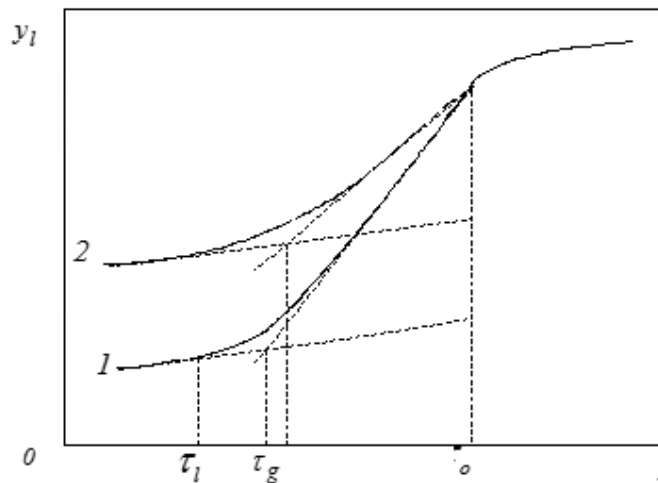


Fig. 3.2.8. The temperature dependence of the reduced mean-square atom displacements along the bond $y_l(a)$ at $(\tilde{q} \rightarrow \tilde{q}_c)$.

Indeed, when the melt is cooled down under highly non-equilibrium conditions, the part of the energy of the system, which is related to the thermal motion of particles, is transformed into the macroscopically organised motion due to the spatial-temporal correlations at the macroscopic scale. This motion is transformed into the parameter fluctuations (i.e. interatomic distances, inter-

bond angles), related to the static displacements of atoms under cooling, on \tilde{q} , one may take the value of thermal displacements of particles in the system in the equilibrium state as the counting level, i.e. $\Delta y_i(\tilde{q}) = y_i(\tilde{q}) - y_i(\tilde{q} = -1)$. The corresponding dependences $\Delta y_i(\tilde{q})$, $\Delta \sigma(\tilde{q})$ at $\tau = 0.1$ are shown in Fig.3.2.9. As seen, the degree of disordering increases with \tilde{q} and, moreover, a sharp increase is observed as we approach the region of the transition to the non-crystalline state from the overcooled liquid side. It gives a way to the quasi-linear dependence for the systems in the interval of \tilde{q} values under study. Therefore, those properties which are proportional to σ , y_i (e.g., the volume of the solid), also undergo the leap at $\tau = \tau_m$, and the properties defined by the increments $\frac{d\sigma}{d\tau}$, $\frac{dy_i}{d\tau}$, (e.g., the heat expansion coefficient and heat capacity) tend to infinity (Fig. 3.2.10).

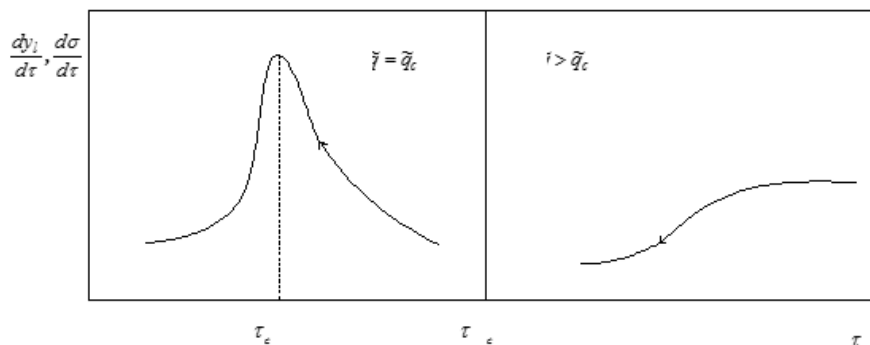


Fig. 3.2.9. The temperature dependences $\frac{d\sigma}{d\tau}$ (a), $\frac{dy_i}{d\tau}$ (b) at the transition to the non-crystalline state ($\tilde{q} \rightarrow \tilde{q}_c$).

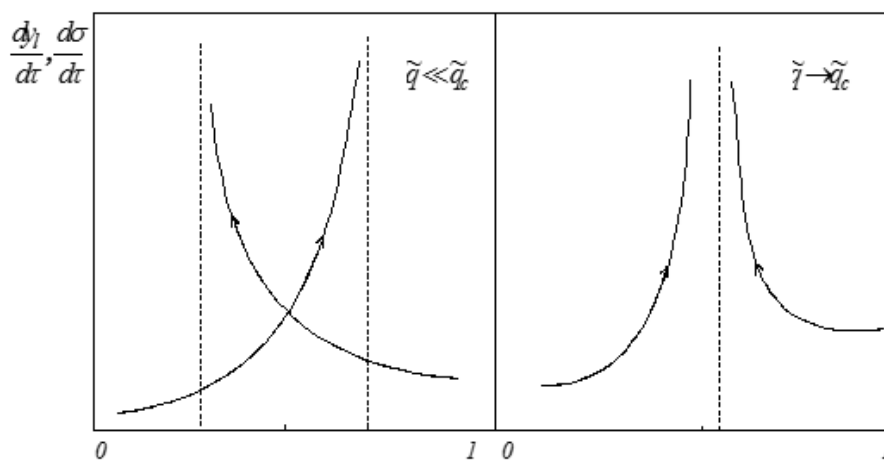


Fig. 3.2.10. The temperature dependences $\frac{d\sigma}{d\tau}$ (a), $\frac{dy_i}{d\tau}$ (b) at different melt cooling rates ($\tilde{q} \ll q_c$).

It should be noted that the type of dependence of the disordering degree on \tilde{q} in non-crystalline solids correlates with the variations of the elastic constants \tilde{f}/f , \tilde{g}/g at the given temperature, when they decrease with increasing \tilde{q} and the structure of the material becomes more easily rearranged under the influence of the external factors. This approach allows the temperature behaviour of both the microscopic and macroscopic parameters (e.g., volume) to be evaluated quantitatively for the case of cooling. The temperature-dependence of the volume reduced to that of the solid at the temperature of synthesis τ_0 is plotted in Fig. 3.2.11. System cooling at low rates $\tilde{q} < \tilde{q}_c$ initiates the spasmodic reduction of V at the transition to the solid state (the volume of the

solid- phase state increases slightly with \tilde{q}). During cooling in the $\tilde{q} > \tilde{q}_c$ conditions, which prevent the crystallization process, the volume of the solid varies continuously and the value of V is determined by the cooling rate. Thus, the peculiarities of the formation of the non-equilibrium stationary state structure depending on the control parameters have been considered within the limits of the present concept.

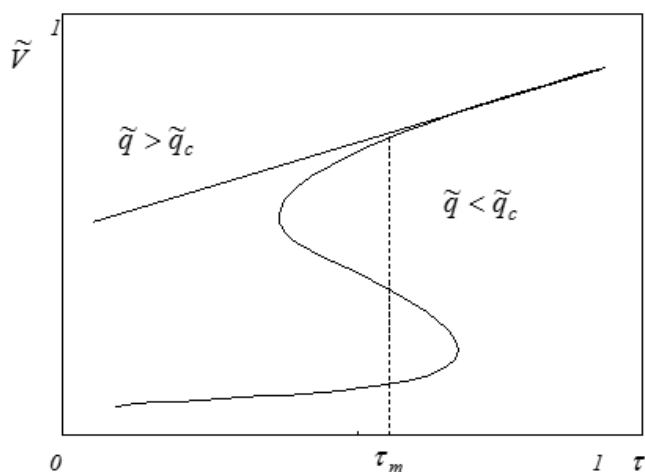


Fig. 3.2.11. The temperature dependence of the reduced volume of the non-crystalline solid.

3.3.2. Bifurcation diagram of the transition to the non-crystalline state

The vitrification process can be considered the cooperative self-organized process. Indeed, the conditions of the occurrence of self-organized structures are as follows [22]:

- the system must be thermodynamically open, i.e. it has to exchange the energy or the matter with environment;
- the state of the system should be far from the thermodynamic equilibrium;
- the structure self-organization has a threshold nature and the behaviour of subsystems forming the system must be consistent;
- the dynamic equations of the system are non-linear and stochastic.

Let us analyze how these requirements hold true in the process of non-crystalline structure formation:

- the technological process of melt cooling and vitreous structure formation takes place in the thermodynamically open system, which exchanges the energy with environment;
- the glass is produced in the system far away from the equilibrium state (melt). The degree of the displacement can be defined by the order parameter calculated as the deviation of a fraction of atoms in the soft configurations of the system (amplitudes of dynamic displacements or force constants) from the corresponding values for the equilibrium state;
- non-crystalline material formation has a threshold character over the dynamic displacement amplitudes and the fraction of atoms in the soft configurations. These materials are produced only at the certain control parameter values (for example, the cooling rate);
- during the glass formation the self-consistent interaction of different subsystems takes place that governs the non-linearity of the system behaviour. A glass as a synergetic system offers stochasticity, i.e. the time evolution of the system depends on the reasons not predicted with absolute accuracy;
- a non-crystalline structure produced from the melt is a more ordered structure compared with the initial (melt) state (the spatial-temporal correlation of the motion of atoms and their groups is considerably larger).

Based on the aforementioned, we shall analyze the peculiarities of the qualitative variation of the system under the control parameter (i.e. the melt cooling rate) variation. Let us rewrite the equation of motion for the order parameter η in the following form:

$$\frac{\partial \eta}{\partial t} = \Phi(\eta, \tilde{q}), \quad \Phi(\eta, \tilde{q}) = a_0 \tilde{q} \eta - c \eta^2 - b \eta^3. \quad (3.2.15)$$

Here, we assume that $a = a_0 \tilde{q}$, and this holds in the vicinity of \tilde{q}_c , c and b are the constants, $\Phi(\eta, \tilde{q})$ is a non-linear function; for large \tilde{q} we can use the approximation $a = a_0 \arctan(\ln\{1 + \tilde{q}\})$ [22]. The characteristic equation for the asymptotically stable stationary states has a form:

$$\bar{\Phi}(\eta, \tilde{q}) = 0, \quad \bar{\Phi}'_\eta(\eta, \tilde{q}) < 0, \quad (3.2.16)$$

where $\bar{\Phi}'_\eta(\eta, \tilde{q})$ is the first derivative with respect to η .

The inequality in (3.2.15) is the condition for the stability of Lyapunov's solution of equation (3.2.16) [31]. The values $\eta \geq 0$ have the physical sense for the solid-phase state, since only these values correspond to the real amplitudes of stationary solutions. From (3.2.15) it is obvious that in the $\{\eta, q\}$ plane, the bifurcation diagram is transformed into a straight line $\eta = 0$ and the second-order curve:

$$a_0 \tilde{q} - c \eta - b \eta^2 = 0.$$

Two bifurcation values of the parameter \tilde{q} exist for the problem under consideration:

$$\tilde{q}_1 = \frac{-c^2}{4a_0 b}, \quad \tilde{q}_2 = 0.$$

At $\tilde{q} < \tilde{q}_1$, the equation has a sole stable root $\eta = 0$ ($\bar{\Phi}'_\eta(\eta, \tilde{q})_{\eta=0} = a_0 \tilde{q} < 0$), which corresponds to the stable focus (Fig. 3.2.11). When \tilde{q} passes the bifurcation value, a couple of non-zero solutions arise (the boundary cycles, whose radii are $\eta = |c| + \frac{\sqrt{c^2 + 4a_0 \tilde{q} b}}{2b}$ and $\eta = |c| - \frac{\sqrt{c^2 + 4a_0 \tilde{q} b}}{2b}$). One of these cycles (with a larger radius, the upper branch b , Fig. 3.2.11) is stable ($\bar{\Phi}'_\eta(\eta, \tilde{q}) \leq 0$), whereas the second one (with a smaller radius η , b' branch, Fig. 3.2.11) is unstable ($\bar{\Phi}'_\eta(\eta, \tilde{q}) > 0$). The character of the singular point $\eta = 0$ is not changed in this case. A stable cycle increases with \tilde{q} , while an unstable one decreases. At the second value of bifurcation parameter $\tilde{q} = 0$, an unstable cycle vanishes, merging with the singular point, which becomes unstable as $\tilde{q} > 0$ ($\bar{\Phi}'_\eta(\eta, \tilde{q})_{\eta=0} > 0$).

Thus, at low melt cooling rates ($\tilde{q} < 0$), the dynamic equation has a sole solution, which corresponds to the crystalline state that is asymptotically stable at $t \rightarrow \infty$. At the cooling rates above the critical velocity ($\tilde{q} > \tilde{q}_1$) the solution that belongs to the branch a is bifurcated (i.e. it becomes unstable with respect to the fluctuations of dynamic displacements of atoms and the fraction of atoms in the soft configurations [32-37]), and the system tends to the stationary non-crystalline state (branch b , Fig. 3.2.11) with the spasmodic change of the order parameter η at the microscopic level. If the melt is cooled with the rate of $\tilde{q}_1 < \tilde{q} < \tilde{q}_2$, then, to ensure the development of the system towards the non-crystalline state, one has to create a certain non-equilibrium in this system (e.g., induced by annealing or irradiation), at which the deviation of the equilibrium state η will exceed the distance from an unstable branch (Fig. 3.2.12). The result obtained, i.e. the possibility of the occurrence of at least two stable states differing in the order parameter values, η ,

in the non-crystalline material at the same control parameter, temperature or pressure, is a measure of the dependence of the final state of the non-equilibrium system on the method of production, i.e. on the system prehistory.

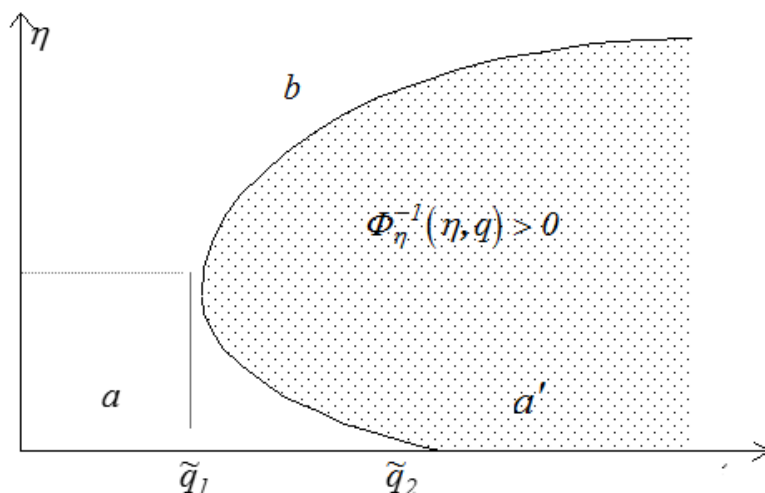


Fig. 3.2.12. Branching of the solutions of the characteristic equation (*a* – a stable part of the state, *a'* – an unstable part of the equilibrium liquid state, *b* – a non-equilibrium stationary state).

The equation of motion for the order parameter $\partial F / \partial \eta = -\gamma \partial \eta / \partial \alpha$ (γ is constant) allows Lyapunov's functional to be determined:

$$F(t) - F(0) = -q \int_0^t \left(\frac{\partial \eta}{\partial \alpha} \right) dt,$$

where the allowance was made for $q = dT/dt$. The multi-stability phenomenon is observed, i.e. the spatial distribution of η , which corresponds to one of the minima of F , is set depending on the initial conditions and the control parameter (Fig. 3.2.13). Typical time dependences of Lyapunov's functional at $x = \eta \cos t$, $\dot{x} = -\eta \sin t$ (t is the time) in the vicinity of the stationary solutions η are presented in Fig. 3.2.14.

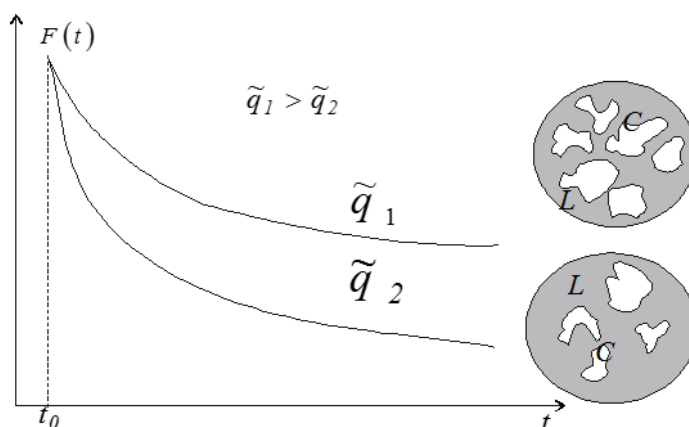


Fig. 3.2.13. Lyapunov's functional as a function of time at different control parameters.

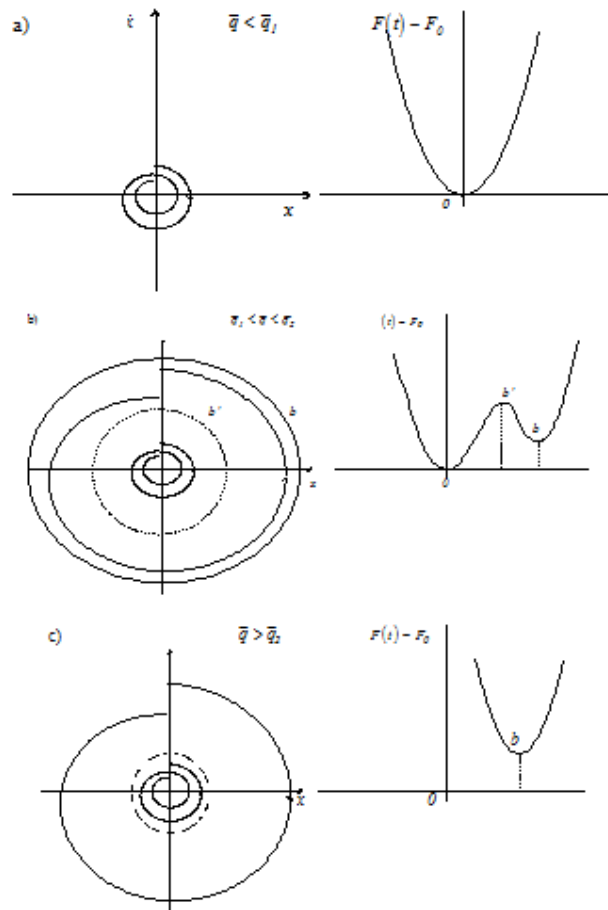


Fig. 3.2.14. Time dependences of the parameter of Lyapunov's functional deviation from the equilibrium state in the vicinity of different bifurcation points: a - a stable focus at $\tilde{q} < \tilde{q}_1$; b - boundary cycles at $\tilde{q} < \tilde{q}_1$.

Given the instability chain, the number of paths to the different states and corresponding dissipative structures increases sharply. The choice of the path is arbitrary, but the non-equilibrium system memorizes this choice. Possible bifurcation cascades and transitions to the stationary non-equilibrium structures are shown qualitatively in Fig. 3.2.15. At $\tilde{q} < \tilde{q}_1$, only one stationary state exists for any \tilde{q} . For $\tilde{q} = \tilde{q}_1$ at any \tilde{q} , the primary bifurcation occurs, i.e. those states, which belong to the branch a , become unstable, whereas two other solutions (branches b and b') appear to be possible. At $\tilde{q} < \tilde{q}_3$, the branch b becomes unstable and two other stable branches (c and c') arise, and so on. That situation may occur, for instance, when the time dependence of the cooling rate is varied during the cooling process.

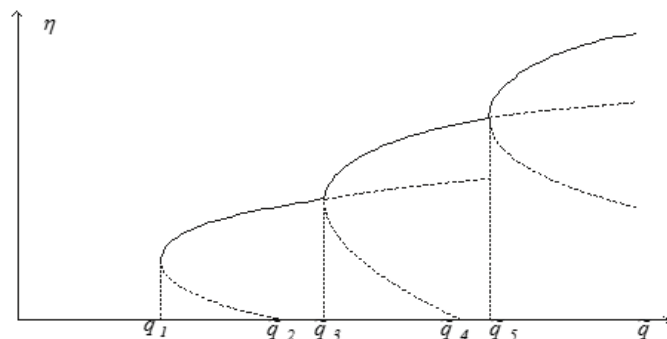


Fig. 3.2.15. The bifurcation diagram of the transition to the non-crystalline state in case of the bifurcation cascade.

Consider the influence of non-locality of the system order parameter η distribution. In that case, equation (3.2.16) assumes the form:

$$\frac{\partial \eta}{\partial t} = a_0 \tilde{q} \eta - c \eta^2 - b \eta^3 + D \Delta \eta. \quad (3.2.17)$$

Here, D is the diffusion coefficient, Δ is a Laplacian which describes the diffusion-type non-locality. Equation (3.2.17) is solved in the closed confined domains with the continuous flux across the boundary, i.e. the boundary conditions are as follows:

$$\left(\frac{\partial \eta}{\partial r} \right)_{r=r_0} = 0.$$

Let us identify the homogeneous stationary solutions of the system, $\eta_s(\tilde{q})$, with the thermodynamic branch of the system evolution in the bifurcation diagram (3.2.17). To clarify stability, we shall consider small perturbations of the thermodynamic branch of solutions:

$$\eta(r, t) = \eta_s + \delta \eta(r, t) \quad (3.2.18)$$

where $\delta \eta(r, t)$ describes the deviation of the system from the homogeneous stationary state η_s due to the random fluctuations $\delta \eta(r, t) \ll 1$.

Let us specify $\delta \eta(r, t)$ in a form of the expansion into a Fourier series:

$$\delta \eta(r, t) = \sum_k \square \exp\{ikr + \lambda t\}. \quad (3.2.19)$$

Here, \square is an amplitude of the mode with the wave-vector k and the damping decrement λ .

Substituting (3.2.18) into (3.2.19) and linearizing over the small parameter $\delta \eta(r, t)$, with the allowance made for (3.2.17), we obtain the dispersion equation which binds the decrement with the wave-vector:

$$\lambda = \lambda(k, \tilde{q}), \quad \lambda(k, \tilde{q}) = -a_0 \tilde{q} + 2c \eta_s + 2b \eta_s^2 - D k^2. \quad (3.2.20)$$

For $k^2 < k_c^2 = \frac{-a_0 \tilde{q} + 2c \eta_s + 2b \eta_s^2}{D}$ the damping decrement is $\lambda(k, \tilde{q}) > 0$ indicating that the mode with the wave-vector k diverges.

Let us make some essential remarks. The mathematical theory of stability of the solutions of differential equations used here starts from the Lyapunov's theory of stability [31]. Several criteria exist, being sufficient to warrant (or not warrant) the asymptotic stability of the stationary state. One of these criteria is based on the analysis of the stability over the linear approximation, while the other one starts from Lyapunov's function concept. The analysis of stability over the linear approximation in the problem under consideration allows one to determine the stability (or instability) of the solutions linearized in the vicinity of the stationary state to which the homogeneous solutions η_s correspond. The instability of the solutions of the linearized equation is sufficient for the stability of the total non-linear equation. Hence, it follows that one may restrict oneself to the finite-order terms in the expansion of functions $\eta(r, t)$. By virtue of the last assumption, we shall confine ourselves to the infinitesimal stability, i.e. to the study of the system response to small perturbations, so that $\partial \eta / \eta_s \ll 1$. That restriction is unessential [37], since the infinitesimal stability provides the necessary condition for instability with respect to any $\eta(r, t)$.

Although the solution of the non-linear equation in this case may also increase exponentially with time, in the presence of non-linear terms, they will tend towards another stationary state with the heterogeneous distribution of domains in the "soft" states.

Beyond that point, solutions η_s remain constant on the macroscopic scale under consideration with simultaneous slow time variation on the instability development scale. The condition of the slow time variation of the $\lambda_s^{-1} \frac{\partial \lambda}{\partial t} \ll \lambda$ type, which is reduced to the condition of slight variation of the function λ on the scale, is imposed on the function λ_s^{-1} (an adiabatic approximation). The period and the lifetime of the dissipative structure produced depend on the control parameter \tilde{q} .

At $\tilde{q} \rightarrow \infty$, $L_c = \frac{2\pi}{k_c} \rightarrow 0$ and $\tau_{life} = \frac{1}{\lambda(\tilde{q}, k)} \rightarrow 0$ (see Fig. 3.2.15).

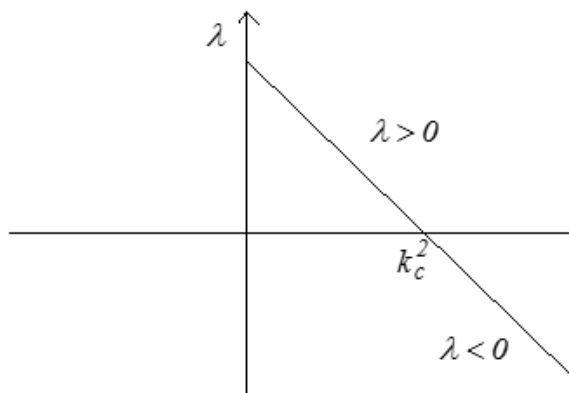


Fig. 3.2.16. The dependence of the damping decrement λ on k^2 .

SELF-ORGANIZING COLLECTIVITY APPROACH IN BIOLOGY

4.1. Self-organizing processes in bio-matters
4.1.1. Global approach

Bioscience knows two different types of philosophies: the Chinese (holistic) and European (reductionalistic) approaches. A summary of the differences is shown in Fig. 4.1.1.

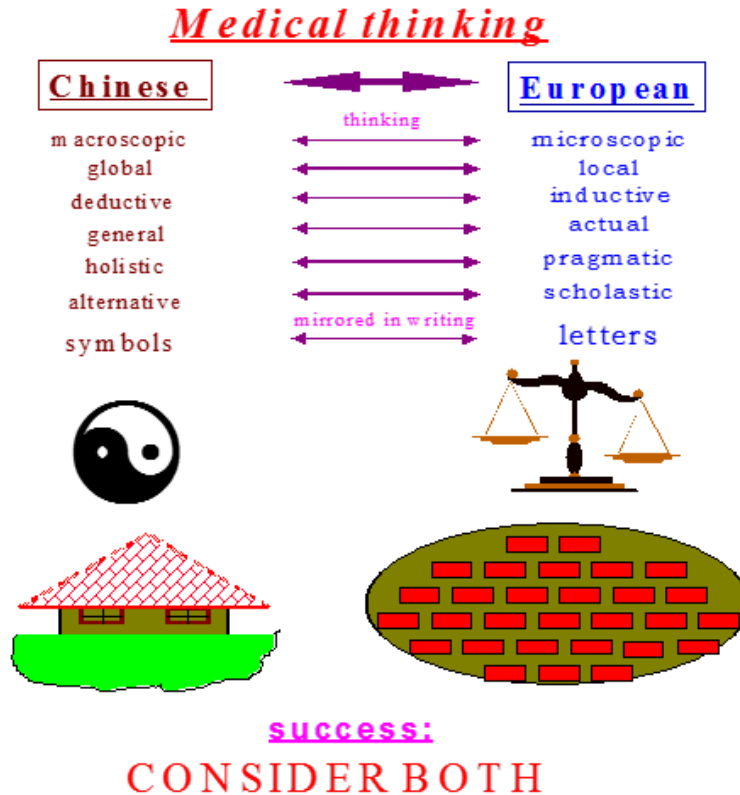


Fig. 4.1.1. Balance of inductive and deductive thinking.

Both approaches are not optimal. We find the explanation for macroscopic processes (the general laws) by examining microscopic processes. On the other hand, however, we have to have a global macroscopic approach of the total system to understand the interdependence of microscopic effects, which build up the system.

It is trivial, that both of the two approaches dominate our thinking. The use of both approaches might explain the complex systems of the living matter.

4.1.2. Self-organization of living processes

From the physical point of view, the average energy and lowering and the average entropy increasing in the system drives the life process. In this sense, life follows the basic thermodynamic laws: the living process continuously “burns” the incoming “nutrition”. The living process lowers the electron energy, which is caused by the oxidation of the outgoing final “products”. The gradual loss of electron energy of the “nutrition” molecules is the energy to sustain life. Simply speaking, the living process is only an entropy producer, an open, dissipative system, Fig. 4.1.2. But in the living process, not only the liberated heat (energy) is the “product”. The living unit has other

advantages as well from the combustion. The organism develops itself, rearranges, reorganizes the incoming chemicals and builds up its own structure, consequently lowers the entropy. The main factor of its local limited stability is just the balance of the entropy production with the entropy sink (neg-entropy production, information generation) (Fig. 4.1.3). This balance is typical in every self-organizing system, so there is no doubt about self-organizing of individual in the living object as another balance also characterizes the life in general: the development (evolution) of self-organizing (Fig. 4.1.4).

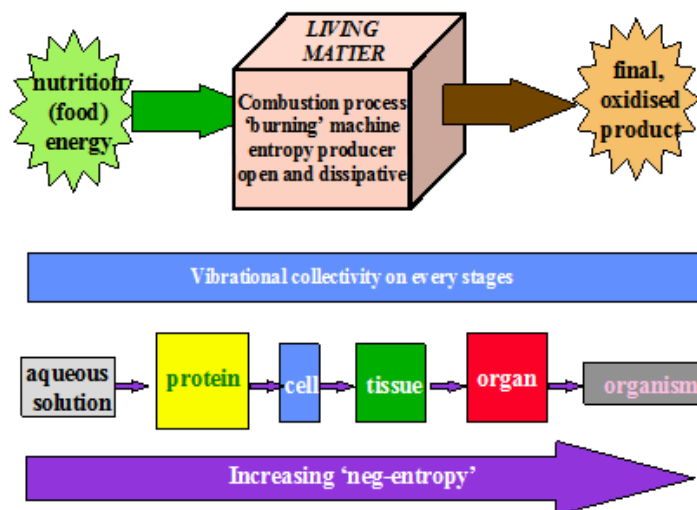


Fig. 4.1.2. Structure of the combustion.

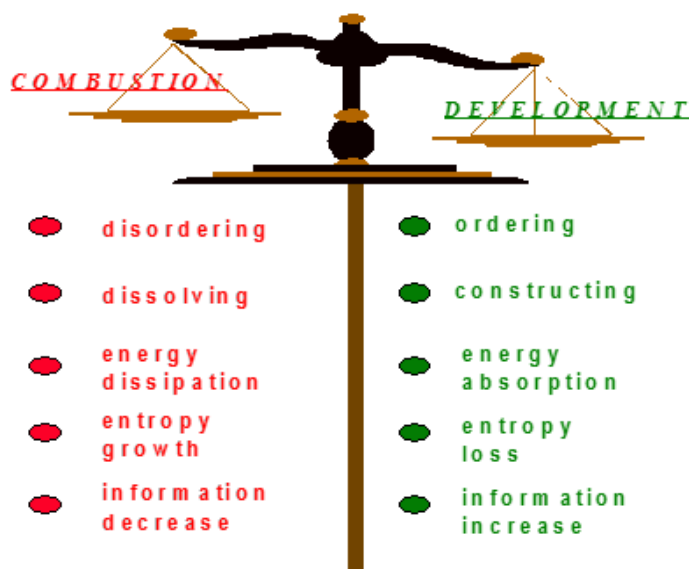


Fig. 4.1.3. Life-function.

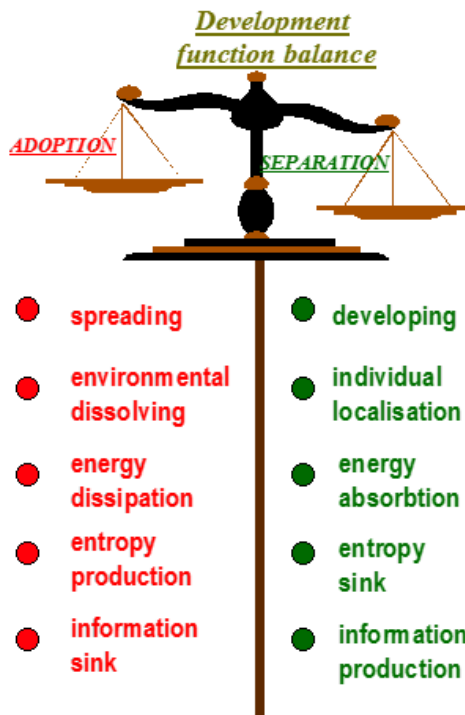


Fig. 4.1.4. Evolution balance.

The bio-oxidation cannot be a fast process. Anyway, the process is limited by the available nutrition being transported to the “combustion” units. A possible uncontrolled “combustion” of a defected unit will consume the energy of others in the close vicinity, blocking to continue this process. This situation can be solved by a positive feedback to limit the extra demand, which is a special self-organized collectivity. From the chemical point of view, the living process is a highly (self-) organized charge transfer with a sophisticated energy accumulation and self-reproduction [1]. To keep the living process ongoing, the nutrition has to be transported to the living unit (e.g. cell) or the living system transports itself to the nutrition. For example, plants transport their nutrition by means of diffusion and osmosis. There is a thermodynamic driving force to overcome the barriers of fixated nutrition: the (sunlight) external energy pump to make the necessary gradients. The gradients are made not only in a thermodynamic meaning, by in a chemical kind as well: chemical reactions and new components can be generated by the energy-pump. However, another mechanism also exists: the movement of the living object by means of external transport processes (convective flows in the surrounding environment) or by an internal mechanical unit (a muscle), which converts the chemical energy into a mechanical one.

The biological energy “combustion” is the general driving force for the development to an increasingly more sophisticated and accommodated bio-system. This evolution causes the living system to be more and more independent of its environment. The life organizes and stabilizes itself.

On the one hand, the evolution forces the system to adapt and improve, developing a perfect “combustion” ability, but on the other hand, self-reproduction is rather conservative: the system sustains itself at the same level. Slight changes in this conservative process lead to evolution, being controlled only by changing the conditions and environmental demands.

4.2. Water: a general solvent of the living matter

Water is essential for the living process. It is the mother, the matrix and the “fuel” of life, and also has the lowest energy as a final product of any chemical processes in life [2]. The liquid water

enhances the external transport with its variability. It promotes the evolution with its cooperativity. It promotes the self-reproduction including its collectivity.

Every living system (irrespective of its complexity) has a considerable amount of water. The molar density of the living systems with such a quantity of water is very dilute and does not reach half a mol. (The human body's molarity is definitely less than half a mol, with 60% water content and its average molecular weight of more than 2000; the molarity, on average, is very close to that of seawater or the artificial infusion solutions, whose diluteness is well known). In complex biostructures, the water-concentration has large gradients, defined by the internal structures of the system.

4.2.1. Water structure

Contrary to its rather simple chemical composition, the liquid water has a complicated peculiar structure, which is the topic of several serious investigations [3-4]. Despite the simplicity, water has unusual properties: the abnormal thermodynamic parameters (melting point, boiling point, vaporization heat, fusion heat, etc. are higher than it would be expected for liquids composed of hydrogen and oxygen). Its physical and structural properties are also peculiar: it has a density maximum at 4°C, and its viscosity decreases with pressure up to ~1000 atm. All of these physical abnormalities make water exceptional and determine a lot of unique properties of living biological matter [5]. Nowadays, there is increased interest in the problem of possible water structures: from crystalline ice-like-structure to the clustered and monomer liquids with different degrees of structural ordering [6-11]. The structure of agglomerations of water molecules and different kind of clusters is definitely complicated and exhibits many unusual properties:

- The hydrogen atoms, bonded to one oxygen atom, can jump to another oxygen atom in another water molecule. Thus, the proton makes bond-like the connection through a lone pair, bridging the oxygen atoms and creating the so-called hydrogen bridge. The bridge has a much weaker bond strength than the normal hydrogen-oxygen bonds.
- Due to the V-shaped dipole structure of water, intermolecular dipole interactions and arrangements are complex.
- The non-regular tetrahedral shape of the water molecule changes the actual occupation status of the proton. Thus, consequently, the whole geometric arrangement fluctuates due to the fluctuating proton bonds, the connected hydrogen-bridges.
- Water-tetrahedrons cannot occupy the space in a closed-packed manner: voids (holes) between the tetrahedron must be present.

4.2.2. Molecule bifurcation: hydrogen bridges

One of the most important dynamic equilibria occurs in the hydrogen bridges. The hydrogen bridge in water systems are not static fixed bonds. It is a special quantum-mechanical effect, based on the migration of a proton (hydrogen ion) between the water molecules. The hydrogen ion (proton) oscillates by tunnelling through the bonds of oxygen atoms, and so it is “frustrated”, not fixed to one oxygen-atom (Fig. 4.2.1). The tunnelling threshold energy (activation energy) depends on the distances between oxygen atoms, dividing two states with an energy barrier that has its maximum energy at a distance of about 0.25 nm. If oxygen molecules are closer to each other, the barrier height is smaller, and if the distance is larger, the possibility of tunnelling sharply decreases.

The proton is caught in a double potential well in which it vibrates between the two energy minima (Fig. 4.2.1). This process causes the proton to become highly delocalized that gives the well-known chemical equilibrium (used for the pH definition):



Despite that, no stable state exists halfway to the two oxygen atoms; the proton averaged over a long stretch time remains exactly in the middle, because of the equal probability of the two states in the minima of the oxygen binding potential.

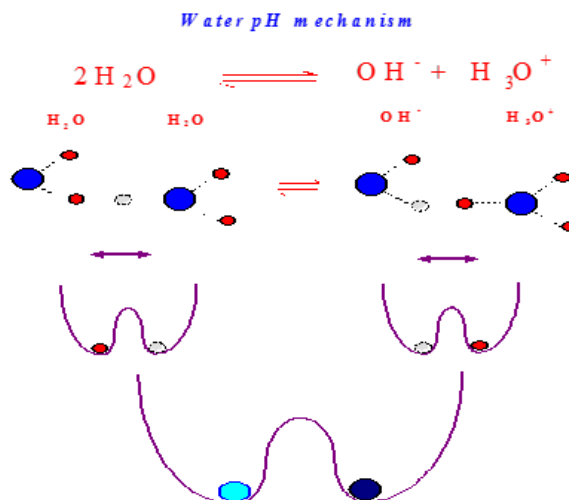


Fig. 4.2.1. Water pH-mechanism.

4.2.3. Geometric bifurcation: water clusters

The situation becomes even more complicated when taking the geometric incompatibilities of the water structure into account. The water molecule forms a tetrahedron with protons in its two vertices, while two other ones are empty (the so-called “lone” pairs) (Fig. 4.2.2). The water tetrahedron is not so dense (the oxygen atom is in the centre), but it is the most stable clustering of these molecules.

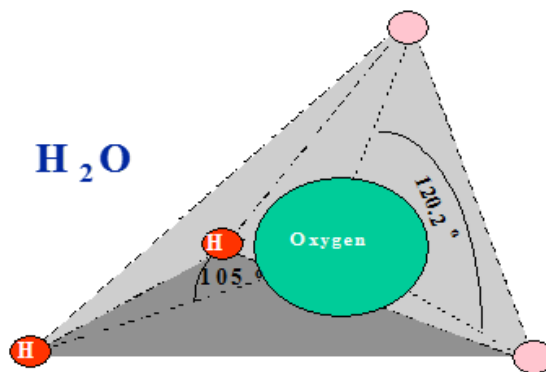


Fig. 4.2.2. Water tetrahedron.

These tetrahedrons are ready for the geometric frustration [5], which was discussed above.

The proton migration effectively changes the geometry of the water tetrahedron. The angle between two oxygen-bonded hydrogen ions is approximately 105° , while that between the hydrogen bridges is approximately 110° and between the lone pairs is approximately 120° . In this way, the water tetrahedron is not a fixed geometric arrangement, but its edges vibrate in accordance with the proton migrations.

Consequently, it can be considered as “smeared” or “soft” polyhedron during a time period considerably longer than the characteristic migration time. The binding energy of the hydrogen bridges is only 0.17-0.29 eV/molecule (4-7 kJ/mol), which is only one order of magnitude larger than the thermal energy at room temperature (~ 0.025 eV at 20°C). In liquid water, the order of water molecules cannot be stabilized because the thermal energy destroys a huge fraction of the

hydrogen bridges. The cohesion effect of the hydrogen bridges in pure water is most trivial in its solid form. Ice has various structures [3] in which the actual hydrogen bridges tightly bind water molecules. A remarkable variability of the structures bonded by the hydrogen bridges originates from various binding possibilities and their geometric forms. Ice has eight main and several additional structures, depending on the formation conditions. Rotating the molecules, which is possible because of their V-like structure, one can modify these structures, Fig. 4.2.3. The three characteristic formations are called the I-, V- and D-forms [3] (Fig. 4.2.4). The I-structure, which instantly changes, has a very short lifetime (10^{-14} – 10^{-16} s) compared to the intermolecular proton vibration frequency; the V-structure vibrates with a medium lifetime (10^{-11} – 10^{-14} s); the D-structure is changed by the diffusion with a relatively large lifetime.

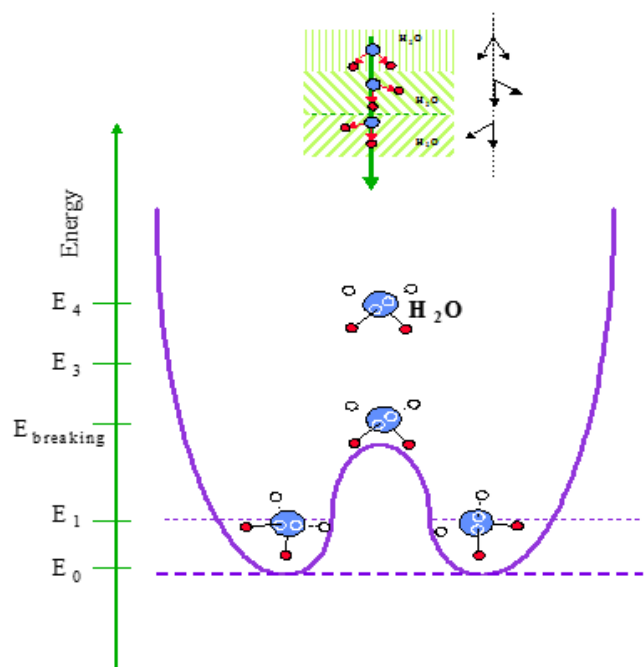


Fig. 4.2.3. The bifurcation of the water molecules due to their V-like structure.

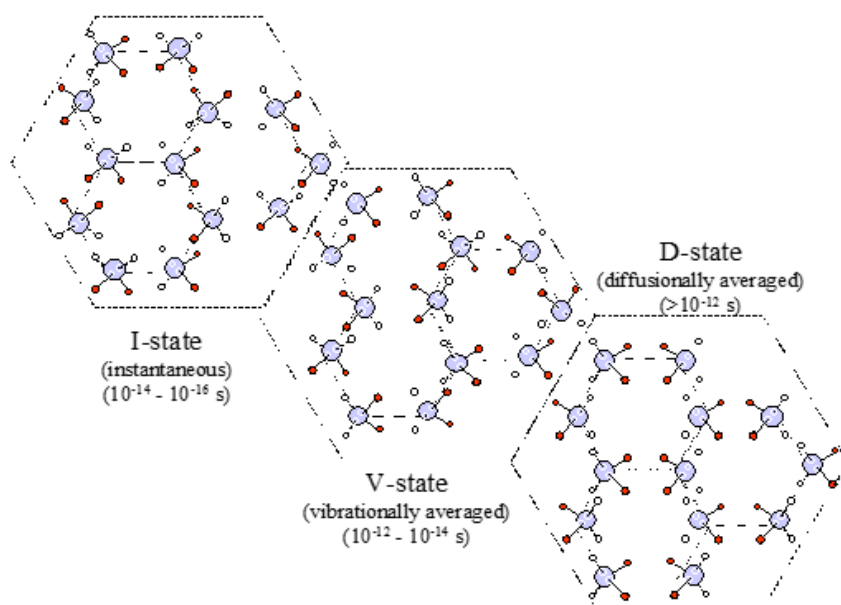


Fig. 4.2.4. Different relaxation structures of water.

Liquid water always has at least two phases (Fig. 4.2.5):

- the phase that contains only the monomer molecules and
- the phase that has clusters: identical and/or different and/or a composition of clusters as well.

The molecular bond in water is 10 eV/molecule (242 kJ/mol), which is about fifty times larger than the average bonding in the hydrogen bridges. However, a significantly large part of the hydrogen bridges exists in the liquid phase, even at temperatures as high as the boiling point. The existence of water clustering is revealed by the radial distribution function measured by the X-ray diffraction. These measured hydrogen bridges show that the "ice structure" does not vanish during the melting process. The effect at the melting point is only that some domains (cluster of water) are disconnected from each other (like islands). When increasing the temperature, these domains are gradually broken down into smaller and smaller ones (Fig. 4.2.6). These domains are not static structures; their size fluctuates, but the average definitely characterizes the actual state [12]. This effect is well known in the solid-state and statistical physics: the order does not vanish at once at the phase transition, but does at the vicinity of the medium-range and the short-range [13]. This effect is also shown theoretically in the two-dimensional Ising model (one of the rigorously solved systems) in the phase transition [14]. The cluster conservation is more effective in the case of water, because six-fold rings in the solid state (ice I) break easier at a certain point due to the incompactness of the angles in the water tetrahedrons with the six-fold ring [3]. The remaining chain appears to be relatively stable.

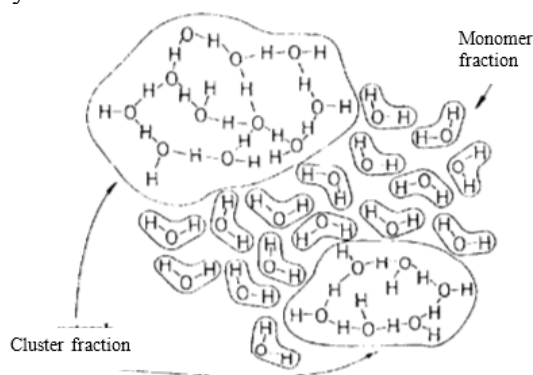


Fig. 4.2.5. Schematic of the phases.

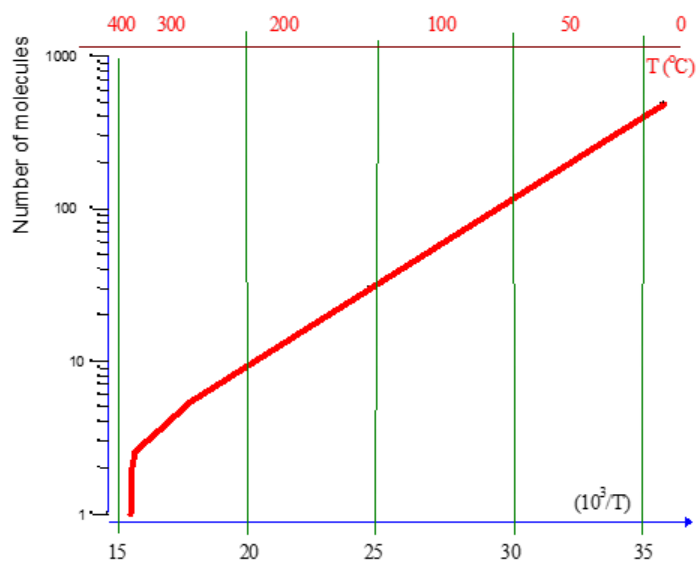


Fig. 4.2.6. Water-cluster size versus temperature.

Structural division of the liquid water into the ordered (clustered, type 1) and disordered (type 2) phases is the most widespread model for the description. The existence of the water clustering is revealed by the radial distribution function measured by the X-ray diffraction [3]. These measured

hydrogen bridges show that the “ice structure” does not vanish at once during the melting process. The effect on melting is only that some domains (water clusters) are disconnected from each other (like the islands). With increasing temperature, these domains are gradually broken down into the smaller and smaller ones. These domains are not static structures, their size fluctuates but the average definitely characterizes the actual state. This fact emphasizes the complexity of normal liquid water which can mostly be prescribed to the hydrogen bridges. The numerous models, taking into account these peculiarities, were formulated for the liquid water:

- the quartz-like structure (based on the tetrahedral units) [15];
- the dodecahedral (chathrate) model (associated with special hydrogen bond rings) [16];
- the bent-hydrogen-bond model (calculates the bent chain of the hydrogen bonds) [16], as well as
- the cluster models: the flickering cluster model [17], the solid-like model [19], etc.

These models reasonably follow the actual systems but fail to yield the maximum density at 4°C.

A more or less adequate model was suggested based on the coexistence of two types of clusters in the liquid [19], so the water in this model consists of three phases.

However, a remarkably large number of hydrogen bridges still exist in the liquid phase even at the temperatures as high as the boiling point (Fig. 4.2.7) [21-25]. This means that the normal water (obtained by gradual melting from ice), has two structurally different phases: the monomer water molecules and the water clusters [26]. Moreover, the water clusters in this phase-mixture can have a large variability depending on their actual structure and phase transitions. The simple approach assumes the presence of ice-like structures: from simple elements of structural network to the quasi-crystalline ones [6,7]. The quasi-crystalline structure is formed from the ice-like clustering due to the structure destruction by heating or other disturbances (the admixtures introduction, ultrasound influence, etc.) and is accompanied by an increase in density, a change in chemical activity, optical and other properties [6-10,27].

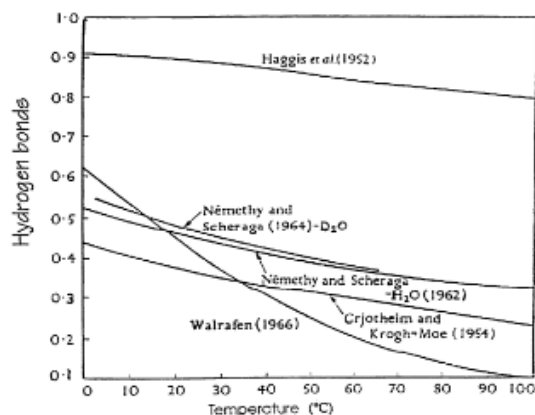


Fig. 4.2.7. The temperature dependence of the hydrogen bonds percentage (100% in ice), according to the different approximations.

The ordering of water structure has also been analyzed. In other models, the clusters are the tetramers or hexamers [6] with 3-4 nm dimensions [6,9]. The thermodynamic approach to the analysis of such systems needs some restrictions [6,8] in case of one- or two-dimensional structures (few layers of H₂O molecules) as is relevant in biological objects [28,29].

However, the living system is not an ordered solid. It is not so trivial to introduce the collective states in the biomatter (contrary to crystals [30]): it is an aqueous solution. In the living state, the water is mostly well-ordered and nearly crystalline (semi-crystalline [31]). A polarized multi-layer of water was described which can be considered to be in a quasi-crystalline state [32-35].

The normal water, gradually melting from ice, has two structurally different phases (the monomer water-molecules and the water-clusters [26]). Moreover, the clusters of water in this phase-mixture can have a large variability depending on their actual structure and phase transitions. This fact emphasizes the complexity of the normal liquid water that can mostly be prescribed to the hydrogen-bridges.

Great attention has been drawn to the problem of the ordered water enclosing the hydrophobic regions creating inert, osmotically inactive zones [36]. Numerous works point out the importance of the ordered water (melted ice) in living objects [37,28], but a suitable model for these effects does not exist at the present time.

In general, the problem of developing an adequate model of water is related to its structure. In this book, we will describe a model and the self-organization in non-crystalline materials, taking into account a number of known facts [6,7] as well as our investigations on the glassy structures and properties [40] combined with different water types. A cluster approach to the two-structure model of liquid water using the ideas of synergetics [40,41] is employed to model the structures and explain the ordering properties of water.

4.2.4. Dissipative structure in water: the synergetic model

The fluctuations of the order parameter are uniform in the homogeneous matter. At the presence of different heterophases various symmetry properties have another physical nature: they determine non-homogenous fluctuations in the macroscopic domains inside the system. All of the available sites of the system are occupied by the clusters with the probability, which defines the actual phase state. The degree of the structural disorder is characterized by the actual arrangements, interatomic distances and space fluctuations in the short-range order and by the bond angles. We consider the system containing N atoms, which have two states:

- The disordered states, characterized by significant values of statistical displacements and, as a consequence, an anharmonicity of the atomic vibrations, shear non-stability and the possibility of regrouping.
- The ordered states.

The concentration and the stability of the disordered states depend on the preparation conditions and the initial conditions. Suppose that the distribution of the atomic positions has a Gaussian form:

$$\mathfrak{R}(\delta_i) = (2\delta_i Q_i)^{-1/2} \exp(-\delta_i^2 / 2Q_i),$$

where Q_i is the distribution parameter which characterizes the disorder in the system, δ_i is the longitudinal ($i=1$) and transverse ($i=2$) mean-square \bar{e}_i deviations, with the following conditions:

$$\langle \bar{e}_i \rangle_c = 0 \quad \text{and} \quad \langle (\bar{e}_i)^2 \rangle_c = \sum_i Q_i.$$

Let us define the average on the random field:

$$\langle \dots \rangle_c = \prod_i \int \dots \mathfrak{R}(\delta_i) d\delta_i.$$

The average distance $\langle \bar{r}_i \rangle_c$ is determined as follows:

$$\bar{r}_i = \langle \bar{r}_i \rangle_c + \bar{u}_i + \bar{e}_i, \tag{4.2.2}$$

where \vec{u}_l and \vec{e}_l are the dynamic and statistical displacements of quasi-equilibrium sites.

The Hamiltonian of the system is:

$$H(\{X\}) = \sum_f \sum_l \left(\frac{(\vec{P}_l^f)^2}{2m} + U_f(\vec{r}_l) - \mu \right) + \frac{1}{2} \sum_{f,f',l \neq l'} \Phi_{ff'}(\vec{r}_l - \vec{r}_{l'}) X_l^f X_{l'}^{f'}, \quad (4.2.3)$$

where X_l^f is the local characteristic function, which is determined as:

$$X_l^f = \begin{cases} 1, & \text{if the } l\text{-th atom is in the } f\text{-th state;} \\ 0, & \text{if the } l\text{-th atom is not in the } f\text{-th state;} \end{cases}$$

($f=1$ corresponds to the ordered state, $f=2$ corresponds to the disordered state),

\vec{P}_l^f is the momentum-operator, m is the particle mass, μ is the chemical potential, and $U_f = \sum_{f',l'} \Phi_{ff'}(\vec{r}_l - \vec{r}_{l'})$ is the one-particle potential, where $\Phi_{ff'}(\vec{r}_l - \vec{r}_{l'})$ is the potential energy of the interaction.

The effective Hamiltonian of the system is

$$\begin{aligned} \tilde{H} &= \int H(\{X\}) d\{X\} = \sum_f H_f \\ H_f &= \omega_f \sum_l \left(\frac{(\vec{P}_l^f)^2}{2m} + U_f - \mu \right) + \frac{\omega_f^2}{2} \sum_{l \neq l'} \tilde{\Phi}_f(\vec{r}_l - \vec{r}_{l'}), \end{aligned} \quad (4.2.4)$$

where: $\omega_f = N_f/N$ is the share of atoms in the f state; $N=N_1+N_2$ and $\omega_1=1-\omega_2$.

The heat capacity C_p and linear expansion coefficient α_T are (see Appendix 3):

$$\begin{aligned} &+ \frac{P}{N} \left(\omega_1 \frac{\partial v_1}{\partial T} + \omega_2 \frac{\partial v_2}{\partial T} \right) + \\ &+ \frac{1}{N} \left\{ 2\omega_2 (\tilde{\Phi}_1 + \tilde{\Phi}_2) - 2\tilde{\Phi}_1 + P(v_2 - v_1) \right\} \frac{\partial \omega_2}{\partial T}, \end{aligned} \quad (4.2.5)$$

$$\alpha_T = \frac{1}{V} \frac{\partial V}{\partial T} \Big|_p = \frac{N}{V} (v_2 - v_1) \frac{\partial \omega_2}{\partial T} + \frac{N}{V} \left\{ \frac{\partial v_1}{\partial T} + \omega_2 \left(\frac{\partial v_2}{\partial T} - \frac{\partial v_1}{\partial T} \right) \right\}, \quad (4.2.6)$$

where V is the volume, P is the pressure, $v_f = v_{0f} l_f^3$, and v_{0f} is the geometric-structure fact.

The results of heat capacity C_p calculations (according to (4.2.5)) are presented in Fig. 4.2.8 (the parameters being: $P^*=0.1$, $f=10^5$ erg·cm, $Q_i=0.03$ a; $a=2.83$ nm and $E=5$ kcal/mol, taken from [9]). When comparing the experimental and theoretical results including the temperature

dependence of the linear expansion coefficient α_T [9], a good agreement is obtained, so the proposed model and the approach appear to be satisfactory (Fig. 4.2.9).

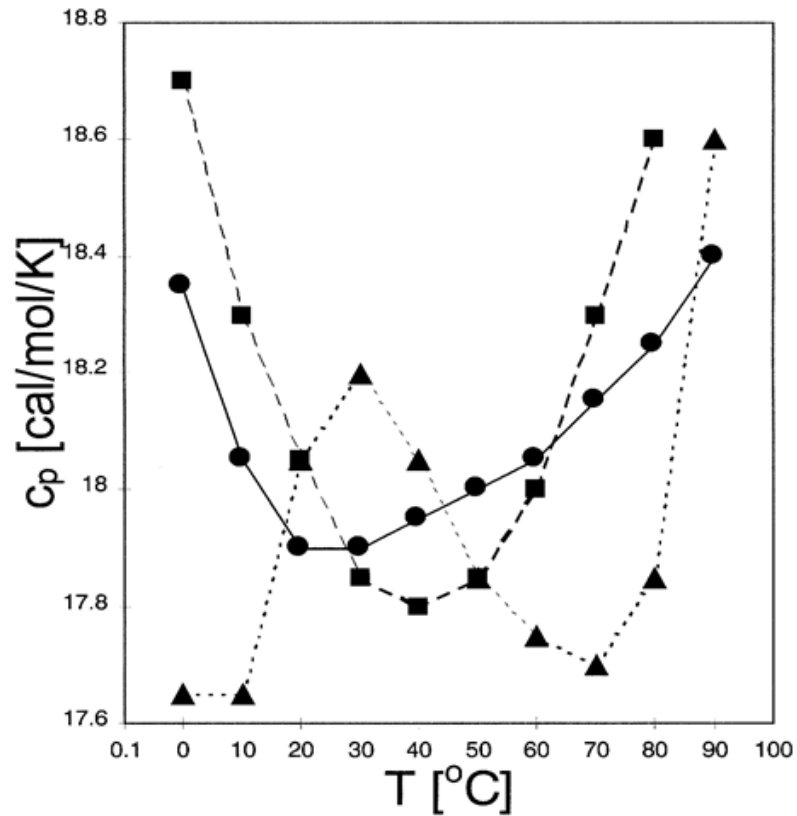


Fig. 4.2.8. A comparison of the measured and calculated heat capacity of water: (Lines are only the guides for eye): ● – experiment, ■ – present calculations, ▲ – previous calculations [9].

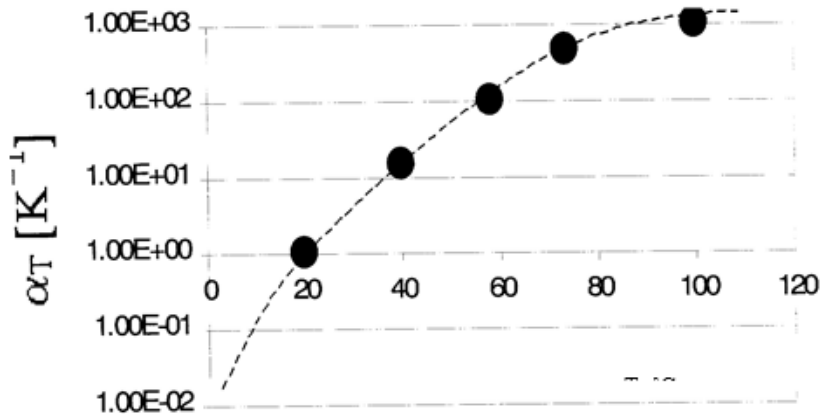


Fig. 4.2.9. The temperature dependence of the linear expansion coefficient α_T .

The nature of the temperature-dependent densification of water may be explained in the frame of this model: the structural inhomogeneity of liquid in the medium-range order leads to inhomogeneity of phononic subsystems (an anharmonic atomic vibration is mostly produced by weak bonds). The vibrational energy (accumulated in clusters) is stored as an elastic deformation energy causing the compression of the system. Anharmonic atomic vibrations for stronger (inter-cluster) bonds become important at higher temperatures, and water expand.

The structural inhomogeneity (degree of order) correlates also with the Urbach tail, namely, the slope of the absorption edge decreases with the disorder of the system. Water, as a condensed

matter, has the electronic excitation within the 7.5~8.9 eV spectral range (X→D-B transitions [44]). The electron absorption gives an exponential dependence of the extinction coefficient on the photon energies and temperature, so Urbach law is fulfilled [45,46]. We have measured the dependence of the absorption spectra ($\ln\alpha$ [cm^{-1}]) on the excitation wavelength (Λ [nm]) for the melted ice and normal water. The sample (water in the special cuvette) was measured using a Hitachi spectrophotometer at room temperature followed by the heating of the melted ice up to 100°C and cooling it down (Fig. 4.2.10). While the “normal water” agrees with the actual liquid disorder corresponding to water type 2. The change in absorption spectrum shows the more ordered state of the melted ice (type 1 water). This was predicted by Eq. (A3.10), which gives a tile decrease of the ordered-state clusters when the temperature increases.

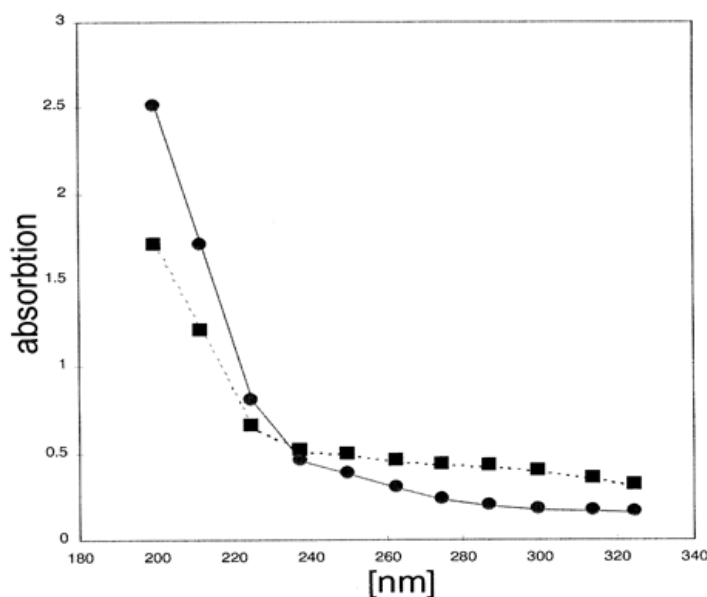


Fig. 4.2.10. Optical absorption edge measurements on water (at room temperature; lines are only the guides for eye): ● – melted ice → (type 1, water), ■ – bolted at 1000°C and cooled down to room temperature and measured there → (type 2, water).

At a fixed temperature $\omega_2 > \omega_2^e$, where ω_2^e characterises the equilibrium disordered state, the relaxation of the ordered state to the equilibrium one is observed with an increase in the degree of disorder, according to the results of calculations Eq. (A3.10) (Fig. 4.2.12).

This result proves that the ordering effects agree with predicted ones and gives the possibility of evaluating the disordering dynamism (Fig. 4.2.12) from the difference of the two curves (Fig. 4.2.11).

Note also, that our model-calculation shows an extreme at the 15–45°C temperature interval, which is the normal body temperature of highly organized living organisms. Our model is generalized enough to be extended to the description of system behaviour in the external fields (electromagnetic, ultrasound), which is especially important for studying the living systems (these problems are considered in detail in chapter 6).

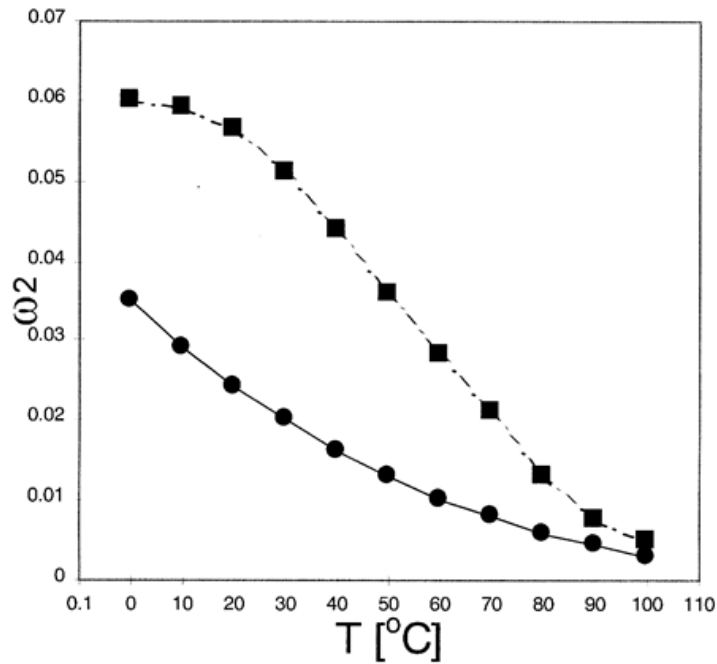


Fig. 4.2.11. Temperature dependence of the two phases (Lines are only the guides for eye): ■ – the ordered phase, ● – the equilibrium disorderes phase.

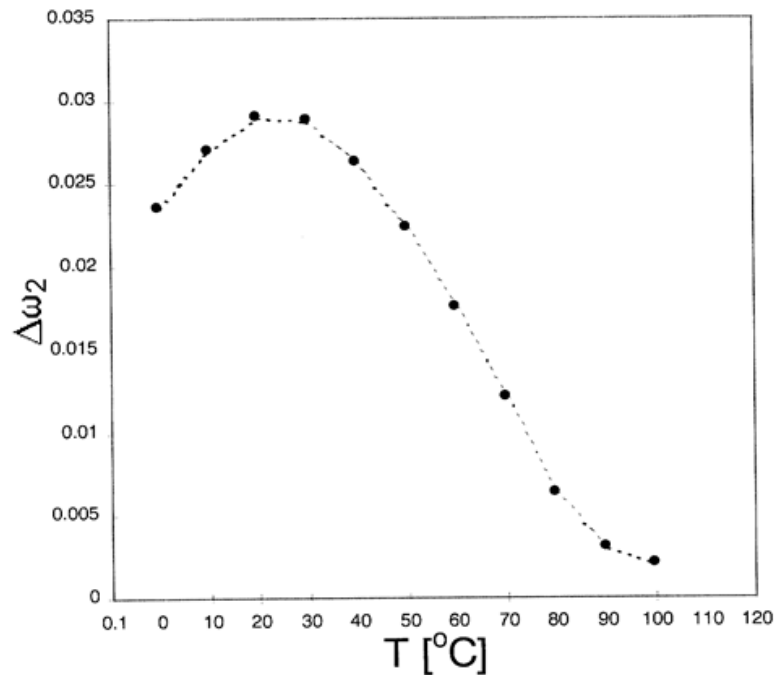


Fig. 4.2.12. Destroying the local order by temperature (Line is only the guide for eye).

4.2.5. Dynamic properties: water network signal transport

The existence of the hydrogen bridges is the most important organizing factor of the water cluster formation. The clusters will be formed in such a way as to minimize their free energy. This effect offers paths in the hydrogen network with energy barriers lower than the hydrogen bonds. This process reconstructs the actual network effectively and relatively fast. The frustration process can be so intensive that the proton migration becomes delocalized for a large area [46], providing instability in the liquid water [47,48]. The structure of water, from the viewpoint of the proton localization, is similar to a gel structure [49]. Regarding quantum mechanical effects, it can be

considered as the so-called quantum-gel state [50]. Consequently, water itself is not homogeneous in this meaning of the hydrogen bond [26]. The bonded clusters can be regarded as a huge water molecule. The estimated mean size of the cluster characteristically depends on the temperature. The mean size of the H-bonded water “molecules” depends linearly on the inverse temperature. As it was shown before, the average size seems to contain 300 molecules at room temperature.

The proton delocalization can be very effective, having jumps (hopping) of protons in a chain, Fig. 4.2.13. During the chain hopping water molecules apparently rotate due to different bond-angles between the empty and filled sites. The path of hydrogen hopping can be a closed loop. These loops can form polyhedrons [26] (Fig. 4.2.14). Among them, icosahedral symmetry is observed in water and is known as the so-called clathrate structures.

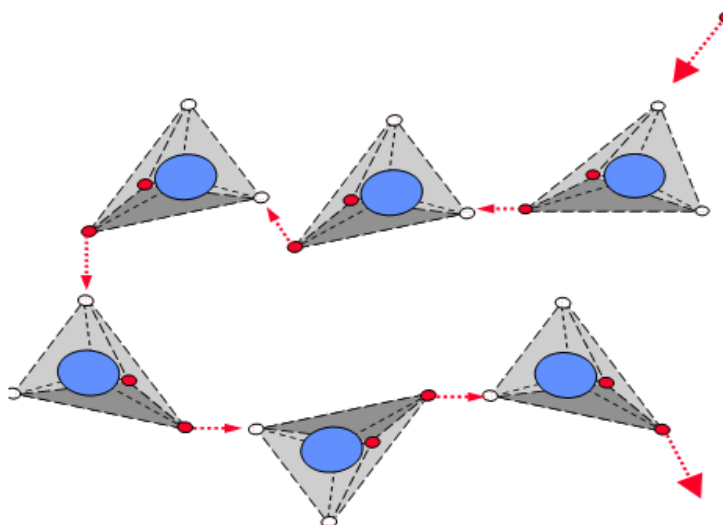


Fig. 4.2.13. Proton hopping in water.

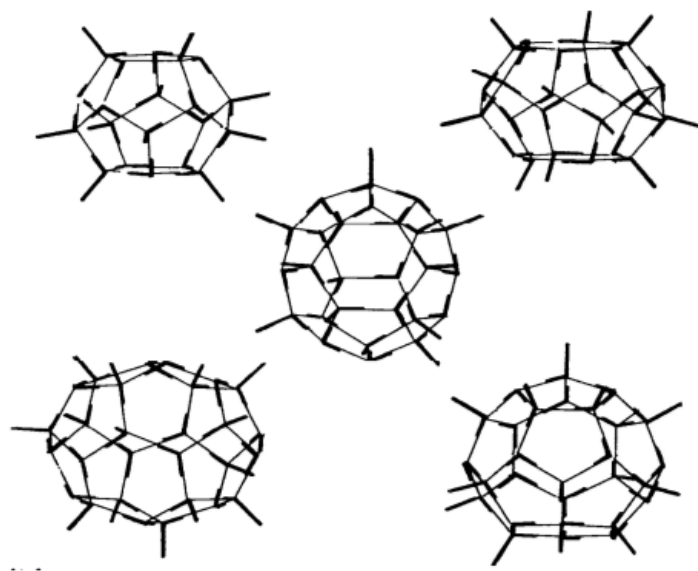


Fig. 4.2.14. Clathrate structure of water.

Water interacts with the surface, creating in its vicinity the well-structured water agglomerates [51]. This structured surface water, observed many times as the bound water or closed water, has a low dielectric constant and more limited absorption for the microwave and radio-frequency radiation. This water passes a shorter relaxation time during the NMR investigations. Temperature-dependent structural phase transition is also observed in these structures [51], showing a highly cooperative order-disorder phenomenon. The hydration orientation of the protein surfaces is well

described in the literature [52]. These types of water have "polymeric" structures similar to the so-called "poly-water" [53,54], but they have an entirely different origin and were later proved to be an artefact [55].

4.3. Bifurcation processes in bio-matter

Living objects are typically open dissipative systems. The life has its meaning only in the open state, because the metabolism (matter and energy exchange between the living object and environment) is an open procedure by definition. The organization procedure can be formulated in the neg-entropy terms, first strictly formulated for living objects by E. Schrödinger in his Dublin lectures [56].

The bistability characterizes life at every level. Even its general solvent and matrix, water itself, has numerous bistabilities and, thus, bifurcation procedures, as described above. Let us follow some of the other bifurcation mechanisms and their inter-connections.

4.3.1. Protein bifurcation

The protein is a huge molecule. It is difficult to interpret its living state because it is dynamic and "screaming and kicking....." [57]. However, the dynamic motion of proteins has been proven both theoretically [58-60] and experimentally [61-62]. The protein *in vitro* is an insulator in which electrons have the lowest possible energy filling up the closed common electron-shells (valence bands). The protein *in vitro*, in an insulating state, is not able to transfer any information, having only coupled electrons in almost localized bonds. The protein *in vitro* has no ESR signal, [63]. However, the protein *in vivo* is different: it has a strong ESR signal [63] representing the uncoupled electrons. *In vivo*, it is a conductor, having a common band with other nearby proteins. The cohesion forces in this system are strongly enhanced compared to their *in vitro* counterparts. Due to the inert protein, the cohesion forces between these molecules *in vitro* are not as large as *in vivo*, thus, the system can, in fact, decay relatively easily to its non-living form.

The adsorbed water supports the isolation of the protein islands [64]. The adsorbed water coverage *in vitro* is almost randomly distributed on the boundary of the protein molecule, producing an insulating layer with large dielectric permeability [65]. To provide a material with collective intermolecular transport, the disordered structure must be rearranged.

In the living state, there is a considerable smaller dielectric permeability around proteins because of the ordered adsorbed water [65], and much larger cohesion forces are observable [65]. The strict isolation as well as the electronic saturation of the macromolecule has been lost and the desaturated proteins do appear in the living state. The system, being an insulator *in vitro*, becomes semiconducting *in vivo*. An electron acceptor, tuning away the molecule from the stable, static equilibrium, produces the protein molecule desaturation. That is responsible for the living state, giving the possibility for a special type of collectivity and co-operativity in the system.

The essential mechanism of life at the submolecular level is the electron-desaturation of proteins by various reagents due to metabolism processes. The living process is realized in a charge flow making the final oxidation through various steps by different reagents (an oxidation process). The oxidation goes step-by-step, transferring only a fraction of the electron charge at each step. This mechanism of the charge transfer is the life itself at the micromolecular level. The collectivity appears in the conduction chain of information between protein molecules. The stable non-conducting protein state has been destabilized *in vivo* and the molecules try to stabilize themselves seeking to fill up their shells in the electronically closed stable configuration. The non-saturated macromolecules try to reach their stable saturated form.

The search for stability at the microscopic level (i.e. that for molecule configuration for the stable insulating state) contradicts the global (macroscopic) stability requirements (Fig. 4.3.1). The latter are stabilized by the transported charge (semiconductor) due to the metabolic process, which causes, by its nature, non-corresponding electronic charges in the stabilization process. Consequently, the non-stable saturated molecules are produced in this process. In the living

system, the local and global energy requirements compete with each other resulting in geometric frustration. It is supposed that their balance has a central role in the formation of the actual phase [66].

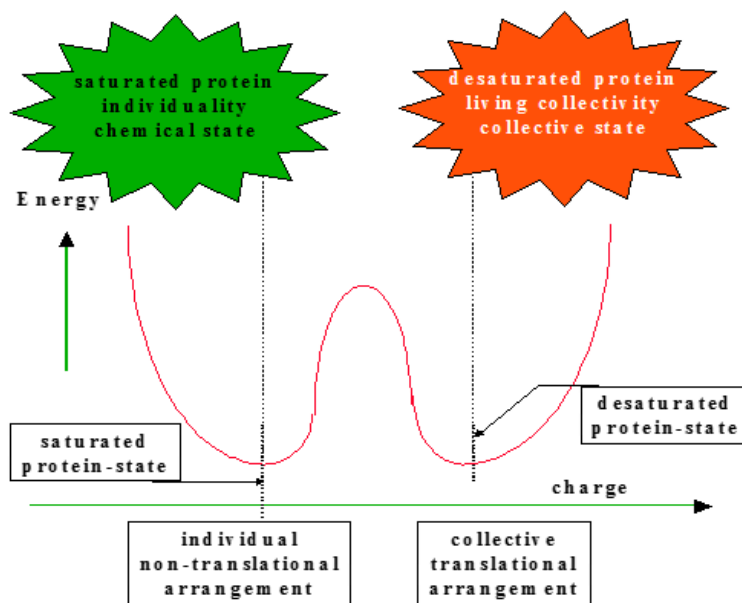


Fig. 4.3.1. Protein bifurcation.

4.3.2. Sliding waves

High electron stability is connected with the perfect saturated state. To reach this state, a small amount of charge is not sufficient because the electron acceptors, which are responsible for the oxidation driving force and transporting this charge in the living state. At perfect saturation, the molecular interactions are weak, only Van-der-Waals interactions exist. However, the long-range requirements are opposite: only the large correlation length, which requires non-saturated, well-interacting molecules, can create the effective long-range order. The momentarily optimal short-range order cannot be frozen because its neighbourhood becomes more unstable due to the stabilization of the given short-range unit (protein). The incompatibility of the energy minima of the short and long-range orders creates an unstable situation. The material (at this level, too) has to be frustrated. The non-saturated proteins meet the long-range requirements well, but in the short-range, the search for the saturated situation will dominate, contradicting global tendencies. Again a “stability-bag” (the so-called “soliton”) will be formed, moving through the material (Fig.4.3.2) [67].

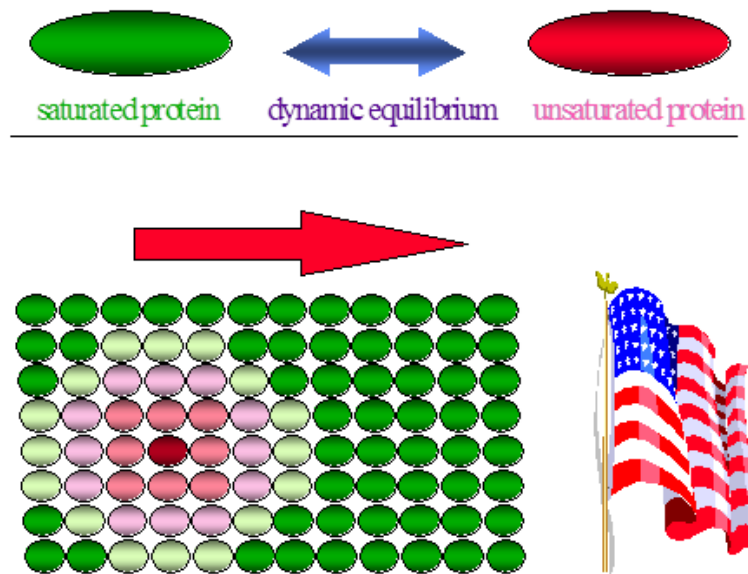


Fig. 4.3.2. Sliding instability bag.

The molecules in the neighbourhood of that, which saturates itself will be unstable due to the missing charge. It is in fact a CDW (Charge Density Wave) based on the Peierls-Frolich instability.

This is one of the forms of frustration discussed before. If the short-range forces are favoured in the total system, the long-range order has no balance (or vice versa), then the life will disappear. A delicate balance in the effective interaction length stabilizes the dynamic frustration, which is, as we suggested [66], the basic behaviour of life. The dynamic frustration of the living protein is a possible explanation of the "screaming and kicking...." [7]. One protein molecule alone is not enough for this dynamism. In any case, the co-operative and collective behaviour is responsible for the long-range interactions. The transported charges in the frustration are one of the most important components of the cohesion forces and without them, life itself vanishes.

4.3.3. Protein structure bifurcation

At the microscopic level of protein arrangement, the geometric organization is trivial: an octahedron and even an icosahedron can be constructed (Fig. 4.3.3 [68]). These structures are very similar to the clusters observed in amorphous materials. The amorphous materials are created under the influence of the effective short-range interactions to obtain the closest packing. However, it is possible that the long-range interactions are not effective enough to build up the long-range order and thereby to occupy the space properly with ordered structures.

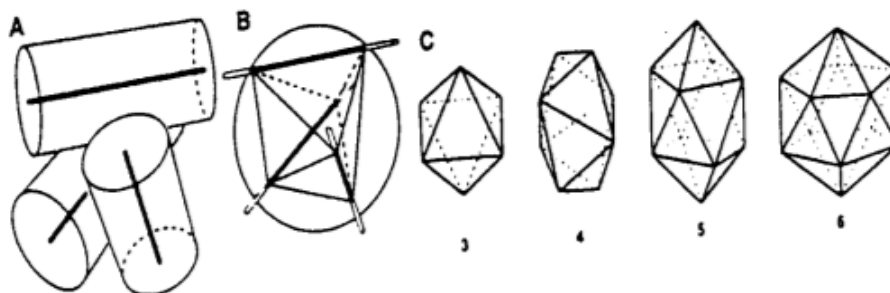


Fig. 4.3.3. Arrangement of helical alpha-proteins.

The protein clustering shows the search for the closest packing in the short-range order, causing the above described conditions. This geometric contradiction between a five-fold symmetry in the closest packing and the prohibited five-fold symmetry in the proper space occupation is a very nice solution to the problem of free surfaces, avoiding the “enticement” of living material to arrange in a genuine crystalline form. The closest packing has free surfaces and does not fit the order that kills internal dynamics without direct contact with the metabolic transport lines and water transmission of the living dynamics. This is exactly the point why DNA also has five-fold helices (α and β forms) and, inside these molecules, some five-fold rings as well. The macroscopic chains of the polyhedral protein units (Fig. 4.3.4 [69]) offer a soliton transfer mechanism through the linear-arrangements with the help of the above-discussed breathing and tilting distortions of the polyhedrons. According to this well-known geometric incompatibility to occupy the space [68,70], the vibrations caused by the frustration occur and can result in the so-called “bioconductive connective system” [71,72], which had been introduced due to other reasons, but are in a good agreement with our assumptions.

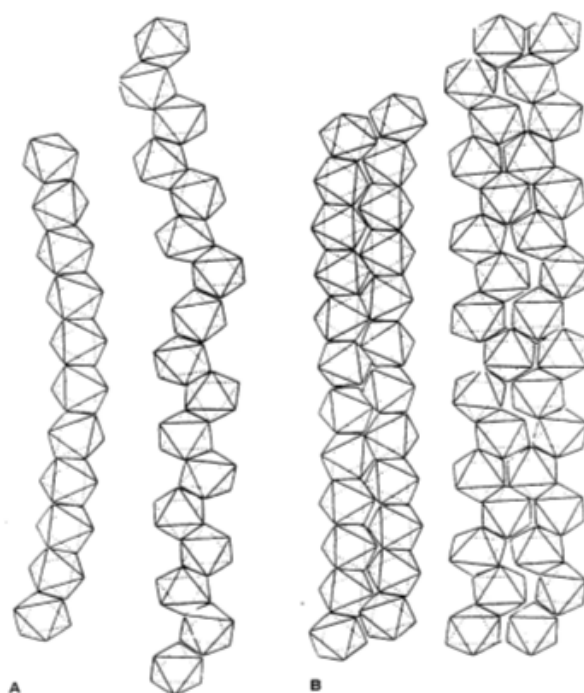


Fig. 4.3.4. Geometric arrangements of proteins.

The geometric frustration is related to the protein vibration (bending vibration) due to the hydrogen bridges, inter-molecular interaction and other (mainly water) molecules (Fig. 4.3.5). This can resemble a collective wave moving through the matter. The picture becomes even more complicated when taking the other internal hydrogen bonds into account. This allows even more freedom of movement for the intrinsic dynamic wave creation.

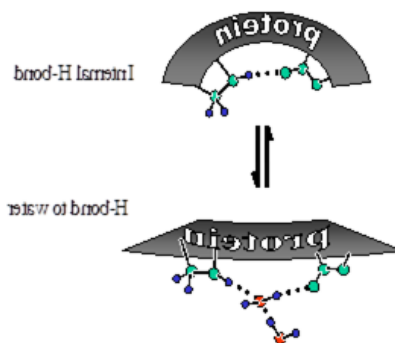


Fig. 4.3.5. Protein-bending by water.

The protein geometric arrangement is determined by the hydrogen bridges (Fig. 4.3.6). The typical bifurcation of the hydrogen bridge has a complex superposition with the “rigid” zigzag and “soft” intermediate channels. This is very similar to the pentagonal bifurcation pattern discussed before.

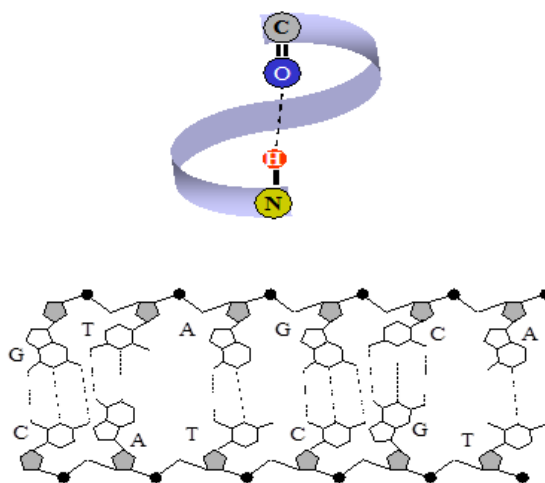


Fig. 4.3.6. Hydrogen bridges and geometric arrangement in DNA.

The dielectric permittivity is drastically lowered in the ordered state arranged by the protein surface. Consequently, the information exchange, due to the enhanced proton migration, is promoted. The importance of the change is the dielectric permittivity was at first pointed out by Szent-Györgyi [63], who experimentally proved this fact, which was postulated much earlier [73,74] (note that some of the actual switching mechanisms (for example the function of black melanin) are also based on water [64] and are related to its reordering [75]).

4.3.4. Membrane bifurcation

The cell membrane is a double-dipole layer constructed of special lipid-molecules. The membrane itself is stabilized by the metabolism like a concentration battery. Generally, the average pH outside of the cell is higher than inside it. The concentration of the element stabilizes the negative charge inside (the acidic pole) and the positive one outside (the alkaline side) of the cell.

The cell membrane divides the active electrolyte and, thus, controls the ion transport. In this meaning, the cell is very similar to the transistor, having a charge (ion) donor on one side, an acceptor on the other side and a layer which controls the charge flux in between electrolytes. The membrane pores (ion channels) are electric-field controlled; so the “transistor” is a field effective

(FET) one (see Fig. 4.3.7). Therefore, the membrane constructs an oscillator (a self-oscillating electronic device). The spontaneous and periodic potential drops (discharge) characterize its dynamics [76-77]. If the polarity is forced to be changed, the cell will become disturbed (an action potential is developed), which is the base for the general information exchange of the overall control. If the metabolism stops, the cell membrane automatically vanishes, as well as the structure of life. Every metabolic change immediately influences the structure of the cell membrane and, thus, the process of life as well.

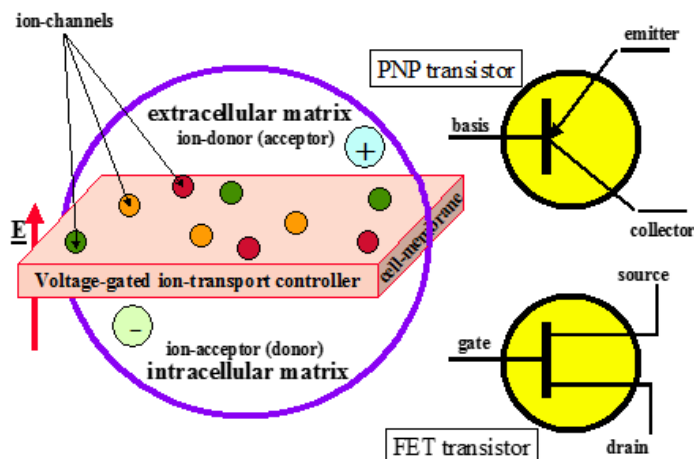


Fig. 4.3.7. The cell membrane schematic.

The porous membrane has a special bifurcation phenomenon (Teorell [78,79], followed by Monnier [80,89] and, more recently, Larter [82]), which is described in a comprehensive form in [83]. Different forces control the actual oscillations: the electric fields, the electro-osmotic flows and the hydrostatic pressure. A rhythmic salt-water oscillation can now be introduced. The membrane oscillation is also an intrinsic vibration, contributing another factor to the dynamic equilibrium of the living matter.

4.3.5. Cell bifurcation

The information exchange in the cell must be the focus of attention if one wants to understand the collectivity in living matter. The message coming from the tissue (see the social signals below) is handled by the receptors in the cell membrane, which jostles the G-protein molecule that activates or inhibits an enzyme to act in a certain manner. However, an abnormal message can give a rise to different effects, causing complicated and fatal diseases like cancer.

The cell life has also a bifurcation behaviour. The cells are tightly connected (“glued”) by the hydrogen bridges. This adhesion makes co-operativity in tissue possible. Each cell receives a defined signal from the organized system, from near or far. Every cell (or group of cells) has a typical characteristic as a member of the specific tissue. The cell membrane is the actual controller of the charge transport manifested in different molecules and ions. The membrane charge is arranged in a double layer, which is able to order the outside water by its electric field and make the structure adequate for the dynamic frustration processes. Note that the ions in the intercellular water disturb the ordered structure and, due to their destroying effect, the geometric frustration is supported.

Finishing the proliferation, the cell membrane builds up the hydrogen bridges once more, increases the adhesion and recreates the long-range order function. At the same time, this process creates the typical shape of the actual cell through the ordering control of the cell membrane. The whole process is collective and cooperative, for which the driving force is the gradual loss of the incoming electron energy in the living system. Forcing the dynamic equilibrium into action and frustration, which makes the living system "screaming and kicking...".

The dividing procedure shows two different cell states: a collective (working) and an individual (dividing) stage in the cell life (see Fig.4.3.8) (A. Szent Gyorgyi denoted these stages by beta and alpha, respectively [84]). At the beta-stage, due to the hydrogen-bridge network (the ordered state), the net regulates the extracellular ion mobility. While in the alpha state, the net is demolished, and the ion mobilities are uncontrolled. Consequently, at the alpha stage the combustion of the cell is uncontrolled. The cell concentrates on its division (Motherhood effect). The cell energies are optimal in both states, which makes the double-well description possible (Fig. 4.3.9).

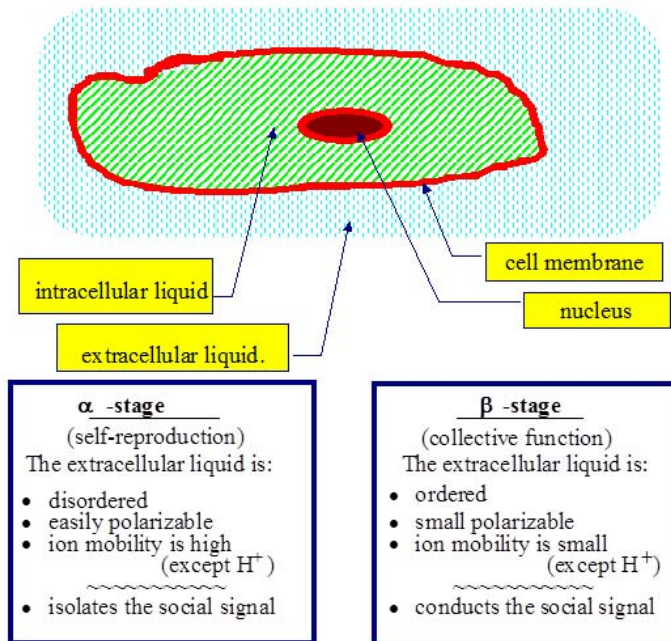


Fig. 4.3.8. Life-stages of a cell.

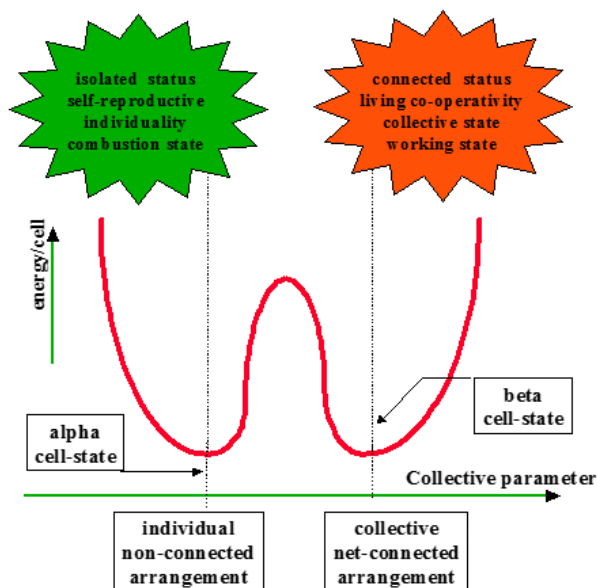


Fig. 4.3.9. Cell bifurcation by the double-well potential.

The cell proliferation is a healthy, standard process, because the life span of a regular cell is generally one order of magnitude less than the average life span of the tissue, where it functions. The proliferation has to be in balance with the normally functioning long-range forces, keeping the system living. The clue for the balance from the statistical point of view is to obtain a recreation of the long-range forces after the cell proliferation. The system becomes intact again. The cell

proliferation is biologically programmed. The divided and renewed cell switches itself into the collectively organized tissue, satisfying the common long-range requests. The division of the cells is statistical in the tissue with the co-operative forces preserving its history. The mutual long-range signal fits later the units back into the tissue. However, the cluster size of the proliferated region can be so large that the signal cannot overcome the critical interaction distance. The co-operativity in the tissue cannot be reconstructed any more. The co-operativity and, therefore, the history of the cell are demolished. This is the point at which the system cannot turn back to its standard balance. The cells are not controlled by the system any more, they live independently and divide unlimitedly, out of control. This is cancer.

The organization of the larger units (cells) also shows the importance of the five-fold arrangements which have already been indicated theoretically [85-88]; numerically [89-95] and even experimentally [96-99]. The enigma about the mystic five in the average co-ordination number of the cells [100] is trivial in the light of these observations. A five-fold symmetry is the closest packing, which minimizes the energy in the short range (the same as in the solids called the Frank-Kasper phases) and creates a five-fold co-ordination (the so called Aboav-Weaire law) in the cell arrangements. The interdependence of the short- and long-range order is studied in detail in three dimension [101]. It is clearly shown that the random microscopic arrangements are well correlated, and develop the long-range order. This process strongly depends on the relaxation derived by the actual pair-potential functions. The two-cell correlation function [100] can also be seen from the point of view of the search for the closest packing. This arrangement also gives a frustration possibility in the dynamic way.

4.3.6. Tissue bifurcation

The organized higher levels (others than the cells) are connected to each other by a special collectivity and transport phenomenon. While the cell individually is similar to a chemical energy plant, the tissue is collective. In the cell, the combustion goes through the definite chemical reactions, so the electron jumps to a lower energetic state, and radiates a definite photon. The energy of this monochromatic emission is absorbed by the cell structure and due to the scattering procedures, a non-monochromatic, blackbody radiation (heat) leaves the cell. The tissue, as the collective system of the cells, is different. This collectivity creates a common function and harmonizes the individual radiation of the cells. The tissue in its proper work emits a collective radiation, which is coherent and relatively narrow in its wavelength spectrum (Fig. 4.3.10).

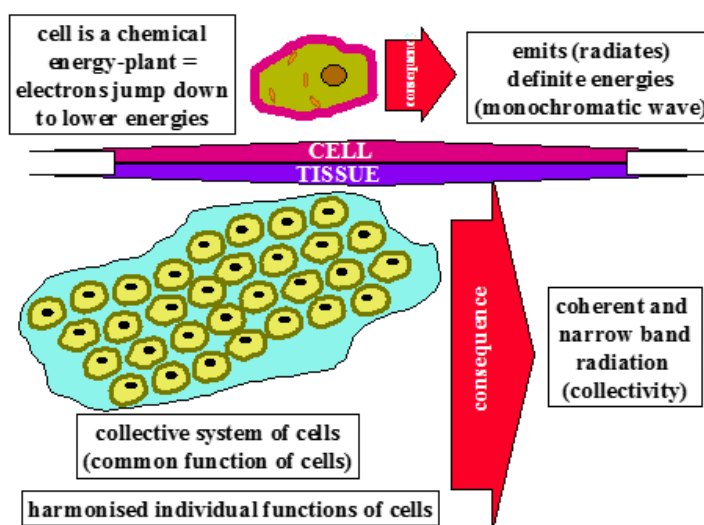


Fig. 4.3.10. Tissue "maser state".

As a consequence of the coherency, the tissue works like a maser (e. g. a laser, which radiates in the microwave region). If the collectivity of cells is broken, the maser state is also demolished.

Fröhlich and their co-workers had first shown these maser states which were called later on "biophotons" by Popp and Co-workers [21] (see below).

The tissue is mainly organized by the social signals. At each level of the living system, water provides the transmission of signals. One can imagine that water is an effective medium for the living process to operate in.

The tissue is geometrically organized by the Aboav-Weaire law, which describes the growing structure as the nearest neighbourhood of newly born cells. Their number changes linearly by a slope which is very close to 5. This rule is a fingerprint of the special self-organizing procedure, which characterizes the non-crystalline materials in general. As emphasized above, in the crystalline material, some definite symmetries can exist. These crystalline symmetries are requested by the proper translational tessellation, which provides a global energy minimum of the system. In non-crystalline materials (such as the living one as well), the symmetry is determined by the shorter correlation, much more central than the translational one. The local cluster energy for the central symmetry is less than that for the translational one (Fig. 4.3.11).

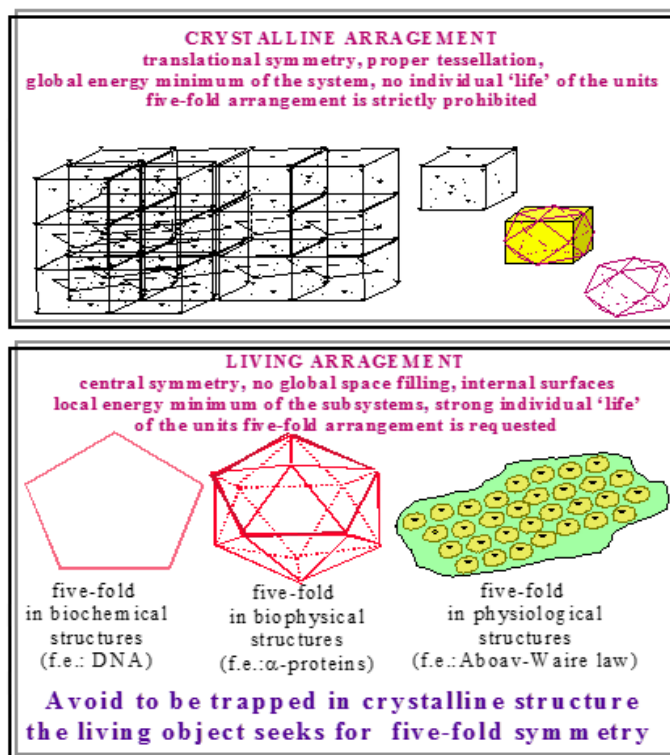


Fig. 4.3.11. Differences between crystalline and non-crystalline structures.

4.3.7. Organism bifurcation

In oriental medicine, there are numerous evidences for the bifurcative properties of the whole organism. The balance of the Yang and Yin (the main ideology behind the acupuncture) is the basis of the healthy organism.

The process of development of an alive organism does not require the interference of external controlling forces, and there is a sequence of the independent acts of self-organization. Handling this process can be carried out with the help of inappreciable effects of controlling parameters. They influence the choice the path of development at the moments when the developing structure is able to bifurcate in the presence of several possible paths of evolution.

With the help of synergetics, various aspects of operation of a human organism are researched. At normal operation of almost all of the systems of vital activity, the intermediate mode between the chaos and the order is characteristic. For example, the extreme modes of heart rate (arrhythmia and excessively ordered rhythms) are dangerous and testify to its illness (too regularly fragile heart is not able flexibly to react to varying external conditions). The health is a particular balance

between chaos and order. The concept of dynamic illness in recognition and treatment of illnesses, and also for warning illnesses will be utilized. The stabilization of the vital activity is reached through the instability, the stationary values of change.

4.4. Collectivity and self-organization

The important balance between short- and long-range effects is controlled by the energetic situation. The system always tries to realize the lowest available energy (which is a cluster (in a microscopic range) with a five-fold symmetry). On the macroscopic scale, it is the ordered occupation of space, which eliminates the five-fold symmetries and therefore contradicts the live requirements. This delicate balance leads to dynamic vibrations, which can be easily frozen by the domination of any force in the system. Protein, with its saturated-desaturated states in the living process also shows this basic dynamic construction and builds up the living system. The self-organization is built up by this dynamic equilibrium in all the organizing levels from the water transfer through the proteins and up to the organism as well. The dynamic vibration is effective for the whole living organism. It has an effect on each level of organization of the system: starting from the protein building up to the total unity:

protein → protein agglomerates → cells → tissues → organs → organism.

Accordingly, the system creates a balance between the nutrients and final products, which breaks down the energy stored in the chemical bonds in the nutrients and creates final products in which the chemically stored energy is low. At the same time, certain biological systems (plants) are capable of executing this process in reverse, for which they receive their energy from the solar energy and the electromagnetic radiation.

4.4.1. Living self-organizing: structure of bistabilities

As observed, the bifurcation mechanism characterizes all levels of the living organism. This is summarized showing some important levels of the complex, multilevel bifurcation mechanism (Fig. 4.4.1).

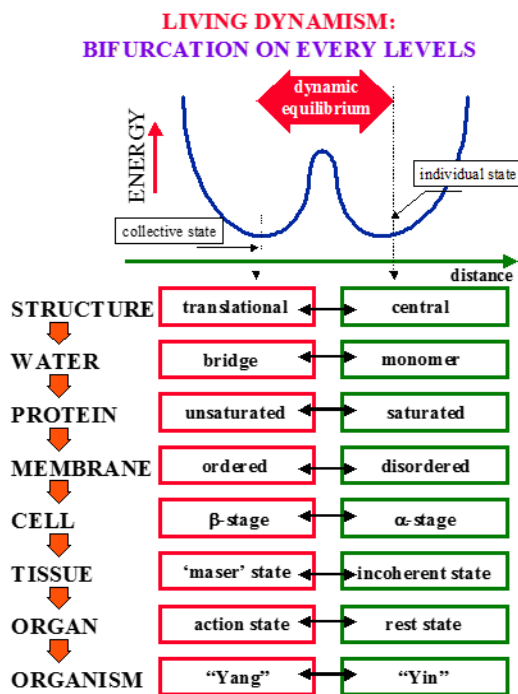


Fig. 4.4.1. The structure of living dynamism.

Of course, these dynamic bistabilities are structurally connected, organized in a specially packed way: the lower levels build up the most actual levels and they construct the next level in the same way. A simple draft of the structure of the well-known bistable potential wells is shown in Fig. 4.4.2.

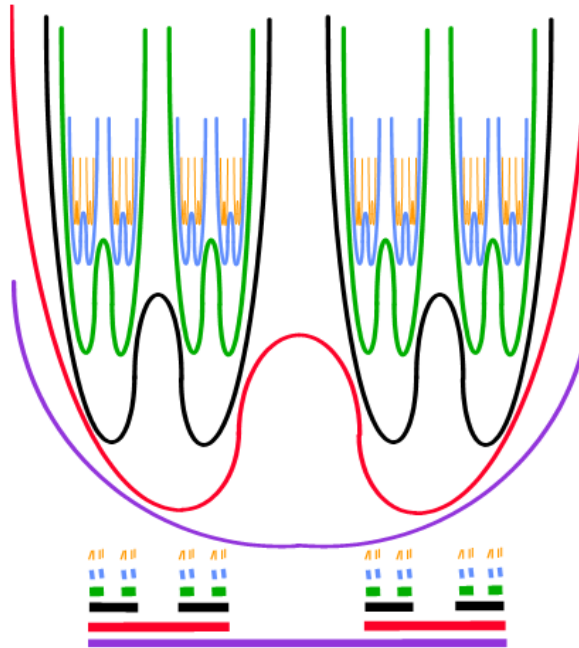


Fig. 4.4.2. Build-up of the bifurcation self-similar structure.

The building up procedure is identical to the so-called Cantor-dust fractal structure (Fig. 4.4.3) whose fractal dimension is $D \approx 0.631$. It was assumed that the structure is organized with three equal intervals. If it is not so, the Cantor-dust is slightly changed.

If the Cantor-dust remains symmetric, but the interval between the bars increases, then the dimensionality decreases and vice versa.

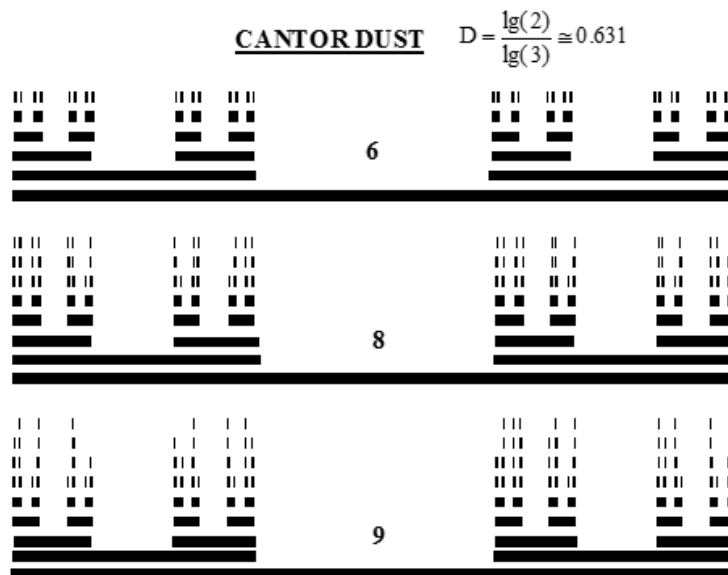


Fig. 4.4.3. The control-dust fractal well characterizes the self-similar structure of bifurcative processes.

4.4.2. System properties

There are tiny, practically molecular, charge transfers which are catalyzed by enzymes. The enzymes are, in essence, those things which promote the electron transfers and bring the microscopic currents into existence – in the simplest terms, they are the microscopic conductors [63].

The charges transmitted during the microscopic (vibration) processes cover a somewhat larger scale and are manifested in a soliton transfer. In case of the living systems, these vibration processes destabilize their next nearest neighbourhood. In this way, the actual unit, as a result of this environmental destabilization, starts to stabilize and, thus, destabilizes its predecessor. In other words, a “stability focal point” runs through the material, something that is one of the most basic forms of the charge flows or the information flows in living systems. This “social signal” also makes connections between proteins, cells, tissues and organs possible. Certain varieties of these social signals trigger the chemical processes and their instant local production increases the efficiency of “social signals” (for example, the rate of production of nitrogen-monoxide in the pericellular systems). During division, the cell isolates itself from its environment in the actual tissue, and breaks a social signal. After division, the signal broken path can even be geometrically re-established.

The frustration process arises at each level of organization in the living material, from the water proton frustration to the intercellular frustration, which is what a social signal produces.

The above vibrations were measured together with protein internal vibrations; the resulting frequencies fall within quite a narrow range in the 100 GHz band and quite close to the proton vibration. To this we must add that the polyhedral structures derived from global proteins are not the sort to fill the fields. They create geometric frustrations within themselves. These frustrated chains are similar to the frustration chain suggested in the high-temperature ceramic superconductors. The concentration batteries, formed by the concentration gradients in the body-electrolyte create significant macroscopic currents, which is part of the body's biological functions. In essence, these concentration batteries form internal surfaces (membranes) on the high electric fields. For instance, a simple cell membrane has a field strength of approx. 2 million V/m as a result of the ordered double-layer's extraordinary thinness and relatively high-membrane potential. A potential difference acts as a driving force between different ions and the charged particles in general. This concentration battery is capable of produce in a general currents in living systems.

Depolarization currents work on an even larger scale and are capable of limiting or forcing the operation of certain organs (e.g., the heart, muscles, etc.). These depolarization currents (i.e. in certain injuries (“wound current”) and in the case of broken bones), play a delimiting feedback role in the acceleration of cell growth.

Different global currents come into the body along with those already mentioned caused by the flow of aqueous solutions within the body.

4.4.3. Bio-signals and their control

The ordered water can probably function as an information exchanger (transducer) between the molecules and, even partly, between the larger units (e.g. cells) by means of the hydrogen-bridges. The measured protein vibration frequencies are quite high (10–1000 GHz, the corresponding lifetime is 10^{-10} – 10^{-12} s) [103,104]. This frequency range is basically in agreement with the measured Brillouin- and Raman-scattering. The calculated water vibration frequencies reach about 200 cm^{-1} and 30 cm^{-1} (2000 GHz in the stretching mode and 900 GHz in the torsion mode, respectively) [105,106], which (the entire torsion mode at 30 cm^{-1} , i.e. at 900 GHz) is tunable by an external electric field [107]. Intercellular communications (introduced by Frolich [108] and Becker postulates the "secondary nervous system" [109]) also occur in this mode (100 GHz [110]), while the proton oscillation (the hydrogen bridge generating solitons [111]) is also

within the range of 100 GHz. The optical radiation in the infrared (1–1000 THz [1 THz = 1000 GHz]) in far infrared (100 GHz) and even in the visible and ultraviolet ranges [69] support the imposed role of the water as the transmitter in the cellular system well. The intercellular communication [112] and the social signal between the cells [113] can be easily explained in this way.

The ordered water is very useful and able to switch quickly, transferring some energy, its time constant ranges up to 10–12 s [114]. The quick energy (and/or disturbance) transport is mainly connected to the tetrahedral structure of the water molecules and, consequently, to the geometric frustration, as discussed before.

The biological charge transfer requires a close donor-acceptor distance: if they are 2 nm from each other, the charge-donation can decrease by 10–12 nm [115]. In case the proteins are in close vicinity, the ordered water makes the charge transfer between them possible [116]. Very recently, it has been observed that haemoglobin binds 60 water molecules during the oxygen transport [107]. This pattern can be expanded to some other switching systems [118]. It is not yet known [119], why there is a definite number of water molecules related to the certain biological process, but the only explanation can be found in the connection with the ordered water. Note that a very small energy effect in the haemoglobin action (8 kcal/mol) [120] is exactly within the range of the hydrogen-bridge energies as well as within the range of the water cluster melting energy [106].

A definite chemical balance defines the function, or rather, the combustion of biological organic material. This balance is fundamentally an energetic one acting between the solar energy on the one side (as a source) and the vital energy – on the other side (as the absorber or user). In essence, both sides of the chemical reactions take place through the electromagnetic interactions, either in the generation or in the combustion of the organic material. The energy exchange goes through the non-ionizing electromagnetic radiation. Thus, the frequency equivalent to electromagnetic radiation involved in the 10^{-4} – 10^{-1} eV biological energy transfers is 10–10,000 GHz. (Naturally, the actual frequency depends on the energy transfer involved (biological metabolism and information exchange), since every type is different).

In essence, the formation, or, rather, decomposition of water works as two basic pillars of the energy equation in the life processes, but these are not immediate processes which are completed in only one step. Of course, in the decisive majority of cases, other elements apart from hydrogen and oxygen participate in the process, which means that we need to direct our attention towards other processes as well.

Biological systems cannot withstand this type of energy release and, so, the activation energy, i.e. the energy release, proceeds step-by-step in these systems. The mechanism, by which these steps are taken, is one of the most characteristic biological properties. By categorizing the energy transfer in a different way from that for the case of the pure chemistry, it brings them in steps, which utilize a fundamentally small amount of energy (characteristically falling within the 10-100 GHz radiation frequency band). This gives a very interesting recognition of different metabolic properties in the given living system, because the energy loss of the electron energy creates the definite radiation in the 100 GHz region (this process is a fundamental conversion, which makes the nutrients available to the other life processes, which are not capable of such a conversion, see later).

The question concerning the influence of external noises on the behaviour of dynamic systems has been widely discussed in the literature [1–4]. Recently, due to the development of synergetics, new interesting results have been obtained resulting in the re-estimation of the role of random factors as well as the effect of external random field on open systems.

At first glance, the external noise in this case appears to be averaged and the macroscopic system essentially matches its state to the average conditions of the medium. Second, the stochastic variability of the conditions results in the state blurring and spreading out around the average state. The concepts that the role of fluctuations is, finally, secondary, are based on a certain linear type of the relationship between the system and environment. However, the behaviour of the non-linear system in the noise-containing medium is testament to the opposite. It has been found, in particular, that the external noise not only causes the evident linear response in dynamic systems, i.e. it results in the linear fluctuations of their characteristics, but also governs the qualitative variation of the system behaviour [5 – 9]. This means that the external noise results in the occurrence of new stationary non-equilibrium states, undamped periodical oscillations, etc. From that point of view, one may conclude that not only the determined external influence but also the random fluctuations of the external medium properties may appear to be the factor which governs the re-arrangement of the behaviour of strongly non-equilibrium system. Recent theoretical and experimental studies [10 – 14] show that, despite its apparent disordering effect, the random character of the medium can initiate much richer variety of structures compared with those structures resulting from the determined conditions. It turns out that the rise of the stochastic variability of the medium can result in the additional structuration of non-linear systems and no analogy can be found with the determinate case [9].

As shown below, the role of external medium fluctuations is quite essential in producing the dissipative structures in non-crystalline solids and biological objects with different functional ordering levels.

5.1. Noise-induced phase transformations: elements of probability theory

5.1.1. Energetic criteria of pink noise

The pink noise characterizes actually almost all dynamic effects in the living objects [15,16]. This behavior is the real fingerprint of self-organization, having a harmonic self-similar time structure of these dynamic effects.

Let $x(t)$ be a function of time. The Fourier transform of this function is defined by the following integration [16]:

$$X(f) = \int_{-\infty}^{\infty} x(t) e^{-j2\pi f t} dt = \mathcal{F}\{x(t)\}. \quad (5.1.1)$$

The Fourier transform of the function $x(at)$, where a is an arbitrary positive scalar, is:

$$\mathcal{F}\{x(at)\} = \frac{1}{a} X\left(\frac{f}{a}\right). \quad (5.1.2)$$

Now, let $x(t)$ be a representation of a stochastic process. One can define the effective power of this process by:

$$\bar{x} = \lim_{T \rightarrow \infty} \int_{-T}^T x^2(t) dt \quad (5.1.3)$$

It follows from the Wiener-Khintchine theorem [16] that this average power may be evaluated by the following integration in the frequency range:

$$\bar{x} = \lim_{T \rightarrow \infty} \int_{-T}^T x^2(t) dt = \int_0^{\infty} S(f) df \quad (5.1.4)$$

where $S(f)$ is the so-called power spectral density function

$$S(f) = \frac{1}{2\pi} X(f) X^*(f) = \frac{1}{2\pi} |X(f)|^2 \quad (5.1.5)$$

and an asterisk denotes the complex conjugation.

A stochastic process is $1/f$ -noise if its power spectral density function has the form of:

$$S(f) \approx \frac{1}{f} \quad (5.1.6)$$

It is convenient to define the self-similarity of a stochastic process: a stochastic process is said to be self-similar if the effective work of the representation $x(t)$ of the stochastic process equals to the effective work of the representation $x(at)$ defined over the time scale at , for every positive scalar a , i.e.:

$$\lim_{T \rightarrow \infty} \int_{-T}^T x^2(t) dt = \lim_{T \rightarrow \infty} \int_{-T}^T x^2(at) d(at) \quad (5.1.7)$$

We can prove that if a stochastic process is self-similar then it is a pink noise. Really, if we apply the Wiener-Khintchine theorem to the equation (5.1.7), we get:

$$a \int_0^{\infty} \frac{1}{a^2} S\left(\frac{f}{a}\right) df = \int_0^{\infty} S(f) df \quad (5.1.8)$$

where the equation (5.1.2) was taken into account. Also, for the power spectral density function, the functional equation holds:

$$S\left(\frac{f}{a}\right) = a S(f) \quad (5.1.9)$$

for every positive scalar a, f .

To solve this equation one has to set for a the value $a = f$. Then can get:

$$S(f) = \frac{S(1)}{f} \sim \frac{1}{f} \quad (5.1.10)$$

which proves the original statement.

5.1.2. The white noise processes and their modelling

One may recognize the following aspects when solving the problem of modelling the external random field influence on the open macroscopic system:

i) The influence of the environment on the non-equilibrium system is described at the phenomenological equation level with the help of the external parameters λ_t being the random values. These values may, in particular, be the random stationary processes represented in the following form:

$$\lambda_t = \lambda + \sigma \xi_t, \quad (5.1.11)$$

where λ corresponds to the average value, ξ_t describes fluctuations around the average value, σ is the external noise intensity ($\sigma^2 = \langle \xi_t, \xi_t \rangle$). The introduction of the phenomenological description of the external noise results in the following stochastic differential equation (SDE) [15]:

$$\frac{dX(r,t)}{dt} = f_\lambda(X(r,t)). \quad (5.1.12)$$

Here $X(r,t)$ is the state parameter, $f_\lambda(X(r,t)) = h(x) + \lambda_t g(x)$ is the functional dependence which expresses the local evolution of $X(r,t)$ components over the time t and the space r , $h(x)$ and $g(x)$ are the functions of $X(r,t)$. The examples of the state parameters are, say, the deviation of the system from the equilibrium state, the portion of the atoms in the amorphized states, the dynamic displacements [11], etc. The equation (5.1.2) with allowance made for (5.1.11) takes the form:

$$\frac{dX(r,t)}{dt} = f_\lambda(X)dt + \sigma g(X)dW_t = h(X) + \lambda g(X) + \xi_t g(X), \quad (5.1.13)$$

where $dW_t = \xi_t dt$.

ii) The determination of the functional dependence between the random values, which simulate the medium fluctuations. A sharp distinction of the time scales is essential for the white noise, namely, the state of the medium varies much more rapidly than the macroscopic state of the system. Denote the characteristic time of the time evolution of the system as τ_m , which is identical to the time of the system relaxation to the stationary state X_s :

$$\tau_m = |1/\omega(X)|_{X=X_s}, \quad \omega(X_s) = \mathcal{D}f_\lambda(X)/\mathcal{D}X|_{X=X_s}.$$

The correlation time τ_{cor} is the measure of the random medium fluctuations and is defined as a process memory time:

$$\tau_{cor} = \int_0^\infty \frac{C(\tau)d\tau}{C_0}.$$

For the correlational function $C(\tau) = C(0)\exp\{-\gamma\tau\}$ we have $\tau_{cor} = \gamma^{-1}$, where γ is a constant, t is the time. The rapidly fluctuating medium is characterized by the fact that the correlation time τ_{cor} of the random process λ_t is much less than the characteristic macroscopic time τ_m of the system:

$$\tau_{cor} \ll \tau_m.$$

A peculiar feature of the white noise is that this process is completely random, i.e. at each moment of time, it attains an independent value and has an infinitely large dispersion. In the white noise spectrum, the energy is evenly distributed over all frequencies similarly to the case of a white light, whereas the correlational function is proportional to the Dirac δ -function.

iii) Time evolution of the probability density for the $\mathfrak{R}(y,t+s|x,s)$ transition is described by the Fokker-Planck equation (FPE), which in the Ito's interpretation and in the Stratonovich's interpretation has a form [9,15]:

$$\begin{aligned} \frac{d\mathfrak{R}(y,t+s|x,s)}{dt} &= \partial_y f_\lambda(y)\mathfrak{R}(y,t+s|x,s) + \frac{\sigma^2}{2} \partial_{yy} g^2(y)\mathfrak{R}(y,t+s|x,s), \quad (5.1.14) \\ \frac{d\mathfrak{R}(y,t+s|x,s)}{dt} &= -\partial_y \left[f_\lambda(y) + \frac{\sigma^2}{2} g(y)\partial_y g(y) \right] \mathfrak{R}(y,t+s|x,s) + \frac{\sigma^2}{2} \partial_{yy} g^2 \mathfrak{R}(y,t+s|x,s), \end{aligned}$$

where ∂_y and ∂_{yy} are the first and the second derivatives with respect to y ; y and x are the states of the system at the moments $t+s$, s , respectively.

iv) The advantage of the white noise approximation lies in the possibility of describing the time evolution of the system by a diffuse Markov process with well-elaborated mathematical methods. Since the correlation time for the real random process is non-zero, one has to take into account the non-Markov behaviour of the system to describe these processes more strictly. To do this one may

use the "colour noise" approximation for which the prehistory of the system and the external noise are correlated due to the environmental memory. In this case, the two-dimensional process described by the variable x and fluctuating parameter ξ_t is considered [9]:

$$\begin{aligned} dx &= f(X)dt + g(X)\xi_t dt \\ d\xi_t &= -\gamma_{colour}\xi_t dt + \sigma dW_t \end{aligned} \quad (5.1.15)$$

where γ_{colour} is a constant of colour noise.

5.2. On the peculiarities of the white noise influence on the formation of dissipative structures

5.2.1. Dissipative structures: influence of white noise

The parameters which describe open systems (i.e. non-crystalline solids or biological objects) are the values which vary due to the mass and heat exchange with the environment and, thus, also fluctuate. These fluctuations can be controlled and considered the "external" noise. The external medium fluctuations of, say, temperature (pressure, radiation) variation rate can affect the system during the process of non-crystalline materials production, biological objects activity at different loads and, more essentially, result in the qualitatively new non-equilibrium phase transformations not predicted within the framework of the determinate influence [11,14].

Consider, as an example, the initial influence of the external random temperature field in the white Gaussian noise approximation on the melt being cooled, as well as on the structure and stability of the non-crystalline materials formation. The non-crystalline structure formation can be simulated by a bifurcation process defined by the solution of the non-linear differential equation:

$$\begin{aligned} \frac{\partial \eta}{\partial t} &= -\frac{\partial \psi}{\partial \eta}, \\ \psi &= -\frac{\lambda}{2}\eta^2 - \frac{\gamma}{3}\eta^3 + \frac{\beta}{4}\eta^4 + \frac{D}{2}\Delta\eta. \end{aligned} \quad (5.2.1)$$

Here ψ is Lyapunov's functional, η is an inner parameter of the system, which describes the deviation of the system from the equilibrium, D is the diffusion coefficient, γ and β are the parameters, λ is a control parameter. Consider the deviation of the portion of atoms in the liquid-like (amorphized) states from their equilibrium value as the parameter η (here, we neglect the spatial fluctuations for simplicity). The control parameter λ of the system during cooling may be approximated by the expression:

$$\lambda = \begin{cases} a\tilde{q}, \frac{q - q_c}{q_c} & \text{at } q \rightarrow q_c, \\ a \arctan(\ln[1 + \tilde{q}]) & \text{in other cases} \end{cases}.$$

Here q is the cooling rate, q_c is the critical cooling rate, which corresponds to the transition to the non-crystalline state. Neglecting the spatial fluctuations, the determinate equation of motion for η may be written according to (5.2.1):

$$\frac{\partial \eta}{\partial t} = \lambda g(\eta) + h(\eta), \quad g(\eta) = \eta, \quad h(\eta) = \gamma\eta^2 - \beta\eta^3. \quad (5.2.2)$$

Assume that the system (melt) under cooling is affected by the external temperature field ξ_t with the intensity σ . Consider the behaviour of the system when the fluctuations around the average cooling rate value occur rapidly enough, which allows one to apply the white Gaussian noise

approximation, i.e. assume $\lambda = \lambda + \sigma \xi_t$. The initial equation (5.2.2) in this case is reduced to the stochastic differential equation in the Stratonovich's interpretation:

$$d\eta(t) = (\lambda\eta + \gamma\eta^2 - \beta\eta^3)dt + \sigma\eta dW_t. \quad (5.2.3)$$

The evolution of the η value distribution density $\mathfrak{R}(\eta, t)$ is given by:

$$\partial_t \mathfrak{R}(\eta, t) = -\partial_\eta \left(\lambda\eta + \gamma\eta^2 - \beta\eta^3 + \frac{\sigma^2}{2}\eta \right) \mathfrak{R}(\eta, t) + \frac{\sigma^2}{2} \partial_\eta^2 (\eta^2 \mathfrak{R}(\eta, t)). \quad (5.2.4)$$

The continuity equation is $\partial_t \mathfrak{R}(\eta, t) + \partial_\eta J(\eta, t) = 0$, where

$$J(\eta, t) = \left(\lambda\eta + \gamma\eta^2 - \beta\eta^3 + \frac{\sigma^2}{2}\eta \right) \mathfrak{R}(\eta, t) - \frac{\sigma^2}{2} \partial_\eta (\eta^2 \mathfrak{R}(\eta, t))$$
 is the probability flux.

In the stationary state, $\partial_t \mathfrak{R}(\eta) = 0$ and, respectively, $\partial_t \mathfrak{R}(\eta) = 0$. The stationary probability density $\mathfrak{R}_s(\eta)$ is defined by the functional relation:

$$\mathfrak{R}_s(\eta) = \frac{N_{norm}}{g(\eta)} \exp \left\{ \frac{2\lambda}{\sigma^2} - \frac{\lambda(u) + h(u)}{g(u)} \right\} = N_{norm} \eta^{\frac{2\lambda}{\sigma^2} - 1} \exp \left\{ \frac{2\lambda}{\sigma} \eta - \frac{\beta}{\sigma} \eta^2 \right\}. \quad (5.2.5)$$

Here N_{norm} is a normalization factor found from the normalization condition:

$$\int_0^\infty \mathfrak{R}_s(\eta) d\eta = 1, \quad 1/N_{norm} = \frac{1}{2} \left(\frac{\sigma^2}{\beta} \right)^{\frac{\lambda}{\sigma^2}} \Gamma \left(\frac{\lambda}{\sigma^2} \right) + \frac{\gamma}{\sigma^2} \left(\frac{\sigma^2}{\beta} \right)^{\frac{\lambda}{\sigma^2} + \frac{1}{2}} \Gamma \left(\frac{\lambda}{\sigma^2} + \frac{1}{2} \right), \quad (5.2.6)$$

and $\Gamma(x)$ is a gamma-function. It follows from (5.2.5) and (5.2.6) that $\mathfrak{R}_s(\eta)$ can be integrated over the (0,1) interval, i.e. the stationary solutions exist only if $\frac{2\lambda}{\sigma-1} > 1$ or $\lambda > 0 (q > q_c)$. At $\lambda < 0$, which is equivalent to $\tilde{q} < 0$ and $q < q_c$, the probability density (5.2.5) with the inclusion of the expression for N_{norm} behaves as a delta-function. The extreme of the stationary density $\mathfrak{R}_s(\eta)$ correspond to the macroscopic stationary non-equilibrium states of the system, and the qualitative variation of the form of $\mathfrak{R}_s(\eta)$, depending on the control parameter and the noise intensity, serves as an indicator of the transition [9]. The solutions of the equation for the stationary density extrema determination have a form:

$$\eta_1 = 0, \quad \eta_{2,3} = \frac{\gamma \pm \sqrt{\gamma^2 + 4\beta(\lambda - \sigma^2/2)}}{2\beta}. \quad (5.2.7)$$

The roots $\eta_{2,3}$ exist at $\lambda > \frac{\sigma^2}{2} - \frac{\gamma^2}{4\beta}$ and always correspond to the maximum $\mathfrak{R}_s(\eta)$, while η_1 corresponds to the maximum $\mathfrak{R}_s(\eta)$ only if $0 < \lambda < \frac{\sigma^2}{2}$ (the positive values of the deflection of an inner parameter of the system from the equilibrium state have a physical sense, therefore, we shall further analyze the $\mathfrak{R}_s(\eta)$ extreme curve at $\eta > 0$). Thus, given the random field affecting the melt during cooling, the qualitatively different transitions to the non-crystalline state may occur. The transition at $\sigma = 0$ and $\lambda = 0$ corresponds to the determinate case ($q = q_c$), while that at $\sigma < 0$ and

$\lambda = \frac{\sigma^2}{2}$ is accompanied by a sharp change in the probability density shape when the δ -like distribution $\mathfrak{R}_s(\eta)$ is blurred towards the non-zero values of η .

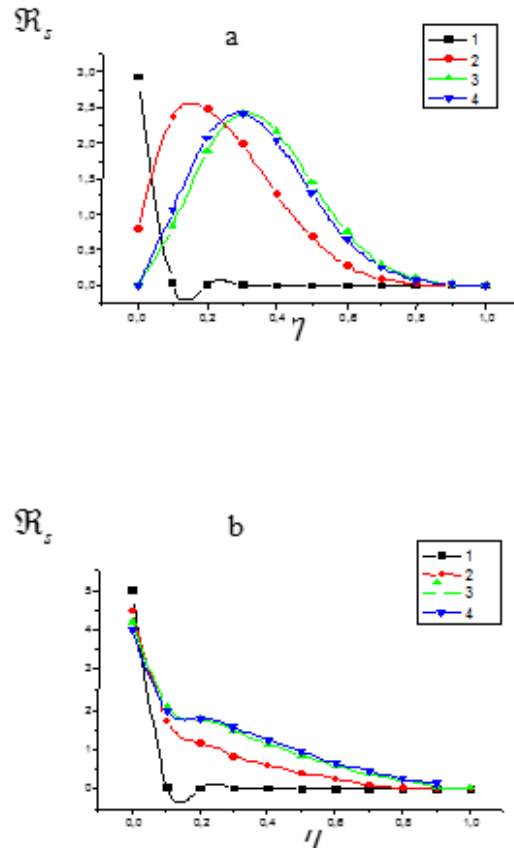


Fig. 5.2.1. The behavior of the stationary probability density for the distribution of the liquid-like domains of *ht* enon-equilibrium system at fixed noise intensities: a - $\sigma = 0.6 (10^{-2}(C/s)^2)$; b - $\sigma = 15(10^{-2}(C/s)^2)$.

5.2.2. The white noise: bifurcation diagram

The behaviour of the stationary density of the distribution for the deviation of a portion of atoms in the liquid-like (amorphized) amorphous states from their equilibrium value as a function of the external noise intensity is plotted in Fig. 5.2.1. The probability density reveals the following peculiarities. If the melt cooling rate is less than the critical one ($\lambda < 0$), then the stationary point $\eta = 0$, which corresponds to the crystalline state, is asymptotically stable (the distribution $\mathfrak{R}_s(\eta)$ in this case behaves as the δ -function). Given the external noise and the control parameter value of $0 < \lambda < \sigma^2/2$, the stationary probability density turns to infinity at $\eta \rightarrow 0$, i.e. a part of the properties of the δ -function is retained, and $\eta = 0$ remains the most probable quantity (see Fig.5.2.1b); however, it is no longer the stable stationary point. Hence, in this case, the transition occurs to the partially disordered (amorphous-crystalline) state, which relaxes to the equilibrium one at $t \rightarrow \infty$; the formation of the non-equilibrium structure is also possible, since $\mathfrak{R}_s(\eta) \neq 0$ at $\eta = 0$, however it is not asymptotically stable. In other words, a random temperature field exerts the disorganizing action on the melt under cooling when the self-consistent interaction of subsystems is partially destroyed. If $\lambda = \sigma^2/2$, the character of the distribution is again sharply changed, although the density of the distribution of $\mathfrak{R}_s(\eta)$ is non-zero at $\eta = 0$, the most probable value of $\mathfrak{R}_s(\eta)$ occurs at $\eta = 0$ (Fig. 5.2.1b). For $\lambda > \sigma^2/2$, the probability of the crystalline-like structure formation tends to zero (Fig. 5.2.1a), and a distinct non-zero extreme value of $\mathfrak{R}_s(\eta)$ is observed. The behaviour of

the extrema in the stationary probability density $\mathfrak{R}_s(\eta)$ as a function of the cooling rate q at fixed noise intensities is plotted in Fig. 5.2.2. The dependence of $\mathfrak{R}_s(\eta)$ on \tilde{q} may be considered a modification of the determinate bifurcation diagram of sorts (Fig. 5.2.3) at which the displacement of the curve $\eta(\tilde{q})$ by $\sigma/2$ over \tilde{q} is observed.

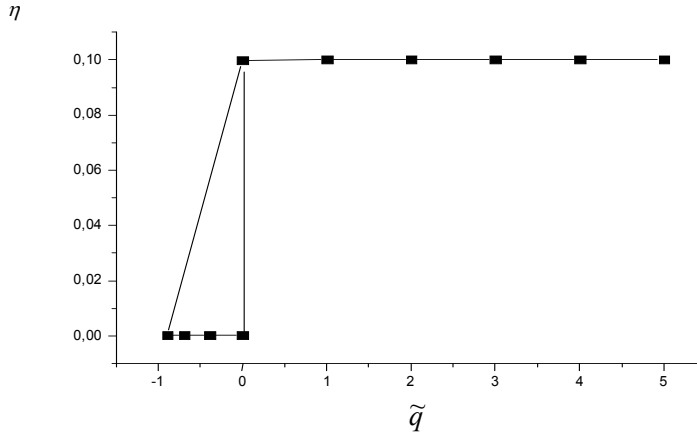


Fig. 5.2.2. The dependence $\mathfrak{R}_s(\eta)$ as a function of the cooling rate \tilde{q} ($\sigma = 0.6 \cdot 10^{-2} (C/s)^2$).

One may conclude from the above character of the $\mathfrak{R}(\eta)$ distribution that the transition in the vitreous-producing semiconductor melt under cooling can be initiated by maintaining or reducing the intensity of the temperature field fluctuations in the external medium. The knowledge of only the average state of the medium is inadequate to predict the macroscopic behaviour of the system: at $\lambda > \sigma/2$ we have $\mathfrak{R}_s(0) = 0$; at $\lambda = \sigma/2$, $\mathfrak{R}_s(0)$ remains finite and at $\lambda < \sigma/2$, $\mathfrak{R}_s(0) \rightarrow \infty$, i.e. the transition to the non-crystalline structure vanishes. Another peculiarity of the noise-induced transitions, which distinguishes these transitions from the determinate case, is the possibility of a set of η values to occur and, hence, that of a set of spatially disordered structures with different ordering domains. Thus, the approach under consideration allows one to calculate the critical values of the parameter fluctuations, at which the structural characteristics of non-crystalline materials do not vary with the conditions of their production, as well as to predict the production of qualitatively new structures at the certain noise intensities [19-22].

5.2.3. The non-stationary probability density

The time of deviation of the probability density of the system from the equilibrium state is described by the Fokker-Planck equation:

$$\partial_t \mathfrak{R}(\eta, t) = -\partial_\eta \left(\lambda \eta + \gamma \eta^2 - \beta \eta^3 + \frac{\sigma^2}{2} \right) \mathfrak{R}(\eta, t) + \frac{\sigma^2}{2} \partial_{\eta\eta} (\eta^2 \mathfrak{R}(\eta, t)). \quad (5.2.8)$$

The initial and boundary conditions of the problem are:

$$\mathfrak{R}(\eta, 0) = \delta(\eta), \quad 0 \leq \eta \leq 1,$$

$$\mathfrak{R}(\eta, t) = \mathfrak{R}(1, t) = 0, \quad t \geq 0. \quad (5.2.9)$$

Rewrite the Fokker-Planck equation (5.2.8) in the following form:

$$\begin{aligned} \partial_t \mathfrak{R}(\eta, t) = & -(\lambda + 2\gamma\eta - 3\beta\eta^2 - \sigma^2) \mathfrak{R}(\eta, t) - \\ & - \left(\lambda \eta + \gamma \eta^2 - \beta \eta^3 + \frac{\sigma^2}{2} \right) \partial_\eta \mathfrak{R}(\eta, t) + \frac{\sigma^2 \eta^2}{2} \partial_{\eta\eta}^2 \mathfrak{R}(\eta, t). \end{aligned} \quad (5.2.10)$$

To numerically solve the differential equation (5.2.10), we shall reduce it to the system of algebraic equations using the finitary-differential method [18]. Namely, we shall put: $\eta = jh$, $t = n\Delta t$, $j, n \leq \infty$. Here h , Δt are the steps over the coordinate η and

time t , respectively. The behaviour of the non-stationary probability density of the system deviation from the equilibrium state and its time evolution as a function of the control parameter and external noise intensity have been calculated.

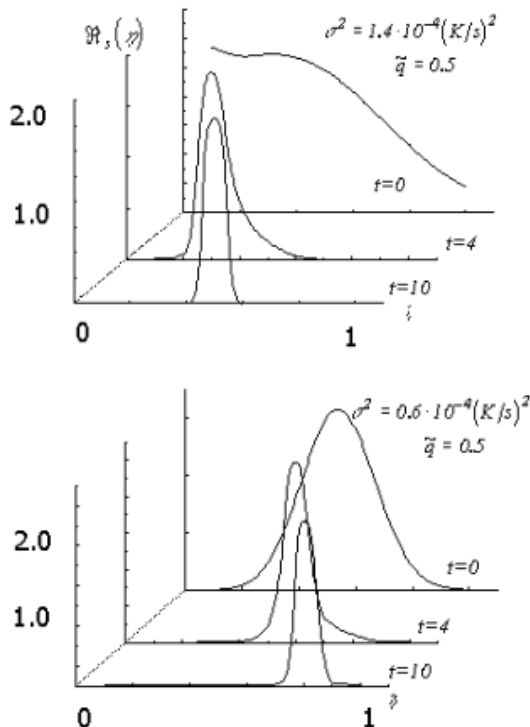


Fig. 5.2.3. Time evolution of the probability density of the system from the equilibrium state at fixed noise intensities.

The following regularities were found:

- At $q > q_c$ the δ -like shape of $\mathfrak{R}(\eta)$ is blurred with time and displaced towards the lower η .
- The domain of the possible sets of η values is narrowed at the same time.
- Momenta are broadened with the external noise intensity rise.

5.3. The colour noise action on the dissipative structure formation

The advantage of a white noise approximation is that it allows one to simulate the temporal evolution of diffuse Markov system by the process with the use of well-known mathematical means. However, for substantial systems, the time of correlation is not equal to zero. The use of a white noise approximation, as a previous history of a system and the state of noise in the given instant correlation due to a storage of a surrounding medium is, in this case not obviously possible. It is especially essential for biological systems.

Consider a two-dimensional process, which is featured by an order parameter of a system $\eta(t)$ and the fluctuating parameter $\xi_i(t)$. In this case, one has to consider two stochastic differential equations with respect to the random processes $\eta(t)$, $\xi_i(t)$ (see (5.1.15)) :

$$\begin{aligned} d\eta &= f_\lambda(\eta)dt + g(\eta)\xi_i dt, \quad f_\lambda(\eta) = \lambda g(\eta) + h(\eta), \\ d\xi &= -\gamma_{\text{colour}}\xi_i dt - \sigma dW_t. \end{aligned} \quad (5.3.1)$$

Here ξ_t is, actually, a white noise for which the following conditions hold:

$$\langle \xi_t \rangle = 0, \quad \langle \xi_t \xi_{t'} \rangle = 2\delta(t - t') = \frac{\sigma^2}{\tau} \exp\left\{-\frac{t - t'}{\tau}\right\}$$

where τ is a noise correlation time, λ is a control parameter, γ_{colour} and σ are the random process constants, and $\delta(t - t')$ is the Dirac function.

The probability density is defined by the solution of the corresponding Fokker-Planck equation [9]:

$$\begin{aligned} \partial_t \mathfrak{R}(\eta, z, t | \eta_0, z_0) &= -\partial_\eta (f_\lambda + zg) \mathfrak{R}(\eta, z, t | \eta_0, z_0) + \partial_z \gamma_{colour} z \mathfrak{R}(\eta, z, t | \eta_0, z_0) + \\ &+ \frac{\sigma^2}{2} \partial_{zz} \mathfrak{R}(\eta, z, t | \eta_0, z_0) \end{aligned} \quad (5.3.2)$$

Here, z is the parameter of the state of the system.

In a general case, one fails to solve the problem for the colour noise. Therefore, we shall restrict ourselves to the consideration of the particular case of the stochastic differential equation:

$$d\eta = -\alpha_{norm} g(\eta) H(\eta) dt + \sigma g(\eta) \xi_t dt$$

where $H(\eta) = \int_\eta dz / g(z)$, α_{norm} is the normalization parameter.

A peculiarity of such systems is that using the transformation $\mathfrak{I} = H(\eta)$, we obtain the linear differential equation:

$$d\mathfrak{I} = -\alpha_{norm} \mathfrak{I} dt + \sigma \xi_t dt. \quad (5.3.3)$$

For the continuous random function ξ_t , the process:

$$\mathfrak{I}_t(\omega) = \mathfrak{I}_0(\omega) \exp\{-a(t - t_0)\} + \int_{t_0}^t \xi_s(\omega) \exp\{-\alpha(t - s)\} ds = \mathfrak{I}_0(\omega) \exp\{-a(t - t_0)\} + Y_t(\omega)$$

is a sole solution of equation (5.3.3) with the initial conditions \mathfrak{I}_0, t_0 .

The present approach is difficult to be realized in practice. Therefore, it is worthwhile to apply the approximate methods using the white noise results as the first approximation. Let us rewrite the system of the stochastic differential equations (5.3.1) in the following form:

$$\begin{aligned} d\eta &= f_\lambda(\eta) dt + \frac{\xi_t}{\varepsilon} g(\eta) dt, \\ d\xi_t &= -\frac{\xi_t}{\varepsilon^2} dt - \frac{\sigma}{\varepsilon} dW_t. \end{aligned} \quad (5.3.4)$$

The factor ε has been introduced as a measure of the removal from the white noise approximation (the limit transition $\varepsilon \rightarrow 0$). Then, the equation for the near-white noise influence has a form [9,23]:

$$d\eta = f_\lambda(\eta)dt + \frac{1}{\varepsilon}g(\eta, \tilde{\xi}_t)dt \quad (5.3.5)$$

where $\tilde{\xi}_t = \xi_t/\varepsilon$ is an effective fluctuation.

The density of the probability of the transitions is defined in this case by solving the following equation:

$$\begin{aligned} \partial_t \mathfrak{R}_\varepsilon(x, z, t) &= \left(\frac{f_1}{\varepsilon^2} + \frac{f_2}{\varepsilon} + f_3 \right) \mathfrak{R}_\varepsilon(x, z, t), \\ f_1 &= \partial_z z + \frac{\sigma^2}{2} \partial_{zz}, \quad f_2 = -z \partial_\eta g(\eta), \quad f_3 = -\partial_\eta f(\eta). \end{aligned} \quad (5.3.6)$$

Let us expand the probability density over a power series in ε , restricting ourselves to the stationary case:

$$\mathfrak{R}_\varepsilon(\eta, z) = \mathfrak{R}_0(\eta, z) + \varepsilon \mathfrak{R}_1(\eta, z) + \varepsilon^2 \mathfrak{R}_2(\eta, z) + \dots$$

The normalization condition is: $\int_{-\infty}^{\infty} \mathfrak{R}_k(\eta, z) d\eta dz = 1$. It is obvious that $\mathfrak{R}_s = \int \mathfrak{R}_k(\eta, z) d\eta$.

Then, in the first approximation of the perturbation theory, we have:

$$\begin{aligned} \mathfrak{R}_0(\eta, z) &= r_0(\eta) \mathfrak{R}_s(z), \quad r_0(\eta) = \mathfrak{R}_0(\eta), \\ \mathfrak{R}_1(\eta, z) &= r_1(\eta) \mathfrak{R}_s(z), \quad r_1(\eta) = -\frac{2}{\sigma} \frac{\lambda g + h}{g^2}. \end{aligned} \quad (5.3.5)$$

Relations (5.3.5) allow one to determine the ordering variation of the dissipative structure for the given shape of the colour noise and frequency. As an example, Fig. 5.3.1 illustrates the dependence of the stationary density of the probability of system removal from the equilibrium state $\mathfrak{R}(\eta, z)$ as a function of various frequencies z and a white noise correlation time ε .

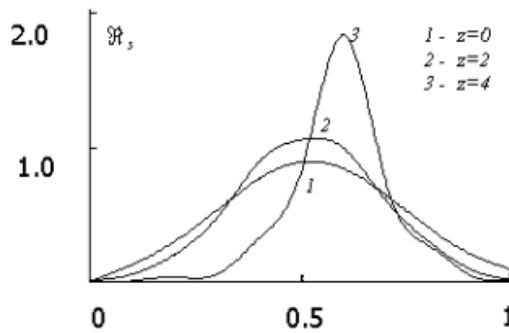


Fig. 5.3.1. The dependence $\mathfrak{R}(\eta, z)$ as a function of various frequencies z and white noise correlation time ε .

5.4. Pink noise in the bistability of the living system structure

The bistable state (corresponding to the bistable potential) can be characterized as a wave (Fig. 5.4.1) with positive and negative amplitudes in the actual states. The above described structural arrangements of the bistabilities can be presented in a form of a set of waves harmonically and self-similarly fitted to each other (Figs. 5.4.2 – 5.4.4).

Wave and bistability

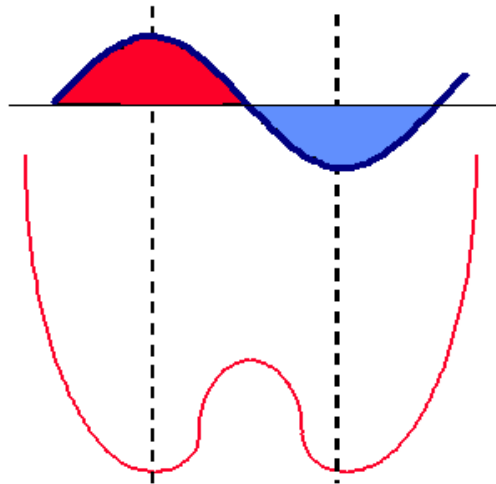


Fig. 5.4.1. Bistable state and wave.

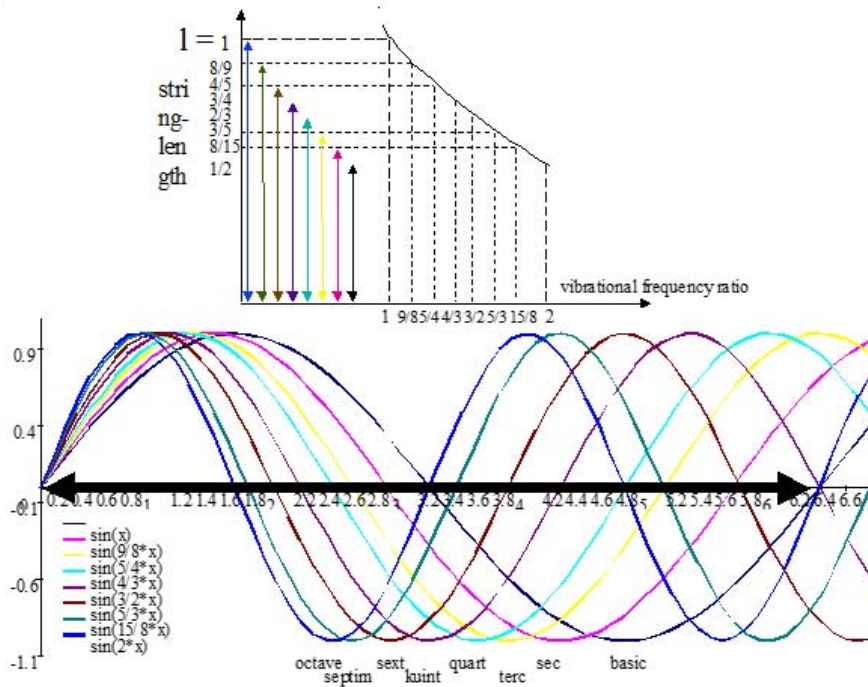


Fig. 5.4.2. String-length as a function of the vibrational frequency ratio.

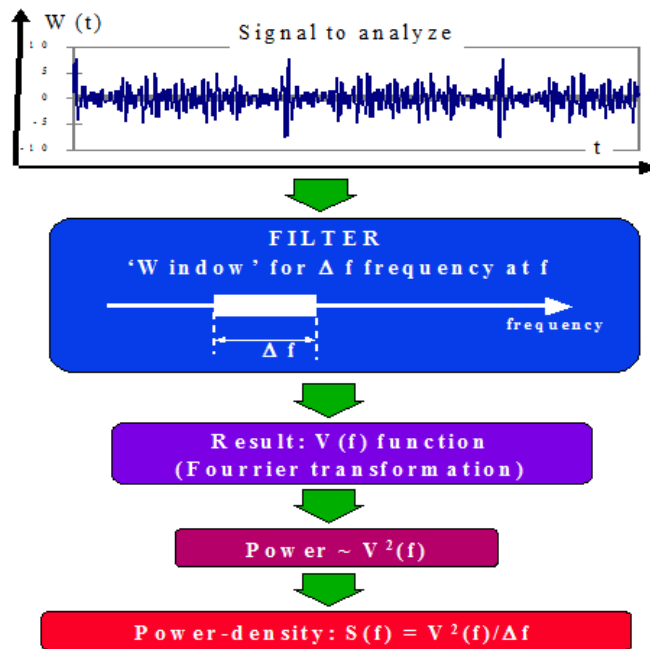


Fig. 5.4.3. Signal to analyse (Fourier transformation).

The sum of these waves (the original living act) is a noise (an example is shown in Fig. 5.4.4), which is exactly a pink noise. This is a simple and model-like explanation of the pink noise dominance in the living dynamic phenomenon (Fig. 5.4.4).

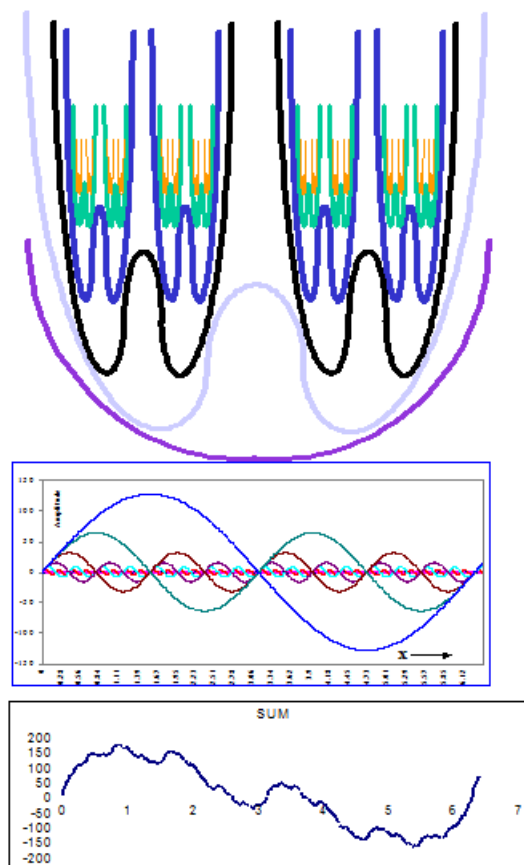


Fig. 5.4.4. Pink noise and self-similarity of waves.

INTERACTION OF ELECTROMAGNETIC RADIATION WITH BIOMOLECULAR STRUCTURES

The studies of dissipative processes at the photo-induced structural changes as well as of the consistent change in the configurational energy on the space scale exceeding the short-range order are of particular interest and essential when analyzing the structural self-organization and complement of the pattern of photo-structural changes occurring in non-crystalline solids. Since radiation with the energy of the quantum corresponding to the absorption region interacts directly with the electron subsystem, an essential role in non-crystalline solids, being the open thermodynamic system, is played by the mechanism of the transformation of the absorbed energy into that of the structural transformation. As a result, the self-organizing phenomena in non-crystalline structures under radiation appear to be diverse, and qualitatively new stationary and non-stationary structures have the possibility to occur. The same is true for an organic matter and living objects.

The interactions in the living matter (to our knowledge) belong exclusively to electrodynamics. The biological processes (and also all the chemical processes) are based only on one fundamental interaction type: the electrodynamic interactions. All interactions in a living organism – chemical or physical – occur on the basis of the electromagnetic interactions (the interaction in the Universe may be divided into four groups; the electromagnetic group is one of the best defined). It means that all of the processes in the living objects to a certain extent are sensitive to the electromagnetic influence and, thus, may be affected. So, it is not surprising that these influences have been extensively discussed and published in a wide range of special papers. The electromagnetic pollution of the environment has nowadays become one of the important problems. The next questions naturally appear:

- How does the electromagnetic radiation interact with a living matter?
- Does any peculiar property, which must be taken into consideration in such cases, exist?
- Do the quantum effects have to be introduced, or is the classical description sufficient?

6.1. Electromagnetic radiation effect

6.2.1. General formulation

The laser radiation interaction with different-type non-crystalline solids produces the photo-induced change in their optical, physicochemical and other properties [1–4]. These processes have been studied fairly well in chalcogenide vitreous semiconductors [5–7], where they are the most effective under the exposure of the light quanta of $h\nu < E$ energy. The interest in the studies of photo-induced transformations in such materials, besides the practical application, is due to the fact that non-crystalline media produced in the strongly non-equilibrium conditions are open for the energy and mass exchange. The interplay of the local transformations in the configuration of the atom location (photo-deformation of the vitreous matrix and the change of its rigidity) with the defect charge state variation, resulted from the excitation localization onto the local centres, has been discussed in [7,8]. Within the framework of this approach the peculiarities of photo-induced structural changes have been studied at the short-range and middle range order level. A series of experimental data on the studies of the dynamics of optical parameter variations and relaxation phenomena at the photo-thermal excitation of light-sensitive amorphous materials [10] indicate the specific features of the wide-spectrum ($\Lambda = 0.3 - 15\mu m$) laser radiation interactions. These data can be analyzed, as shown below, from the viewpoint of photo-induced instabilities and the dissipative structure formation. The present chapter is devoted to the discussion of this problem.

The nature of the feedback and the development of a laser-induced instability under the laser radiation interaction with non-crystalline materials is as follows. The non-crystalline solids have

different degrees of structural ordering that emerges in the presence of at least two spatially separated and structurally different states. They differ in the amplitude of dynamic displacements, shift instability and space rearrangement ability. Such states can be described in terms of a two-level model modified to fit the vitreous solids [7].

An electromagnetic wave $E(r,t) = E_0 \exp\{-i\omega t + ikr\}$ falling with the wave-vector k , frequency ω ($\hbar\omega > E_g$, E_g is the energy gap) and the wave amplitude $E_0 = E(r)f(t)$ ($f(t) = 1$ at $0 < t < \tau_p$, $f(t) = 0$ at $t > \tau_p$, τ_p being the exposure time), induces the transition of the system to the excited state with a subsequent relaxation to the certain metastable state [7,8]. Assume that when the light is absorbed, the excitation of the electron subsystem occurs first and then an extremely fast ($\approx 10^{-8} - 10^{-10}$ s) radiationless transition takes place with partial conversion to the heat. The change in electron subsystem state also results in the local atomic potentials renormalization when the charge state of the defects changes and induces the rearrangement of the structure of the system in the excitation region. The relationship between the contributions of thermal and electron mechanisms of the laser radiation action is defined primarily by the energy density. At moderate energy densities ($\leq 10\text{W}/\text{cm}^2$), the contribution related to the change in the state of electron subsystem and subsequent vibrational spectrum transformation is predominant. At higher energy densities ($\geq 10\text{W}/\text{cm}^2$) the photocrystallisation processes due to the thermal component of the laser radiation action are observed for many non-crystalline materials. Such processes will be considered in sect. 6.4.

Since non-crystalline solids have locally heterogeneous structure (at the short-range and medium-range order levels), the process of light quantum absorption results in the spatially heterogeneous distribution of the temperature T , related to heating by the external field and a portion of atoms N_2 located in the soft atomic configurations. The forces resulted from the T and N_2 gradients govern the photodeformation of the structure and the production of the thermal and diffuse fluxes. This flux related to the rearrangement of atoms in soft and rigid configurations is defined by the size of soft configuration regions and their location. The spatial variation of the temperature and concentration of atoms in soft configurations affects the activation energy and the width of the quasi-forbidden band (i.e. the absorption coefficient) and thus executes the reverse effect of the medium on the radiation.

For the "radiation + medium" system, when the non-crystalline material is used as a medium, two feedback channels are possible. The first of these channels is due to the thermodiffusion processes, which lead to spatial rearrangement and the displacement of certain soft atomic configurations of heterogeneously absorbing medium and change the optical properties. This, in its turn, causes the redistribution of energy over the cross-section of the beam as the radiation passes through the medium and governs the reverse action of the medium on the radiation.

The second feedback channel is related to the change in the activation energy of the atom transition into the metastable state, the generation of the energy accumulated in a form of deformations and the reverse influence on the formation of the spatial-temporal structure.

6.1.2. Electromagnetic effects on living objects

A successful progress in studying the biomolecular structures and the peculiarities of the influence of the external fields is connected with the studies of the role of non-linear waves and stochastic signals in the biological system operation. Switching of the types of the stationary non-equilibrium structures in such systems may also result, in particular, from the influence of external electromagnetic fields. Most of the ordering processes in biological objects are so complicated that the unified theory of such processes active in any area of the process appears to be constructed only in very rare instances. In this case, it seems quite effective to expand the experience and the results gained for less complicated processes occurring in the adjacent fields, in particular, when investigating the physicochemical systems, to more complicated processes in biological objects.

The example is the study of the influence of the electromagnetic radiation on non-crystalline materials and the related structures on their basis.

The specific nature of the action of the electromagnetic millimetre radiation on the dielectric media of the human organism (water, blood, liquor) is a matter of general experience. It should be noted that the fraction of liquid in humans constitutes nearly 65%. The physicochemical mechanism of the transition of the system to the ordered state under the influence of the radiation may be based on the effective variation of the coordinates of bifurcation points (in particular, the critical values of the temperature and pressure). As a result, the former stable structureless system is transferred below the boundary of the reaction stability, where the thermodynamic instability is stabilized by the occurrence of the coherent spatially ordered structures.

During last few decades, theoretical studies on the mechanisms of the influence of electromagnetic radiation on biological objects are being developed extensively along with the experimental investigations of that influence on the non-crystalline organic and inorganic materials. Various mechanisms of the influence can operate at the different levels of the structural organization of biological objects, i.e. at the organism level, at the biomembrane level and at the biomolecular level [11,12]. The complex description of different levels of the biological system organization is also possible with the allowance made for their interaction with the external fields. One can adduce a number of examples of the increased sensitivity of living organisms to the external electromagnetic fields. The influence of the wave processes has been discussed both at the molecular and cellular levels, in the chemical reactions (Belousov-Zhabotinsky reactions) and in the process of vital activity of the organism [12-14].

The sensitivity of biological systems to external electromagnetic fields depends primarily on the frequency range and radiation power. This influence on the organism can be either useful or deleterious. The medical effect of electromagnetic waves is achieved, for instance, in the hypertension treatment (destructive malignant tumour heating), laser surgery, etc. Therefore, the analysis of different aspects of the interaction of electromagnetic fields with biological objects is not only of scientific but also of applied interest. We shall dwell upon the consideration of the physical principles of electromagnetic waves interaction with biomolecular structures and related self-organizing processes. Among the experimentally observed effects of the influence of low-intensity ($\cong 10 \text{ MW/cm}^2$) high-frequency radiation on different biological objects, the studies of the radiation-induced heat transfer processes in the skin are of specific interest. This is primarily due to the development of non-crystalline materials and related systems which can simulate the biological processes.

Consider the main model representations of that phenomenon. In the coherent excitation conception introduced by G. Froelich, the existence of a single distinguished degree of freedom in the biological macromolecules is assumed, and the amplitude of the normal vibrations of this degree significantly exceeds those of the other degrees of freedom. Hence, the phonons are concentrated on the distinguished degree of freedom (the so-called Bose-condensation). To change the conformations in the biomacromolecules one has to accumulate the energy of about 0.5 meV on the distinguished degrees of freedom. In terms of the conception considered here, the macromolecule is treated as a construction of sorts, which comprises the universal elements, i.e. the levers, hinges, energy reservoirs and fixers. The macromolecules are classified into the rigid constructions with no distinguished degrees of freedom and the systems to that degree. The energy transfer along the certain direction is possible if the distinguished degree of freedom is available.

A constant energy source, which supplies the system with the quanta of radiation within a reasonably narrow frequency region close to the main frequency, is the necessary element of the Froelich's coherent excitation model. Depending on the coherent state dampening, the pumping radiation power must exceed some critical value in the system of the Bose-condensation mentioned above.

The soliton mechanism of the electromagnetic radiation action on the biological structures has been developed by A. Davydov [15]. In accordance with the concept of A. Davydov and his school, the hydrolysis of the ATP molecule attached to the end of the protein molecule is

accompanied by the release of the energy, which is further spread in the form of a soliton. It turned out that in the case when the energy transport takes place due to the soliton propagation in the biological molecules, the external radiation can effectively violate this process.

An informational theory of the low-intensity millimetre radiation influence on the living organisms is of an indisputable interest [16]. The living organisms, being complex systems comprising a host of organs and subsystems, must operate in coordination over a long period under the varying internal and external conditions.

In this relation, the vital activity of the organisms cannot be provided in the absence of well-developed informational control systems. A huge amount of information processed and considered by the living organism becomes possible only in the case of low-power signals whose production requires the energy consumption compatible with the energy abilities of the organism. For a human being, this power constitutes 10^{-3} – 10^{-4} of the heat power produced by the organism and is about 1–10 mW.

The principal concepts of the present approach are as follows:

- the action of the millimetre radiation on the vital activity of the organisms is of informational, not energy, character;
- the effects of the external radiation of non-thermal intensity on the organism are defined by the fact that the radiation simulates the informational signals produced by the organisms themselves under the changing conditions of their operation.

6.2. Production of ordered structures: the feedback mechanism

6.2.1. Simulation of the visible laser radiation influence on ordering processes

In the absence of lighting, certain soft atomic configurations are statistically homogeneously distributed over the sample volume. An external light field results in the rise of the concentration of soft domains described by the distribution function $g(x, r, t)$ over the dimensions x . The behaviour of the system under illumination is described by the dynamic equation for the number of atoms in soft configurations and the thermal balance equation with laser heat source, which depends only on the radiation intensity [7,8]:

$$\frac{\partial N_2}{\partial t} = G - \frac{N_2 - N_{2s}}{\tau} - 4\pi \int_0^{\infty} x^2 V(x) g(x, r, t) dx + D \Delta N_2 \quad (6.2.1)$$

$$\rho C \frac{\partial T}{\partial t} = \text{div}(k_0 \cdot \text{grad}(T)) + P(T) - Q(T) + L_a \frac{\partial N_2}{\partial t} \quad (6.2.2)$$

Here r is a spatial coordinate, $V(x) = v/x = D(N_2 - N_{2s})$ is the rate of the change of the soft domain dimensions (v is defined by the difference between the atom concentrations in the soft configuration domains under illumination, N_2 , and that without illumination, N_{2s}); $D = D_0 \exp\{-\xi_D/kT\}$ is an atom diffusion coefficient; ξ_D is the diffusion activation energy; τ is the life-time of atoms in the soft configurations; $G = \gamma\beta/\hbar\omega$ is the photo-generation rate for atoms in the soft configurations; β is a quantum yield; $I = E^2/(s_0\tau_p)$ is the intensity density of the incident wave (consider first the heterogeneous distribution of the intensity over the beam cross section s_0); ρ is the density of the non-crystalline sample; C and κ_0 are the heat capacity and the heat conduction coefficient, respectively; $P = \gamma I$ is the laser heat source intensity defined by the density of the radiation power absorbed during the exposure time; $Q(T) = \int_{T_0}^T \eta_h(\xi) d\xi$ is the heat exchange with the environment; η_h is the heat exchange constant; T_0 is the ambient temperature,

and the parameter L_a defines the difference of the energies of the transition between the states within the limits of the amorphous phase or during the photocrystallisation; Δ is a Laplacian.

The first term on the right side of equation (6.2.1) describes the rate of atom transformation into the soft configurations, the second and the third ones describe the loss of atoms during the transition to the rigid configuration and at the soft domain drains, while the fourth term describes the spatial photodiffusion (displacement) of several soft configurations. Similarly, the second term on the right side of equation (6.2.2) describes the sample temperature rise at the expense of radiation absorbed, the first and third terms define the temperature change due to the heat capacity and heat exchange with the environment, whereas the fourth term describes the latent heat evolution at the transition.

The kinetics of time variation of $g(x,r,t)$ can be described by the following Fokker-Planck equation [8,17]:

$$\frac{\partial g(x,r,t)}{\partial t} = -\frac{\partial}{\partial x} [V(x)g(x,r,t)] + D_0(x)\Delta g(x,r,t). \quad (6.2.3)$$

Here, the first term on the right side describes the photo-induced variation of the soft domain dimensions $g(x,r,t)$, and the second one defines their spatial diffusion $D_0(x) = \beta_0/x^2$. The dependence of $g(x,r,t)$ on the space coordinate is governed by the forces f_N and f_T ($f_N = \mathcal{G}_E \text{grad}(N_2)$; $f_T = -\kappa\alpha_T \text{grad}(T)$; κ being the uniform compression modulus; \mathcal{G}_E being the energy band deformation potential; α_T being the thermal expansion coefficient), which result in the production of the thermal and diffuse fluxes and, hence, in the redistribution and displacement of the soft domain centres.

The system of equations (6.2.1) to (6.2.3) is closed if the initial and boundary conditions are specified at the surface:

$$\left. \frac{\partial T}{\partial z} \right|_{z=0} = 0, \quad \left. \frac{\partial T}{\partial z} \right|_{z=d} = 0, \quad \left. \frac{\partial T}{\partial r} \right|_{r \rightarrow \infty} = 0.$$

The spatial variation of the atom concentration in the soft configurations and that of the medium temperature inversely affect the width of the quasi-forbidden band and the absorption coefficient γ . At the laser radiation absorption frequency ω , we have (in the approximation linear over N_2 and T):

$$\gamma(\omega) = \gamma_0 + \frac{\partial \gamma}{\partial \omega} \Delta \omega, \quad \hbar \Delta \omega = \beta_T T + \beta_N N_2, \quad (6.2.4)$$

where $\beta_T = (\partial E_g / \partial T)$, $\beta_N = (\partial E_g / \partial N)$, γ_0 is the absorption coefficient prior to lighting. It is seen from (6.2.4) that the feedback between the medium and the radiation is formed due to the dependence $\gamma = f(T, N, \xi)$, and $D_0 \neq 0$. The exclusion of one of these factors (i.e. if $\gamma = \text{const}$ or $D_0 = 0$) breaks the relationship, and these degrees of freedom behave almost independently. We shall consider separately the cases of the photo-induced changes, which occur in non-crystalline materials, depending on the intensity of radiation.

6.2.2. Quast-stationary solution and their stability

At low laser radiation densities, one can neglect in (6.2.2) the thermal effect of the transition between different states in the amorphous phase and allow parameters κ_0 , η_h to be constant. In

this case, the quasi-stationary solutions of the system of equations (6.2.1) to (6.2.3) $\frac{\partial N_2}{\partial t} = 0$, $\frac{\partial T}{\partial t} = 0$, $\frac{\partial g}{\partial t} = 0$ are defined from the system of equations

$$\alpha_{11}N_{2c} + \alpha_{12}T_c + G_0 + \frac{N_{2s}}{\tau} - 4\pi \int x^2 V_c(x) g_c dx = 0 \quad (6.2.4)$$

$$\alpha_{21}\rho CN_{2c} + \alpha_{22}\rho CT_c + P_0 \eta_n T_0 = 0 \quad (6.2.5)$$

$$g_c(x) = N_0 \delta(x - \bar{x}). \quad (6.2.6)$$

Here: $\alpha_{11} = \frac{I\beta}{\hbar^2 \omega} \beta_N \left(\frac{\partial \gamma}{\partial \omega} \right) - \frac{1}{\tau}$, $\alpha_{12} = \frac{I\beta}{\hbar^2 \omega} \beta_T \left(\frac{\partial \gamma}{\partial \omega} \right)$, $\alpha_{21} = \frac{I\beta_N}{\rho C \hbar} \left(\frac{\partial \gamma}{\partial \omega} \right)$, $\alpha_{22} = \frac{I\beta_T}{\rho C \hbar} \left(\frac{\partial \gamma}{\partial \omega} \right)$ and \bar{x} is the average size of the soft configuration domains, N_0 is the defect state density. Let us check the stability of stationary solutions N_{2c} , T_c and g_c . We shall represent the quantities $N_2(r, t)$, $T(r, t)$ and $g(x, r, t)$ in the form of an expansion into a power series in the infinitely small deviations from the quasi-stationary state, restricting ourselves to the linear approximation [9]:

$$N_2(r, t) = N_{2c} + \delta N_2(r, t), \quad T(r, t) = T_c + \delta T(r, t), \quad g(x, r, t) = g_c + \delta g(x, r, t).$$

Let us linearize the system of equations (6.2.1) to (6.2.3) over the quantities δN , δT , δg , with the allowance made for boundary conditions. As a result, we get:

$$\begin{aligned} \frac{\partial(\delta N_2)}{\partial t} &= \alpha_{11}\delta N_2 + \alpha_{12}\delta T - 4\pi \int_0^\infty (xv\delta g + Dxg_c\delta N_2)dx + D^2(\delta N_2), \\ \frac{\partial(\delta T)}{\partial t} &= \alpha_{12}\delta N_2 + \alpha_{22}\delta T + a^2(\delta T), \\ \frac{\partial(\delta g)}{\partial t} &= -\frac{\partial}{\partial x} \left(v \delta g + g_c \frac{D}{x} \delta N_2 \right) + D_0^2(x)\delta g, \end{aligned} \quad (6.2.8)$$

where $a = k_0 / (\rho C)$. Let us represent the fluctuations δN , δT and δg as:

$$\delta N_2, \delta T, \delta g \approx J_m(kr) \exp\{\lambda t\}. \quad (6.2.9)$$

Here, $J_m(qr)$ is the m^{th} -order Bessel's function, k is the wave vector, and the parameter λ defines the time interval of the evolution of the photo-induced instability.

Substituting (6.2.9) into the system of equation (6.2.8), we obtain:

$$(\lambda - \alpha_{11} + 4\pi D\bar{x}N_0 + k^2 D)\delta N - \alpha_{12}\delta T + 4\pi v \int_0^\infty x \delta g dx = 0, \quad (6.2.10)$$

$$(\lambda - \alpha_{22} + ak^2)\delta T - \alpha_{21}\delta N = 0,$$

$$(\lambda + k^2 D_0(x))\delta g + v \frac{\partial}{\partial x} \left(\frac{\delta g}{x} \right) + \frac{\partial}{\partial x} \left(\frac{D}{x} \delta N g_c \right) = 0. \quad (6.2.11)$$

Setting the determinant of the system of equations (6.2.10) and (6.2.11) to zero, we arrive at the following dispersion equation:

$$\lambda = \frac{[3v\tilde{\alpha}_1 - \beta_0(4\pi N_0\bar{x} + \tilde{\alpha}_o)]k^2 - \beta_0\tilde{\alpha}_1k^4 + 3v\tilde{\alpha}_o}{4\pi N_0\bar{x}^3}, \quad \tilde{\alpha}_o = \frac{\alpha_{12}\alpha_{21} - \alpha_{11}\alpha_{22}}{D\alpha_{22}}, \quad \tilde{\alpha}_1 = 1 + \frac{a\alpha_{12}\alpha_{21}}{D\alpha_{22}^2} \quad (6.2.12)$$

The analysis of equation (6.2.12) shows that at $3\tilde{\alpha}_1 > \beta_0(4\pi N_0\bar{x} + \tilde{\alpha}_o)$ or $G > G_{min}$, where $G_{min} = \frac{(4\pi N_0\bar{x})^2 \beta_0}{3\tilde{\alpha}_1}$, the homogeneous quasi-stationary distribution of the soft configuration domains becomes unstable, i.e. if $\lambda \geq 0$ or $\beta_0k^4\tilde{\alpha}_1 - [3v\tilde{\alpha}_1 - \beta_0(4\pi N_0\bar{x} + \tilde{\alpha}_o)]k^2 - 3v\tilde{\alpha}_o < 0$, such eigenvalues of k^2 exist that fluctuations δN_2 , δT , δg tend to the infinity at $t \rightarrow \infty$. The eigenvalues of k^2 must obey the following conditions:

$$k_{c(+)}^2 < k^2 < k_{c(-)}^2 \quad (6.2.13)$$

where $k_{c(\pm)}$ are the solutions of a biquadratic equation $\lambda(k^2) = 0$:

$$\beta_0k^4\tilde{\alpha}_1 - [3v\tilde{\alpha}_1 - \beta_0(4\pi N_0\bar{x} + \tilde{\alpha}_o)]k^2 - 3v\tilde{\alpha}_o = 0$$

and are equal to:

$$k_{c(\pm)}^2 = (2\beta_0\tilde{\alpha}_1)^{-1} \left\{ [3v\tilde{\alpha}_1 - (4\pi N_0\bar{x} + \tilde{\alpha}_o)\beta_0] \pm \sqrt{(3v\tilde{\alpha}_1 - (4\pi N_0\bar{x} + \tilde{\alpha}_o)\beta_0)^2 + 12v\beta_0\tilde{\alpha}_o\tilde{\alpha}_1} \right\} \quad (6.2.14)$$

For each q^2 , which obeys the condition:

$$\lambda(k^2) > 0 \quad (6.2.15)$$

Hence, the spatially homogeneous solution g_c , N_{2c} , T_c at $G > G_{min}$ is unstable with respect to the fluctuation with the wave vector taken from the $k_{c(+)}^2 < k^2 < k_{c(-)}^2$ interval.

Let us determine the k^2 quantity at which the function $\lambda(k^2)$ attains the maximum value.

From the equation $\frac{d\lambda}{dk^2} = 0$, we find:

$$k_{max}^2 = \frac{3v\tilde{\alpha}_1 - \beta_0(4\pi N_0\bar{x} + \tilde{\alpha}_o)}{2\beta_0\tilde{\alpha}_1} \quad (6.2.16)$$

The maximum value of the function $\lambda(k^2)$ is:

$$\lambda_{max} = \lambda(k_{max}^2) = \frac{(3v\tilde{\alpha}_1 - (4\pi N_0\bar{x} + \tilde{\alpha}_o)\beta_0)^2 + 12v\beta_0\tilde{\alpha}_o\tilde{\alpha}_1}{16\pi N_0\bar{x}^3\beta_0\tilde{\alpha}_1} \quad (6.2.17)$$

The main mechanism of the instability stabilization is related to the spatial localization of the excitation on the defects [3,4] and the competition of the transfer processes, which tend to sustain the uniformity of the mean sample. Thus, in the system of randomly distributed soft domains, the transition to the heterogeneous stationary state is possible, i.e. in non-crystalline solids under illumination, the periodical structure of the distribution of soft atomic configuration domains with

the wave vector of $k_{\max} = \frac{2\pi}{L}$ is formed. One may write down the following expression for the period of the structure produced:

$$L = L_0 \sqrt{\frac{G_{\min}}{G - G_{\min}}}, \quad L_0 = \frac{2\pi\tilde{\alpha}_1}{N_0\bar{x} \left[1 + \frac{4\pi N_0\bar{x}\beta_0\beta_T\omega(\partial\lambda/\partial\omega)}{3\tilde{\alpha}_1\gamma_0\rho C} \right]}. \quad (6.2.18)$$

The specific lifetime of the dissipative structure is $\tau_{\text{life}} = (\lambda_{\max})^{-1}$.

Hence, in terms of the model under consideration, the inclusion of local heterogeneity of non-crystalline solids results in a new quality revealed in the possibility of the spatial self-organization of the structure at the order level exceeding the average. In this case, the disordering of the structure of non-crystalline solids at the short-range order level at the sample photodarkening is accompanied by the ordered structure formation on the macroscopic spatial scale. Such stationary non-equilibrium structures are separated in the configurational energy space by the low potential barriers. These processes can occur in a time of laser radiation action and, hence, define the character of radiation interaction with non-crystalline media.

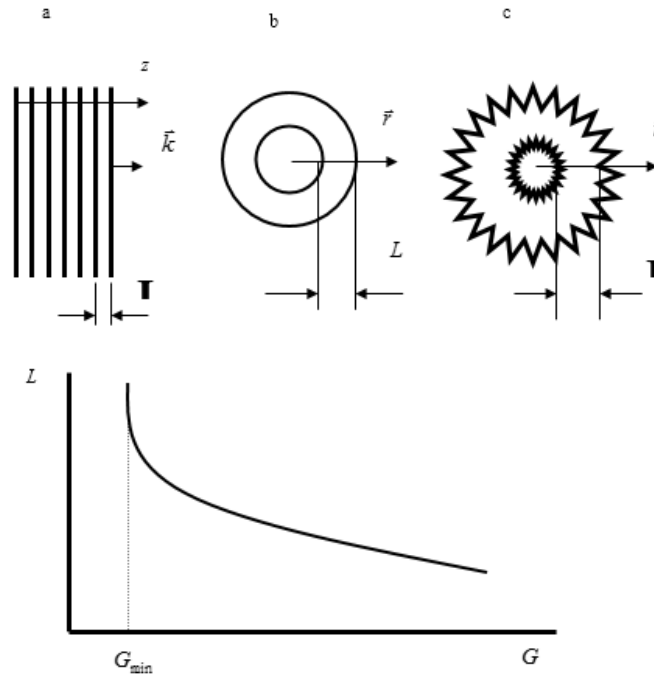


Fig. 6.2.1. The dependence of the period L of ordered configuration on the radiation power (a – linearly – periodic structure, b – periodic structure as rays, c – periodic structure as concentric rings).

Consider the dependence of the ordered configuration period of the soft domain spatial location and the time of its existence for non-crystalline substances (Fig. 6.2.1.). At specific values, the period of dissipative structure formed at $G > G_{\min}$ is about $10^{-2} - 5 \cdot 10^{-1} \mu\text{m}$, and the time of its occurrence is $\tau_{\text{life}} \approx 10^{-1} - 10^{-5} \text{ s}$. The minimum value of the quantum flux is $G_{\min} \approx 10^{18} - 10^{19} \text{ quanta/cm}^2\text{s}$ and is determined by the structural defectiveness (it decreases with this parameter) and its rigidity. These structures are also revealed as distinctive features in the behaviour of optical and structural-sensitive parameters. The photo-induced increment of the absorption coefficient at growing instability is about $\delta\gamma/\gamma_c \approx (1-3)10^{-3}$.

6.3. Simulation of the electromagnetic radiation interaction with biomolecular structures

Consider the possible physicochemical mechanism of the radiation influence on a human organism as the formation of dissipative structures. Let us first consider the certain principle facts. Biological objects are of the threshold character with respect to power [22]. The number of bone marrow cells is reduced from standard under the influence of X-ray radiation. At the additional exposure to UHF-radiation, the marrow cells become protected from further X-ray action, starting with the certain threshold level ($P_{\min} \cong 1 - 10 \text{ mW/cm}^2$). As $P > P_{\min}$, the magnitude of the effect remains virtually constant.

The observed threshold power effect can be explained by the formation of the ordered dissipative structure in the initially statistically heterogeneous structureless system. Let us make some estimates. According to equation (6.2.2), one obtains for the radiation power:

$$P_{\min} = \gamma I_{\min} \quad (6.3.1)$$

where γ is an absorption coefficient, and the intensity rate can be defined from the expression:

$$G_{\min} = \mathcal{A}_{\min} \beta / \hbar \omega \text{ or } G_{\min} = \mathcal{A}_{\min} \beta / h \nu$$

From here:

$$I_{\min} = G_{\min} h \nu / \gamma \beta \quad (6.3.2)$$

Substituting into (6.3.2) in (6.3.1), we obtain the expression for a power of radiation relevant to a threshold value:

$$P_{\min} = G_{\min} h \nu / \beta \quad (6.3.3)$$

According to equation (6.3.3) for $\nu = 37.4 \text{ GHz}$, $\Lambda = 8 \text{ mm}$ and radiation penetration depth of $G_{\min} = 10^{18} \text{ quanta/cm}^2 \text{ s}$, this value is about $P_{\min} \cong 2.7 \text{ mW/cm}^2$.

Water defines the extremely important functions of the vital activity of biological objects. Therefore, the millimetre radiation heats up various substances almost in a thin near-surface layer with a great temperature gradient. In the water solutions of different substances, the energy absorption will also be determined by the water molecules and has a local nature. Such a selective microheating may result in the biologically substantial effects even at low radiation powers when the integral heating is minor. The temperature increase, as noted above, is negligible ($< 0.1^\circ \text{ K}$), and is not the dominant factor of the useful effect.

The investigation of the dependence character of the biological effect on the power density and wave frequency is of special interest. As follows from (6.2.18), the dependence of the period of the dissipative structure under formation on the power determines the variation of the ordering scale without the change in the character of the system itself (i.e. the energy effect). The efficiency of the radiation influence on the living object depends on the initial state of the organism, which is determined by the dependence of the system parameters on the initial and boundary conditions.

The irradiation of the organism at the certain frequencies can set its normal operation under new conditions. Depending on the causes and the character of the disease or pathological status, the larger therapeutic effect is reached at the different-frequency millimetre radiation action. The electromagnetic radiation of a certain frequency sets at $P > P_{\min}$ the character of the dissipative structure under formation and is able to return the open system to the structural stability domain and, consequently, eliminate arising malfunctioning.

Consider some changes in the biological objects (i.e. in the dissipative structures) under the influence of a certain-frequency radiation. Let us analyze these changes from the standpoint of the

non-linear thermodynamics. Since the entropy variation dS is determined by that inside the system, $(dS)_i$, and the entropy flux from the environment, $(dS)_e$, i.e. $dS = (dS)_i + (dS)_e$, then:

$$\frac{dS}{dt} = \frac{(dS)_i}{dt} + \frac{(dS)_e}{dt}, \quad (6.3.4)$$

where $(dS)_e/dt = \sum X_j J_j$ is the entropy production determined by the dissipative processes inside the system, J_j is the velocity of the j -th irreversible process (i.e. the diffusion, the convection and the heat transfer) and X_j are the relevant driving forces ($\propto \text{grad}(T), \text{grad}(N)$).

For the isolated systems:

$$\frac{dS}{dt} = \frac{(dS)_i}{dt} \geq 0. \quad (6.3.5)$$

The stability condition for the local equilibrium in the volume element for $S(r, t) = \int \rho s(r, t) dr$ is described by inequalities:

$$\delta^2 s \leq 0, \quad \frac{d}{dt}(\delta^2 s) \geq 0 \quad (6.3.6)$$

where $\delta^2 s$ is a specific entropy "curvature" (negatively defined quadratic form which plays a role of the Lyapunov's function) and ρ is the density.

Therefore, in this case the equation of the balance for the excessive entropy is

$$\frac{1}{2} \frac{d}{dt}(\delta^2 s) = \sigma([\delta s]) - p([\delta s]), \quad \text{here } \sigma([\delta s]) \text{ is the generalized entropy production, } p([\delta s]) \text{ is the generalized entropy.}$$

The necessary condition for the stability of the dissipative structure under formation is $\frac{1}{2} \frac{d}{dt}(\delta^2 s) = \sigma([\delta s]) - p([\delta s]) \geq 0$.

Let us analyze possible variations of $\sigma([\delta s])$ and $p([\delta s])$ depending on the radiation frequency (Fig. 6.3.1). At the certain frequency ν in the system, $p([\delta s])$ attains some minimum value. In this state, $\sigma([\delta s])$ may be a finite positive quantity. If $\sigma([\delta s]) > p([\delta s])$, then the condition holds within the entire region of ν (a dot-and-dash line in Fig. 6.3.1). This case corresponds to the absence of the biological effect at $P < P_{\min}$; i.e. no formation on the dissipative structure is observed.

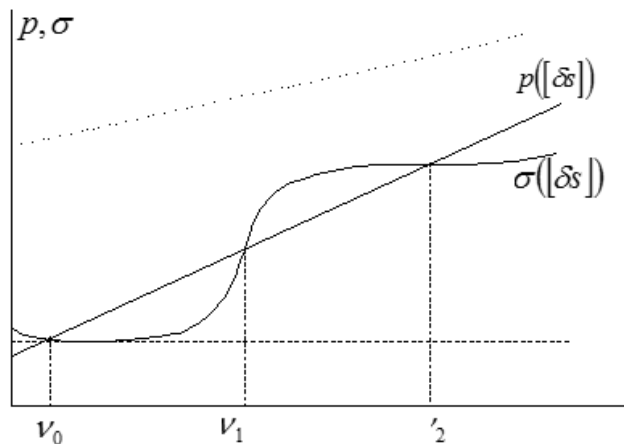


Fig. 6.3.1. Schematic of the formation of stable structures under the radiation frequency variation.

At $\nu = \nu_0$, $\sigma([\delta s]) = p([\delta s])$ and $P > P_{\min}$, the crossing of the curves takes place accompanied by the transition to the unstable heterogeneous mode. Namely, for $\nu > \nu_0$, $\sigma([\delta s]) < p([\delta s])$ (a dotted line).

For $\nu \geq \nu_l > \nu_0$, the repeated crossing of the curves is possible and the following inequality holds: $\sigma([\delta s]) > p([\delta s])$. In this case, the distinguished (with respect to the frequency) region of the existence of the dissipative structure takes place and a new type of organization arises. The similar situation may occur over and over with increasing ν .

Note in conclusion that the dissipative structures under formation are extremely sensitive to the external changes that are essential in defining the status of the organism or in diagnosing its diseases as well as in determining the character of the interaction of radiation producing the desirable therapeutic effect. For this reason, the local interaction of very low intensity UHF-radiation with a skin tissue may be considered also as a “switch”, which influences the transmitted signal (neuron), the greater part (organ) or the whole dissipative system – the living organism.

6.4. Thermal instability and ordered structure formation

Production of the spatial-temporal structures and thermal instabilities with the bistable behaviour under the influence of the ultra-short nanosecond and picosecond pulses or the powerful continuous radiation on semiconductor layers and biostructures is one of the possible examples of the systems which allow the formation of dissipative structures far away from the equilibrium state [18 – 21]. The mechanism of the production of these structures is based on the linear interaction of radiation with the substance, when the reverse influence of the medium on the radiation absorption occurs, and the stationary non-equilibrium mode is possible possessing the spatial and time characteristics, which differ qualitatively from those for the linear energy transfer mechanism. In this section, we shall study the model of the development and stabilization of the thermal instabilities with a simultaneous formation of dissipative structures in non-crystalline layers under the influence of radiation.

Consider the model system comprising the cover layer, the non-crystalline material and the substrate. Let the radiation of $P(x) = I(x)/\pi x_0^2$ power with the Gaussian intensity distribution $I(x) = I_0 \exp\{-x^2/x_0^2\}$ over the beam cross section (x_0 is the effective beam radius) and with the t pulse duration, whose intensity decreases along the z -axis, be absorbed completely by the system volume. The peculiarities of the behaviour of the IR-transparent layers of non-crystalline semiconductors [20] are defined by the substrates, which absorb the radiation of a given wavelength, and the heat removal mechanism. In the IR-region of the spectrum, the strong temperature dependence of the absorption cross section appears to be essential. The absorbing capacity can be approximated by the expression $\gamma = \gamma_0 \exp\{-\alpha_a T_a/T\}$, where γ_0 is the absorption depth and α_a is the non-linearity parameter. A considerable increase of the absorption and the rise of the reverse influence of the medium on the radiation take place with the increasing radiation energy density. The self-consistent increase of the absorption at the presence of the feedback between the radiation and the substance as well as the occurrence of the non-stationary temperature mode at the non-crystalline boundary may result in the appearance and development of thermal instability self-organization.

In order to study the formation of the structures due to thermal instabilities, consider the dynamics of the temperature variation in the "substrate + layer" system. This problem is described by the non-linear differential equation, which accounts for the heat generation, propagation and transfer:

$$\rho C \frac{\partial T}{\partial t} = \text{div}(\kappa_o \text{grad} T) + G(T) - Q(T). \quad (6.4.1)$$

Here C , ρ and κ_o are the heat capacity, density and heat conduction, respectively; $G(T) = \gamma U P \delta(z) f(t)$ is the heat source; U is the optical transmission of the layer at the

wavelength Λ , which allows for the power variation at the absorption; $Q(T) = \int_{T_0}^T \frac{\eta_h(\xi) d\xi}{d}$ is the heat exchange with the non-crystalline layer (η_h being the heat exchange constant, T_0 being the initial temperature),

$$\delta(z) = \begin{cases} 1, & z \leq d, \\ 0, & z > d, \end{cases} \quad f(t) = \begin{cases} 1, & t \leq t, \\ 0, & t > t. \end{cases}$$

The boundary conditions are:

$$T(x, z, t)|_{z=0} = T_0, \quad \left. \frac{\partial T(x, z, t)}{\partial z} \right|_{z=0} = 0. \quad (6.4.2)$$

To solve equation (6.4.1) and analyze the obtained results it is convenient to use the dimensionless values: $\Phi = \frac{T}{T_a}$, $\Phi_0 = \frac{T_0}{T_a}$, $\tilde{p} = \frac{UP\delta(z)}{\eta_h T_a}$, $\tau_t = \frac{\eta_h t}{\rho C d}$, $\tilde{k} = \frac{\kappa_o d}{\eta_h x_0^2}$ in terms of which the equation (6.4.1) attains the form:

$$\frac{\partial \Phi}{\partial \tau_t} = \tilde{k} \Delta \Phi + \tilde{p} \exp\left\{-\frac{\alpha_a}{\Phi}\right\} f(\tau_t) - \Phi + \Phi_0. \quad (6.4.3)$$

Here Δ is the Laplace operator in the cylindrical coordinate frame. The stationary temperature field Φ_s , which specifies the bifurcation diagram in the $\{\Phi, \tilde{p}\}$ plane, is given by equation $\frac{\partial \Phi}{\partial \tau} = 0$.

The stationary temperature field configuration depends on the geometry of the two-layer "non-crystalline layer + substrate" system, the heat source density and the heat removal value. The system possesses the bistability over the \tilde{p} parameter related to the radiation intensity. Depending on \tilde{p} , one or three stationary states do exist differing in the reduced temperature Φ . The type of the singular points in the bifurcation diagram $\{\Phi, \tilde{p}\}$ and their stability are studied by expanding Φ over the small deviations from the stationary solutions $\Phi = \Phi_s + \delta\Phi$, where Φ_s is a root of equation (6.4.1), $\delta\Phi$ is a variation of Φ [20]. Substituting $\Phi = \Phi_s + \delta\Phi$ into equation (6.4.3), we left only the terms linear over $\delta\Phi$. The quantitative analysis of the stability of the solutions of equation (6.4.3) with respect to the perturbations of the form:

$$\delta\Phi = J_m(k\xi) \cos(m\varphi) \exp\left\{\int_0^\tau \omega dt\right\} \quad (6.4.4)$$

where $J_m(k\xi)$ is the first-order Bessel function over m , leads us to the following dispersion dependence:

$$\omega(k) = \tilde{p}/\tilde{p}_c - 1 - \tilde{k}k^2, \quad \tilde{p}_c = \frac{\Phi_s^2}{\alpha_a} \exp\{\alpha_a/\Phi_s\} \quad (6.4.5)$$

It is seen that $\omega(k)$ depends on the radiation density in such a way that a certain value of $\tilde{p} = \tilde{p}_c$ exists (\tilde{p}_c being the thermal instability threshold), starting from which the unstable modes

appear in the perturbation spectrum. One can distinguish the interval of the wave vector values k , which obeys the inequality $k^2 < k_c^2 = \varepsilon / \tilde{k}$ ($\varepsilon = (\tilde{p} - \tilde{p}_c) / \tilde{p}_c$), where $\omega(k) > 0$ and the quasi-stationary solution ϕ_s is unstable with respect to the fluctuation with the wave vector taken from the given interval specific spatial instability zone, which defines the formation of the dissipative structure, is $2\pi / k_c = 2\pi / \sqrt{\varepsilon / \tilde{k}}$ and depends on \tilde{p} . The short-wave modes, for which $\omega(k) < 0$ and the modulus is rather large, are dampened rapidly. For such perturbations, the additional increase in the absorption cross-section caused by the temperature is compensated by the heat removal.

The physical pattern of the thermal instability resides in that the heat removal through the non-crystalline layer boundary and the heat transfer fail to compensate the rise of the energy absorbed due to the temperature increase in the absorption cross section. The threshold intensity \tilde{p} and the temperature ϕ are defined provided the rate of the absorbed energy increase is equal to that of heat removal. The thermal instability stabilization occurs at the cost of the self-regulated mechanisms resulting in the saturation of the absorption non-linearity, which governs the equalization of the rate of the absorbed energy increase and that of heat removal. Note that the self-organizing modes combine the high intensity of the thermal processes with the perturbation resistance, while the form of the structure is retained due to the joint action of the non-linear absorption and heat removal.

Let us analyze the threshold power density of the instability as a function of t_p , taking into account the kinetics of the heat instability evolution. Consider the situation when t_p is much more than the time of the temperature change due to the heat conduction $t_\kappa = \rho C x_0^2 / 3\kappa_o$ and the heat transfer $t_\eta = \rho C d / \eta_h$, i.e. $t_p \gg t_\kappa, t_\eta$. A specific time interval of the instability evolution t_i is defined by the $\omega(k)$ value and for the long-wave perturbation $t_i = (p/p_c - 1)^{-1}$. As is seen, the time of heat instability evolution depends on the radiative power and is decreased with the latter, while close to the threshold p_c is large. Therefore, in the hypercritical region, the evolution equation (6.4.1) at $\tilde{k} \ll 1$ is reduced to the quasi-stationary one:

$$\frac{dQ(T, T_0)}{dt} = -\frac{Q(T, T_0)}{t_\eta} + \frac{qQ(T_c, T_0)}{p_c t_\eta} f(t), \quad (6.4.8)$$

$$Q(T_c, T_0) = \int_{T_0}^{T_c} \eta_h(\xi) d\xi. \quad (6.4.9)$$

From equation (6.4.8) we obtain the threshold capacity of instability as a function of t :

$$p = p_c \left(1 - \exp\left\{-\alpha_a t / 2t_\eta\right\} \right)^{-1}. \quad (6.4.10)$$

At the radiative power density $p < p_c$, a stationary temperature distribution is set, and the temperature of the "substrate + layer" system is increased monotonically with p and t_p reproducing the spatial beam profile. In the hypercritical region, $p > p_c$, the substrate temperature increases sharply, and the time of the stationary temperature field relaxation, at which the absorption non-linearity is saturated, is defined by t_p . At $t_p > t_{0p}$ (t_{0p} is the threshold value of t_p defined at a given radiative power p by formula (6.4.10)), the heat instability does not occur and a continuous increase in the amorphous layer temperature with exposure time is observed. At $t_{0p} < t_p < t_i$, the establishment of the stationary temperature field at the interface is impossible since the energy increase rate at the absorption exceeds considerably the heat removal rate and, in

the region of the $2\pi/\sqrt{\varepsilon/k}$ order, the homogeneous temperature distribution with the maximum at $\xi=0$ becomes unstable. In the highly hypercritical region ($\tilde{p} \gg \tilde{p}_c$), $t_{0p}/t_\eta \approx \tilde{p}/\tilde{p}_c$ and $t_i/t_\eta \approx \tilde{p}/\tilde{p}_c$, and, therefore, $(t_{0p} - t_p) \rightarrow 0$. In the weakly hypercritical region ($(\tilde{p} - \tilde{p}_c)/\tilde{p}_c \ll 1$), $t_i/t_\eta \approx \tilde{p}_c/(\tilde{p} - \tilde{p}_c)$ and $t_{0p}/t_\eta \approx \ln\{\tilde{p}_c/(\tilde{p} - \tilde{p}_c)\}$ and $t_{0p} < t_i$. Thus, the above situation occurs only in the weakly hypercritical region.

At $t_p > t_i$, a non-linear absorption saturation is observed during a laser action resulting in the establishment of a stationary temperature mode, and the temperature profile again corresponds to the spatial distribution of the beam.

The model considered above allows one to explain the regularities of the IR laser radiation with condensed media. The studies of the influence of the laser radiation (with $\Lambda = 10.6\mu m$ wavelength, $P = (3-5)W/cm^2$ power and $t_p(0-30s)$ pulse duration) on the two-layer "non-crystalline layer + substrate" system [20] allow the above mechanism to be confirmed. The structural changes in the layer occurring under irradiation were detected by measuring the optical density D in the visible spectral region ($\Lambda = 0.63\mu m$).

The time evolution of D deposited amorphous layers determined by the densitogram is shown in Fig. 4.6.1. For the given radiative power at low exposures the spatial profile of the beam is repeated with the continuous increase of D in its centre. With increasing t , D at first decreases and then again increases tending to saturation. The change in the optical density at the centre of the laser spot in the region of the leap for the materials under consideration is about 10% (see Fig. 6.4.1). The radiation record under the conditions of thermal heating of the "substrate + layer" system is characterized by a rise of the material sensitivity and a decrease of the threshold density at which the effect of non-monotonic variation of the optical density is observed. The effect of the non-monotonic variation of D can be treated as a result of the thermal instability evolution.

Let us perform some estimations in accordance with formulae (6.4.7) to (6.4.10). The dependence of the threshold radiative power on the pulse duration is plotted in Fig. 6.4.2 together with the bifurcation diagram in the $\{T, P\}$ plane. As follows from the bifurcation diagram $\{T, P\}$, the temperature of the system increases at first monotonically with increasing radiative power density P (a stationary temperature distribution defined by the diagram at the ab area is established during the laser radiation). At $P > P_c$ (here P_c is a density threshold defined by the maximum in the dependence $P(T)$), a considerable temperature rise occurs (the bb' area). The substrate temperature increases sharply being stabilized at the saturation of the absorption non-linearity (the $b'c$ area). The bb' area, which corresponds to the thermal instability of the system, is characterized by the time of its evolution, i.e. the time required to achieve the stationary temperature field (10^{-2} to 10 s for the system under study). For $P = 7.9W/cm^2$ ($I = 0.3W$, $x = 0.11cm$), the threshold pulse duration, at which the instability is produced, is about $0.35 - 0.4s$ and correlates with the exposure times in the interval of the non-monotonic behaviour of D (Fig. 6.4.1).

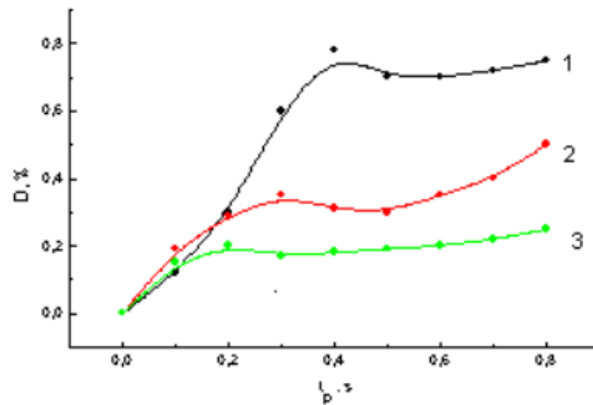


Fig. 6.4.1. Relative variation of the optical density of the Ge-As-Te layers as a function of the radiation influence duration [20]).

With reference to the bio-object (e.g. plants), the model reviewed above attracts an interest at the examination of the processes heat transfer in the skin under the influence of radiation. Indeed, the skin has a layered structure. The heat transfer processes occurring in the skin are described by the heat conduction, which involves the terms responsible for the heat influx due to the blood flow, the heat evolution resulted from the metabolism processes occurring in the skin, and the radiation absorption by the skin. The biological objects absorb radiation mainly by water contained in them. The fact that the radiation of about 10 MW/cm^2 density results in the substantial change of heat fluxes is a distinctive feature of this process.

The mechanism of the low-intensity high-frequency radiation effect on the organism under the skin irradiation may be related to the reduction of heat drain from the irradiated area. Thus, the increase of the flux incident onto the outer skin surface is due to the drain of the heat evolved at the radiation absorption. Moreover, the radiation-induced reduction of heat fluxes in the inner skin layers is observed. One might expect that the biologically active areas of the irradiated skin will appear to be especially sensitive to the heat flux variation. Here one has to take into account the spatially heterogeneous processes in the skin plane related to the spatial heterogeneity of the skin structure. The conformation variations of the bio-macromolecules (i.e. rotation around the unit bonds, valence angle variation) appear to be essential when considering the mechanisms of interaction with electromagnetic fields on the biomolecular level. The conformation variations of the macromolecules occur against the background of the thermal fluctuations inherent in the biological systems and are related to them.

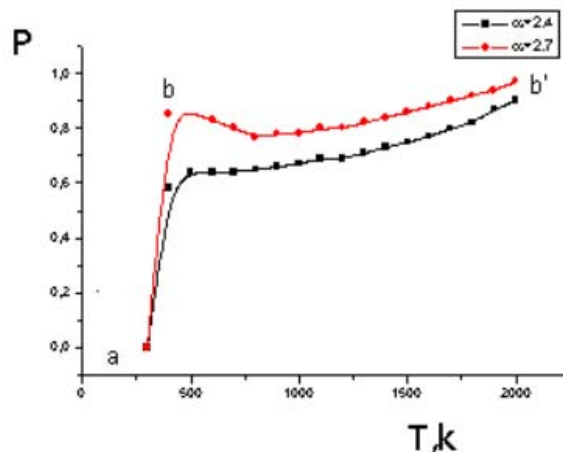


Fig. 6.4.2. Thermal instability intensity as a function of the pulse duration.

APPENDIX

1. Self-consistent phonom approximation

In most cases, the dynamic theory of the crystalline lattice is based on the harmonic approximation, while the anharmonic terms in the expansion of the crystal potential energy are considered as a slight perturbation [1,2]. This approach is based on the assumption about the low amplitudes of oscillations of atoms around their equilibrium position. The ratio of this amplitude to the interatomic distance is used as a small parameter of the perturbation theory series. However, for a number of cases (close to the phase transition points, e.g. non-crystalline materials melting and other cases [3,4]), when the anharmonic effects are essential, the harmonic theory or the lower orders of the perturbation theory fail to give an adequate description. Thus, to study systems with strong anharmonicities, i.e. the anharmonic solids, one requires other approaches. Among them, the principal role is played by the self-consistent harmonical approach. In one of his first papers [5], M. Born suggested the method for self-consistent determination of the frequencies of lattice oscillations with the allowance made for the first anharmonic terms in the expansion of the crystal potential energy. Later on, this method was applied to study the dynamics of quantum crystals [3], at zero temperatures [6], for doped crystals [7] and non-crystalline solids [8,9].

Consider N.M. Plakida's approach [1,4] based on the Green's function method. For the simple crystalline lattice of N atoms with mass M, the Hamiltonian H of the system is written as:

$$H = \frac{1}{2} \sum_{l=1}^N \frac{\vec{P}_l^2}{2M} + U(\vec{r}_1, \dots, \vec{r}_N) , \quad (\text{A1.1})$$

where $U(\vec{r}_1, \dots, \vec{r}_N)$ is the potential energy, \vec{P}_l is the momentum of the l -th atom, \vec{r}_l is the immediate position of the l -th atom.

Let us represent the immediate position of the l -th atom \vec{r}_l for the strongly anharmonic solid as:

$$\vec{r}_l = \vec{R}_l + \vec{u}(l) , \vec{R}_l = \langle \vec{r}_l \rangle \quad (\text{A1.2})$$

Here \vec{R}_l is an average equilibrium position of the l -th atom, $\vec{u}(l)$ is the displacement of the l -th atom from its equilibrium position, $\langle \dots \rangle$ defines the temperature averaging over the equilibrium state of the system with the Hamiltonian (A1.1):

$$\langle \dots \rangle = Sp(\exp(-\frac{H}{\theta}) \dots) / Sp(\exp(-\frac{H}{\theta})) , \quad (\text{A1.3})$$

$\theta = k_B T$, k_B is the Boltzmann constant.

At the expansion of the potential energy $U(\vec{r}_1, \dots, \vec{r}_N)$ over the displacement degrees, the Hamiltonian of the system assumes the form:

$$H = \frac{1}{2} \sum_{l=1}^N \frac{\vec{P}_l^2}{2M} + \sum_{n=1}^{\infty} \frac{1}{2} \sum_{l_1 \dots l_n} \Phi(l_1, \dots, l_n) \bar{u}(l_1) \dots \bar{u}(l_n). \quad (\text{A1.4})$$

Here,

$$\Phi(l_1, \dots, l_n) = \left[\nabla_{l_1} \dots \nabla_{l_n} U(\vec{r}_1, \dots, \vec{r}_N) \right]_0$$

is the n-th-order force constant, index 0 indicates that the expression in brackets is calculated at the equilibrium positions of atoms.

Let us obtain the equation of motion for the time-dependent Green's function [4]:

$$G^{ra}(ll', t) = \langle\langle u(lt); u(l'0) \rangle\rangle$$

$$\text{Here, } \langle\langle A(t); B(t') \rangle\rangle = -\frac{i}{\hbar} \theta(t-t') \langle [A(t), B(t')] \rangle,$$

$\theta(t-t')$ is the Heaviside's function,

$A(t), B(t)$ are the arbitrary operators.

To do this, we use the equation of motion for operators $\bar{u}(l), \vec{P}(l)$:

$$[\bar{u}(l), H] = i\hbar \frac{\vec{P}(l)}{M} \quad (\text{A1.5})$$

$$[\vec{P}(l), H] = -i\hbar \sum_{n=0}^{\infty} \frac{1}{n!} \sum_{l_1 \dots l_n} \Phi(l_1, \dots, l_n) u(l_1) \dots u(l_n)$$

obtained with the allowance made for that the force constants are symmetric functions l_1, l_2, \dots, l_n .

Thus, we obtain:

$$-M \frac{d^2 G(ll', t)}{dt^2} = \delta(t) \delta(ll) + \sum_{n=0}^{\infty} \frac{1}{n!} \sum_{l_1 \dots l_n} \Phi(l, l_1, \dots, l_n) \langle\langle u(l_1, t) \dots u(l_n, t); u(l', 0) \rangle\rangle \quad (\text{A1.6})$$

where $\delta(t)$ is the Kronecker symbol. Performing the Fourier transformation of equation [7]:

$$G(ll', \omega) = \int_{-\infty}^{\infty} dt \exp(i\omega t) \langle\langle \bar{u}(l, t) \bar{u}(l', 0) \rangle\rangle$$

we obtain:

$$M\omega^2 G(ll', \omega) = \delta_{ll'} + \sum_{n=0}^{\infty} \frac{1}{n!} \sum_{l_1 \dots l_n} \Phi(ll_1 \dots l_n) \langle\langle u(l_1, t) \dots u(l_n, t); u(l', 0) \rangle\rangle_{\omega} \quad (\text{A1.7})$$

If one leaves only the term with $n=1$, then (A1.7) coincides with the equation that describes the lattice oscillations in the harmonic approximation.

Using Wick's theorem [4], we split Green's functions in the right-hand part of equation (A1.7):

$$\begin{aligned}
\langle\langle u(l_1, t) \cdots u(l_n, t); u(l', 0) \rangle\rangle_\omega &= \sum_i \langle \prod_{j \neq i} u(l_j, t) \rangle \langle\langle u(l_1, t); u(l', 0) \rangle\rangle_\omega + \\
\sum_{i < j} \langle \prod_{k(\neq i, j)} u(l_k, t) \rangle \langle\langle u(l_i, t) u(l_j, t); u(l', 0) \rangle\rangle_\omega &+ \\
\sum_{i < j < k} \langle \prod_{m(\neq i, j, k)} u(l_m, t) \rangle \langle\langle u(l_i, t) u(l_j, t) u(l_k, t); u(l', 0) \rangle\rangle_\omega &. \quad (A1.8)
\end{aligned}$$

Substituting (A1.8) into (A1.7), we obtain:

$$M\omega^2 G(l', \omega) = \delta_{l'} + \sum_{n=0}^{\infty} \frac{1}{n!} \sum_{l_1 \dots l_n} \tilde{\Phi}(l_1 \dots l_n) \langle\langle u(l_1, t) \cdots u(l_n, t); u(l', 0) \rangle\rangle_\omega, \quad (A1.9)$$

here

$$\begin{aligned}
\tilde{\Phi}(l_1 \dots l_n) &= \nabla_{(l_1)} \cdots \nabla_{(l_n)} \langle \Phi(\vec{r}) \rangle, \quad (A1.10) \\
\langle \Phi(\vec{r}) \rangle &= \langle \exp(\sum_l u(l) \nabla_l) \rangle \Phi(\vec{r})
\end{aligned}$$

are the effective potential and effective force constants, respectively.

The physical essence of the effective potential and effective force constants is as follows. In the anharmonic solid, all the atoms oscillate around the medium equilibrium positions with substantial amplitude, so that atom is exposed to the strongly anharmonic forces from the surrounding atoms. When calculating these forces, the atoms cannot be considered to be rigidly fixed since the forces depend on the type of motion of surrounding atoms. Therefore, the motion of any separate atom is defined by the potential produced by all other atoms, the oscillations of which induce the chaotic thermal modulation of the potential of a separate atom. The condition should hold that the motions of all the atoms must be self-consistent. Thus, in the anharmonic solids, the motion of atoms is defined by the effective potentials or effective force constants, not the initial potentials or initial force constants.

If a series in the right-hand side of (A1.9) is cut off at $n=1$, we obtain the non-interacting re-normalized harmonic phonons. To take into account the scattering processes for the re-normalized phonons, one has to cut a series off at $n > 1$. We shall restrict ourselves to the case with $n=1$. According to (A1.9), we get in this approximation:

$$M\omega^2 G(l', \omega) = \delta_{l'} + \sum_l \tilde{\Phi}(l_1) G(l_1 l', \omega),$$

where the following relation is used:

$$\tilde{\Phi}(l') = \Phi(l') + \sum_n \frac{1}{n!} \sum_{l_1 \dots l_n} \Phi(l', l_1 \dots l_n) \langle u(l_1) \cdots u(l_n) \rangle. \quad (A1.11)$$

The correlation functions in (A1.11) are approximated in accordance with Wick's theorem [10] in the following way:

$$\begin{aligned}
\langle u(l_1) \cdots u(l_n) \rangle &\approx (n-1) \langle u(l_1) u(l_2) \rangle \langle u(l_3) \cdots u(l_n) \rangle \approx \\
(n-1)(n-3) \cdots &\langle u(l_1) u(l_2) \rangle \cdots \langle u(l_{n-1}) u(l_n) \rangle, \quad (A1.12)
\end{aligned}$$

where the force constant symmetry with respect to the index replacement was accounted for. Substituting (A1.11) into (A1.10), we get:

$$\tilde{\Phi}(ll') = \nabla(l)\nabla(l') < \exp(-\frac{1}{2} \sum u(l_1)u(l_2)\nabla(l_1)\nabla(l_2)) > \Phi(r). \quad (\text{A1.13})$$

Thus, Green's function $G(ll', \omega)$ is defined by the force constants from (A1.13), which, in their turn, depend on Green's function via the correlation functions. First the force constants are found, which, being substituted into (A1.11), allow the correlation functions to be calculated. This procedure is repeated as long as convergence is reached. The thermodynamic parameters of the anharmonic system may be calculated in the similar way.

The motion of atoms in the self-consistent field is defined by the effective pair interaction potential obtained from the initial potential by averaging with the used Gauss distribution for interatomic distances. The effective potential as a function of interatomic distance is smoother than the initial potential, i.e. its depth is less, and the minimum corresponds to the distance larger than that in the initial one. Since the width of the Gauss distribution is determined by the correlation displacement matrix, the difference between the potentials is especially sensitive to the considerable anharmonism.

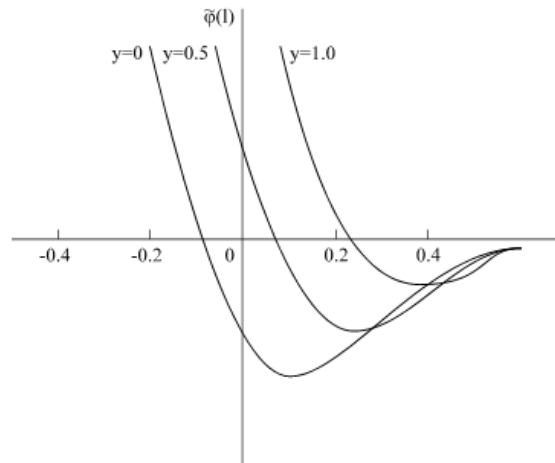


Fig. A1.1. Pair potential within the self-consistent phonon approximation for the one-dimensional chain with the Morse potential.

To illustrate the self-consistent potential, the interaction of the nearest neighbours in the one-dimensional chain with the Morse potential should be considered (Fig. A1.1). In this case we obtain:

$$C_{\alpha\alpha'}(l, l+1) = \delta_{\alpha\alpha'} < (u(l) - u(l+1))^2 > \equiv \delta_{\alpha\alpha'} \bar{u}^2(l) \quad (\text{A1.14})$$

Here, $\bar{u}^2(l)$ is a mean-square relative displacement of the adjacent atoms. The effective pair potential in this case assumes the form:

$$\Psi(r) = V_0 \{ \exp(-12r/a) \exp(2y) - 2 \exp(-6r/a) \exp(y/2) \}$$

where $y = 36\bar{u}^2(l)/a^2$, V_0 and a are the potential parameters.

2. Variational principle for the free-energy functional

Let us find the functional equations to determine the probability of the liquid-like states formation, force constants and mean-square displacement of atoms. Using equations (3.2.3) and (3.2.4) for σ :

$$\delta F = \left[\frac{\partial F}{\partial \sigma} \right]_{y_{\alpha\beta}, \tilde{\Phi}_f^{\alpha\beta}} \cdot \delta \sigma + \left[\frac{\partial F}{\partial \tilde{\Phi}_f^{\alpha\beta}} \right]_{\sigma, y_{\alpha\beta}} \cdot \delta \tilde{\Phi}_f^{\alpha\beta} + \left[\frac{\partial F}{\partial y_{\alpha\beta}} \right]_{\sigma, \tilde{\Phi}_f^{\alpha\beta}} \cdot \delta y_{\alpha\beta}$$

$$F \leq F_0 + \langle H - \tilde{H}_0 \rangle_0, F_0 = \sum_f F_{0f} - TS, F_{0f} = -\Theta \ln \left\{ SP \left(e^{\frac{-H_f}{\Theta}} \right) \right\}$$

we find:

$$\frac{\partial F}{\partial \sigma} = \frac{\partial F}{\partial \sigma} + \frac{\partial}{\partial \sigma} \langle H - \tilde{H} \rangle_0 = \tilde{T}_2 - \tilde{T}_1 + 2\sigma(\tilde{\Phi}_2 - \tilde{\Phi}_1) - 2\tilde{\Phi}_1 - 4\tilde{I}(1 - \sigma)\sigma -$$

$$- 2IN \ln \frac{\frac{g_2 - 1}{\sigma}}{\frac{g_1 - 1}{1 - \sigma}} \quad (\text{A2.1})$$

Here, the following notation has been introduced: F is the free energy functional for the effective Hamiltonian, S is the entropy, g_f is a statistical weight of the state f , σ_f is the fraction of atoms in the liquid-like states, $\tilde{\Phi}_f^{\alpha\beta}(l, l')$ is the force constants and the mean-square relative displacements

$$\text{of atoms } y_{\alpha\beta}(l, l') = \langle u^\alpha(l, l') u^\beta(l, l') \rangle, \quad \Theta = k_B T, \quad \tilde{T}_f = \sum_l \left\langle \frac{\bar{P}_f^2(l)}{2M} \right\rangle, \quad \tilde{\Phi}_f = \frac{1}{2} \sum_{l, l'} \langle \Phi_f(l, l') \rangle,$$

$$\tilde{I} = \left\langle \sum_{l, l'} \sum_{\alpha, m} I_\alpha(\bar{r}_{ll'}) v_\alpha(l/m) \right\rangle. \text{ Similarly, the functional equations with respect to the quantities } y_{\alpha\beta}(l, l')$$

and $\tilde{\Phi}_f^{\alpha\beta}(l, l')$ are found:

$$\frac{\partial F}{\partial y_{\alpha\beta}(l, l')} = \frac{\partial}{\partial y_{\alpha\beta}(l, l')} \langle H - \tilde{H} \rangle_0 = \frac{1}{4} \left(\langle \nabla_{ll'}^\alpha \nabla_{ll'}^\beta \Phi_f(\bar{r}_{ll'}) \rangle \sigma_f^2 - \tilde{\Phi}_f^{\alpha\beta}(l, l') \right) \quad (\text{A2.2})$$

$$\frac{\partial F}{\partial \tilde{\Phi}_f^{\alpha\beta}(l, l')} = \frac{\partial F_0}{\partial \tilde{\Phi}_f^{\alpha\beta}(l, l')} + \frac{\partial}{\partial \tilde{\Phi}_f^{\alpha\beta}(l, l')} \langle H - \tilde{H} \rangle_0 = \frac{\hbar}{2MN} \sum_{\bar{k}} \frac{\sin^2 \frac{\bar{k}\bar{r}_{ll'}}{2}}{\omega(\bar{k})} \coth \frac{\hbar\omega}{2\Theta} - \frac{y_{\alpha\beta}(l, l')}{4}. \quad (\text{A2.3})$$

In the non-equilibrium non-crystalline state, $\delta F \neq 0$, expanding F into a power series in the system deviation from the equilibrium state and restricting ourselves to the first terms of the expansion, we have:

$$F = F_0 + \frac{1}{2} \sum_{i, j} a_{ij} \eta_i \eta_j + \frac{c}{3} \eta^3 + \frac{b}{4} \eta^4 \quad (\text{A2.4})$$

where the following notations are used:

$$\eta = \sigma - \sigma_e, \eta_y = \{ \eta_y^\alpha \}, \eta_y^\alpha = y_\alpha(l, l') - y_\alpha(l, l')_e, \eta_\Phi = \{ \eta_\Phi^\alpha \}, \eta_\Phi^\alpha = \tilde{\Phi}^{\alpha\alpha}(l, l') - \tilde{\Phi}^{\alpha\alpha}(l, l')_e,$$

$$a_{ij} = \left(\frac{\partial^2 F}{\partial \eta_i \partial \eta_j} \right)_e, \quad c = \frac{1}{2} \left(\frac{\partial^3 F}{\partial \eta^3} \right)_e, \quad b = \frac{1}{6} \left(\frac{\partial^4 F}{\partial \eta^4} \right)_e$$

and the allowance was made for $\left(\frac{\partial F}{\partial \eta_i} \right)_e = 0$ (the subscript "e" corresponds to the equilibrium state).

Based on (A2.4), we can write:

$$\begin{aligned}\frac{\partial F}{\partial \sigma} &= a_{11}\eta + a_{12}\eta_y + a_{13}\eta_\Phi + c\eta^2 + b\eta^3, \\ \frac{\partial F}{\partial \eta_y} &= a_{12}\eta + a_{22}\eta_y, \quad \frac{\partial F}{\partial \eta_\Phi} = a_{13}\eta + a_{33}\eta_\Phi.\end{aligned}\tag{A2.5}$$

To describe the kinetics of the order parameter variation, we shall use the Landau-Khalatnikov regression equation [11] $\frac{\partial \eta_i}{\partial t} = -\gamma_i \left(\frac{\partial F}{\partial \eta_i} \right)$, which allows one to obtain in relations (A2.5) the following system of non-linear kinetic equations:

$$\begin{aligned}\gamma_1 \frac{\partial \eta}{\partial t} &= -a_{11}\eta - a_{12}\eta_y - a_{13}\eta_\Phi - c\eta^2 - b\eta^3, \\ \gamma_2 \frac{\partial \eta_y}{\partial t} &= -a_{12}\eta - a_{22}\eta_y, \quad \gamma_3 \frac{\partial \eta_\Phi}{\partial t} = -a_{13}\eta - a_{33}\eta_\Phi.\end{aligned}\tag{A2.6}$$

The first terms in these equations describe the energy dissipation with the relaxation time of $\tau_{ij} = a_{ij}^{-1}$, while the second terms define the collective mode interaction.

Consider the Prigogine principle of mode subordination, which holds for the highly non-equilibrium systems [12]. According to this principle:

$$\frac{\partial \eta_y}{\partial t} = 0, \quad \frac{\partial \eta_\Phi}{\partial t} = 0.$$

This allows one to reduce the number of order parameters: $\eta_y = -\left(\frac{a_{12}}{a_{22}}\right)\eta$, $\eta_\Phi = -\left(\frac{a_{13}}{a_{33}}\right)\eta$ and rewrite (A2.6) in the following form:

$$\gamma_1 \frac{\partial \eta}{\partial t} = -a_0\eta - c\eta^2 - b\eta^3, \quad a_0 = -\left(a_{11}^2 - \frac{a_{12}^2}{a_{22}^2} - \frac{a_{13}^2}{a_{33}^2} \right).\tag{A2.7}$$

The expansion coefficients are the functions of the temperature, pressure and control parameter, i.e. the cooling rate is $a_0 = a_0(T, P, q)$. Since in the equilibrium state $\delta F = 0$, $\delta^2 F > 0$ and $\eta = 0$, then, to ensure this, $a_0(T, P, q)$ must be a positively defined matrix, i.e. $a_0(T, P, q) > 0$. In the non-equilibrium state, $\delta F \neq 0$, $\eta \neq 0$. To provide the formation of the stationary states with a non-zero order parameter, it is essential that $a_0(T, P, q) < 0$. Thus, at the transition to the non-equilibrium state

with the non-zero order parameter: $\eta = \frac{-2c \pm \sqrt{4c^2 - 4a_0b}}{6b}$, and the expansion coefficient is $a_0(T_c, P_c, q_c) = 0$. Here, the following conditions must hold: $c(T_c, P_c, q_c) = 0$, $b(T_c, P_c, q_c) > 0$, since, with approaching the point T_c, P_c, q_c from the equilibrium state side, an even derivative should be positive. Thus, in the process of melt cooling and at the transition to the non-crystalline state, $a_0(T_c, P_c, q_c)$ can be approximated by:

$$a_0(T_c, P_c, q_c) = -\tilde{a}_0 \ln(\arctan[\tilde{q}]), \quad \tilde{q} = \frac{q - q_c}{q_c}$$

which is transformed to $a_0(T_c, P_c, q_c) \approx -a_0\tilde{q}$ as $\tilde{q} \ll 0$.

Thus, having started from expressions (A2.1)-(A2.7), we arrive at the following self-consistent system of equations with respect to the relative fraction of atoms in the liquid-like states, the mean-square atomic displacements $y_{\alpha\beta}(l, l')$ and the force constants $\tilde{\Phi}_f^{\alpha\beta}(l, l')$:

$$F_1(\sigma) = 0, F_2(y) = 0, F_3(\Phi) = 0 \quad (\text{A2.8})$$

Here:

$$F_1(\sigma) = \tilde{T}_2 - \tilde{T}_1 + 2\sigma(\tilde{\Phi}_2 - \tilde{\Phi}_1) - 2\tilde{\Phi}_1 - 4\tilde{I}(1-\sigma)\sigma - 2\Theta N \ln \frac{\frac{g_2}{\omega_2} - 1}{\frac{g_1}{\omega_1} - 1} + \tilde{a}_0 \tilde{q} \eta - c \eta^2 - b \eta^3 - D_\eta \nabla^2 \eta,$$

$$F_2(y) = \frac{\hbar}{2MN} \sum_{\vec{k}} \frac{\sin^2 \frac{\vec{k} \vec{r}_{l'}}{2}}{\omega(\vec{k})} \coth \frac{\hbar \omega}{2\Theta} - \frac{y_{\alpha\beta}(l, l')}{4} - \frac{\eta_y}{\tau_y},$$

$$F_3(\Phi) = \frac{1}{4} \left(\left\langle \nabla_{l'}^\alpha \nabla_{l'}^\beta \Phi_f(\vec{r}_{l'}) \right\rangle \sigma_f^2 - \tilde{\Phi}_f^{\alpha\beta}(l, l') \right) - \frac{\eta_\Phi}{\tau_\Phi}.$$

This system allows the temperature properties of the system to be studied both at the equilibrium ($\eta = 0$) and highly non-equilibrium ($\eta \neq 0$) transformations.

3. The variational principle for the free-energy functional in the liquid water

Solving the variational problem in the linear approximation of the non-equilibrium thermodynamics gives:

$$\delta F / \delta \omega_2 = -a(\omega_2 - \omega_2^e), \quad (\text{A3.1})$$

where the free-energy functional F is:

$$F = \sum_f F_{0f} - TS, \quad (\text{A3.2})$$

$$F_{0f} = -\theta \ln \left[Sp \left(\exp \left(-\frac{\tilde{H}_f}{\theta} \right) \right) \right],$$

$\theta = k_B T$, k_B is the Boltzmann constant, $S = -k_B \ln \left[\prod_f \frac{g_f!}{N_f! (g_f - N_f)!} \right]$ is the entropy, g_f is a

statistic weight of the f state, and the equilibrium fraction of the disordered states is

$a = \left(\partial^2 F / \partial \omega_2^2 \right)_{\omega_2^e}$, so we have the functional equation for ω_2 :

$$\tilde{T}_2 - \tilde{T}_1 - 2\tilde{\Phi}_1 + 2\omega_2(\tilde{\Phi}_2 - \tilde{\Phi}_1) - \Theta N \left(\ln \left(\frac{g_2}{\omega_2} - 1 \right) - \ln \left(\frac{g_1}{\omega_1} - 1 \right) \right) = a(\omega_2 - \omega_2^e). \quad (\text{A3.3})$$

Let us denote:

$$\tilde{T}_f = \sum_i \left\langle \left\langle \left(\frac{\langle \bar{P}_i^f \rangle^2}{2m} \right) \right\rangle_c \right\rangle, \quad \tilde{\Phi}_f = \left\langle \frac{1}{2} \sum_{i \neq i'} \left\langle \left\langle \Phi_{ff'}(\vec{r}_i - \vec{r}_{i'}) \right\rangle_c \right\rangle \right\rangle, \quad (\text{A3.4})$$

which are the kinetic and potential energies of the corresponding phase states averaged on the random field and heterophase fluctuations.

The statistical micro-displacements of the liquid particles have to be calculated. To describe the thermal behaviour of the system we take into account strong anharmonic effects as well as the structure transformations. We apply a self-consistent anharmonic approach, which makes it possible to re-normalize the force constants and local potentials as a consequence of the anharmonicity of the atomic vibrations [13,14].

Functional equations similar to Eq. (A3.3) for relative to re-normalized force constants $\tilde{\Phi}_{ll'}^{\alpha\beta}$ and the mean-square of atomic displacements:

$$\tilde{D}_{ll'}^{\alpha\beta} = \left\langle \left(u_i^\alpha - u_{i'}^\alpha \right) \left(u_i^\beta - u_{i'}^\beta \right) \right\rangle$$

are obtained:

$$\frac{\delta F}{\delta \tilde{\Phi}_{ll'}^{\alpha\beta}} = 0, \quad \frac{\delta F}{\delta \tilde{D}_{ll'}^{\alpha\beta}} = 0.$$

Therefore for $\tilde{T}_f, \tilde{\Phi}_f$ from Eq. (A3.4) and $\tilde{\Phi}_{ll'}^{\alpha\beta}, \tilde{D}_{ll'}^{\alpha\beta}$ we have:

$$\tilde{T}_1 = \sum_{\vec{k}} \frac{\hbar \omega(\vec{k})}{4} \text{cth} \frac{\hbar \omega(\vec{k})}{2\theta}, \quad \tilde{\Phi}_1 = \sum_{i, i'} \exp \left\{ \frac{1}{2} \sum_{\alpha, \beta} \tilde{D}_{i, i'}^{\alpha\beta} \nabla_i^\alpha \nabla_{i'}^\beta \right\} \Phi_1(\vec{r}_i - \vec{r}_{i'}), \quad (\text{A3.5})$$

$$\tilde{\Phi}_{ll'}^{\alpha\beta} = \nabla_l^\alpha \nabla_{l'}^\beta \tilde{\Phi}_1(\vec{r}_l - \vec{r}_{l'}), \quad \tilde{D}_{ll'}^{\alpha\alpha} = \frac{\hbar}{MN} \sum_{\vec{k}} \frac{2 \sin^2 \left(\frac{\vec{k}(\vec{r}_l - \vec{r}_{l'})}{2} \right)}{\omega(\vec{k})} \text{cth} \frac{\hbar \omega(\vec{k})}{2\theta},$$

$$m \omega^2(\vec{k}) = \sum_{i, i'} \sum_{\alpha} \exp(i\vec{k}(\vec{r}_i - \vec{r}_{i'})) \tilde{\Phi}_{ll'}^{\alpha\alpha} \omega_i,$$

where \vec{k} is a wave-vector, $\omega(\vec{k})$ is a vibrational frequency.

The atomic interaction is written as $\Phi(r) = \Phi_1(r) + \Phi_2(r)$. Here $\Phi_1(r)$ is a long-range term (approximated by a Morse-type potential $\Psi(r) = V_0 \left(\exp(-12(r-a)/r) - 2 \exp(-6(r-a)/r) \right)$ and a non-central potential $G(\delta) = G_0 \exp(-4(\delta/a)^2)$, where δ is the deviation of an atom from the plane, perpendicular to the bond direction, G_0 and V_0 are the potential parameters) and $\Phi_2(r)$ is a short-range term (approximated by a hard sphere-type potential).

In a self-consistent approach, averaging on the random field interaction potentials Eq. (A3.5), we get:

$$\tilde{\Psi}(r) = \omega_1^2 V_0 \exp(-\tilde{Q}_1) \left(e^{-12(r-a)/r} e^{2Y_1} - 2e^{-6(r-a)/r} e^{Y_1/2} \right), \quad (\text{A3.6})$$

$$\tilde{G}(\delta) = -\omega_1^2 V_0 \left[1 + 2(Y_t + \tilde{Q}_t) \right]^{-1} \exp\left(-\frac{4(\delta/a)^2}{1 + 2(Y_t + \tilde{Q}_t)} \right).$$

Here $Y_l = 36\tilde{D}_{ll}/a^2$ and $Y_t = 4\tilde{D}_{tt}/a^2$ are the average square atomic displacements along the bonding and in transversal directions; $\tilde{Q}_l = 36\tilde{Q}_l^2/a^2$ and $\tilde{Q}_t = 4\tilde{Q}_t^2/a^2$ are the fluctuations of the distance and angle between the bonds, $a = \langle l \rangle_c = a_0(1 + \tilde{Q}_l/4)$ is the average interatomic distance taking into account the statistical spread of the equilibrium sites.

According to the local equilibrium principle for the system $P = -\frac{zN\omega_1^2 \tilde{\Psi}'(l)}{V}$, the average distance is:

$$l = a \left(1 + \frac{Y_l}{4} - \delta_l \right), \quad (\text{A3.7})$$

where

$$\delta_l = \frac{\ln[B(Y_l)/2]}{6}, \quad B(Y_l) = 1 + \left[1 + \frac{P^* r^2 \exp(Y_l)}{6\omega_1^2 a^2} \right], \quad P^* = \frac{PV \exp(\tilde{Q}_l)}{6zNV_0}$$

is the reduced pressure, z is the number of the nearest neighbours, P is the pressure, V is the volume.

So, the potential energy and force constants are defined by equations:

$$\tilde{\Psi}(r) = -\frac{\omega_1^2 V_0 e^{-Y_l} e^{-Q_l}}{2} \left[B(Y_l) - \frac{P^*}{12\omega_1^2} \left(\frac{r}{a} \right)^2 e^{Y_l} \right], \quad (\text{A3.8})$$

$$\tilde{G}(0) = -\frac{G_0 \omega_1^2}{1 + 2(Y_t + \tilde{Q}_t)},$$

$$\tilde{f}(\theta) = \tilde{\Psi}'(r) = \omega_1^2 f \left[\frac{P^*}{12\omega_1^2} \left(\frac{r}{a} \right)^2 + \frac{e^{-Y_l}}{2} B(Y_l) \right], \quad f = 72V_0 \exp(-\tilde{Q}_l)/a^2. \quad (\text{A3.9})$$

From Eq. (A3.4) and Eq. (A3.5), the kinetic and potential energies are calculated as follows:

$$\omega_1^2 \tilde{\Phi}_1(r) = zN \left[\tilde{\Psi}(r) + \tilde{G}(0) \right] / 2, \quad \tilde{\Phi}_2 = N\varphi/2, \quad \tilde{T}_f = 3N_f \theta/2,$$

$$\varphi = \int \rho(r) \Phi_2 dr.$$

Hence, the self-consistent system of Eqs. (A3.3) – (A3.5), (A3.8), (A3.9):

$$\frac{2\omega_1 Y_l}{\tau} = \frac{e^{Y_l} e^{Q_l}}{B(Y_l) + \frac{P^*}{6\omega_1^2} \left(\frac{r}{a} \right)^2 e^{Y_l}},$$

$$\frac{0.27Y_l\omega_1}{\tau} = \frac{g}{f} \left[\frac{(1 + 2(Y_l + \tilde{Q}_l))}{\left(\frac{P^*}{12\omega_1^2}(r/a)^2 + B(Y_l)/2e^{-Y_l}\right)^{1/2}} \right], \quad (\text{A3.10})$$

$$\begin{aligned} \omega_2 \xi_p + \omega_1 z \left\{ \frac{e^{-Y_l} e^{\tilde{Q}_l}}{2} \left[B(Y_l) - \frac{P^*}{12\omega_1^2} \left(\frac{r}{a}\right)^2 e^{Y_l} \right] \right\} + \\ + \left\{ \frac{0.1}{1 + 2(Y_l + \tilde{Q}_l)} \exp\left(-\frac{4(z/a)^2}{1 + 2(Y_l + \tilde{Q}_l)}\right) \right\} - \\ - \tau \ln\left(\frac{(g_2 - \omega_2)\omega_1}{(g_1 - \omega_1)\omega_2}\right) = a(\omega_2 - \omega_2^e). \end{aligned}$$

Here $\tau = \theta/V_0$ is the reduced temperature, $\xi_p = \varphi/V_0$ and G_0/V_0 are assumed to be 0.1. The solution for ω_2, Y_l, Y_t of the self-consistent system of equations (A3.10) in the $T < 100^\circ\text{C}$ temperature range was found numerically using the iteration procedure.

The internal energy is:

$$\tilde{E} = \omega_1 \tilde{T}_1 + \omega_2 \tilde{T}_2 + \omega_1^2 \tilde{\Phi}_1^2 + \omega_2^2 \tilde{\Phi}_2^2 \quad (\text{A3.11})$$

and the volume is:

$$V = N(\omega_1 v_1 + \omega_2 v_2), \quad (\text{A3.12})$$

where $v_f = v_{0f} l_f^3$, and v_{0f} is a geometric-structure factor. Consequently, the heat capacity C_p and the linear expansion coefficient α_T are:

$$\begin{aligned} C_p = \frac{1}{N} \left. \frac{\partial(\tilde{E} + PV)}{\partial T} \right|_p = 3R + \omega_1^2 \frac{\partial(\tilde{\Phi}_1/N)}{\partial T} + \omega_2^2 \frac{\partial(\tilde{\Phi}_2/N)}{\partial T} + \\ + \frac{P}{N} \left(\omega_1 \frac{\partial v_1}{\partial T} + \omega_2 \frac{\partial v_2}{\partial T} \right) + \\ + \frac{1}{N} \left\{ 2\omega_2(\tilde{\Phi}_1 + \tilde{\Phi}_2) - 2\tilde{\Phi}_1 + P(v_2 - v_1) \right\} \frac{\partial \omega_2}{\partial T}, \quad (\text{A3.13}) \end{aligned}$$

$$\alpha_T = \frac{1}{V} \left. \frac{\partial V}{\partial T} \right|_p = \frac{N}{V} (v_2 - v_1) \frac{\partial \omega_2}{\partial T} + \frac{N}{V} \left\{ \frac{\partial v_1}{\partial T} + \omega_2 \left(\frac{\partial v_2}{\partial T} - \frac{\partial v_1}{\partial T} \right) \right\}. \quad (\text{A3.14})$$

REFERENCES

Introduction

1. Koblo A.B. The visible Hand. Synergetic Microfoundation of Macroeconomic Dynamics. – Karlsruhe. Lecture Notes in Economics and Mathematical. V. 369. 1991.
2. Haken H. Information and Self-Organisation. – Berlin-Heidelberg-Stuttgart. Springer-Verlag. 1999.
3. Livin S.A., Hallam T.G., Gross L.J. Applied Mathematical Ecology. – Berlin-Ithaca-Knoxville. Springer. 1989.
4. Schwable U. The Core of Economies with Asymmetric Information. – Berlin-Heidelberg-Mannheim. Springer-Verlag. 1995.
5. Portugali J. Self-Organisation and the City. – Berlin-Tel Aviv. Springer-Verlag. 2000.
6. Glansdorff P., Prigogine I. Thermodynamic Theory of Structure, Stability and Fluctuations. – New York. Wiley. 1971.
7. Shuster G. Deterministic Chaos. An Introduction. – Weinheim. Physik - Verlag. 1984.
8. Vorontsov M.A., Miller W.B. Self-Organization in Optical Systems and Applications in Information Technology. – Berlin-Heidelberg. Springer-Verlag. 1995.
9. Patashinskii A.Z., Pokrovskii V.L. Fluctuation Theory of Phase Transitions. – Oxford-New York-Toronto-Sydney-Paris-Frankfurt. Springer. 1995.
10. Hilborn R. C. Chaos and Nonlinear Dynamic. – New York-Oxford. Springer. 1994.
11. The Nature of Chaos. – Edited by T. Mullin. Oxford-New York. Springer. 1994.
12. Stehle P. Order, Chaos, Order. The Transition from Classical to Quantum Physics. – New York- Oxford. Oxford University Press. 1994.
13. Kauffman S.A. The Origins of Order: Self-Organization and Selection in Evolution. – New York Oxford. Oxford University Press. 1993.
14. Mott N.F., Davis E.A. Electron Process in Non-Crystalline Materials. – Oxford. Clarendon Press. 1979.
15. Penrose P. Shadows of the Mind: Search for the Missing Science of Consciousness. – Vintage. 1994.
16. Amorphous Semiconductors. – Ed. M. Brodsky. Berlin-Heidelberg-New York. Springer - Verlag. 1979.
17. Haken H. Principles of Brain Functioning. A Synergetic Approach to Brain Activity. Behaviour and Cognition. – Berlin-New York. Springer. 1996.
18. Peacocke A.K. The Physical Chemistry of Biological Organization. – Clarendon Press. Oxford. 1983.
19. Babloyantz A. Molecules, Dynamics, and Life. An Introduction to Self-Organisation of Matter. – John Wiley & Sons. Inc. 1986.
20. Metters M. On the Material of the Cognitive Activity of Mind. – Berlin. Springer. 1997.
21. Tass P.A. Phase Resetting in Medicine and Biology. Stochastic Modelling and Data Analysis. – Berlin-Heidelberg. Springer-Verlag. 1999.
22. Uhl C. Analysis of Neurophysiological Brain Functioning. – Berlin-Heidelberg. Springer-Verlag. 1999.

Chapter 1

1. Haken H. Self-Organization and Information. – Phys. Script. (1987) **35**, N 3, 247-254.
2. Nicolis G., Mansour M. – Phil.Mag. (1987) **9**, N 4, 281-297.
3. Walgraef P., Borckmans P., Dewel G. Dissipative Structures in Chemical Systems as Non-Equilibrium Phase Transitions. – Non-Equilibrium Phase Transitions. London-New York (1986), 29-54.
4. Sornette D. Chaos, Fractals, Self-Organization and Disorder: Concepts and Tools. – Berlin-Los Angeles. Springer-Verlag. 2000.
5. Haken H. Advanced Synergetics. – Berlin-Heidelberg-New York-Tokyo. Springer. 1984.
6. Maeland B. Fractal Geometry of Nature. – Freeman. 1983.
7. Peitgen H.O., Richter P.H. The Beauty of Fractals. – Springer-Verlag. 1986.
8. Pietronevo L., Tosatti E. Fractals in Physics. – North-Holland. 1986.
9. Tou D., Casas-Vazquez J., Lebon G. – Rep. Prog. Phys. (1988), **51**, N 8, 1105-1179.
10. Haken H. – Rep. Prog. Phys. (1989), **52**, N 5, 115-153.
11. Kaneko K. – Physica D. (1989), **39**, N 1-2, 1-41.
12. Hu Gang, Haken H. – Z.Phys. B: Condens. Matter (1989), **76**, N 4, 537-545.
13. Bhatti F.M., Brak R., Essam J.M. and Lookman T. – J. Phys. A.: Math. Gen. (1997) **30**, N 18, 6217-6232.
14. Fokas A.S., Kaup D.J., Newell A.C., Zakharov V.E. Nonlinear Processes in Physics. – Berlin-Heidelberg-Postdam-Tucson. Springer-Verlag. 1993.
15. Prigogine I. From Being to Becoming: Time and Complexity in Physical Sciences. – San Fransisco. Freeman. 1980. (Nicolis G., Prigogin I. Self-Organization in Non-Equilibrium Systems. From Dissipative Structure to through Fluctuations. – New York. Wiley. 1977).

16. Kravtsov Y.A., Kadtko J.B. *Predictability of Complex Dynamic Systems. –Berlin-Heidelberg-San Diego. Springer. 1996.*
17. Pragma Shucla. – J. Phys. A: Math. Gen. (1997), **30**, 6313-6326.
18. Glendinning P. *Stability, Instability and Chaos: an Introduction to the Theory of Non-Linear Differential Equations. – Cambridge. 1994.*
19. Heinrichs J. – J. Phys. A: Math. Gen. (1997), **30**, N 15, 5289-5298.
20. Mukku C., Sriram M.S., Segar J., Bindu A. – J. Phys. A: Math. Gen. (1997), **30**, N 9, 3003 - 3020.
21. Kruse P., Stadler M. *Ambiguity in Mind and Nature. Multistable Cognitive Phenomena. – Berlin-Bremen. Spinger. 1995.*
22. Mikhailov A.S., Loskutov A.Y. *Foundation of Synergetics. Chaos and Noise. – Berlin-Heidelberg. Springer-Verlag. 1996.*
23. Huseby O., Thovert J.F., Adler P.M. – J. Phys. A: Math. Gen. (1997), **30**, N 5, 1415-1444.
24. Gould H, Tobochnik J. *An Introduction to Computer Simulation Methods Applications to Physical Systems. – Addison-Wesley. 1988.*
25. Chatterjee S., Bhui B. – IL nuovo cimento (1995) **110**, N 11, 1277-1286.
26. Fournier J., Boitex G., Seytre G. – Phys. Rev. B: (1997), **56**, N 9, 5207-5212.
27. Colaioni F., Flamini A. – Phys. Rev. E. (1997), **55**, N 2, 1298 - 1310.
28. Paul J.M., Hubert J.F. – J. Phys. A: Math. Gen. (1997), **30**, N 6, 1791-1801.
29. Dominguez D.R.C., Theumenn W.K. – J. Phys. A: Math. Gen. (1997), **30**, N 5, 1403 – 1414.
30. Haken H. *Laser Light Dynamics. – Amsterdam-New York-Oxford-Tokyo. North-Holland Physics Publishing. 1985.*
31. Yannacopoulos A.M., Rowlands G. – J. Phys. A: Math. Gen. (1997), **30**, 1507 - 1525.
32. Battezzati M. – IL Nuovo cimento (1995), **110B**, N 11 , 1287 – 1289.
33. Lange K. *Mathematical and Statistical Methods for Genetic Analysis. – Berlin- Ann Arbon. Springer. 1997.*
34. Wechsler H., Phillips J.P., Bruce V., Fogelman S.F., Huang T.S. *Face Recognition. From Theory to Applications. – Gaitherburg-Urbana. NATO ASI. 1998.*
35. Tass P., Haken H. –Biological Cybernetics (1995), **74**, N 1, 31-39.
36. Kruse P., Carmasin H.-O., Pahlke P., Striber D., Stadler. – Biological Cybernetics (1996), **75**, N 4, 321 - 330.
37. Finke E., Simon D. – Applied Physics A: Materials Science and Processing (1995), **60**, N. 5, 487- 495.
38. Pribe C., Grossberg S., Cohen M.A. – Biological Cybernetics (1997), **77**, N 8, 141-152.
39. Hoppensteadt F.C., Izhikevich E.M. – Biological Cybernetics (1996) **75**, N 8 , 117 - 127.
40. Ditzinger T., Tuller B., Haken H., Kelso J.A.S. – Biological Cybernetics (1997) **77**, N 1, 31 - 40.
41. Lin J., Takisawa N., Shirahawa K. – Colloid & Polymer Science (1999), **277**, 247 - 251.
42. Huerta R., Bazhenov M., Rabinovich M.I. – Europhys Lett. (1998), **43**, N 6,719 -724.
43. Ratner V.A., Zharkikh A.A., Kolchanov N.A., Rodin S.N., Solovjov V.V., Antonov A.S. *Molecular Evolution. – Berlin. Springer. 1996.*
44. Lyubich Y.I., Akin E. *Mathematical Structures in Population Genetics. – Berlin-New York. Springer. 1992.*
45. Basar E. *Brain Function and Oscillations. Vol. II. Interactive Brain Function. Neurophysiology and Cognitive Processes. – Berlin. Springer. 1999.*

Chapter 2

1. Hume-Rothery W. – J. Inst. Met. (1926), **35**, 295. (Hume-Rothery W., Mabbott G.W. and Channel-Evans K.M. – Phil. Trans. Roy. Soc. A (1934), **233**, 1).
2. Pauling L. *The Nature of the Chemical Bond. – Ithaca, Cornell Univ. Press. 1960. (Pauling L. Theory of Alloy Phases. – Cleveland, Am. Soc. Metals, Ohio, (1956)220).*
3. Pearson W.B. *The Crystal Chemistry and Physics of Metals and Alloys. – Wiley Interscience, New York. 1972.*
4. Hume-Rothery W. *Electrons, Atoms, Metals and Alloys. – Iliffe and Sons, Ltd. 1948. (Hume-Rothery W. and Raynor G.V. – The Structure of Metals and Alloys.- Inst. Metals, London. 1954).*
5. Laves F. *Theory of Alloy Phases. – Cleveland, Am. Soc. Metals, (1956)124.*
6. Frank F.C. and Kasper J.S. – Acta Cryst. (1958), **11**, 184. (Frank F.C. and Kasper J.S. - Acta Cryst. (1959), **12**, 483).
7. Jones H. *The Theory of Brillouin Zones and Electronic States In Crystals. – North Holland Publ. Co., Amsterdam, 1960.*
8. Mott N.F. and Jones H. - *The theory of the properties of metals and alloys.– Dover Publ. Inc. New York. 1958.*
9. Evesque P. – Contemp. Phys. (1992), **33**, 245.
10. Bideau D., Hansen A. (Eds.) *Disorder and Granular Media. – Elsevier, New York. 1993.*
11. Knigth J.B., Jager H.M., Nagel S.R. – Phys. Rev. Lett. (1993), **70**, 3728.
12. Bak P., Tang C., Wiesenfeld K. – Phys. Rev. A (1980), **38**, 364.
13. Kadanoff L.P., Nagel S.R., Wu L., Zhou S. – Phys. Rev. A (1989), **39**, 6524.
14. Lee J. – J. Phys. I. (France) (1993), **3**, 2017.
15. Poschel T., Buchholtz V. – Phys. Rev. Lett. (1993), **71**, 3963.
16. Stepanyuk V.S., Katsnelson A.A., Szasz A., Trushin O.S., Nayak P.– Phys. Stat. Sol. (b) (1991), **164**, 395.
17. Stepanyuk V.S., Katsnelson A.A., Szasz A., Trushin O.S. – Phys. Stat. Sol. (b) (1990), **161**, K77.
18. Stepanyuk V.S., Szasz A., Katsnelson A.A., Trushin O.S. – J. Non-Cryst. Sol. (1990), 125, 139.

19. Johnson W.A. and Mehl R.F. – Trans. Amer. Inst. Mining. (Metal) (1939), **135**, 416.
20. Avrami M. J. – Chem. Phys. (1939), **7**, 1103. (Avrami M. – J. Chem. Phys. (1940), **8**, 212. Avrami M. – J. Chem. Phys. (1941), **9**, 117).
21. Kolmogorov A.N. – Izv. Acad. Nauk. SSSR, Ser. Mat. (1937), **1**, 355.
22. Jellinek J. Theory of Atomic and Molecular Cluster. – Berlin-Argonne. Springer. 1999.
23. Cope F.W. – Physiol. Chem. & Phys. (1976), **8**, 519. (Cope F.W. – Physiol. Chem. & Phys. (1977), **9**, 443. Cope F.W. – Physiol. Chem. & Phys. (1980), **12**, 537).
24. Munster A. Statistical Thermo-dynamics. – Springer Verlag Berlin and Acad. Press, New York. 1974, Vol. 2., p.98.
25. Munster A. Statistical Thermo-dynamics. – Springer Verlag Berlin and Acad. Press, New York. 1974, Vol.2., p.88.
26. Bethe H. – Proc. Roy. Soc. London. A (1935), **150**, 552.
27. Widom M. Introduction to Quasicrystals, (Ed.: M.V. Jaric). – Acad. Press, Boston. 1988, p.77.
28. Guggenheim E.A. Mixtures. – Oxford University Press. 1952.
29. Batirev I.G., Katsnelson A.A., Kertesz L., Szasz A. – Phys. Stat. Sol. (b) (1980), **100**, 479.
30. Batirev I.G., Katsnelson A.A., Kertesz L., Szasz A. – Phys. Stat. Sol. (b) (1980), **101**, 163.
31. Widom M. Introduction to Quasicrystals, Ed. M.V. Jaric. – Acad. Press, Boston, 1988, p.59.
32. Hoare M. – Ann. N.Y. Acad. Sci. (1976), **279**, 186.
33. Torres M., Pastor G., Jimenez I. and Fayos J. – Phil. Mag. Lett. (1989), **59**, 181.
34. Nelson D.R. and Spaepen F. – Solid State Physics (1989), **42**, 1.
35. Proceedings of International Meetings on Small Particles and Inorganic Clusters. – J. de Physique (1977) **38**, C2. (Second: Surf Sci. 106, 1981. Third: Surf Sci. 156, 1985. Fourth: Z. Phys. D.12, No.14, 1989).
36. Shindhom H. and Portler R. – Phil. Mag. Lett. (1989), **59**, 131.
37. Shoemaker D.P. and Shoemaker C.B. Introduction to Quasicrystals. – Ed.: M.V. Jaric, Acad. Press, Boston, 1988, 1. (Samson S. Structural Chemistry and Molecular Biology. Eds.: A. Rich and N.Davidson, Freeman, San Francisco, 1968, 687).
38. Emin D. – Physics Today (1987), **41**, 55.
39. Haggin V. – Chem. Eng. News (1987), **65**, 9.
40. Voronoi G.F. – J. Rome Angew. Math. (1908), **134**, 198.
41. Finney J.L. – Proc. Roy. Soc. London, Ser. A (1970), 319, 479. (Finney J.L. – Proc. Roy. Soc. London, Ser. A (1970), **319**, 495).
42. Cundy H.M. and Rollett A.P. – Mathematical Models, Oxford at the Clarendon Press. 1976.
43. Widom M. – Phys. Rev. B (1985), **31**, 6456.
44. Penrose R. Introduction to the Mathematics of Quasicrystals. – Ed.: M.V. Jaric, Acad. Press, Boston, 1989, 53.
45. Stepanyuk V.S., Szasz A., Katsnelson A.A., Trushin O.S. – J. Non-Cryst. Sol. (1991) **130**, 311.
46. Stepanyuk V.S., Grigorenko B.L., Szasz A., Katsnelson A.A., Watson L.M. – J. Non-Cryst. Sol. (1994) **176**, 133.
47. Grigorenko B.L., Nemukhin A.V., Sergeev G.B., Stepanyuk V.S., Szasz A. – Phys. Rev. B (1994) **50**, 1866.
48. Stepanyuk V.S., Katsnelson A.A., Trushin O.S., Szasz A. – Phys. Stat. Sol. (a) (1990) **122**, K7.
49. Coxeter H.S.M. Regular Polytopes. – Methuen, London. 1947.
50. Stepanyuk V.S., Szasz A., Katsnelson A.A., Trushin O.S., Muller H., Kirchmayr H. – J. Non-Cryst. Sol. (1993) **159**, 80.
51. Sadoc J.F. – J. de Physique (1980) **41**, C8, 326.
52. Zsoldos I, Szasz A. – Submitted to Non-Cryst. Solids, 1998.
53. Stepanyuk V.S., Katsnelson A.A., Szasz A., Kalibaeva G.M., Muller H., Kirchmayr H. – Phys. Stat. Sol. (b) (1993) **178**, K1.
54. Stepanyuk V.S., Katsnelson A.A., Szasz A., Wolf O.V., Gyarmati E., Kalibaeva G.M. – J. Phys.: Cond. Mat. (1993) **5**, 6139.
55. Stepanyuk V.S., Katsnelson A.A., Szasz A., Trushin O.S., Muller H., Watson L.M., Kirchmayr H. – J. Non-Cryst. Solids (1992) **151**, 169.
56. Harris I.A., Kidwell R.S. and Northby J.A. – Phys. Rev. Lett. (1984) **53**, 2390.
57. De Heer W.A., Knight W.D., Chou M.Y. and Cohen M.L. – Solid State Physics (1987) **40**, 93.
58. Iniguez M.P., Lopez M.J., Alonso J.A. and Soler J.M. – Z. Phys. D. (1989) **11**, 163.
59. Manninen M. – Solid State Comm. (1986) **59**, 281.
60. Knight D.W., de Heer W.A. and Saunders W.A. – Z. Phys. D. (1986) **3**, 109.
61. Narashimhan S. and Jaric M.V. – Phys. Rev. Lett. (1989) **62**, 454. (Narashimhan S. and Jaric M.V. – Phys. Rev. Lett. (1989) **63**, 2769).
62. Buck U. – Europhys. Lett. (1989) **20**, 41.
63. Sadoc J.F. – J. de Physique (1983) **44**, L707.
64. Nelson D.R. – Phys. Rev. B (1983) **28**, 5515.
65. Szasz A. Strongly Correlated Electron Systems and High Tc Superconductivity. –Eds.: E. Zipper, R. Manka, M. Maska), World Scientific, Singapore, London, 1991, 168.
66. McAdon M.H. and Goddard W.A. – J. Phys. Chem. (1987) **91**, 2607.
67. Northby J.A., Xie J., Freeman D.L. and Doll J.D. – Z. Phys. D. (1989) **12**, 69.
68. Phillips J.C. – Chem. Rev. (1986) **86**, 619.
69. Shith A.P. and Rolson A.P. – Phys. Rev. Lett. (1989) **62**, 2768. (Narasimhan S. and Jaric M.V. – Phys. Rev. Lett. (1989) **63**, 2769).

70. Rokshar D.S. – Phys. Rev. B (1987) **35**, 5487.
71. Mosseri R. and Sadoc J.F. – J. de Physique Letters (1984) **45**, L827. (Sadoc J.F. – J. de Physique (1980) **41**, C8, 326. Sadoc J.F. and River N. – Phil. Mag. B. (1987) **55**, 537).
72. Mosseri R. and Sadoc J.F.- Z. Phys. D. (1989) **12**, 89. (Kreibig U., Fauth K., Quinted M. and Schonauer D. – Z. Phys. D. (1989) **12**, 505).
73. Ichicava T. – Phys. Stat. Sol. (1973) **19**, 707. (Barker J., Hoare M.R. and Finney J.L. – Nature (1975) **257**, 120).
74. Sadoc J.F. and Mosseri R. – Phil. Mag. B. (1982) **45**, 467.
75. Anlage S.M. Icosahedral Order in Metastable Metallic Alloys. – Ph.D. Thesis, California Institute of Technology, Pasadena California, USA, 1988.
76. Anlage S.M. – Mat. Sci. Forum (1987) **22-24**, 269.
77. Szasz A. – J. Supercond. (1993) **6**, 99.
78. Emin D. – Physica C (1989) **162-164**, 799. (Emin D.- Phys. Rev. Lett. (1989) **62**, 1544. Emin D., Hillery M.S.- Phys. Rev. B. (1989) **39**, 6575).
79. Teller E. Proc. World Congress Supercond. Huston, 1988, (Eds.: Burnham C.C., Kane R.D.) World Scientific Singapore, 1988, 303.
80. Szasz A., Kopajev Yu. A., DasGupta A. – Phys. Lett. A (1991), **152**, 361.
81. Szasz A. – Physiol. Chem. Phys. (1991), **23**, 43.
82. Szasz A., Kertesz L., Hajdu J., Kollar J. – Aluminium (1985), **61**, 515. (Stepanyuk V.S., Szasz A., Katsnelson A.A., Kozlov A.V., Hendry A. – Phys. Stat. Sol. (b) (1992) **170**, 189. Szasz A., Aysawy M.A., Dankhazi Z., Kertesz L., Muller H., Kirchmayr H. – J. Non-Cryst. Solids (1993) **163**, 49).
83. Szasz A., Watson L.M., Kertesz L., Kollar J. – Phys. F. Met. Phys. (1988), **18**, 1849. (Kerr A., Watson L.M., Szasz A., Muller H., Kirchmayr H. – J. Phys. Chem. Solids (1995) **57**, 1285).
84. Kertesz L., Kojnok J., Szasz A. – Cryst. Latt. Def. and Amorphous Mat. (1982), **9**, 219. (Negm N.Z., Watson L.M., Szasz A. – J. de Physique (1987) **48**, C9-1033. A. Kerr, L.M. Watson, A.Szasz: J. Phys. Condens. Matter. (1995) **7**, 5405).
85. Brewer L. In Phase Stability of Metals and Alloys. – Eds: P.S. Ruchman, J. Stringer, R.I. Jaffec, McGraw Hill, 1967.
86. Szasz A., Fabian D.J. – Physica C (1988), **153-155**, 1205.
87. Heine V. and Weaire D. – Solid State Physics (1970), **24**, 249.
88. Heine V., Weaire D. – Sol. St. Phys. (1970), **24**, 287.
89. Massalsky T.B., Mizutani U. – Prog. Mat. Sci. (1978), **22**, 151.
90. Stroud D., Aschcroft N.W. – J. Phys. F (Metal. Phys.) (1971), **1**, 113.
91. Dalton N.W., Deegan R.A. – J. Phys. C (1969), **2**, 2369.
92. Coveney P.V. – Nature (1988), **333**, 409.
93. Pettifor D.G. – J. Phys.C (1970), **3**, 367. (Andersen O.K., Jepsen O., Glotzel D. Highlights of Condensed Matter Theory. –Eds: F. Bassani, F. Fumi, M.P. Tosi North Holland, Amsterdam, 1985).
94. Darker L., Gurry R.W. Physical Chemistry of Metals. – McGraw Hill, New York, 1953. (Pettifor D.G. – Phys. Rev. Lett. (1983), **53**, 1080).
95. Miedema A.R. – J.Less-Common Met. (1973), **32**, 117. (Miedema A.R., de Boer F.R. and de Chatel P.F. - J. Phys. (1973), **F 3**, 1558. Miedema A.R. and de Chatel P.F. - Metall Soc. AIME Proc. 1980. Miedema A.R., de Chatel P.F. and de Boer F.R. - Physica (1980), **100**, 1.
96. Rudman P.S., Stringer J., Jaffee R.J. Phase Stability In Metals and Alloys. – McGraw Hill New York, 1966. (Toyozaava Y. Highlights of Condensed Matter Theory. – Eds: F.Bassani, F.Fumi and M.P.Tosi, North Holland Amsterdam 1985. Pettifor D.G. – Sol. St. Phys. (1987), **40**, 43. Pettifor D.G. Physical Metallurgy. – Eds: Cahn R.W., Haasen P. Elsevier Science Publisher BV, Amsterdam, Ch.3, 1983).
97. Hafner J. – J. Phys. (1976), **F 6**, 1243.
98. Hafner J. From Hamiltonians to Phase Diagrams. – Springer Verlag, Berlin, Heidelberg, 1987.
99. Alonso J.A., March N.H. - Electrons In Metals and Alloys. – Acad. Press, Harcourt Brace Jovanovich, Publ., London, 1989.
100. Szasz A., Kertesz L., Aysawy M.A., Kirchmayr H., Muller H., Watson L.M. – J. Non-Cryst. Solids (1991), **130**, 211.
101. Szasz A., Fabian D. – Solid State Commun. (1988), **65**, 1045.
102. Szasz A. – J. Non-Cryst. Sol. (1991), **127**, 121.
103. Butler W.H. and Kohn W. – NBS Special Publ. (1971), **323**, 465. (Proc. 3rd Materials Res. Symp., Garthersburg Maryland, USA, 1969).
104. Morgan G.G. and Weir G.F. – Phil. Mag. (1983), **47**, 177.
105. Haussler P. – Z. Phys. (1983), **B 53**, 15.
106. Mizutani U. – Progr. Mat. Sci. (1983), **28**, 97. (Narlicar A.V., Ekbote S.N. – Superconductivity and Superconducting Materials. - Southern Asian Publ. New Delhi India, 1985).
107. Nagel S.R. and Tauc J. – Phys. Rev. Lett. (1975), **35**, 380.
108. Niessen A.K., Miedema A.R., de Boer F.R. and Boom R. – Physica B (1988), **151**, 401.
109. Sato S. and Tamegai T. – Jap. J. Appl. Phys. (1989), **28**, LI620.
110. Khait Y.L. – Z. Phys. B: Cond. Mat (1988), **71**, 7.
111. Khait Y.L. – Phys. Rep. (1983), **99**, 237. (Khait Y.L. – Physica (1986), **C139-140**, 237).

112. Kleman M. – J. de Physique (1982), **43**, 1389.
113. Heritier M., Montambaux G. and Lederer P. – J. de Physique Letters (1979), **40**, L439.
114. Szasz A., Fabian D.J. Physics and Materials Sciences of High Temperature Superconductors. – Eds.: R. Kossowsky S. Methfessel and D. Wohlleben, NATO ASI Series, Kluwer Acad. Publ., Dordrecht-Boston, 1990.
115. Amand R. St. and Glessen B.C. – Scr. Metall. (1978), **12**, 1021. (Sommer F., Duddek G. and Predel B. – Z. Metallkunde (1978), **69**, 587. Predel B. and Hulse K. – J. Less-Common Metals (1979), **63**, 45).
116. Polk D.E. – Scr. Metall. (1970), **4**, 117.
117. Chen M.S. – Mater. Sci. Eng. (1976), **34**, 151.
118. Mizutani U., Yoshida T. – J. Phys. F.: Met. Phys. (1982), **12**, 2331. (Johnson W.L. - Glassy Metals I. Eds. H.J. Guntherodt H. Beck Springer Verlag, 1981).
119. Waseda Y. – Prog. Mat. Sci. (1981), **26**, 1.
120. Sommer F., Fripan M., Predel B. – Proc. 4th Int. Conf. Rapidly Quenched Metals (Sendai, 1981) 209.
121. Haussler P., Baumann F. – Z. Phys. B (Cond. Mat.) (1983), **49**, 303.
122. Donald I.W., Ward K.D., Davies H.A., Craugle J. – Free. 4th. Int. Conf. Rapidly Quenched Metals Sendai, Japan (1981) 597.
123. Lovas A., Granasi L., Zambo-Balla K., Kiraly J. – Proc. Cent. Metallic Glasses: Science and Technology, Budapest, 2, 291, 1980.
124. Aysawy M.A., Szasz A., Kojnok J., Lovas A., Stepanyuk V.S., Kertesz L. – Periodica Polytechnica (Chem. Eng.) Techn. Univ. Budapest, 34, 149, 1990.
125. Kemeny T., Vincze I., Fogarassy B., Arajcs S. – Phys. Rev. B (1979), **20**, 476.
126. Stavola M. – Phys. Rev. Lett. (1987), **58**, 1571.

Chapter 3

1. Physical and Chemical Properties. – Berlin-Kobe-Ibarak. Springer. 1999.
2. Szwarc H. – Thermochemica Acta. (1986), **109**, N 1, 91-103.
3. Gibbs J.H., DiMarzio E.A. – J. Chem. Phys. (1958), **28**, N 3, 373-383.
4. Rivier N. – Advanced in Physics. (1987), **36**, N 1, 95-134.
5. Richter A., Romanov A.E., Pompe W., Vladimirov V.I. – Phys. Stat. Solidi (b) (1987), **143**, 43-53.
6. Ziman J.M. Models of Disorder. The Theoretical Physics of Homogeneously Disordered Systems. – Cambridge. Cambridge University Press, 1977.
7. Singh N. – Physica B: Condensed Matter. (1999), **270**, N 1-2, 298-306.
8. Cao Biao and Chen Zhenhua. – Physica B: Condensed Matter. (1999), **266**, N 2, 152-161.
9. Kawashima N., Shirahama K. And Kono K. – Physica B: Condensed Matter. (1999), **259**, 373-375.
10. Damker T., Bryksin V.V. and Botger H. – Physica B: Condensed Matter. (1999), **263-264**, N 1-4, 133-135.
11. Bach H., Krause D. Analysis of the Composition and Structure of Glass and Glass Ceramics. – Berlin-Mainz. Springer. 1999.
12. Lauter-Pasyuk V., Lauter H.J., Lorenz M., Aksenov V.L., Leiderer P. – Physica B: Condensed Matter. (1999), **266**, N3, 149-153.
13. Miyagawa M., Hiwatari Y., Bernu B., Hansen J.P. – J. Chem. Phys. (1988), **88**, N 6, 3879-3886.
14. Wright O.B. – Physica B: Condensed Matter. (1999), **263**, N 1-4, 321-323.
15. Yonezawa F., Nose S., Sakamoto S. – J. Non-Cryst. Sol. (1987), **95/96**, N1, 83-93.
16. Weher Th.A., Stillinger F.H. – Phys. Rev. B: Condens. Matter. (1987), **36**, N 13, 7043-7050.
17. Baxter R.J. Exactly Solved Models in Statistical Mechanics. A Subsidiary of Harcourt Brace Jovanovich. – London-Toronto. 1982.
18. Tanaka M. – J. Phys. Soc. Jap. (1986), **55**, N 9, 3108-3116.
19. Reksan S. – J. Non-Cryst. Sol. (1987), **95/96**, N1, 131-141.
20. Hiki Y., Takahashi H. and Kogure Y. – Physica B: Condensed Matter. (1999), **263**, 353-356.
21. Mar'yan M.I. – Izv. VUZov. Fizika (1990), N 12, 15-19.
22. Mar'yan M.I. – The Scientific Herald of Uzhgorod State University (1998), N 2, 43-48.
23. Amorphous Semiconductors. – Edited by Brodsky M.H. Springer. Berlin-New York. 1979.
24. Glassy Metals (Ionic Structure, Electronic Transport and Crystallisation). – Edited by H.-J. Guntherodt and H. Beck. - Springer. Berlin-New York. 1981.
25. Dynamics of Solids and Liquids by Neutron Scattering. – Edited by S.W. Lovesey and T. Springer. Berlin-New York. 1982.
26. Barrat A., Franz S. and Parisi G. – J. Phys. A: Math. Gen. (1997), **30**, 5597-5612.
27. Mitsutaka Nakamura, Osamu Matsuda, Yong Wang and Kazuo Murase. – Physica B: Condensed Matter. (1999), **263**, N 1-4, 330-332.
28. Borsari I., Degly Esposti M., Graffi S., Unguenddi F. – J. Phys. A: Mat. Gen. (1997), **30**, N 7, L155-L159.
29. Mar'yan M.I., Khiminets V.V. – Pis'ma v Zh. Tehn. Fiz. (1989), **15**, N 5, 5-9.
30. Mar'yan M., Mishak A., Kikineshy A., Rosola I. – XVIIth Int. Congr. on Glass. China. Beijing. (1995), **7**, 217-222.
31. Andronov A., Vit A., Khalkin C. Theory of Oscillators. – Oxford. Pergamon Press. 1966.
32. Hunklinger S., Raychaudhuri A.K. Thermal and Elastic Anomalies in Glass at Low Temperatures. Progress in Low Temperature Physics. – Amsterdam (1986), **9**, 265-344.

33. Fleurov V.N., Trakhtenberg L.I. – J. Phys. C: Sol. St. Phys. (1986), **19**, N 28, 5529-5553.
34. Clare C. Yu. – J.Non-Cryst. Solids. (1987), **95**, N 2, 163-165.
35. Phillips J.C. – J.Non-Cryst. Solids. (1981), **43**, N 1, 37-77.
36. Mar'yan M.I., Khiminets V.V., Turyanitsa I.I. – Fiz. Khim. Stekla. (1990), **16**, N 2, 293-299.
37. Mar'yan M.I., Dobosh M.V., Tsygyka V.V., Khiminets V.V. Self-Consistent Approach to the Study of Thermodynamic Properties of Vitreous Semiconductors in the Softening Temperature Region. – Non-Cryst.Sem.'89. Uzhgorod (1989), **1**, 148-150.

Chapter 4

1. Kuhn H. – Molec. Eng. (1992) **1**, 377.
2. Szent-Gyorgyi A. – Bioelectronics, Acad. Press. New-York, London, 1968.
3. Eisenberg D. and Kauzmann W. Structure and Properties of Water. – Oxford at Clarendon Press, 1969.
4. Franks F. (ed). Water A Comprehensive Treatise (in seven volumes) Plenum Press, NY, London.
5. Szasz A., van Noort D., Scheler A., Douwes F. – Phys. Chem. Phys. (1994), **26**, 299-322.
6. Fisher I.Z. Structure and role of water in living organism. – Publ. Leningrad State Univ. (1968), **34**–44.
7. Vdovenko V.M., Hurinov Yu. V., Lety E. Ibid, 3-6.
8. Benson S.W., Siebert E.D. – J Chem.Soc. (1992), **114**, 4269-4276.
9. Mezel M. – Physics of many body systems. (1991), **19**, 37-50.
10. Baranova A.V., Petrov V.I., Fedorov A.V., Chernyakov G.M. – Pisma v ZhETF (1993), **57**, 356-359.
11. Walrafen G.E. – J.Chem. Phys. (1986), **86**, 6980.
12. Structure of Water and Aqueous Solutions. – Ed. by W. P. A. Luck, Verlag Chemie and Physics, Weinheim, 1974, p.247.
13. Münster A. Statistical Thermodynamics. – Springer-Verlag, Berlin, v. 2, 1974.
14. Wannier G. H. – Rev. Mod. Phys. (1945), **17**, 50.
15. Berecz E. Physical Chemistry (in Hungarian). – Tankonyvkiado Budapest, 1988.
16. Haggis G.H., Ballasted J.B., Buchanan T.J. – J. Chem. Phys. (1952), **20**, 1452.
17. Crotheim K., Kaoch-Mor J. – Acta Chem. Scand. (1954), **8**, 1193.
18. Nemethy G., Scheraga H.A. – J. Chem. Phys. (1962), **36**, 3382.
19. Nemethy G., Scheraga H.A. – J. Chem. Phys. (1964), **41**, 680.
20. Walrafen G.E. – J. Chem.Phys. (1966), **44**, 1546.
21. Geiger A., Stillinger F.H., Rallmann A. J. – Chem. Phys. (1979), **70**, 4185.
22. Angell C.A. – J. Phys. Chem. (1971), **75**, 3698.
23. King W.T., Barletta R.E. – J. Chem. Phys. (1974), **78**, 1531.
24. Hasted J.B. Aqueous Dielectrics. – Chapman and Hall, 1985.
25. Bernal J.B., Fowler R.H. – J. Chem. Phys. (1933), **1**, 515.
26. Pauling L. Hydrogen Bonding. – (Hadzi L. ed.) Pergamon Press London, p.I, 1959.
27. Frank H.S., Wen W.Y. – Discussions Faraday. Soc. (1957), **24**, 133.
28. Marchi R.P., Eyring H. J. – Phys.Chem. (1964), **68**, 221.
29. Smith C.W. In Biological Coherence and Response to External Stimuli. – Ed. Frohlich H., Springer Verlag. Berlin-Heidelberg (1988), 205.
30. Mott N.F., Davis E.A. Electron Process in Non-Crystalline Materials. – Oxford. Clarendon Press. 1979.
31. Cope F.W. – Biophys. J. (1969), **9**, 303.
32. Ling G.N. A Physical Theory of the Living State. – Blaisdell Publishing Co. New York, 1962.
33. Ling G.N. – Intern. Rev. Cytology (1969), **26**, 1.
34. Ling G.N. In Search of the Physical Basis of Life. – Plenum Publishing Co., New York, 1984.
35. Ling G.N. A Revolution in the Physiology of the Living Cell. – Kreiger Publishing Co., Malabar, FL, 1992.
36. Wiggins P.M. – Microbiological Reviews (1990), **54**, 432-449.
37. Devjatkov N.D., Beckij O.V., Putvinskij A.V. – Proc. 1st Biophysical Congress, USSR, Moscow (1982), 116.
38. Antonchenko V.J. Physics of Water. – Kiev, Publ. House "Naukova Dumka". 1986.
39. Mar'yan M., Mishak A.A., Rosola I.J., Kikineshy A.A. – Proc. XVII Int. Congress on Glass, Beijing, China (1995), **7**, 217-223.
40. Mar'yan M.I., Kurik M.I, Kikineshy A.A., Watson L.M., Szasz A.– Modelling Simul. Mater. Sci. Eng. (1999), **7**, 321-331.
41. Mar'yan M.I., Kurik M.I, Kikineshy A., Watson. L.M., Szasz A. – Ukrainian Journal of Phys. (1999), **10**, 1227-1233.
42. Plakida N.M. Statistical Physics and Quantum Field Theory. – Moscow, Nauka (1973), 205-240.
43. Jellinek J. Theory of Atomic and Molecular Clusters. – Berlin-Argonne. Springer. 1999.
44. Quickender T.I., Irvin J.A. – J. Chem. Phys. (1980), **72**, 4416.
45. Honce-Levin C. – J. Phys. Chem. (1989), **93**, 70.
46. Kurik M.V. – Phys. St. Solidi (1977), **8**, 9.
47. Sacchetti F. – J. Molec. Struct. (1991), **250**, 329.
48. Sasai M. – J. Chem. Phys. (1990), **93**, 7329.
49. Mayer E. – J. Molec. Struct. (1991), **250**, 403.
50. Dore J. C. – J. Molec. Spectr. (1991), **250**, 193.

51. Peschel G., Belouschek P. Hyperthermia and the structure of water in biological tissues. – "Cancer Therapy by Hyperthermia and Radiation, Urban and Swarczenberg (1978), 154-156.
52. Van Oss C. J. Water and biological macromolecules. – Ed.: E. Westhof, The Macmillan Press Ltd., Haundmills (1993), 393.
53. Lippincott E. R, Stromberg R. R, Grant W. H. and Cessac G. L. – Science (1969), **164**, 1482.
54. Derjaguin B. V, Churaev N. V. – Nature (1973), **244**, 430.
55. Rousseau D.L. – J. Coll. Interf. Sci. (1971), **36**, 434.
56. Schrodinger E. – What is the Life? Cambridge University Press.
57. Weber W. – Adv. Protein Chem. (1975), **29**, 1.
58. McCammon J. A and Harvey S. C. Dynamics of Proteins and Nuclear Acids. – Cambridge Univ. Press., Cambridge, 1987.
59. Brooks C. L, Karolus K. and Pettitt B. M. Proteins, a Theoretical Perspective of Dynamics, Structure and Thermodynamics. – John Wiley, New York, 1988.
60. Freuenfelder H., Sligar S. G. and Wolynes P. G. – Science (1991), **254**, 1598.
61. Gurd F. R. N. and Rothgegh V. – Adv. Protein Chem. (1979), **33**, 74.
62. Wagner W. – Rev. Biophys. (1983), **16**, 1.
63. Szent-Györgyi A. The Living State and Cancer. – Marcel Dekker Inc. 1978.
64. Cope F. W. – Adv. Biol. Med. Phys. (1970), **13**, 1.
65. Hazelwood C. F. – Nature (1969), **222**, 747.
66. Szasz A. – Phys. Chem. Phys. USA (1991), **23**, 43.
67. Schriffier J.R., Wen X.G., Zhang S.C.-Physica (1989), **C 162-164**, 300.
68. Chothia C. – Nature (1989), **337**, 204.
69. Bistolfi F. Biostructures and Radiation order-disorder. – Edizioni Minerva Medicina, Torino. 1991.
70. Murzin A.G., Finkelstein A. V. – J. Molec. Biol. (1988), **204**, 749.
71. Bistolfi F. – Radiol. Med. (1990), **80**, 203.
72. Bistolfi F. – Panminerva. Med. (1990), **32**, 10.
73. Hamburger H. J. – Z. Biol. (1989), 26, 414.
74. De Vries H. – Jahrb. Wiss. Botan. (1985), 16, 465.
75. Cope F. W. – Physiol. Chem. Phys. (1980), 12, 537.
76. Musha T. and Sawada Y. – Physics of the Living State, Rhythms and Bifurcation in Membranes and Interfaces, IOS Press, Amsterdam (1994) 45.
77. Musha T. and Sawada Y. – Physics of the Living State, Self-organisation of Electric Currents in Artificial Lipid Membranes, IOS Press, Amsterdam (1994) 57.
78. Teorell T. – J. Gen. Physiol. (1959), 42, 831.
79. Teorell T. – J. Gen. Physiol. (1959), 42, 847.
80. Monnier M. – JU. Membr. Sci. (1977), 2, 49.
81. Monnier M. – JU. Membr. Sci. (1977), 2, 67.
82. Larter R. – Chem. Rev. (1990), **90**, 355.
83. Musha T. and Sawada Y. Physics of the living state. – IOS Press, Amsterdam. 1994.
84. Szent-Gyorgyi A. Electronic Biology and Cancer. – Marcell Dekker, New York, Basel, 1976.
85. Iglesias J. R. and de Almedia R. M. C. – Phys Rev. (1991), **A 43**, 2763.
86. Dellanay R., Caër G. Le, and Khatum M. – J. Phys. (1992), **A 25**, 6193.
87. Stavans J., Domany E. and Mukamel D. – Europhys. Lett. (1991), **15**, 479.
88. Flyvbjerg H. and Jeppesen C. – Phs. Scr. (1991), **38**, 49.
89. Glazier J. A., Anderson M. P. dan Grest G. – Philos. Mag. (1990), **B 62**, 615.
90. Anderson M. P., Srolovitz D. J., Grest G. S. and Sahni P. S. – Acta Metall. (1984), **32**, 783.
91. Srolovitz D. J., Anderson M. P., Sahni P. S. and Grest G. S. – Acta Metall. (1984), **32**, 793.
92. Weaire D. and Kermode J. P. – Philos. Mag. (1983), **B 48**, 245.
93. Weaire D. and Kermode J. P. – Philos. Mag. (1984), **B 50**, 379.
94. Wejchert J., Weaire D. and Kermode J. P. – Philos. Mag. (1986), **B 53**, 15.
95. Fradkov V. E., Schvindlerman L. S. and Udler D. G. – Philos. Mag. (1987), **B55**, 289.
96. Aboav D. A. – Metallography (1980), **13**, 43.
97. Aboav D. A. – Metallography (1983), **16**, 265.
98. Aboav D. A. - Metallography (1984), **17**, 383.
99. Mombach J. C. M., Vasconcellos M. A. Z., and Almeida V. – J.Phys. (1990), **D23**, 600.
100. Mombach J. C. M., de Almeida R. M. C. and Iglesias J. R. – Phys Rev. (1993) **E47**, 3712.
101. Zsoldos I., Szasz A. – J. Non-Cryst. Solids, 1998.
102. Chang J.J., Fisch J., Popp F.A. – Biophotons, Kluwer Acad. Publ. Boston London, 1998. (Ho M.W., Popp F.A., Wanke U. – Bioelectrodynamics and biocommunication, World Scientific, Singapore, London, 1994).
103. Kell D. B. and Hitchens G. D. – Coherent Excitations in Biological Systems, Eds.: H. Frölich and F. Kremer, Springer Verlag, 1983.
104. Hameroff S. R. Biological coherence and response to external stimuli – Ed.: H. Frölich, Springer Verlag (1988) 242.
105. Nardone M., Ricci M. A and Benassi I. P. – J. Molec. Str. (1992), **270**, 287.

106. Vegiri A. and Farantos S. C. – J. Chem. Phys. (1993), **98**, 4059.
107. Andres J. L., Marti J., Duran M., Leedos A., Bertran J. – J. Chem. Phys. (1991), **95**, 3521.
108. Rowland S. Coherent Excitations in Biological systems. – Eds.: H. Frölich and F. Kremer, Springer Verlag, 1983, 145.
109. Becker R.O., Selden G. – The Body Electric (Electromagnetism and the Foundation of Life), Quill William Morrow, New York, 1985.
110. Barrett T.W., Pohl H.A. Energy Transfer Dynamics. – Springer Verlag Berlin-Heidelberg New York, 1987.
111. DelGuidence E., Doglia S., Milani M., Vitiello G.- Biological Coherence and Response to External Stimuli. – Ed.: H. Frölich, Springer Verlag, 1988.
112. Singer S. J. – Science (1992), **255**, 1671.
113. Raff M. C. – Nature (1992), **356**, 397.
114. Morgan G. G., Weir G. F. – Phil. Mag. (1983), **47**, 177.
115. Moser C. C., Keske J. M., Warncke K., Farid R. S and Dutton P. L. – Nature (1992), **355**, 769.
116. Ling G. N. – Int. Rev. Cytology (1960), **26**, 1.
117. Colombo M. F., Rau D. C. and Parsegian V. A. – Science (1992), **256**, 655.
118. Parsegian V. A., Rand R. P., Fullere N. L and Rau D. C. – Methods of Enimol. (1989), **127**, 400.
119. Rand P. – Science (1992), **256**, 618.
120. Rau D. C. and Parsegian V. A. – Science (1990), **249**, 1278.

Chapter 5

1. Mayer J., Goepfert Mayer M. Statistical Mechanics. – New York-London-Sydney-Toronto. Wiley. 1977.
2. Garcia-Ojalvo J., Sancho J. Noise in Spatially Extended Systems. – Berlin-Catalunya-Barcelona. Springer. 1999.
3. Atkins P.W. The Second Law. – New York. Freeman. 1984.
4. Risken H. The Fokker-Planck Equation. Methods of Solutions and Applications. – Berlin. Springer. 1996.
5. Nicolis G., Prigogine I. Self-Organisation in Non-Equilibrium Systems. From Dissipative Structure to through Fluctuations. – New York. Wiley. 1977.
6. Gardiner C.W., Zoller P. Quantum Noise. – Berlin. Springer. 2000.
7. Arnold L. Stochastic Differential Equations. Theory and Application. – New York. Wiley. 1974.
8. Mar'yan M., Yurkovich N., Kikineshy A. – Third Inter. School-Conf. Of PPMSS'99, 7-11 Sept., Chernivtsi, (1999) 190.
9. Horsthemke W., Lefever R. Noise-Induced Transitions. – Berlin-Heidelberg-New York-Tokyo. Springer-Verlag. 1984.
10. Kawashima N., Shirahama K. And Kono K. – Physica B: Condensed Matter. (1999), **259**, 373-375.
11. Mar'yan M.I., Khiminets V.V. – Inzh. Fiz. Zhurn. (1991), **61**, N 1, 52-55.
12. Mar'yan M.I. External Noise Influence on the Vitrification of the Glass-Forming Melts. – 2nd All-Un. Conf. Phys. Glass. Solid. Riga. 1991.
13. Horsthemke W., Lefever R. – Phys. Lett. (1977), **A64**, 19.
14. Mar'yan M.I., Khiminets V.V. – Ukrainian Journal of Phys. (1991), 36, N 5, 757-761.
15. Nigam N.C. Introduction to Random Vibrations. – The MIT Press Cambridge, Massachusetts, London, England. 1983.
16. Gillespie D.T. Markov Processes: An Introduction for Physical Scientist. –Academic Press, San Diego. 1992.
17. Schweitzer F. On the Kinetics of Nucleation: Stochastic Description and Fokker-Planck Equation. – Winssenschaft. Zeit. Wilhelm-Pieck-Universitat. Rostok. (1986), **35**, N 4, 19-23.
18. Fletcher C.A. Computational Techniques for Fluid Dynamics. – Berlin-Heidelberg-New York-London-Paris-Tokyo. Springer-Verlag. 1988.
19. Klimontovich Yu.L. – Annalen der Physik (1988), **45**, N 5, 340-352.
20. Graham R. – J.St.Phys. (1989), **54**, N 5/6, 1207-1215.
21. Brand H.R., Doering C.R., Ecke R.E. – J. St. Phys. (1989), **54**, N 5/6, 1111-1119.
22. Teitsworth S.W. – Appl. Phys. A. (1989), **N 2**, 127-136.
23. Mangioni S., Deza R., Wio H.S. Toral R. – Phys. Rev. Let. (1997), 79, N 13, 2389-2393.
24. Grassman J., Herwaarden O.A. Asymptotic Methods for the Fokker-Planck Equation and the Exit Problem in Applications. – Berlin. Springer. 1999.

Chapter 6

1. Tanaka K. – J.Non-Cryst.Sol. (1980), **35/36**, N 2, 1023-1034.
2. Phillips J.C. – J.Non-Cryst.Sol. (1981), **43**, N 1, 37-77.
3. Bercha D.M., Mar'yan M.I. – Ukrainian Journal of Phys. (1981), **26**, N 6, 978-981.
4. Bercha D.M., Mar'yan M.I. – Ukrainian Journal of Phys. (1982), **27**, N 2, 235-259.
5. Bercha D.M., Mikla V.I., Mar'yan M.I., Semak D.G., Kikineshy A.A. – Fiz. Tv. Tel. (1983), 17, N **9**, 1627- 1630.
6. Mikla V.I., Mar'yan M.I., Semak D.G., Bercha D.M., Kikineshy A.A. – Proc. Int. Conf. on Semicond. Bucuresti (1982), **1**, 202-204.
7. Mar'yan M.I., Kikineshy A.A., Mishak A.A. – Phil. Mag. B. (1993), **68**, N 5, 688-695.
8. Mar'yan M.I., Kikineshy A.A., Mishak A.A. – Ukrainian Journal of Phys., (1993), **38**, N 7, 97-104.
9. Mar'yan M.I., Kikineshy A.A., Mishak A.A. – Quantum Electronics (1994), 46, 3-8.

10. Bach H., Krause D. *Thin Films on Glass*. – Berlin. Springer. 1997.
11. Babloyantz A. *Molecules, Dynamics and Life*. – New York. Wiley. 1986.
12. Fife P. *Nonlinear Problems in Physical Sciences and Biology*. – Berlin. Springer-Verlag. 1972.
13. Wingfree A.T. *The Geometry of Biological Time*. – New York. Springer-Verlag. 1980.
14. Lefever R., Erneux T. *Nonlinear Electrodynamics in Biological Systems*. – New York. Plenum Press. 1974.
15. Davydov A.S., Kislukha N.I. – *Phys. Stat. Solidi (b)* (1973), **59**, 465-473.
16. Devyatkov N.D. *Medico-Biological Aspects of Low-Intensity Millimetre Radiation*. – Moscow. IRE AN SSSR. 1985.
17. Keizer J. *Statistical Thermodynamics of Non-Equilibrium Processes*. – New York. Springer-Verlag. 1987.
18. Tengroth C., Borjesson L., Kagunya W.W., Mindherdorf H.O. – *Physica B: Condensed matter* (1999), 266, N 2, 27-34.
19. Turyanitsa I.I., Mar'yan M.I. – *Ukrainian Journal of Phys.* (1992), **37**, N 2, 256-260.
20. Mar'yan M.I. – *The Scientific Herald of Uzhgorod State University* (1998), N 3, 114-119.
21. Mar'yan M.I., Palyok V. Yu. – *Functional Materials* (1999), **6**, N 3, 485-488.

Appendix

1. Bottger H. *Principles of the Theory of Lattice Dynamics*. – Academie-Verlag, Berlin. 1983.
2. Horton P., Maradudin A.A. *Dynamic Properties of Solids*. – North-Holland, Amsterdam. V.1. 1974.
3. Wette F.W., Nijhoer R.A. – *Phys. Lett.* (1965), **18**, 19.
4. Plakida N.M., Siklos T. – *Phys. Stat. Sol.* (1969), **33**, 103.
5. Born M. *Festschrift Acad. Wiss. Gottingen. Math. Phys.* 1951.
6. Plakida N.M., Siklos T. – *Acta Phys. Hungary.* (1978), **45**, 37.
7. Shukla K.A., Paskin A., Welch D.O., Pienes G.J. – *Phys. Rev* (1982), **B24**, 724.
8. Wojtczak L., Siklos T., Mrygon B., Mielnicki J. – *Phys. Stat. Sol. (b)* (1982), **109**, 483.
9. Stasjuk I.V., Trachenko K.O. – *Condensed Matter Physics* (1997), **N 3**, 89-106.
10. Mar'yan M.I., Khiminets V.V. – *Melting* (1991), **N 1**, 56-62.
11. Yukalov V.I. – *Phys. Rev. B: Condens. Matter.* (1985), 32, **N 32**, 436-446.
12. Mar'yan M.I. – *Izv. VUZov. Fizika.* (1990), **N 12**, 15-19.
13. *Dynamics of Solids and Liquids by Neutron Scattering*. Edited by S.W. Lovesey and T. Springer. Berlin-New York. 1982.
14. Awrejcewicz J., Andrianov I.V., Manevich L.I. *Asymptotic Approaches in Nonlinear Dynamics. New Trends and Applications*. – Berlin-New York. Springer. 1996.
15. Landau L.D., Lifshitz E.M. *Statistical Physics*. – Moscow. Nauka. 1964.